Experimental and Analytical Study on Mixed Sediment (Sand-Mud) Transport Processes

A thesis submitted in partial fulfilment of the requirements for the degree of Doctor of Philosophy (PhD) by:

Olugbenga Samuel IBIKUNLE

BSc (Hons), MSc (Engr.)

Heriot Watt University, Edinburgh

School of Energy, Geosciences, Infrastructure and Society

February, 2017

Abstract

Estuaries and tidal inlets are often characterised by the co-existence of cohesive (i.e. mud: clay and silt, $D<65\mu m$) and non-cohesive (i.e. sand, $D>65\mu m$) sediments in different fractional concentrations. Knowledge of the dynamic sedimentation behaviour of sand-mud mixtures is therefore crucial to the physical understanding and prediction of the time-dependent structure (i.e. mixed or segregated), composition and erodibility of sediment bed deposits developing within these sedimentary environments.

The current study develops and applies a new, non-invasive electrical resistivity measurement technique (ERMT) to capture both temporal and spatial changes in density, porosity and composition of the evolving sand-clay bed deposits, complemented by time-lapsed images of the sedimentation processes. A series of settling column tests are then conducted to investigate spatial and temporal variations in sediment bed structure and composition resulting from differential settling of a range of sand-clay mixtures over three different parametric conditions (i.e. sediment composition, initial mixture concentration and ambient pore fluid salinity). Further experiments on erosion and deposition of mixed-sediment beds are conducted with benthic annular flume. Therefore, discussion, analysis and critical reflection on the current experimental results and findings have provided new insight into mixed (sand-clay) sedimentation and erosion processes.

The results show that the formation of segregated (sand-clay) bed layers within bed deposits is largely controlled by the initial fractional composition (i.e. relative sand and clay concentrations). Specifically, mixtures with low clay contents are shown to form well-defined (sand-clay) layer segregation within the resulting deposits, while higher clay contents result in more transitional segregation patterns or no layer segregation (for very high clay concentrations). The physical mechanism under which these different segregation types can be generated are illustrated through predictions from an existing polydisperse hindered settling model of Cuthbertson *et al*. (2008). This model indicates that the degree of bed segregation, and time scale over which this occurs, correlates well with the difference in predicted hindered settling characteristics and upward displacements associated with the sand and clay fractions, respectively. From the erosion experiments, a negative correlation between the proportion of cohesive sediment and the inception of erosion is further established. Specifically, a 5% clay fractional content

within sand-clay sediment bed is identified as the critical cohesive fractional content that delineates the non-cohesive and cohesive bed erosion regimes.

Dedication

To all visa nationals living (or those that have lived) in the United Kingdom, who, in one way or the other, have been *victimised* by some of the *inhumane* immigration policies of Tories led government of the UK. Also to those who are currently enduring such *inhumane* immigration policies.

Also, to all hard-working, loving and supportive wives and parents.

Acknowledgements

"No one can receive anything unless God gives it from heaven" – John 3:27 (NLT). *"For I can do everything through Christ, who gives me strength"* – Philippians 4:13 (NLT). In the light of these scriptural passages, I give my unreserved thanks to God-the Father, God-the Son and God-the Holy Spirit for making this dream a reality.

Happy you are if you have a true friend, but you are fulfilled if that friend is your spouse - I wholeheartedly appreciate my friend and wife (Oluwafunmilola) for her priceless supports and understanding in all ramifications, we were together in this throughout. Also to my children (Bliss, Emmanuel and Shalom), thank you for your understanding during those periods I have denied you the precious *play-time-with-daddy*. I cannot but acknowledge the roles of my lovely parents-in-law and my parents; thanks for your financial and spiritual supports.

Dr A.J.S. Cuthbertson and Prof. W.J. McCarter, I am grateful for your priceless supports in your roles as my supervisors, your relentless efforts and contributions towards the success of my study shall be forever remembered.

Special thanks go to all the technical members of staff at the School (EGIS); in all honesty, this project may not have been successful if not for your efforts and contributions. The roles of all other academic and supporting staff members within the school are equally acknowledged. I thank the school's scholarship board for the *fees-waiver scholarship*. Also, The Royal Society (RG120540) for additional funds provided for specialist laboratory equipment.

Special thank-you goes to Hon. Michelle R. Thomson (MP for Edinburgh West) and her wonderful team, for standing by us during our long and difficult immigration battle over the senseless and heartless decision of UK Home Office to impede the success of my PhD programme. Jacqueline Moore of Drummond-miller LLP, your passionate and professional support during those difficult moments is equally acknowledged.

Friends and colleagues from all over the world, you are highly appreciated.

Declaration Statement

Table of Contents

Page No.

List of Tables

Page No.

List of Figures

Page No.

Chapter Two Literature Review

Chapter Three Method, Materials and Equipment

Chapter Four Experimental Results: ES-1

Chapter Five Experimental Results: ES-2

Chapter Seven Analysis and Discussion

Notations

Alphabetic Notation

A - Electrodes cross-sectional surface area (L^2) (m^2)

B - Grain surface average mobility of the counter ions (mho cm^2/meg)

C_0 (or C_s) - Initial sediment concentration ($M.L^{-3}$) ($g\ l^{-1}$)

C_D (or F_D) - Particle-fluid drag coefficient

C_u - Soil undrained shear strength ($M.L^{-1}.T^{-2}$) (Pa)

C_v - Soil coefficient of pore water dissipation ($L^2.T^{-1}$) ($m^2\ s^{-1}$)

D - Bed material grain size (L) (mm or μm)

D_n - Sediment particle nominal diameter (L) (mm or μm)

d_p - Fine sediment particle/grain size (L) (μm)

d'_{p*} - Modified dimensionless sand particle diameter (L) (mm or μm)

E - Sediment bed erosion rate ($M.L^{-2}.T^{-1}$) ($kg\ m^{-2}s^{-1}$)

E_a - Conduction process activation energy (kJ/mol).

E^P - *Activation energy* for products rate of reaction (kJ/mol)

E^R - *Activation energy* for Reactants rate of reaction (kJ/mol)

E_{sa} - Sand particle erosion rate ($M.L^{-2}.\ T^{-1}$) ($kg\ m^{-2}s^{-1}$)

e_v - Void ratio of consolidating clay layer

F - Archie (1942) formation factor

F_C - Particle cohesive-adhesive force ($M.L.T^{-2}$) ($kg\ m\ s^{-2}$)

F_g - Particle buoyant weight ($M.L.T^{-2}$) ($kg\ m\ s^{-2}$)

F_L - Sediment grain vertical lifting force ($M.L.T^{-2}$) ($kg\ m\ s^{-2}$)

g - Gravitational acceleration ($L.T^{-2}$) ($m\ s^{-2}$)

h_p - Planck's constant (J s)

k_B - Boltzmann constant (ca 1.3807 x 10^{-23}) ($J.\ K^{-1}$)

K_k - Permeability parameter ($L.T^{-1}$) ($m\ s^{-1}$)

K_w - 'Retardation factor' applicable to Stokes' settling ($M.L^{-3}$) ($g\ l^{-1}$)

LL	- Kaolin Clay Liquid limit (%)
M	- Empirical erosion parameter ($M.L^{-2}.T^{-1}$) (kg $m^{-2}s^{-1}$)
M_E	- Erosion parameter (related to soil mechanical parameters) ($M.L^{-2}.T^{-1}$) (kg $m^{-2}s^{-1}$)
m	- Rock cementation factor related to the tortuosity and pore network
n (or φ)	- Porosity (%)
n_f	- Floc fractal dimension
PI	- Plasticity index (%)
PL	- Kaolin Clay Plastic Limit (%)
Q_v	- Cation concentration per unit pore volume (meg ml^{-1})
R	- Gas constant (8.314 kJ/mol/K)
R_{e*}	- Particle roughness Reynolds number relating to shear velocity ($\overline{u_*}$)
Re_s	- Particle Reynolds number ($w_s \frac{D}{v}$)
SG (or G_s)	- Specific gravity
T	- Absolute temperature (K)
$\overline{u_*}$	- Shear velocity ($L.T^{-1}$) (m s^{-1})
$\bar{u}$	- Mean flow velocity ($L.T^{-1}$) (m s^{-1})
u_{*c}	- Friction velocity critical value ($L.T^{-1}$) (m s^{-1})
v	- Kinematic viscosity ($L^2.T^{-1}$) (m^2 s^{-1})
v_s'	- Effective sand-fluid mixture viscosity ($L^2.T^{-1}$) (m^2 s^{-1})
w_c	- Water content (%)
w_s	- Settling velocity ($L.T^{-1}$) (m s^{-1})
w_{sc}	- Primary consolidation stage settling rate ($L.T^{-1}$) (m s^{-1})
$w_{sf,0}$	- Stoke's settling velocity of floc ($L.T^{-1}$) (m s^{-1})
w_{sh}	- Hindered settling regime settling rate ($L.T^{-1}$) (m s^{-1})
w_{sm}	- Hindered settling velocity for pure mud suspensions ($L.T^{-1}$) (m s^{-1})
$w_{ss,0}$	- Stoke's settling velocity of sand ($L.T^{-1}$) (m s^{-1})

w_{ss} - Hindered settling velocity of the sand through the mud suspension ($L.T^{-1}$) ($m\ s^{-1}$)

w_{su} - Uniform settling regime settling rate ($L.T^{-1}$) ($m\ s^{-1}$)

w_{s-mean} - Mean settling rate for uniform and hindered settling regimes ($L.T^{-1}$) ($m\ s^{-1}$)

Symbols

θ_{ec} - Shields' entrainment parameter

σ - Total pressure (or stress) ($M.L^{-1}.T^{-2}$) (Pa)

σ' - Effective stress ($M.L^{-1}.T^{-2}$) (Pa)

$\emptyset_s$ - Particle volume concentration of sand ($M.L^{-3}$) ($g\ l^{-1}$)

$\emptyset_p$ - Particle volume concentration of mud ($M.L^{-3}$) ($g\ l^{-1}$)

$\emptyset_v$ - Solids volume fraction (= C/ρ_s)

$\emptyset_{vf}$ - Flocs volume fraction

ϕ_s - Solids volume concentration ($M.L^{-3}$) ($g\ l^{-1}$)

φ_a - Angle of repose

γ_{bulk} - Sediment deposits bulk density ($M.L^{-3}$) ($kg\ m^{-3}$)

γ_p - Interstitial fluid bulk density ($M.L^{-3}$) ($kg\ m^{-3}$)

γ_s - Density of the sediment particles ($M.L^{-3}$) ($kg\ m^{-3}$)

μ - Molecular viscosity ($M.L^{-1}.T^{-1}$) ($kg\ m^{-1}\ s^{-1}$)

π - *pi* (= 3.142)

ρ - Fluid densities ($M.L^{-3}$) ($kg\ m^{-3}$)

ρ_{bulk} - Bulk resistivity of the saturated rock ($\Omega \cdot m$)

ρ_p - Resistivity of the saturating liquid ($\Omega \cdot m$)

ρ_s - Particle density ($M.L^{-3}$) ($kg\ m^{-3}$)

σ_{bulk} - Bulk conductivity of the saturated rock ($S\ m^{-1}$)

σ_m - Conductivity of sediment-water mixture ($S\ m^{-1}$)

σ_p (or σ_w) - Conductivity of the saturating pore liquid ($S\ m^{-1}$)

ζ_m - Gibson height (L) (m)

τ_b - Bed shear stress ($M.L^{-1}.T^{-2}$) (Pa)

τ_c - Critical shear stress of the particle ($M.L^{-1}.T^{-2}$) (Pa)

τ_{cs} - Critical bed shear stress ($M.L^{-1}.T^{-2}$) (Pa)

τ_e - Erosion threshold ($M.L^{-1}.T^{-2}$) (Pa)

τ_{es} - Sand particles critical stress for erosion ($M.L^{-1}.T^{-2}$) (Pa)

τ_{sc} - Bed characteristic shear strength ($M.L^{-1}.T^{-2}$) (Pa)

τ_{so} - Bed surface shear strength ($M.L^{-1}.T^{-2}$) (Pa)

Ú - Pore-water pressure ($M.L^{-1}.T^{-2}$) (Pa)

$Ú_h$ - Total hydrostatic pressure on the sediment suspension ($M.L^{-1}.T^{-2}$) (Pa)

Publications

1) Cuthbertson, A.J.S., Ibikunle, O.S., McCarter, W.J. and Starrs, G. (2016). Monitoring and Characterisation of Sand-Mud Sedimentation Processes. Ocean Dynamics, 66 (6): 867-891. (Appendix P-1)

2) Cuthbertson, A.J.S., Samsami, F. and Ibikunle, O.S. (2015). Model studies of the flocculation of sand-mud mixtures. E-proceedings of the 36th IAHR World Congress 28 June – 3 July, 2015, The Hague, the Netherlands.

3) Ibikunle, S. O., Cuthbertson, A. J. S., and McCarter, W.J. (2015). Measurement of density and porosity profiles within mixed sediment deposits using an electrical resistivity technique. Proceedings of Intercoh 2015. Gainesville, Leuven Belgium, 7-11 September, 2015.

4) Ibikunle, S. O., Cuthbertson, A. J. S. and Haynes, H. (2013). Exploring electrical impedance techniques to study sedimentation and bed deposits of sand-mud mixtures. Proceedings of Intercoh 2013. Gainesville, Florida USA, 21-24 October, 2013.

CHAPTER ONE

Introduction

"The secret of change is to focus all your energy, not on fighting the old, but on building the new"
—Socrates

1.1 General Background

Processes such as flocculation, sedimentation and consolidation involving cohesive, non-cohesive or mixed sediments are very common in the world's shorelines and, to a large extent, play vital roles in events such as coastal erosion and flooding, environmental pollution and destruction of sensitive habitats and ecosystems. As recorded by Small and Nicholls (2003), 23% of the world's population live in Global Coastal zones and 19% of the total Earth's land surface is a 100km wide coastal zone. Therefore, physical understanding of the processes associated with estuaries and nearshore coastal zones is very important, due to the high environmental, economic and social value of such ecosystems. This explains why various policy makers around the world have put in place policies and regulations aimed at managing them in sustainable and integrated ways, by making sure that a safe balance exists between economic deliverables from coastal engineering projects (e.g. ports, dam, channelling, etc.), and, for example, socio-economic impacts from coastal erosion and flooding risk (e.g. EC, 2004; HM Government, 2011 and USGCRP, 2009). This reinforces the general acknowledgement that shorelines are amongst the most productive, dynamic and complex environments in the world, not least, due to the common occurrence of mixed sediment beds containing both cohesive (i.e. mud and silt, D<65μm) and non-cohesive (i.e. sand, D>65μm) fractions. The structure and composition of these sediment beds, however, are largely influenced by the combined action of flocculation, settling, deposition and consolidation processes, as well as their subsequent entrainment and erodibility (Manning *et al*., 2010; Grabowski *et al*., 2011).

It is, therefore, essential to have fundamental understanding of physical processes controlling the dynamic behaviour of mixed sediments within estuarine and coastal systems; specifically, the temporal and spatial changes to mixed sediment beds due to mobilisation and deposition from combined current and wave actions. This is required to provide accurate and more generic models of sediment transport dynamics, which will account for variability in sedimentary environments, for the assessment and prediction of the impacts of sediments (cohesive, non-cohesive or mixture of both) and their derivatives (e.g. sediment-bound contaminants) on aquatic ecosystem, and marine structures and human health. This is of major importance for the maintenance and management of navigation channels, ports and harbours, as well as in assessing the effects of increased turbidity on water quality and aquatic habitats within these environments (Torfs *et al*., 1996; Cuthbertson *et al*., 2008, Grabowski *et al*., 2011).

There are a number of other industrial applications whose success depends on an adequate understanding of physical processes involving sediment-fluid interactions within sediment suspensions and the properties of the resulting sediment deposits. In the water and sewage treatment industries for example, turbulence is introduced into raw water or sewage to enhance particle aggregation, thereby facilitating speedy settling and deposition of the larger aggregates into bed deposits called '*sludge cake'*, which is easily removed and disposed. It should be noted, however, that other factors such as biological properties of the sediment in this type of process influence the particle aggregation and by extension the properties of the resulting bed deposits.

1.2 Ancient and Recent Sediment Dynamics Problems

It is interesting to discover that the ancient Book of Isaiah in the Bible, written in Palestine about 792-722 BC, recorded how *tossing sea with its waves cast up mire and mud* (Isaiah 57:20 NIV). Records of historical developments in civil engineering technology, also show that, for more than 8000 years, humanity has been facing problems associated with sediment dynamics in the marine environments and that various methods have been devised to solve them (Mehta, 2014). Furthermore, there have been many historical incidents reported as consequences of uncontrollable settling and deposition of sediments in the marine environments, one such example is that of the ancient *port of Ostia*, near Rome. In the first two centuries, *Ostia* was arguably the most important city in the Roman Empire serving as their naval base and because its all-important port was renowned for

supporting various commercial activities. Later it became impossible for heavy vessels to navigate through the port because the Tiber River was uncontrollably filled with too much sediment and that resulted in the ruin of the port (BBC, 2014; Steves, 2015). More recently, as of the end of 2012, the total actual dredging cost as a result of U.S. Army Corps and industrial activities in the U.S. was $12.201 billion and 237.9million cubic yards of sediment dredged[1] generally during activities associated with dams, canals and flood protection and ecosystem restoration. In Somerset (UK), there were two major flooding incidents between 2013 and 2014, before the recent flooding incidents that occurred in most major cities and towns across UK between late 2015 and early 2016. Failure to maintain regular dredging of the rivers Parrett and Tone by the Environment Agency (EA) has been widely blamed to have played a vital role in the flooding incidents which caused devastating damage to lives, homes, land and wildlife in that area and also in many parts of England and Wales[2]. An investigation on River Wharfe (in Yorkshire, UK) has established that even in channels with stabilised banks, sedimentation can significantly increase flood risk (Raven, *et al*. 2010). In the report on '*Foresight Future Flooding 2004 qualitative risk analysis'* commissioned by Sir Michael Pitt; Evans, *et al*. (2008) stated that: "approximately a year and a half of aggradation produced an increase in the flooded area equivalent to nearly half a century of the impact of climate change on catchment runoff." Various other researchers and even flood victims have established significance of sediment-related flood risks and their corresponding damage.

Although, dredging is often not regarded as the best long term or economic solution when compared with other available flood risk measures, it is however, obvious that it is an integral part of Environment Agency and U.S. Army Corps maintenance regimes. It has been reported that the effects of flooding, and managing flood risk, including dredging activities cost the UK around £2.2bn each year[3]. In addition, the cost of managing and disposing dredged materials is on the increase every year especially with significant changes in EU-UK waste management legislations with significant impact on the dredging industry and navigation authorities' operations (AINA, 2013).

1.3 Basis for Current Study

Clear evidence exists that in most estuaries and near-shore regions, cohesive (i.e. mud: clay and silt, D<65μm) and non-cohesive (i.e. sand, D>65μm) sediments co-exist in different fractions under different tidal and/or wave actions resulting in either segregated

bed layers or mixtures (Williamson, 1991; Torfs, 1994; Torfs *et al*., 1996). The implication of such coexistence is that it makes accurate prediction of sediment transport and morphological changes in these environments very challenging, not least as both types of sediments (i.e. cohesive and non-cohesive) can be mobilised easily under tidal and/or wave actions. For example, in a situation where sand and mud fractions behave independently, i.e. having minimal interaction during settling and deposition processes, a well-sorted and layered or segregated bed is the result (Torfs, 1994; Amy *et al*., 2006). It is worth noting that, these changes and differences in sediment distribution within sediment beds have economic consequences and results in visible changes in nearshore coastal-zone morphology, siltation and erosion of navigation channels, dredging impact, etc. (POL, 2009). Apart from sediment composition, research has shown correlation between structure and erosional strength of sediment bed deposits and other factors such as water chemistry (e.g. salinity, pH), initial sediment concentration (i.e. bulk density), organic components (e.g. EPS), etc. (Torfs *et al*., 1996; Been & Sills, 1996; Spears *et al*., 2008; Grabowski *et al*., 2011).

A variety of process (or physically)-based modelling approaches (e.g. Waeles *et al*., 2008; Le Hir, 2011; Van and Pham Van Bang, 2013, Grasso *et al*., 2015, etc.) have been formulated to simulate mixed sediment settling and deposition processes and structural development in mixed sediment beds. One such approach is the *Kynch theory*, which assumes that settling rate of particles in a suspension is determined by the local particle density only (Kynch, 1952). Based on the proposed relationship between these two physical parameters, sedimentation rate has been related to sediment concentration and composition (e.g. Le Hir *et al*., 2001). Some of the models (e.g. Winterwerp and Van Kesteren, 2004; Le Hir, 2011; Grasso *et al*., 2015) were based on *Gibson's theory* from soil mechanics, which assumes that an increase in density is a result of the vertical exchange of pore water brought about by changes in pressure gradient within the structure (Gibson, *et al*., 1967). However, general applicability of these models is limited, especially when handling a wide range of initial sediment concentrations and sand contents (e.g. with sand content $\geq$ 15%) [Torfs *et al*., 1996; Grasso *et al*., 2015, etc.]. These models also largely require extensive experimental data for their validation; this is particularly a problem, as sufficient data constraining the main variability are required to test the performance of any of such models (POL, 2009). In addition, the capacity of these models to accurately simulate occurrence of segregation in mixed sediment

conditions is a challenge, not least because the presence of sand strongly modifies hindered settling of its cohesive counterpart (Grasso *et al*., 2015).

Therefore, with the crucial goal of improving the applicability and accuracy of sediment transport models, sediment modellers attempt to comprehensively validate these process-based models and/or initialise them. It is necessary for coastal modelling systems to, for instance, fully account for the influence of mixed sediment dynamics (i.e. in terms of wide range of initial sediment conditions) on structural formation and *segregational* behaviour and, by extension, on the dynamics of sand-mud erosion and deposition processes in sedimentary environments. These developments indisputably require more process-driven studies on sand-mud interactions within mixed sediment environments, both at small and large scale. This is with the view of providing robust laboratory experimental data necessary to validate and improve some of these mixed sediment transport models, thereby, making them more applicable to a wider range of variability in mixed sediment environments; consequently, addressing some of the current knowledge gaps and uncertainties associated with mixed sediment dynamics.

Clearly, there is a need for a fundamental understanding of the physical processes controlling the dynamic behaviour of sediments (especially mixed sediments) in estuarine and coastal systems. An adequate understanding of these processes together with the hydraulics of these sedimentary environments will aid provision of accurate and more generic models, for example, necessary for the prediction and estimation of the cost of managing and maintenance of dredging volumes.

1.4 Electrical Resistivity Measurement Technique (ERMT)

One of the major challenges for improved understanding of the physical processes of sediment dynamics in estuaries and coastal zones, is the availability of simple, non-destructive measurement techniques to characterise the spatial and temporal variation in sediment bed structure and composition [Been, 1981; Ha, *et al*., 2010]. From traditional experimental studies on sedimentation process, volume concentration, bulk density profiles and porosities of the resulting sediment deposits have been obtained (for example) by *high energy X-rays or attenuated gamma rays, acoustic & wave attenuation* and *turning fork*. Although these are non-intrusive methods, they have drawbacks and limitations, such as being relatively inflexible, expensive and have clear health and safety

implications. Therefore, there is a need for alternative methodologies that are simple, reliable and less complicated in terms of usability and safety. Previous studies have shown that, although knowledge of the electrical properties of marine sediments is scant, the increasing use of electrical resistivity techniques to study soils has shown significant promise as a viable investigative tool, (Blewett *et al*., 2001; Lovell, M. A., 1985; Dai *et al*., 2009; Samouelian *et al*., 2005, te Slaa, *et al*., 2013; Ibikunle *et al*., 2013). Therefore, in the current work, a simple, non-invasive electrical resistivity measurement technique (ERMT) to characterise the spatial and temporal variation in sediment bed structure and composition resulting from differential settling behaviour of the sediment mixtures has been developed.

1.5 Research Aims and Objectives

Physical processes associated with mixed sediments on a small scale are generally influenced by occurrence of time-dependent flow conditions (i.e. tidal, waves), mixed sediment composition (e.g. sediment types, proportions and initial concentrations), water chemistry (e.g. salinity, pH, temperature) and concentration gradients generated by unsteady flow conditions. This study thus aims to advance the current understanding of the underlying characteristics of physical processes governing dynamics of mixed sediments in the marine environments and to further establish, some of the important connections between fluid-sediment interactions and structural characteristics of the resulting mixed sediment bed deposits.

The specific aims of this study are therefore to;

1) systematically investigate and quantify these fundamental dynamic processes (such as settling, bed structural formation and onset of consolidation) for mixed sediments containing cohesive clay and non-cohesive sand within a settling column and over a wide range of unsteady turbulent flow conditions; and,
2) investigate the development and properties of mixed sedimentary bed structures over a range of sediment mixture compositions, ambient fluid salinity and initial mixture concentration.

Also, the specific objectives of the study are to:

1) explore the potential of employing non-invasive electrical resistivity measurement technique (ERMT) to characterise the spatial and temporal

variation in sediment bed structure and composition resulting from differential settling behaviour of the sediment mixtures.

2) extend existing knowledge on the spatial and temporal variation of sediment bed structure and composition resulting from differential settling of mixed sediments over a wide range of parametric conditions.
3) provide a significant dataset on sand-clay sedimentation processes, over a wide range of initial mixture concentrations and compositions required to (i) investigate further the parametric dependence of mixed and segregated bed deposit formation and (ii) test the polydisperse hindered settling formulation proposed by Cuthbertson, *et al*. (2008) in terms of its predictive capabilities for the generation of these mixed and segregated bed deposits.
4) relate new experimental data on time-dependent sand-mud erosion and deposition processes, measured over a range of unsteady flow events, to the nature and extent of bed restructuring, segregation, stabilisation and bedforms generation in mixed sedimentary environments.
5) suggest appropriate criteria from (1) - (3) to describe likely parametric conditions under which well-mixed or segregated bed layers will form in mixed sediment environments.

Meeting the highlighted aims and objectives, will undoubtedly extend the much-needed understanding of fundamental dynamics of mixed sediment processes in estuaries and coastal regions as required by practitioners involved in management, planning and the implementation of legislations in these dynamic and complex ecosystems. Three experimental series (ES) have been developed, to meet the study's aims and objectives, namely: (i) ES-1: Development of the electrical resistivity measurement technique (ERMT), (ii) ES-2: Systematic mixed sediment suspension experiments, and (iii) ES-3: Mixed sediment bed erosion experiments.

1.6 Contents of the Thesis

This introductory chapter is followed by literature review (Chapter-2) on topics relevant to the current study. Chapter-3 describes, in detail, the experimental facilities, equipment/instrumentation and procedures utilised in each experimental series. Chapter-4 describes initial results of continuous density and porosity profiles that have been obtained for sand-clay mixtures using the developed ERMT (i.e. ES-1). Chapters 5 and

6 describe the experimental findings from ES-2 and ES-3 experiments respectively. Chapter 7 presents a general discussion and analysis of these results, and their corresponding wider implications, while Chapter 8 draws together the conclusions from all the main experimental findings and ends with recommendation for future work.

[1] <http://www.navigationdatacenter.us/db/dredging/ddcost/> accessed on 15/12/16
[2] <http://www.telegraph.co.uk/topics/weather/10644101/How-Somerset-Levels-river-flooded-after-it-was-not-dredged-for-decades.html> accessed on 15/12/16
[3]<http://www.theguardian.com/environment/2014/feb/12/uk-floods-the-facts> accessed on 15/12/2016

CHAPTER TWO

Literature Review

"All truths are easy to understand once they are discovered; the point is to discover them"
— Galileo Gililei

2.1 Introduction

'Flocculation, settling and deposition, consolidation, erosion and transport in suspension, are typically interlinked by the cyclic nature of the tide dominated environments' (Mehta *et al*., 1989). Characterizing these interlinked processes in the marine environment is, nevertheless, complex due to the dual dependence of sediment aggregate properties on the physical, geochemical and biological properties of the sediment-water mixture, as well as the intensity of turbulent flow field (Mehta *et al*., 1989; Winterwerp and Van Kesteren, 2004; Grabowski *et al*., 2011; Mehta, 2014). However, characterisation and understanding of these complex processes are needed to be able to provide accurate models of the resulting sediment transport dynamics. This, in turn, allows assessment of the impacts of sediment (i.e. cohesive, non-cohesive or mixtures of both), and their derivatives (e.g. sediment-bound contaminants), on aquatic ecosystems, marine engineering structures and human health (Grabowski *et al*., 2011). Therefore, this chapter, reviews the literature directly relevant to the issues being addressed in the current study.

2.2 Sediments in Marine Environment

In many rivers, lakes, estuaries, coastal waters and intertidal (littoral) zones; sediments constitute major components of the suspended load and sediment bed. They are generally heterogeneous with regard to their composition and also display a considerable degree of spatial and temporal variations due largely to intensive anthropogenic activities, decreasing precipitation and some other natural factors (Zhao *et al*., 2014; Syvitski *et al*., 2005 and Futterer, 2006). For instance, owing to the continuous activity of tidal current and waves, sediments in the intertidal zone have been found to be commonly well sorted

in terms of size and forms of the sediment grains (Eisma, 1998). Marine sedimentary particles are generally classified according to their structures and, the most common element used is sediment grain diameter (Soulsby, 1997; Winterwerp and Van Kesteren, 2004 and Futterer, 2006). The percentage in which the various sedimentary particles are present in a sediment depends markedly on the grain-size distribution. Therefore, based on their diameters, sediment grains are classified as clay, silts, sands, granules, pebbles, cobbles and boulders. The combination of clays and silts is called '*mud*'; whereas granules and pebbles, are collectively called gravel. (Soulsby, 1997). In sedimentology, sediment classification system based on the grain size distribution is commonly carried out with the use of sand-silt-clay triangle (i.e. Ternary diagram, see Figure 2.1). This allows a more quantitative approach to sediment classification (van Ledden *et al*.,2004). The three common size fractions in (fine) sediment dynamics are clay particles (e.g. kaolinite, illite, montmorillonite and chlorite) with particles < *2µm*; silt-sized particles (e.g. quartz and feldspar minerals) ranging from *2µm to 63µm*, and sand sized particles > *63µm*.

Another interesting classification is the one that classifies sediments based on combination of their mechanical and geochemical properties. Based on this, marine sedimentary particles are classed into two groups, namely cohesive and non-cohesive sediment. The clay fraction of mud, for instance, is cohesive while sand and silt are non-cohesive. Individually, the characteristics and behaviour of cohesive and non-cohesive sediments are significantly different, however, when mixed, their behaviour is much more complex. For example, their (i.e. cohesive, non-cohesive and mixture of both) resistance to erosion under hydrodynamic and waves actions, transport and deposition phenomena are significantly different (Cuthbertson *et al*., 2008, 2010; Manning *et al*., 2011; etc.).

Generally, the following bulk sediment characteristics influence the behaviour and dynamics of cohesive, non-cohesive and mixture of both in the marine environment: (i) grain size distribution, (ii) orientation and packing arrangement, (iii) porosity (or void ratio), and (iv) moisture content. In turn, these characteristics, to a large extent, govern the properties such as cohesiveness, deformability, elasticity, permeability, bulk density, internal friction and shear strength (Pye, 1994). It is therefore correct to say that, physical properties of marine sediments depend predominantly on the properties (or characteristics) and arrangement of the solid and fluid constituents. If Figure 2.2 is considered as being the components of marine sediments, then the single particles are the

sediment grains; the voids (i.e. the pores) between these grains of particles are filled with pore fluid (e.g. sea water) assuming the sediments are water-saturated; and finally, the connected particles and the sediment grains in close contact build the overall sediment frame (Breitzke, 2006).

For the purpose of this study, sediments with higher size range than sand are not considered;, sand is taken as the non-cohesive sediment whilst clay (kaolin) the cohesive sediment.

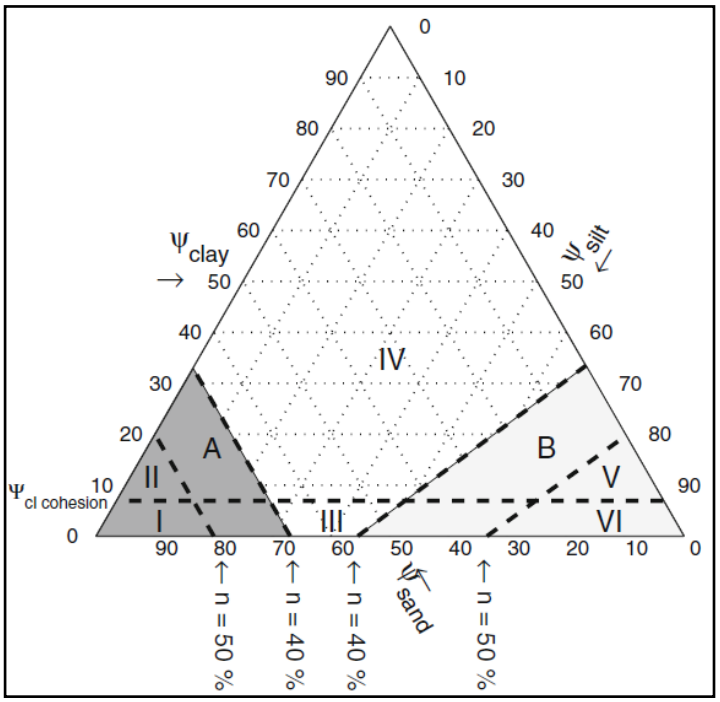

Figure 2.1 Sand-silt-clay ternary diagram based on grain size distribution, showing transition for cohesion & network structure (From: te Slaa *et al.* 2013)

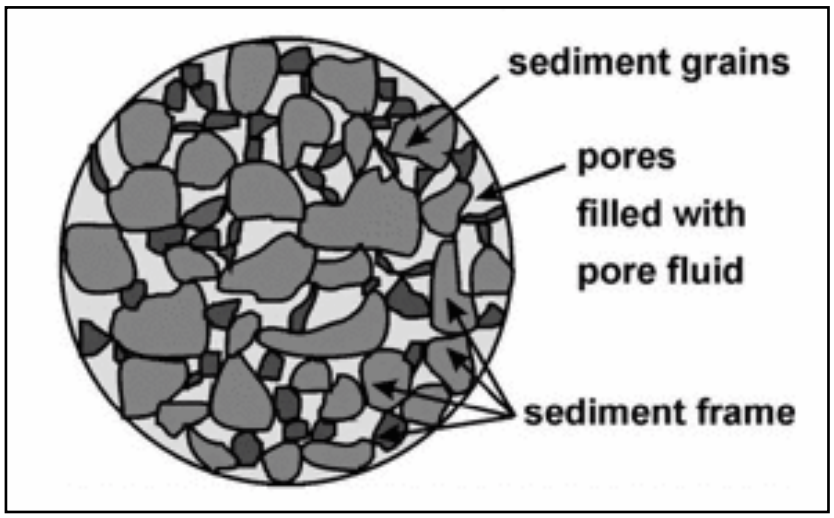

Figure 2.2 Components of marine sediments (From: Breitzke, 2006)

2.2.1 Non-cohesive sediment: General characteristics

The silica tetrahedron is the basic unit from which major sedimentary grains (i.e. non-cohesive fractions) of the marine environment are made. In a silica tetrahedron, four oxygen atoms are arranged at the corners of a tetrahedron with a silicon atom at the centre (Dyer, 1986). Sand and gravel are examples of non-cohesive sediments. Silt-sized particles ranging from *2µm to 63µm* form as a result of physical weathering of primary minerals, are generally classified as non-cohesive from a mineralogical point of view; although, silt constituents -quartz and feldspar- are commonly found, along with clays, in both suspended and bed sediment (te Slaa *et al*., 2013). However, erosion studies (e.g. Jin *et al*. 2002 and Roberts *et al*. 1998) on silt-rich sediment have shown silt particles to exhibit cohesive-like behaviour.

Non-cohesive sediments generally consist of larger, discrete particles than that of their cohesive counterparts. It is typical of non-cohesive particles to majorly react to forces exerted upon them by the inherent hydrodynamic condition and their corresponding movement to these forces is predominantly affected by the physical properties of the particles (e.g. size, shape and density). Unlike in the case of cohesive sediments, the particle's size and its terminal fall velocity of the non-cohesive sediments are the most important parameters commonly use to relate their properties with sediment motion (Dyer, 1986; Van Rijn, 1993; Julien, 1995). This explains why, in most cases, deposition of coarse particles is regarded as characteristic of high energy depositional locations, e.g. fluvial environment (Grabowski *et al*., 2011).

2.2.2 Cohesive sediments: General characteristics and compositions

In sedimentary environments, cohesive and non-cohesive sediments are significantly different from each other, particularly when considering the following two processes; i.e. flocculation and consolidation of deposited material. Almost all cohesive sediment found in marine environment is flocculated due to their physico-chemical characteristics (Winterwerp & Van Kesteren, 2004), which is not the case with non-cohesive sediments. Floc formation affects the settling velocity and bed structure (this will be discussed in detail later in this chapter), hence the sediment dynamics of cohesive particles is different and much more complex than that of sand (Toorman, 2001; Berlamont *et al*. 1993). The term 'cohesive', according to Winterwerp and Van Kesteren (2004), relates to ductile behaviour of the sediment when it is remoulded. In soil and sediment erosion research, Jumars and Nowell (1984) described 'cohesion' as attraction between chemically similar

sedimentary particles or substances, this as recorded by Grabowski *et al*. (2011) refers typically to the attraction of clays and colloids by electro-chemical forces, such as van der Waals forces and electrostatic attraction.

Cohesive sediments found in the marine environment are often with a mixture of clay, silt, sand, organic material, water, and in some cases, gases (e.g. methane); when mixed in water they form what is commonly known as mud. The term mud is often used interchangeably with cohesive sediment, it can therefore be said that there are some non-cohesive fractions in marine cohesive sediments (Soulsby, 1997; Winterwerp and Van Kesteren, 2004; and Grabowski *et al*., 2011). However, the cohesive behaviour of marine sediments is determined by the proportion of clay particles and organic material present, in conjunction with the pore water chemistry, i.e. chemical properties of the liquid phase (Winterwerp and Van Kesteren, 2004; Mehta, 2014).

Generally, cohesive sediment is a heterogeneous, particulate and porous material that is composed of *solid, liquid* and *gas* phases (Grabowski *et al*., 2011; Mehta, 2014). Both the solids and liquid phase largely govern their cohesive behaviour; whereas, inorganic and organic materials are the constituents of the solid phase of the cohesive sediment (Winterwerp and Van Kesteren, 2004). Inorganic minerals include clay minerals (e.g. silica, alumina, illite, montmorillonite and kaolinite) and non-clay minerals (e.g. quartz, mica, carbonates and feldspar). Clay minerals (typically $< 2\mu m$ in diameter when classified with '*Wentworth scale'*) are formed foremost from chemical weathering of primary, rock forming aluminous silicates or minerals such as like feldspar, hornblende and pyroxene or even volcanic glass (Futterer, 2006; and Grabowski *et al*., 2011). Futterer (2006) stated that 'the clay minerals are of special importance, as they not only constitute the largest proportion of fine-grained and non-biogeneous sediment, but they also have the special geo-chemical properties of absorbing and easily releasing ions' and therefore the most electro-chemically active portion of the cohesive sediment (i.e. major contributors to cohesiveness). Clay minerals of cohesive sediments were described as a very effective working "*geochemical factory*" due to their ability to absorb ions internally within the crystal structure, or bind them superficially by means of reversible adsorption, as well as their capacity to temporarily bind larger amounts of water. The non-clay mineral components of cohesive sediment are mainly originated from physical weathering of continental rocks (i.e. the primary minerals) (Futterer, 2006; Grabrowski *et al*. 2011).

All types of clay mineral (e.g. kaoline, illite, montmorillonites and chlorite) can, to varying degrees, undergo ion exchange within them or with those within their ambient solution. This property of clay thus mean that their character can change depending on the concentration of ions in their environment. Their mineralogy is, therefore, difficult to predict and their behaviour (e.g. settling) in the marine environment is largely influenced by the ionic charges on their surfaces. For example, particle flocculation can result, if their ionic charges interact with the ions in the ambient solution (Dyer, 1986; Winterwerp and Van Kesteren, 2004). On the other hand, when deposited on the bed, their electromagnetic properties can cause the charged particles to bind together giving cohesive forces that are much stronger than the gravitational forces on the particles (Dyer, 1986).

Organic materials in the solid phase may exist as living organisms (e.g. bacteria, benthic algae, etc.), detritus (e.g. dead particulate organic material, fecal material, etc.), extracellular polymeric substances (EPS) and organic colloids (Grabrowski *et al*. 2011). Integrated biofilms (e.g., diatoms) are found majorly on sediment surface, while EPS (diatoms' major constituents) are present deeper in the sediment (Figure 2.3). Organic materials are equally electro-chemically active similar to the inorganic material counterparts and therefore contribute considerably to the cohesion and adhesion characteristics of cohesive sediments. Even a small amount of organic matter can have a significant impact on sediment aggregation and sediment erodibility (Winterwerp and van Kesteren, 2004).

The liquid phase of cohesive sediments in the marine environment is predominately saline water, which can occupy a significant proportion of the sediment. Although, as reported by Bale *et al*. (2007), water quantity can often exceed that of the solids, this is particularly the case at the surface of unconsolidated sediment. Gases may be significantly present in estuarine sediment exposed to air, especially at low tides, but generally, relatively lower volumes of gases are seldom found in fine riverine sedimentary environments (Grabrowski *et al*. 2011). The gases (e.g. methane) are primarily formed when the organic component of the sediment is broken down by the actions of inherent organisms (e.g. bacteria, protozoans, fungi, diatoms, polychaetes, etc.) within the sediment (Gebert *et al*., 2006; Sanders *et al*., 2007)

On a final note, the composition or behaviour of cohesive sediment varies both spatially and temporally and it is governed by the availability of the sediment and its components (see Figure 2.3), the meteo-hydrodynamics conditions, biological activity, history, etc. (Winterwerp and Van Kesteren, 2004). For instance, structure and interactions of different subcomponents present in cohesive sediment, to a large extent, determine its erodibility (Grabrowski *et al*. 2011).

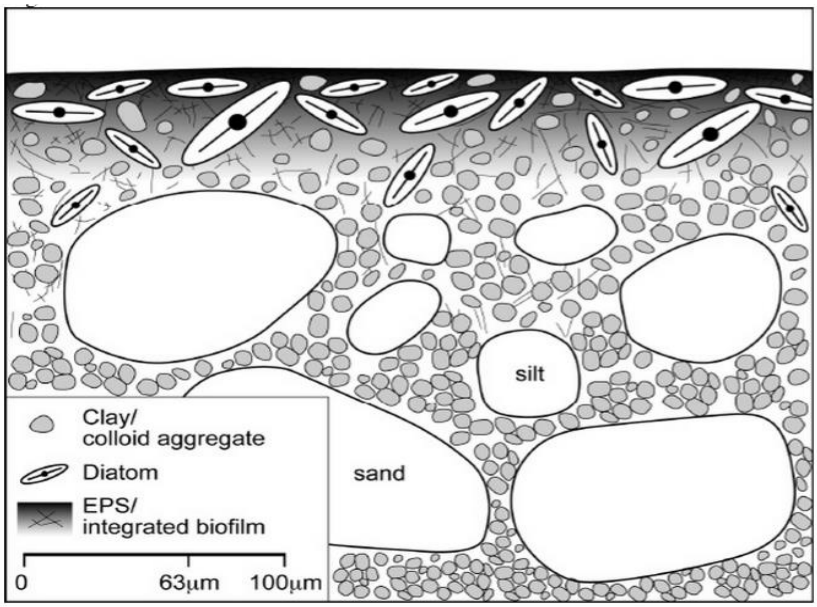

Figure 2.3 Diagrammatic presentation of cohesive microstructure and composition (From: Grabrowski *et al*., 2011)

2.2.3 Mixed-sediment dynamics

The formation of sediment beds under different natural flow conditions is a common occurrence in many sedimentary environments such as estuarine and near-shore coastal marine environments. The structure and composition of these sediment beds are largely influenced by the combined action of settling, deposition and consolidation processes, as well as their subsequent entrainment and erodibility caused by changes in hydrodynamic conditions, i.e. change in energy level. In the context of coastal and estuarine waters, accurate prediction of the transport, interactions and fate of sand-mud mixtures is strongly associated with these sedimentation processes because, for instance, sediment beds in estuaries and tidal basins often consist of both sand (non-cohesive) and mud (cohesive).

Until recently, literature contains an overwhelming amount of work on the development and behaviour of bed deposits for monodisperse sediments in the marine environment (e.g. Winterwerp & Kesteren, 2004). More recently however, there have been

considerable amount of laboratory tests that have revealed primarily, that, the rate or nature of settling, flocculation and consolidation processes characterise bed formation for polydisperse sediment (e.g. sand-mud mixtures) [Williamson, 1991; Torfs *et al*., 1996; Cuthbertson *et al*., 2008, 2010; Manning *et al*., 2011, Mehta, 2014]. For example, Cuthbertson *et al*. (2010) and Manning *et al*. (2011) revealed that processes controlling flocculation and settling rates (which, by extension, influence bed formation processes) can alter dramatically when cohesive and non-cohesive sediments are mixed. It is therefore clear from the literature (e.g. Torfs, 1994; Uncles *et al*., 1998; Whitehouse *et al*., 2000; van Ledden, 2003; and Amy *et al*., 2006; Le Hir, 2011), that sand and mud within these mixed sediment environments can be thoroughly mixed, may exhibit a horizontal gradient (e.g. resulting from gradients in the current or wave patterns), or can be layered in the bed, and witness the history of forcing events. In a situation where the sand and mud fractions have minimal interaction during the settling and deposition processes, then segregation of each fraction within the resulting bed deposits dominates, resulting in a well-sorted, layered bed structure (Torfs, 1994; Amy *et al*.,2006; and Manning *et al*., 2011).

Torfs *et al*. (1996) extensively described the results of various settling and consolidation experiments involving sand-mud mixtures based on many laboratory and field tests carried out by the Hydraulics Laboratory of the Katholieke University Leuven (KUL) and by HR Wallingford Ltd, with the aim to (i) investigate the nature of deposition of mixed sediments, (ii) follow the development of the density structure in time, (iii) study properties of the bed, and, (iv) look at different features of deposition and consolidation behaviour that occur in mixed sediments. However, effects of some parametric conditions such as ambient salinity (which has been identified to significantly alter the dynamics of sedimentation processes (Owen; 1970; Dyer, 1986; Winterwerp and van Kesteren, 2004; Mehta, 2014; etc.) were not fully considered and this is one of the areas the current study addresses. One of the observations of Torfs *et al*. (1996) was occurrence of segregation in mud-sand mixtures, they found that in some sand-mud mixtures heavier sand particles settled faster to the bottom of the column to form a sand rich base layer, and noticed this continued as long as the mud concentration is not high enough to form a continuous network structure to prevent this segregation. Figure 2.4 shows the size grading of the bottom and top layer (1 *mm*) of two of the experiments with Hong Kong mud and King's Lynn Sand (C_0 = 1 -3 $g\ l^{-1}$, $D_{50\ sand}$ = 230 μm) before and after the input of sand.

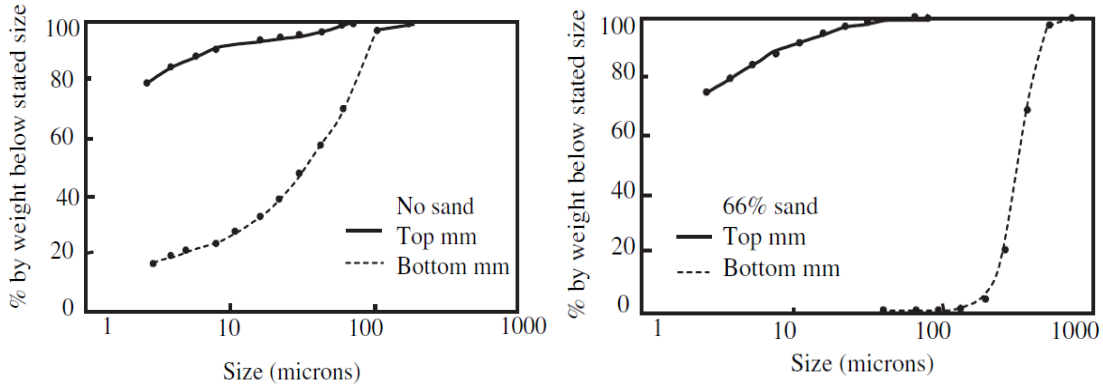

Figure 2.4 Size grading of the top and bottom millimetre of the bed before and after a single input of sand. Left: no sand; Right: 66% added sand (From: Torfs *et al.*, 1996)

It is obvious from the size grading in Figure 2.4 that clear segregation occurs between the top and the bottom of the bed for both tests, although strong segregation is seen in the test with added 66% sand, consisting entirely sand base layer. The segregation observed in the sand free experiments was attributed to strong, compact flocs that rapidly sank to the bottom of the bed. Torfs *et al*. (1996) therefore concluded that the occurrence of segregation may depend on factors, such as the type of mud (i.e. in terms of mineralogical and chemical composition, organic content and biological processes) and the initial input density, as segregation occurs for initial mud concentrations below the gelling point. They added that the degree of segregation is limited to a maximum sand content, which is a function of the mud type as well.

The mineral composition in combination with particle size distributions are important discriminators when consideration is being given to the mechanical behaviour of mixed sediments (especially in terms of textures and structure). For instance, the presence of clay minerals is a vital criterion for sediment mixtures to show cohesive behaviour, in other words, the cohesiveness or non-cohesiveness of mixed sediment matrix is largely dependent on the clay content within the matrix (van Ledden *et al*., 2014; te Slaa *et al*., 2013). A transition between non-cohesiveness to cohesiveness has been reported in mixed sediment bed at clay contents of 5-10% (van Ledden *et al*., 2014). From the sediment classification approach presented in the sand-silt-clay triangle (Figure 2.1), it is clear that network structures can be formed by solid fractions of sand, silt and clay which has been reported to be largely dependent on the overall porosity (te Slaa *et al*., 2013). For example, from the ternary diagram (Figure 2.1), the following network structures can be seen: (i) non-cohesive sand dominated; (ii) cohesive sand dominated; (iii) non-cohesive mixed; (iv) cohesive clay dominated; (v) cohesive silt dominated; and (vi) non-cohesive

silt dominated. Transition to sand or sand–silt-dominated network structures for overall porosities of n = 40 % and n = 50 % are represented by the bold broken lines; while the horizontal bold broken line represents a clay content (i.e. 8 %) at which the transition between cohesive and non-cohesive behaviour can be initiated. Areas of sand- and silt-dominated network structures are respectively indicated by the shaded areas A and B (te Slaa *et al*., 2013 and Van Ledden *et al*., 2004)

2.3 Settling and Deposition

2.3.1 General overview

The processes involving settling and deposition of particles that are heavier than the fluid in which they are suspended (i.e. negatively-buoyant particles) are very common in many natural and industrial systems such as rivers, estuaries, water and waste-water treatment systems, etc. The importance of these processes has resulted in extensive studies being carried out, especially in the context of coastal and estuarine waters, where accurate prediction of the transport, interactions and fate of cohesive and non-cohesive sediment is essential.

Settling involves the rate of falling of particles in carrier fluid, while deposition occurs when the forces responsible for keeping the particles in suspension are no longer sufficient to overcome the forces of the particles' weight and friction (i.e. inter-particle force of attraction). Mehta (2014) described deposition as removal of particles from flow as they settle to form part of the bed-bottom material. This implies that when flow is absent, settling and deposition will mean the same thing. In other words, deposition describes a phenomenon where suspended or eroded sediment being transported within a fluid is deposited at the loss of enough kinetic energy in the fluid, thereby, resulting in the building up of layers of sediment. In intertidal zones (or shorelines) for instance, this phenomenon explains why sediment of a particular size moves across the shoreline profile to a position where it is in equilibrium with the wave and flows acting on that sediment grain. In such scenario or process, the finer sediments are transported away from the region of high energy and subsequently settle out of suspension, or deposit in region of low energy (see Figure 2.5). This results in the coarse sediments being deposited at the upper part of the shoreline profile and sorted by the wave-generated hydraulic regime (see Figure 2.5) [Horn, 1992]

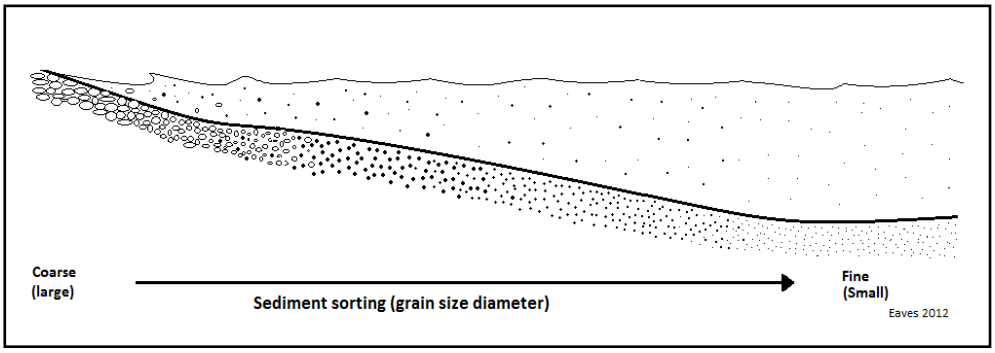

Figure 2.5 Illustration of the sediment size distribution over a shoreline profile (Horn, 1992)

Various modes of settling of fine sediments have been recorded; they are (i) '*free settling'* (Type I settling), which is common to all particles; (ii) '*flocculation settling'* (Type II settling), which is unique to cohesive sediments; and (iii) '*hindered settling'* (Type III settling), which occurs predominantly at higher concentration of sediment particles; this could be the case in monodisperse non-cohesive or flocculated suspensions and in polydisperse suspension containing cohesive and non-cohesive particles (Winterwerp and van Kesteren, 2004; Cuthbertson *et al*., 2008). Detailed descriptions of the above highlighted modes of settling are given in the following sections. Within each mode of settling described above however, the settling rate (or velocity) is generally influenced by a number of factors namely: particle physical properties (e.g. size, shape, structure); ambient fluid physico-chemical properties (e.g. salinity, temperature, viscosity); initial mixture concentration; the turbulence levels/ types within the fluid (e.g. shear rate, oscillating flow) and presence of organic matter (Scott, 1984; Cheng, 1997; Winterwerp, 2002; Dankers, 2006; Cuthbertson *et al*., 2008; Le Hir *et al*., 2011; and Mehta, 2014).

2.3.2 Monodisperse particles settling in quiescent fluid

Basically, when considering the interaction between sediment particles and carrier fluid, settling velocity describes the influence of gravitational force on the motion of discrete particles. Generally, the physical properties governing the fall velocity of a single sediment particle in motionless carrier fluid are its sizes, shape and density. For monodisperse particles settling at infinite dilution, individual spherical particle will settle within the still, homogeneous fluid conditions at a *terminal* fall velocity w_s when the drag forces on the spherical particle equal the immersed weight. Stokes (1851) derived an expression to describe the drag force, which can be written in terms of drag coefficient (C_D), i.e.

$$F_D = C_D \pi \frac{D^2}{4} \rho \frac{{w_s}^2}{2} \quad (2\text{-}1)$$

The 'immerse weight' I, can be expressed as:

$$I = \frac{4}{3} \pi \frac{D^3}{8} (\rho_s - \rho)\, g \quad (2\text{-}2)$$

where D is the particle diameter, ρ_s and ρ are the particle and fluid densities respectively, w_s is the settling velocity and g is the gravitational acceleration.

The nature of the flow around the falling spherical particle is determined by whether it falls gradually, when viscosity will be important, or rapidly, when the particle inertia will dominate. To account for these effects, a Reynolds number can be formed from the fall velocity and the particle diameter:

$$Re_s = w_s \frac{D}{v} \quad (2\text{-}3)$$

where $v = (\mu/\rho)$ is the kinematic viscosity

When $Re_s << 1$, laminar settling conditions exist, the particle then creeps through the carrier fluid, distorting the flow in the process for relatively large distances from the particle with no wake occurring. At $Re_s << 1$, the drag force becomes:

$$F_D = 3\pi\mu D w_s \quad (2\text{-}4)$$

where μ is the molecular viscosity. From equating Equations (2-2) and (2-4), the following expression can be derived:

$$w_s = \frac{D^2}{18} ((\rho_s - \rho)/\mu) g = cD^2 \quad (2\text{-}5)$$

Equation (2-5) is known as the Stokes' law and it demonstrates that $w_s \propto D^2$ in the viscous regime. The value of 'c' in the expression varies from 8975 $(m\ s)^{-1}$ at 20^0C and 6880 $(m\ s)^{-1}$ at 10^0C, to 5920 at 5^0C for quartz particles. These values are further reduced by about ca 5% for salinity of 35*ppt* (Dyer, 1986). The coefficient, 'c' depends on particle characteristics such as, density, composition, etc.

The relationship between drag coefficient and Reynolds number is obtained from Equation (2-1) and (2-4) as:

$$C_D = \frac{24}{Re_s} \tag{2-6}$$

2.3.2.1 Effect of higher Reynolds number

It should be noted that C_D is not only dependent on Re_s (i.e. flow conditions) but also on the effect of ambient fluid temperature. Therefore, the linear relationship between C_D and Re_s is only valid for low Reynolds number (i.e. $Re_s \leq 1$); consequently, the fall velocity cannot be theoretically predicted from Equation (2-5) because the condition for creeping motion (i.e. Stoke's flow) is greatly exceeded once the effect of drag associated with inertia becomes significant (Dyer, 1986; Julien, 1995; Mehta, 2014).

At $Re_s > 1$, the particle ceases to act independently. In this case, the flow separates in the lee of the particle, and vortices are shed, this occur periodically at the initial stage and then randomly thereafter, resulting in the boundary layer around the particle becoming turbulent (Dyer, 1986). Figure 2.6 shows how this relationship significantly deviates from experimental data obtained by Engelund and Hansen (1967) for natural sand and gravel particles. Therefore, for higher values of Re_s, various attempts have been made by many researchers (e.g. Oseen, 1927; Goldstein, 1929; Rubey, 1933; Dallavalle, 1948; Julien, 1995; Soulsby, 1997; and Cheng, 1997) to extend the applicability of the Equation (2-6) to a wider range of flow conditions by introducing empirical corrections for the C_D. Equation (2-7) is the general form of such expressions especially for $Re_s > 10^5$, as presented by Mehta (2014), and Table (2-1) presents the experimental values of coefficients A_D, B_D and exponent m.

$$C_D = \left[\left(\frac{A_D}{Re_s}\right)^{1/m} + {B_D}^{1/m}\right]^m \tag{2-7}$$

Table 2-1 Experimental values of Equation *G* coefficients

Investigator	**A_D**	**B_D**	***m***
Dallavalle, 1948*	24.0	0.40	2.0
Julien, 1995	24.0	1.50	1.0
Soulsby, 1997	26.4	1.27	1.0
Cheng, 1997	32.0	1.00	1.5

*For spherical particles (Adapted from Mehta, 2014)

From consideration of the above studies, Cheng (1997) proposed an explicit formula for the settling velocity of individual natural sediment particles over a range of Stokes' flow conditions (i.e. $1.0 \geq Re_s \leq \sim 10^4$);

$$w_s = \frac{v}{d_p}\left(\sqrt{25 + 1.2d_{p*}^2} - 5\right)^{1.5} \tag{2.8}$$

where,

$$d_{p*} \text{ (the dimensionless particle parameter)} = \left(\frac{g'}{v^2}\right)^{\frac{1}{3}} d_p \tag{2.9}$$

and,

$$g' \text{ (the reduced gravity)} = g(\rho_s - \rho)/\rho \tag{2.10}$$

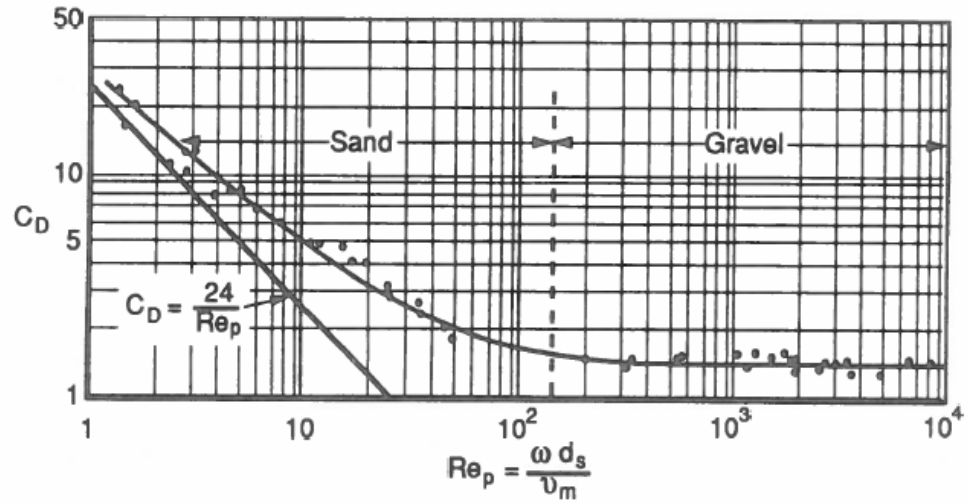

Figure 2.6 Drag coefficient for natural sand and gravel particles (From Julien, 1995)

Particle shape is another parameter, whose influence on fall velocity depends on Re_s. This influence is negligible within the Stokes' law range (i.e. $Re_s \leq 1$), as the drag coefficient is essentially independent of particle shape; but the influence becomes significant at higher Re_s (i.e. in the viscous regime). This is because the particle will tend to settle with its maximum cross-sectional area normal to the direction of motion; clay minerals are likely to settle in this manner (Dyer, 1986; Cuthbertson, 2001). To account for the influence of particle shape on fall velocity, a shape factor (*SF*), based on the triaxial dimensions of the particle is usually used. Dyer (1986) and Garde and Ranga Raju (1977) recommended that for naturally worn sediment particle, *SF* values ranging from 0.6 to

0.7 can be considered appropriate. The curves in Figure 2.7 show the relationship between C_D and Re_s for a sphere and particles of various shape factors. It is clear from Figure 2.7 that particles of different shapes have different curves in the range above $Re_s \sim 1$. Particles with a disc shape for example, tend to have a constant C_D of about 1 at high Re_s (Dyer, 1986). Theoretically, the expression for fall velocity of a disc in viscous regime is given as:

$$w_s = \frac{1}{2k\mu}\frac{\bar{D}}{D_c}(\rho_s - \rho)\, g\overline{D^2} \qquad (2\text{-}11)$$

where $\bar{D} = 0.5(D_a + D_b)$. The coefficient k as reported by Dyer (1986) has a value of 5.1 for broadside settling of infinitely thin particles and 9 for natural particles.

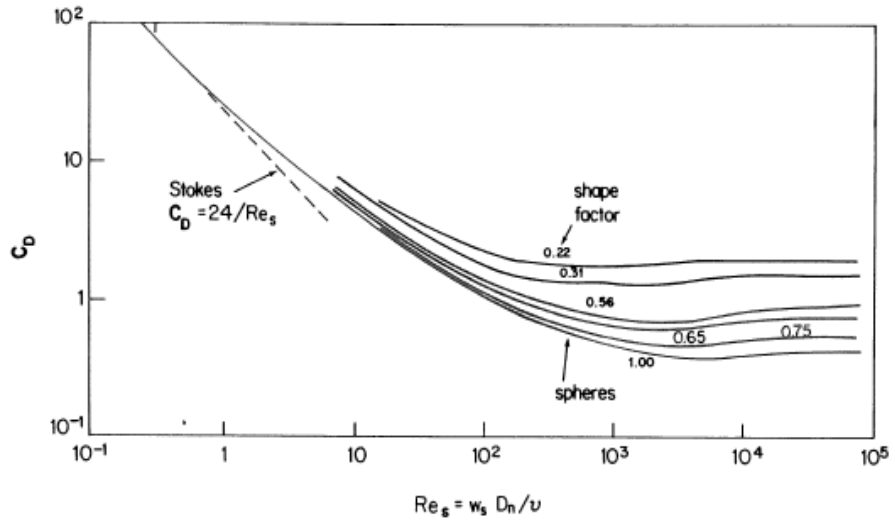

Figure 2.7 Drag coefficient of spheres and non-spherical particles with various shape factors as a function of Reynolds number, based on the nominal diameter D_n (From Dyer, 1986)

It is important to state at this point that the relationships described and derived above are for non-cohesive sediments only and the settling mode described here is an example of Type-I settling mode (i.e. dilutes, non-flocculent, free-settling regime, where every particle settles independently).

2.3.3 Effect of aggregation processes

The properties of flocs differ markedly from those of individual solid particles from which they were formed. Therefore, because flocculating particles constantly change in size and shape during aggregation processes; *flocculation settling* (i.e. Type II settling) of flocs cannot be described adequately by Stoke's law (i.e. Equation 2-5). Additionally, as water gets trapped in the floc, specific gravity increases and this explains why there is a scarcity of adequate mathematical models to describe Type II settling, hence reliance has been on

settling column tests to determine settling characteristics during *flocculation settling*. Winterwerp and van Kesteren (2004), suggested that Equations (2-5) and (2-7) are valid for flocs of cohesive sediments if it is implicitly assumed that the fluid flows only around and not through the flocs. They concluded that flocs can be treated as porous but effectively impermeable entities as an approximation to determine their settling characteristics in marine conditions. This assumption has, however, been proved not to be trivial (e.g. Johnson *et al*., 1996; Gregory, 1997; Mehta, 2014). For example, Mehta (2014) suggested that for the settling velocity of suspended flocs at concentration in excess of $\boldsymbol{C_f}$, aggregation processes (i.e. floc growth and breakup) must be accounted for. Based on Stoke's law, by considering the particle collision frequency which is expected to vary with concentration $\boldsymbol{C}$, a general relationship between settling velocity and the suspended flocs concentration was proposed;

$$w_s = a'_w C^{n_w} = a''_w \emptyset_v^{n_w} \tag{2-12}$$

where a'_w and $a''_w = \rho_s^{n_w}$ are empirical velocity scaling coefficients dependent on the sediment and n_w *(number of particle per volume)* = 1.33 (i.e. 4/3, see Figure 2.8). He cautioned that a'_w and n_w vary with flow shear and the fractal dimension n_f of the floc. Krone (1962) and Burt (1986) conducted tests that confirmed the applicability of the Equation (2-12) in the flocculation settling range in the laboratory (see Figure 2.8) and in-situ experiments respectively.

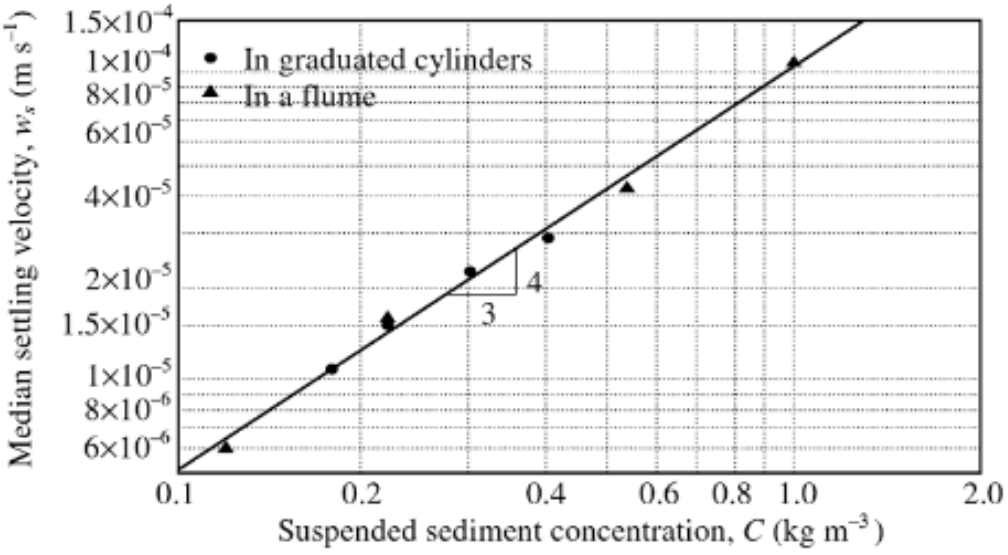

Figure 2.8 Krone (1962): Flocculation settling of San Francisco bay sediment (From Mehta, 2014)

2.3.4 Hindered settling

In practical terms, groups of particles will be settling through the carrier fluid rather than solitary particles. During settling, mutual interactions will normally occur amongst these settling particles, thereby modifying the settling velocities regime from what is observed for solitary particles (Cheng 1997). In other words, when the concentration of sediment grains in a carrier fluid increases, the grains cease to act independently, their motions are therefore correlated through hydrodynamic and grain-grain interactions, which often results in lower settling velocities in comparison to that of a solitary grain (Scott, 1984; Whitehouse *et al*., 2000; Cuthbertson *et al*., 2008), this phenomenon is known as '*hindered settling'* (i.e. Type III settling). The characteristics of hindered settling arise predominantly as indicated by previous studies [e.g. Winterwerp (2002) for mud flocs; and Cheng (1997) for sand particles] from: (i) return flow generation and wake formation, (ii) increased viscosity of the mixture, and (iii) buoyancy effects.

The exact form of the Richardson and Zaki (1954) formulae and/or some related variation have mostly been employed by many scholars to calculate or predict these hindered settling characteristics for coastal sediment transport modelling. However, as proposed by Cuthbertson *et al*. (2008) when modelling suspensions containing both mud flocs and sand particles, a multi-fraction or polydisperse approach is required to fully account for the relative influence of each individual fraction on the settling characteristics of other fractions present in the mixture. In an attempt to achieve this, they developed a two-fraction analytical model, based on the polydisperse formulations of Batchelor (1982) and Davis and Gecol (1994), to predict the hindered settling of both sand particle and mud floc fractions under a wide range of mixture compositions and concentrations (the testing of the Cuthbertson *et al.* (2008) analytical model, in terms of its predictive capabilities for the generation of mixed and segregated bed deposits, is discussed extensively in *section* 7.6, pg. 194). The following subsections present more comprehensive literature review on the characteristics of hindered settling in suspensions containing cohesive, non-cohesive and combination of both sediments.

2.3.4.1 Cohesive sediments

For cohesive sediments, hindered settling effect increases with increasing sediment concentration and becomes more significant with sediment flocculation. For instance, given a situation where the concentration of the sediment in suspension exceeds a given upper limit value (say C_h) of flocculation settling (Equation 2-12), [which, according to

Mehta (2014), may range between approximately 1 to 10 kg/m^3 and largely dependent on the composition of the sediment], w_s will rapidly decrease with corresponding increase in concentration, *C* (Figure 2.9) [Whitehouse *et al*., 2000]. Mehta (2014) reported that this reduction is largely due to the decreasing rate at which the settling slurry dewaters as its permeability decreases with time. If w_s in Equation (2-12) is now taken as w_{sm} (i.e. hindered settling velocity for pure mud suspensions) at C_h and assuming that w_{sm} (see Figure 2.9) can be estimated from Equation (2-5), w_s at a given concentration can be represented by the product of $K_w w_{sm}$, where K_w has been described as the 'retardation factor' applicable to Stokes' settling (Mehta, 2014). Richardson and Zaki (1954) found from settling column experiments an expression for retardation factor, K_w as;

$$K_w = (1 - \emptyset_{vf})^{4.65} \tag{2-13}$$

where $\emptyset_{vf}$ is the flocs volume fraction. Therefore, settling velocity w_s can then be expressed as;

$$w_s = K_w w_{sm} \text{ ; i.e. } w_{sm} (1 - \emptyset_{vf})^{4.65} \tag{2-14}$$

Winterwerp (2002) suggested that the *retardation factor* (i.e. K_w) can be attributed to the effects of (i) increased viscosity, (ii) particle buoyancy, and (iii) return-flow of fluid due to the continuity as particles settle. In order to account for these three effects, Equation (2-14) has been revised as:

$$K_w = \frac{(1 - \emptyset_{vs})(1 - \tilde{\emptyset}_v)^m}{(1 + 2.5\tilde{\emptyset}_v)} \tag{2-15}$$

From Equation (2-15), $\emptyset_v$ (solids volume fraction) is C/ρ_s; $\emptyset_{vs}$ (volumetric concentration of primary mud particles contained within the flocs) is C_s/ρ_s (C_s *is* the space-filling concentration) and $\tilde{\emptyset}_v$ is C/C_s. The value of 1 was assigned to the exponent m by Winterwerp (2002); Letter (2009) and Dankers (2006) found $m = 2$ appropriate for simulating the density profiles of the settling of a fine-grained slurry tested by Kynch (1952). Equation (2-15) is the final hindered settling formula for a concentrated suspension of mud flocs (i.e. cohesive sediments) [Winterwerp, 2002; Mehta, 2014], and the description of each fraction in the Equation is given in Table (2-2).

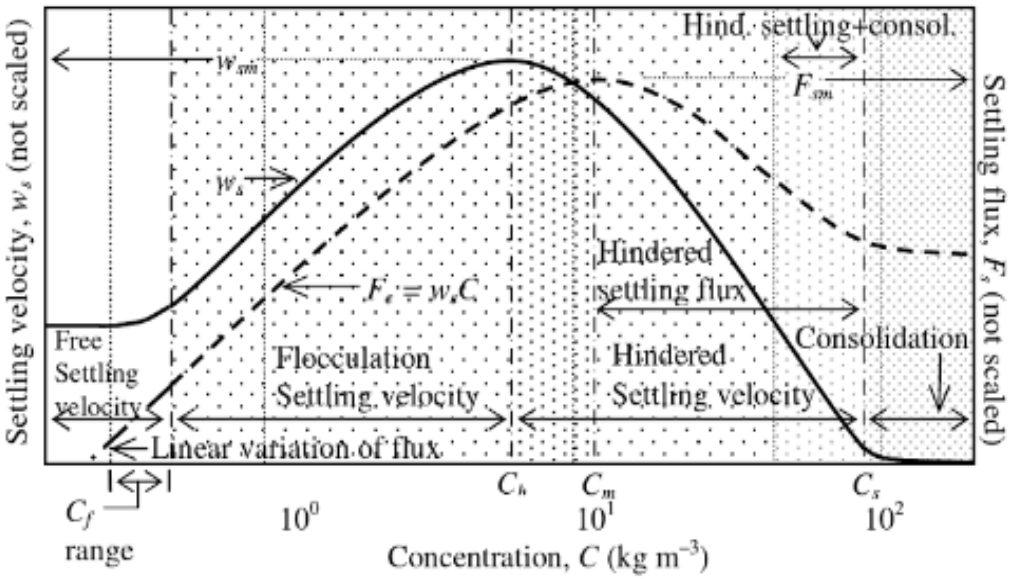

Figure 2.9 Variations of settling velocity and settling flux with concentrations (From: Mehta, 2014)

Table 2-2 Descriptions of fractions in the expression for $\boldsymbol{K_w}$ in Equation (2-15)

Fractions	Descriptions
$(1 - \emptyset_{vs})$	It accounts for decrease in w_s due to return-flow through the slurry pores and micro-channels.
$(1 - \tilde{\emptyset}_v)^m$	It accounts for buoyancy effect which acts against the weight of settling particles.
$(1 + 2.5\tilde{\emptyset}_v)$	It accounts for an increase in drag force on the particle due to the viscosity of suspension being higher than water.

(Adapted from Mehta, 2014)

2.3.4.2 Non-cohesive sediments

As stated above, Equations (2-13) and (2-15) are applicable to cohesive sediments; for non-cohesion sediments, Cheng (1997) proposed an approach for concentrated suspensions of sand particles which was formulated by considering the settling sand particles within the fluid as a two-phase flow problem. The determination of the slip velocity (i.e. the difference in velocities) between the particles and the fluid was based on continuity arguments. The sand particle slip velocity obtained was then expressed in the form identical to Equation (2-8), as:

$$W'_s = \frac{v'_s}{d_p}\left(\sqrt{25 + 1.2d'^2_{p*s}} - 5\right)^{1.5} \quad (2\text{-}16)$$

where v'_s = effective sand-fluid mixture viscosity; and d'_{p*}= $[\left(\frac{g'_s}{v'^2_s}\right)^{\frac{1}{3}} d_p]$ is the modified dimensionless sand particle diameter [with $g'_s = g(\rho_s - \rho')/\rho'$]. It should be noted that, Equation (2.8) differs from Equation (2.16), in that it is proposed for the settling velocity of individual natural sediment particles (i.e. predominantly cohesive sediment).

2.3.4.3 Hindered settling of sand-mud mixtures

The settling velocity of mono-dispersed particles in the hindered settling phase is more or less uniform, this is also true in the consolidation phase but with relatively lower settling velocity. However, this cannot be said of the poly-dispersed particles, such as in mud-sand mixtures, due largely to the complex nature of the inter-related behaviour (including settling characteristics) of the two distinct phases. For example, segregation occurs in the hindered settling phase when the sand particles settle faster than the mud flocs; however, sand particles are trapped within the mud matrix that has gained strength in the consolidation phase and all particles then tend to settle as one (Cuthbertson *et al*., 2008; Dankers, 2006; Torfs *et al*., 1996).

In much diluted suspensions, Van Ledden (2003) suggested that, the sand and mud fractions within the suspension can be assumed to settle independently. This is obviously not acceptable in more concentrated suspensions because, the fractional settling characteristics for the sand and mud constituents are according to Cuthbertson *et al*. (2008) not only governed by the total sediment concentration, but also affected critically by their relative fractional content within the mixture. For instance, in a *sand-rich* mixture, Amy *et al*. (2006) suggested that the settling sand particles may generate return flow large enough to upwardly displace the mud particles (or flocs) within the fluid. In *mud-rich* mixture on the other hand, significant reduction in the settling velocity of the sand particles can occur due to the increased apparent viscosity and return flow resulting from high mud fraction within the mixture (e.g. Winterwerp, 2002)

The work of Wang *et al*. (1995) was one of the few on analysis of settling behaviour of non-cohesive sand in clay suspensions. They performed experiments with large amounts of quartz sand, plastic beads and gravel in both dilute and concentrated mud suspensions and thereafter proposed a purely empirical equation based on the Richardson and Zaki

(1954) and Maude and Whitmore (1958) formulae to describe the settling characteristics of sand in mud suspensions:

$$\frac{w_{ss}}{w_{ss,0}} = (1 - \emptyset_s)^n \left(1 - \emptyset_p\right)^{2.5} \quad (2\text{-}17)$$

where w_{ss} is the hindered settling velocity of the sand through the mud suspension, $w_{ss,0}$ is the Stoke's settling velocity of sand, $\emptyset_s$ the particle volume concentration of sand, $\emptyset_p$ the particle volume concentration of mud and n is a function of the particle Reynolds number, as in the Richardson and Zaki (1954) formula.

Equation (2-17) modelled their experiments well, although with much higher values of n (i.e. $n \approx 8$) than suggested by Richardson & Zaki (1954) [$n \approx 2.5$-5.5]. Wang *et al*. (1995) then concluded that their model only works well for the hindered settling of sand in dilute mud suspensions but significantly deviates from experimental data where the mud concentration is so high that the critical diameter approaches the median diameter of the particles. However, volume effects are important in the hindered settling phase; therefore, for suspensions in which $\emptyset_s << \emptyset_p$, the return flow effect and viscosity effect will be mainly determined by the mud fraction in the mixture (Dankers, 2006). Winterwerp & Van Kesteren (2004) in an attempt to address this, proposed a model under some limiting conditions to predict separately, the hindered settling velocity of both the cohesive mud and non-cohesive sand fraction: (1) the slip velocities of sand particles and mud flocs are equal to their terminal settling velocities measured in clear fluid; and (2) the mixture is predominantly mud with only a small sand fraction (i.e. $\emptyset_s << \emptyset_p$):

$$w_{sf} = \frac{(1-\emptyset)(1-\emptyset_p-\emptyset_s)}{(1+2.5\emptyset)} w_{sf,0} \quad (2\text{-}18)$$

Expanding Equation (2-18) gives;

$$w_{ss} = \frac{(1-\emptyset)(1-\emptyset_p-\emptyset_s)}{(1-\emptyset_f)(1+2.5\emptyset)} \left(w_{ss,0} - \emptyset_f w_{sf,0}\right) \quad (2\text{-}19)$$

In the model presented in Equation (2-19), buoyancy, viscosity and the non-linear return flow effect are all accounted for. However, the model is unable to account adequately for the enhanced hindered settling effects on the mud fraction that may arise from increasing

the volumetric sand content $\emptyset_s$ within the sand-mud mixtures; therefore, its applicability is restricted to *mud-rich* suspensions. This is also the case with the *modified Cheng's model* (this has not been covered here) proposed by Cheng (1997) to predict the hindered settling velocity of the non-cohesive sand fraction. The highlighted shortfalls of the models mentioned above formed one of the major aims of the work of Cuthbertson *et al*. (2008) as noted above (see *section 2.3.4*). Their new polydisperse approach for example defined mixture conditions under which the mud flocs would be displaced upwards due to return flow effects generated by the hindered sand fraction settling. They also suggested that this differential settling phenomenon is likely the prime mechanism for layer segregation within resulting sand-mud bed deposits. A similar polydisperse model was developed by Van and Pham Van Bang (2013) to investigate segregation (and trapping) effects that occur between mud flocs and sand grains during the hindered settling phase of sedimentation processes. The authors acknowledged, however, that limitations in the extent of calibration data available (i.e. one 20 % sand − 80 % kaolin test mixture) meant the model needed further validation over a wider range of sand-clay mixtures.

Grasso *et al*. (2014) analysed data from a number of previous settling column studies (e.g. Merckelbach and Kranenburg, 2004a; te Slaa *et al*., 2013; van and Pham Van Bang, 2013; etc.) which investigated hindered settling of sand-mud mixtures over a wide range of initial concentrations and sand contents. The outcome of the analysis showed that the sand fraction segregation within the resulting bed deposits was not a regular occurrence and appeared to be prevented at a particular initial concentration threshold of the cohesive sediment fraction. Therefore, the spatial and temporal variations observed in sediment bed texture and structure (e.g. the formation of mixed or segregated deposit layers) are believed to be largely defined by hindered settling characteristics within sand-mud suspensions.

2.3.5 Effect of salinity on settling

From Stoke's law (Equation 2-5) and all its offshoots, it is clear that the settling velocity is influenced by the effects of changing salinity on floc characteristics (e.g. diameter, density) and, to some extent, fluid viscosity. Dyer (1986) suggested that as flocculation rate increases with increase in salinity, a particular settling velocity will occur at a lesser concentration in a higher salinity, and that, depending on the ratio of particle size *D* to the spacing of adjacent particles *s*, peak settling velocity should occur at a lower

concentration (McNown and Lin, 1952; Dyer, 1986). Ambient fluid salinities ranging from ~0.5-5.0 *psu* (i.e. oligahaline) and ~5.0-18.0 *psu* (i.e. mesohaline) are broadly reported to enhance flocculation and settling of clay and clay flocs (Ani *et al*., 1991; Uncles *et al*., 2006; Sutherland *et al*.,2014; etc.). For example, one of the studies (e.g. Cerco *et al.*, 2013) in modern estuaries reported a decrease in suspended sediment content in the seaward direction. This was interpreted to be a result of clay sedimentation in the inner estuary and dilution from sea water. Although, the qualitative link between salinity and settling of suspended inorganic solid particles, is somehow complicated (Sutherland *et al*.,2014); however, this qualitative link has been clearly observed in the Gironde Estuary, France (Allen and Posamentier, 1993), the Jiaojang Estuary, China (Guan *et al.*, 2005), Kouchibouguac Bay, Canada (Hauck *et al*., 2009) and in Avonmouth Estuary, England (Owen, 1970).

The series of laboratory settling experiments of Owen (1970) conducted with natural clay from the Avonmouth Estuary in England, revealed that, for each initial sediment concentration, a measurable increase in their settling velocity can be seen with increase in salinity up to 30 *ppt*, and above which, the settling process was retarded (Figure 2.10). There is a generally consistent trend of the gradual rise in the settling velocity with salinity, attainment of a peak value at about 30 *ppt*, and a relatively rapid decrease with a further increase in salinity (especially above 30 *ppt*) for all the sediment concentration tested. Similarly, Sutherland *et al*. (2014) reported that, increasing the salinity beyond a nominal value (~20 *psu*) does not change the settling rate, and that, this rate was found to be retarded with increase in particle concentration (Note: *psu* is approximately equivalent to *ppt*). Specifically, the trend in Figure 2.10 appears to indicate that, above 4 $kg\ m^{-3}$, initial sediment concentration plays significant roles in hindering settling. The flatness of the curve for 32 $kg\ m^{-3}$ (see Figure 2.10) suggests however, that hindrance due to high concentration may likely suppress the effect of salinity (Mehta, 2014). Also, because natural mud was used (Owen, 1970), another likely, and possibly very important, factor responsible for this reduction in settling velocity is the effect the benthic organisms can have on settling process, as they are capable of altering sediment dynamics by changing the structure and composition of the sediment (Jumars and Nowell, 1984; Jones *et al*., 1997). High salinities can chemically alter organic matter and influence, for example, microbial community (e.g. cynobacteria) to produce mucus-like substance which can bind the particles and hence alter their settling characteristics (Mehta, 2014; Grabowski *et al*., 2011; Winterwerp and Van Kesteren, 2004).

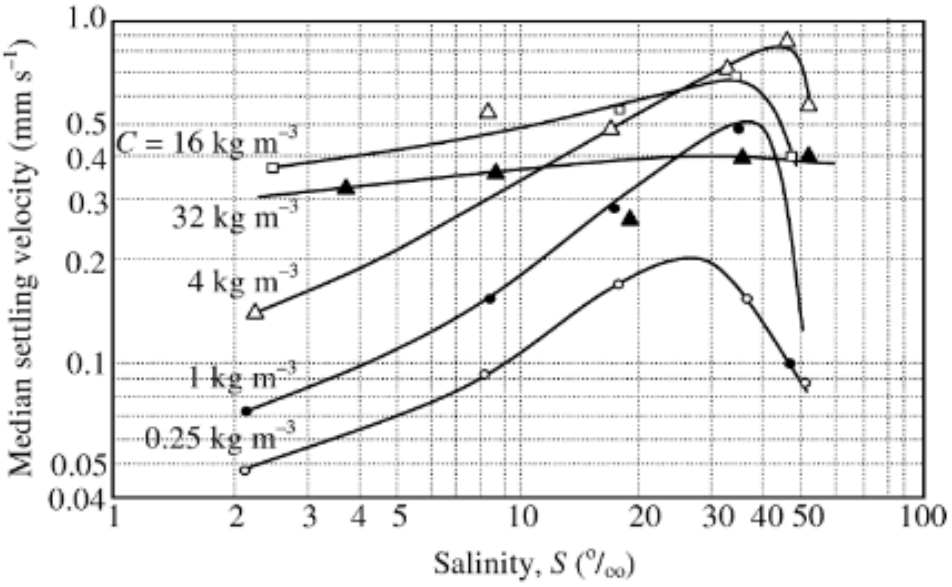

Figure 2.10 Effects of salinity on the settling velocity of Avonmouth (England) mud [After Owen (1970); from Mehta (2014)].

2.4 Sediments Bed Formation Process

2.4.1 Brief introduction

Understanding the dynamics of natural sediment bed formation processes is important to accurately assess and predict erosion and deposition processes that take place in estuarine and near-shore coastal marine environments. For example, in the event such as, dredging excavation or disposal of waste slurries (which is more practical to be dumped on land rather than back into the water due to the possibility of the dredged material being already polluted), accurate prediction of settling and consolidation of such dumped material is necessary to optimize the disposal process (Torfs, *et al*., 1996; Van and Pham Van Bang, 2013).

2.4.2 Bed formation concept

Two major mechanisms are responsible for bed formation, namely: sedimentation of particles or flocculated particles and consolidation (Ross, 1988; Mehta, 2014). Sedimentation can be defined as the process by which particles, or aggregates of particles, under the influence of gravitational force leave suspension and settle to form a bed deposit. Consolidation in a fully saturated environment is a process which results from the deformation of the bed deposit particle framework under an applied stress. The applied stress could either be as a result of net negative buoyancy i.e. self-weight or imposed overburden loading (Dyer, 1986; Ross, 1988; Mehta, 2014).

In the context of bed formation by sedimentation and consolidation, when a column of suspended sediment settles in still water under gravity, the sequence of the complete processes is (Dyer, 1986; Mehta, 2014): flocculation, settling, deposition and consolidation (Figure 2.11). Depending on factors such as sediment types, composition and concentration, the sequence may be altered, for example, the first three processes can occur simultaneously and flocculation can be omitted completely in predominantly non-cohesive sediments (this is discussed further in Chapter 5). A general description and graphical model of the bed formation processes (Figure 2.11) was given by Imai (1981). Due to low submerged weight that makes flocculated sediments to settle more slowly than coarse or non-cohesive sediment of the same size as flocs, the model therefore describes the three general stages that flocculated sediments undergo to form bed deposits:

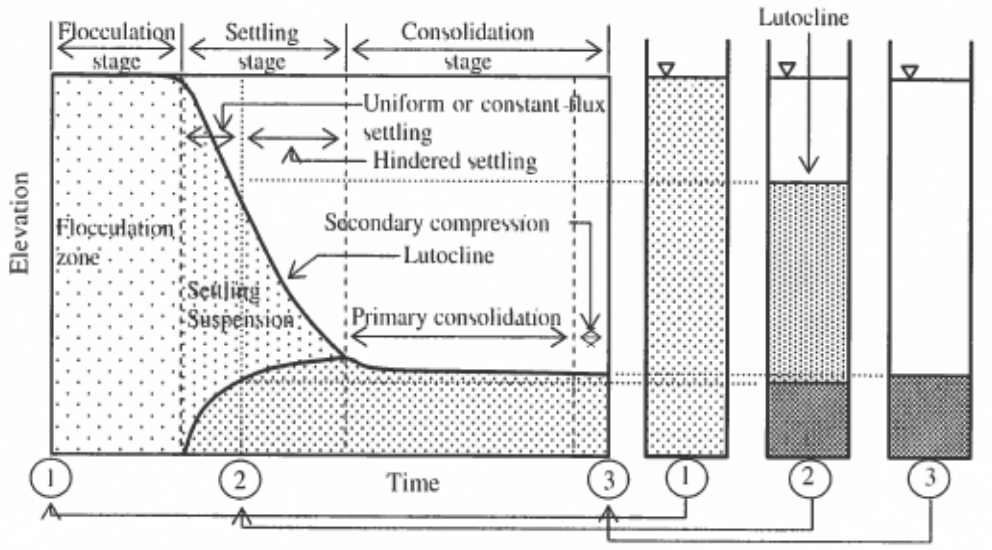

Figure 2.11 Imai (1981) description and graphical model of bed formation process (From Mehta, 2014)

Flocculation stage

Aggregation in particular is the defining process in this stage. The process of aggregation (flocs building-up) and breaking-up is called flocculation. Particles aggregation results when two particles collide and stick together and the rate of aggregation is driven by frequency of collisions, the efficiency of the collisions in getting the particles to stick together and the particle concentration. Particle collisions are initiated by Brownian motion of particles, turbulence within the suspending liquid and differential settling of the suspended particles (Van Leussen, 1994; Winterwerp and van Kesteren, 2004; Mehta, 2014). At this stage, floc formation due to coagulation will occur if the initial particles

are primary or dispersed and conducive to cohesion (Mehta, 2014). Depending on the mineralogy of the sediment involved, this stage may last for seconds or minutes. The onset of rapid fall in the water-sediment interface at the end of the stage (Figure 2.11) shows a smooth transition to the next stage (i.e. settling stage; Figure 2.11) [Imai, 1981; etc.].

Settling stage

This stage is characterised by two phases, namely: uniform settling/constant flux settling phase and hindered settling phase (see Figure 2.11). In the former, the rate of fall of water-sediment interface is relatively uniform due to negligible hindrance against the fall; in the latter phase, however, the fall of the interface (i.e. lutocline) is hindered, this phase is characterised by the decrease in the interface falling rate with time and the formation of second interface below the lutocline (see Figure 2.11), which defines the building up of bed above the bottom (Imai, 1981; Mehta, 2014). Detailed description of this stage has been given earlier in this chapter (i.e. *section 2.3.4*)

Consolidation stage

The last identified stage is the consolidation stage, and the transition from the settling stage to this stage happens at a time (t) when the lutocline meets the rising bed height (see Figure 2.12). Beyond the meeting point between the lutocline and the rising bed height, the surface of the freshly formed bed falls very slowly until there is no significant reduction in the bed deposit height, and this is due mainly to consolidation (Imai, 1981; Mehta, 2014). At the initial stage of consolidation, as mud flocs settle, subsequently settled flocs will squeeze the flocs that settle before them and in the process pore-water is expelled out of the flocs and out of the space between the flocs. This process has been described as self-weight consolidation process by Terzaghi (1943). Self-weight consolidation process basically describes the transition from a fluid-supported suspension to a solid-supported suspension (e.g. soil), which is characterised by a change of state in which pore-fluid pressures and vertical total stress are equal, to a state where pore-fluid pressures are less than the total vertical stress (i.e. there is existence of effective stress) [Sills (1998)]. Figure 2.12 shows (a) a typical density profile; and (b) the calculation of its effective stress (i.e. difference between total pressure and pore pressure) for experiment REDMO5 from Sills (1998). Figure 2.12(a) clearly shows, the fluid supported part, the hindered settling phase, solid-supported part, and the consolidation phase. In Figure 2.12(b), the hindered settling phase is characterised by equal pore-fluid pressures

and total pressure; in the consolidation phase, however, the pore pressures are less than the total pressure (i.e. showing existence of effective stresses). The process described above is widely used in soil mechanics to characterise soil structures; for example, the onset of consolidation is identified by the development of effective stresses, therefore from Figure 2.12(b), it is clear that consolidation starts at *Pressure* = ca 0.17 *kPa*. The pressure value corresponds to a density of ca 1200 $Kg\ m^{-3}$ in Figure 2.12(a), this referred to as the *structural density* (i.e. the concentration at which a space-filling network occurs where particles within the mixture support each other at their loosest packing).

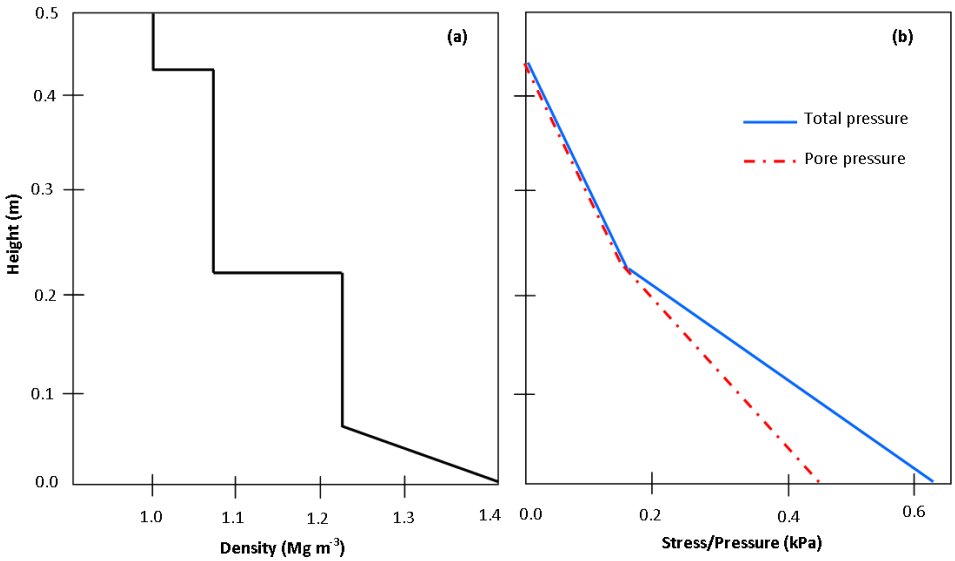

Figure 2.12 Sketch of a typical density profile (a) and the calculation of its effective stress [i.e. difference between total pressure and pore pressure] (b), for experiment REDMO5 from Sills (1998). [Adapted from Lintern, 2003]

Figure 2.13 shows the density profiles for the initial 79 *hours* of a settling column experiment to investigate sedimentation process of estuarine mud (from Combwich, Somerset in England), Been and Sills (1981), described the density (i.e. 1070 $Kg\ m^{-3}$ or 1.07 $g\ cm^{-3}$) of the initial mud suspension as almost uniform (i.e. at flocculation stage), but with time, as settling continues, an interface separating the pool of clear water and the sediment slurry forms which falls linearly with time and maintains an almost constant concentration (i.e. settling stage, similar to Figure 2.11). Meanwhile, at the bottom, a layer of relatively high density is formed, due to (i) coarse particles settling quickly before becoming involved in the flocculation process (which is the case most of the time with sand-mud mixtures) and (ii) partly because of rapid consolidation at the base while the sediment layer is still relatively thin (Been and Sills, 1981).

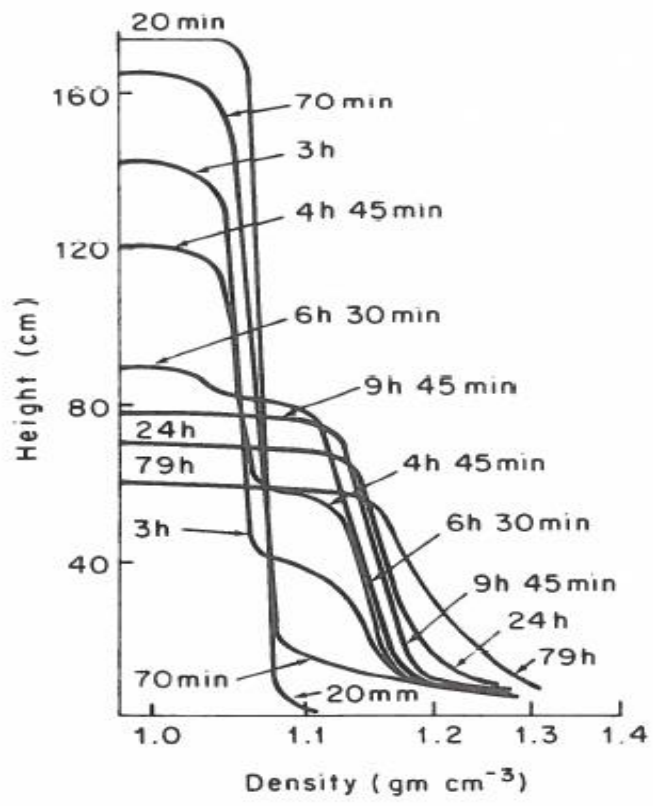

Figure 2.13 Density profiles in a settling suspension with initial density of 1.07 g cm^{-3} (From Been and Sills, 1981)

2.4.3 Effective stress and pore-water pressure

Sediment bed deposits are examples of porous media, comprising a deformable mineral skeleton filled with an incompressible fluid (water) [Ross, 1988; Craig, 1992]. For such a system, settling in hindered mode and consolidation (see Figure 2.11) are both governed by the rate of pore water dissipation (Winterwerp and van Kesteren, 2004; Mehta, 2014). The *effective normal stress* within the settling suspension is insignificant, i.e. pore-water pressure (Ú) is approximately equal to the total hydrostatic pressure ($Ú_h$) on the sediment suspension; but within consolidating bed deposits, it is significantly less than total pressure (σ) [see Figure 2.12(b)]. This difference has been attributed to the fact that part of the suspension total weight is supported by the particle matrix (Winterwerp and van Kesteren, 2004; Mehta, 2014). This difference in pressure is represented by a concept of effective stress σ' (Equation 2-20) which represents load supported by particles matrix as opposed to pore fluid. This has been found to be the controlling parameter in determining soil strain, deformation and strength (Been and Sills, 1981; Schiffman *et al*., 1986). According to the principle of *'effective stress'*, the strength and compressibility (i.e. degree of looseness) of a soil or bed deposit depend on the difference between the *'total*

stress' and the stress carried by the pore fluid i.e. pore-water pressure (Mitchell, 1960 and Craig, 1992).

$$\sigma' = \sigma - Ú \tag{2-20}$$

Total stress at a point in the bed can be obtained by integrating density profile from the top of the bed down to that point. So, from total stress values and pore-water pressure, the distribution of '*effective stress'* over the settling column height can be calculated from Equation (2-20) [Torfs *et al*., 1996; Been &and Sills, 1981; Sills, 1998; Craig, 1992; Winterwerp & Van Kesteren, 2004; etc.].

In addition to effective stress, another important parameter in this context is excess pore pressure (Δu) (Equation 2-21), which is the difference between actual pore water pressure ($Ú$) and hydrostatic pressure($Ú_h$).

$$\Delta \cup = Ú - Ú_h \tag{2-21}$$

The dissipation of pore water has been used to explain consolidation processes; nevertheless, pore water pressure gradient has also been demonstrated to be useful to explain freshly deposited bed behaviour (Lintern, 2003; Ross, 1988; Been and Sill, 1981; etc.). For example, if total stress, σ, is approximately equal to $Ú$ under dynamic conditions (i.e. $\sigma' \approx 0$), liquefaction of the sediment slurry can occur (e.g. fluid mud) (Ross, 1988). In a highly porous sediment bed, the effective stress everywhere within the bed is non-zero and the pore pressure is everywhere hydrostatic. In a freshly deposited bed, the pore water pressure in the upper part of the deposit will be equal the total stress, the implication of this is that the sediments are in suspension, and therefore the water bears the sediment weight. With time, the pore-water pressure will drop below the total stress allowing particle interaction, and a weak bed structure begins to from which is able to bear some of the weight of the sediment (Ross, 1988). These illustrations confirm that the development of effective stress provides a fundamental distinction between suspension and structural bed deposits (Ross, 1988; Been and Sills, 1981; Sills and Elder, 1986; Sills, 1998).

Been and Sills (1981) and Sills and Elder (1986) carried out extensive laboratory studies on the development of effective stress in settling and consolidating estuarine silty-clay

mud from Combwich (UK) in a settling column. Figure 2.14 shows the instantaneous density and effective stress profiles for one of the tests 4.75 *hours* after the start of the settling test. In their experiments, they could not find a particular concentration level at which effective stress will develop, but they did observe that structural development occurred over a range of concentrations (80 – 220 $kg\ m^{-3}$) which largely depended on the initial mixture density. Ross (1988) suggested that their observation seems to imply that structural phase development is dependent on sedimentation rate especially in low concentration quiescent conditions. However, according to the findings of this study on laboratory tests on wave erosion, hydrodynamic agitation also influences structural phase development.

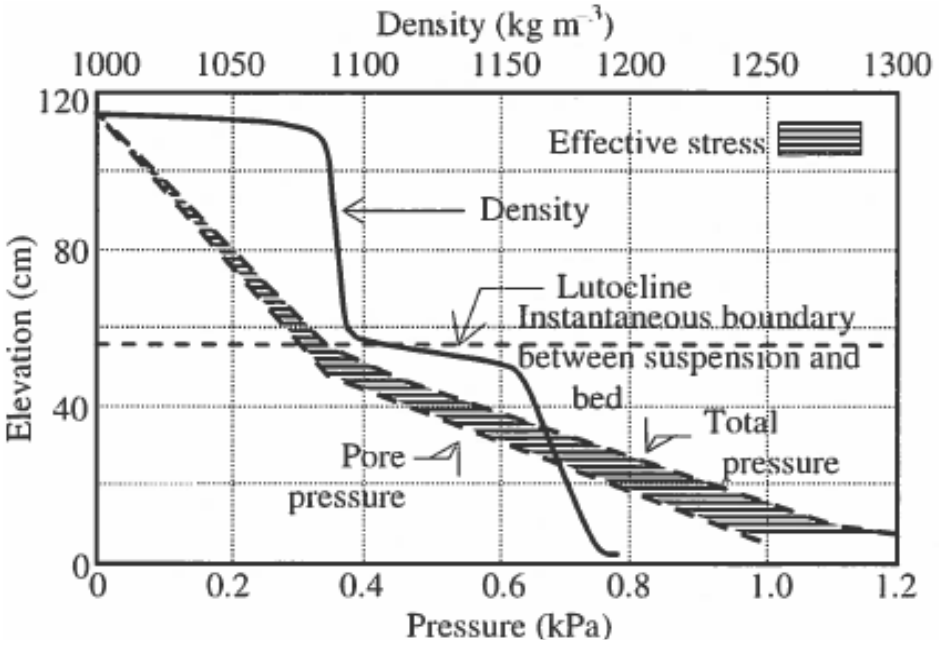

Figure 2.14 Instantaneous density, total pressure and pore pressure profiles of settling Combwich-UK mud (From Mehta, 2014)

2.5 Erosion and Entrainment

2.5.1 General overview

The stability of bed sediment in the marine environment as reported by Grabowski *et al*. (2001) is largely dependent on the balance between hydrodynamic forces that cause erosion and the forces within the sediment that resist it. Amos *et al*. (1998) and Winterwerp and Van Kesteren (2004) described these hydrodynamic forces (erosive forces) as being the embodiment of fluid-transmitted forces (e.g. boundary layer shear stress) and prevalent turbulent conditions. They added that, the characteristics of these erosive forces are largely influenced by the nature of fluid flow and solid transmitted

stresses from particles moving along the bed. The potential of these forces are hindered by aspects of the near-bed environment (e.g. increased bed roughness, presence of organic component, etc.) that control fluid velocity and turbulence intensity (Jumars and Nowell, 1984; Madsen and Warncke, 1983). Therefore, Grabowski *et al*. (2011) stated that erosion occurs when erosive forces are larger than the resistive forces within the sediment which include gravity, friction, cohesion and adhesion. Based on these submissions, erodibility, often expressed as 'erosion threshhold' or as an 'erosion rate', is a measure of these resistive forces (Sanford, 2008; Grabowski *et al*., 2011). Erosion rate is defined as the mass of sediment eroded per unit time once the threshold is exceeded (i.e. at an excess shear stress); while erosion threshold is the water velocity or critical bed shear stress (τ_{cs}) that initiates sediment erosion.

2.5.2 Main properties affecting cohesive sediment erodibility

Findings of various studies (e.g. Torfs *et al*, 2001, Le Hir *et al*., 2008; Grabowski *et al*., 2011; Baas *et al*., 2013; etc.) conducted on erosion of sediments from bed deposits have shown that erodibility of these beds is influenced by a number of physical, geochemical and biological sediment properties and processes. These include; average size of particle/aggregate constituting the bed; particle size distribution within the beds (e.g. clay, silt and sand content); bed bulk density and water content; temperature, clay mineralogy, total salinity, relative cation concentration, pH, metal concentration, bioturbation, feeding and egestion by organisms and biogenic substances (e.g. extracellular polymeric substances -EPS). Figure 2.15 presents some of the main sediment properties and processes that significantly influence erodibility. Grabowski *et al*. (2011) noted that these properties are dynamically linked and the net impact of any individual property on erodibility for natural sediment is more often dependent on the interactions between two or more properties.

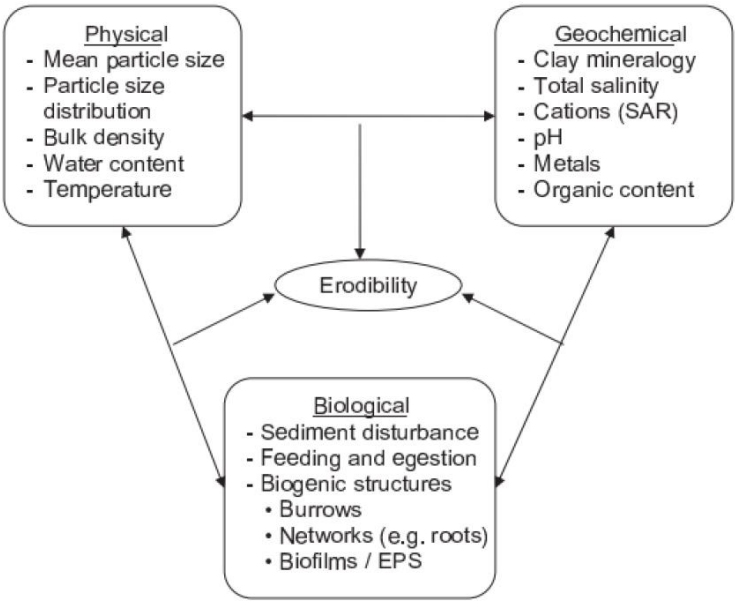

Figure 2.15 Conceptual model of the sediment properties and processes that affect erodibility (From Grabrowski *et al.*, 2011)

2.5.2.1 Physical property: particle size distribution

Various studies both in the field and laboratory (e.g. Yallop *et al*., 2000; Amos *et al*., 2004; Gerbersdorf *et al*., 2008; Tolhurst *et al*., 2008) have identified physical properties of the sediment (e.g. mean particle size distribution, bulk density, etc.) as the most important of the properties that influence erodibility. This explains why they are frequently identified to underlie the significant spatial and temporal variation in erodibility observed in natural marine environments (Amos *et al*., 2004; Bale *et al*., 2007) and commonly used in site-specific models of sediment transport to predict erodibility (Sanford, 2008; Paarlberg *et al*., 2005). A negative correlation between critical bed shear stress and average particle size was reported (Figure 2.16) in the experiment on natural marine mud. Grabowski *et al*. (2011) attributed the reduction in erosion threshold of the unconsolidated bed with increase in particle size to a decrease in density. Dade *et al*. (1992) however, found a directly opposite trend, i.e. positive correlation between critical shear stress and particle size (grain diameter ranging between 10-170 μm). These findings suggest that correlation between particle size and critical bed shear stress can be negative or positive, Grabowski *et al*. (2011) suggested that this variation may depend on how the aggregates are deposited and sediment beds are formed.

Therefore, using cohesive sediments as an example, the relative proportions of clay, silt and fine sands within them will substantially affect their erodibility (Winterwerp and van Kesteren, 2004; Le Hir *et al*.,2008; Grabowski *et al*., 2011; Mehta, 2014).

Grabowski *et al*. (2010), Panagiotopoulos *et al*. (1997), Mitchner and Torfs (1996) and Le Hir *et al*.(2008) reported a measurable increase in erosion threshold, up to a maximum erosion threshold at 30-50% mud, when mud was added to a sand bed [see Figure 2.17 (a)]. A sharp increase in critical shear stress for erosion occurred when clay content exceeds 4.5% in Le Hir *et al*. (2008) erosion experiment with mixture of 280 μm sand and 'St Yves' mud (Figure 2.17b). Torfs *et al*. (2001) analysed various experimental data on erosion of mixed (sand-mud) sediment beds, and found also that erosion threshold increased with increasing mud content, except at mud content of few percent (less than 5%) as presented in Figure 2.18. Their findings show majorly that, combination of hydrodynamic smoothing (i.e. fluid-sediment interactions); clay-sand adhesion and clay cohesion are responsible for the observed increase in erosion threshold. At low clay contents (e.g. 2% bentonite by weight in Lick *et al*., 2004), the voids between the sand and/or silt grains are filled by the clay minerals helping the sand and silt grains to stick together resulting in bed with smoother surface that is more resistant to erosion (Grabowski *et al*., 2011). With high clay contents (e.g. 4-10% by weight), the structural framework of the sediment changes from sand (or silt) grain skeleton framework to a clay mineral framework, indicating a transition from a non-cohesive sediment to a cohesive sediment (van Ledden *et al*., 2004; Winterwerp and van Kesteren, 2004; Grabowski *et al*. 2010).

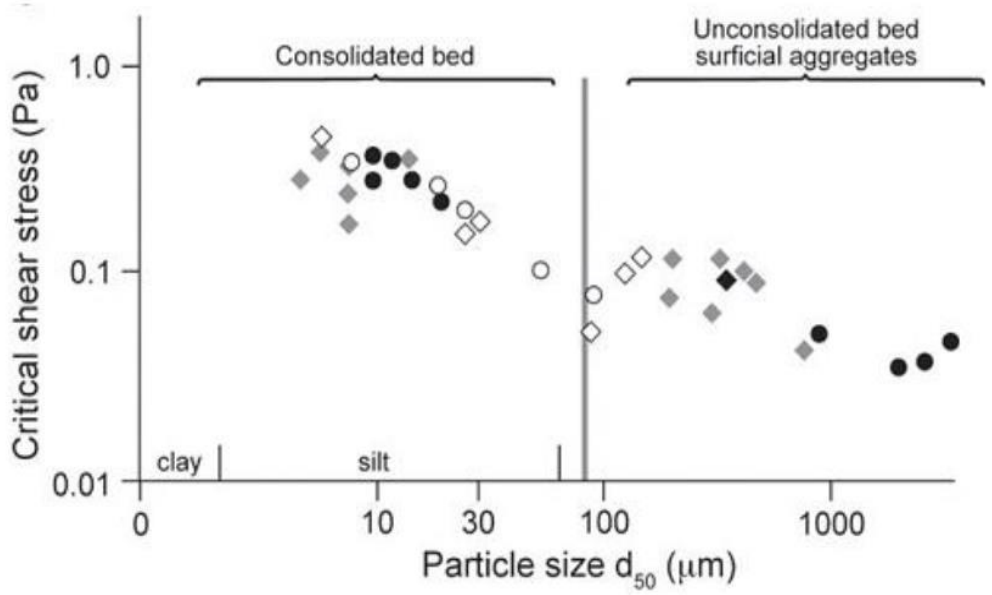

Figure 2.16 Critical shear stress variations with particle size for different beds (From Grabowski *et al*., 2011)

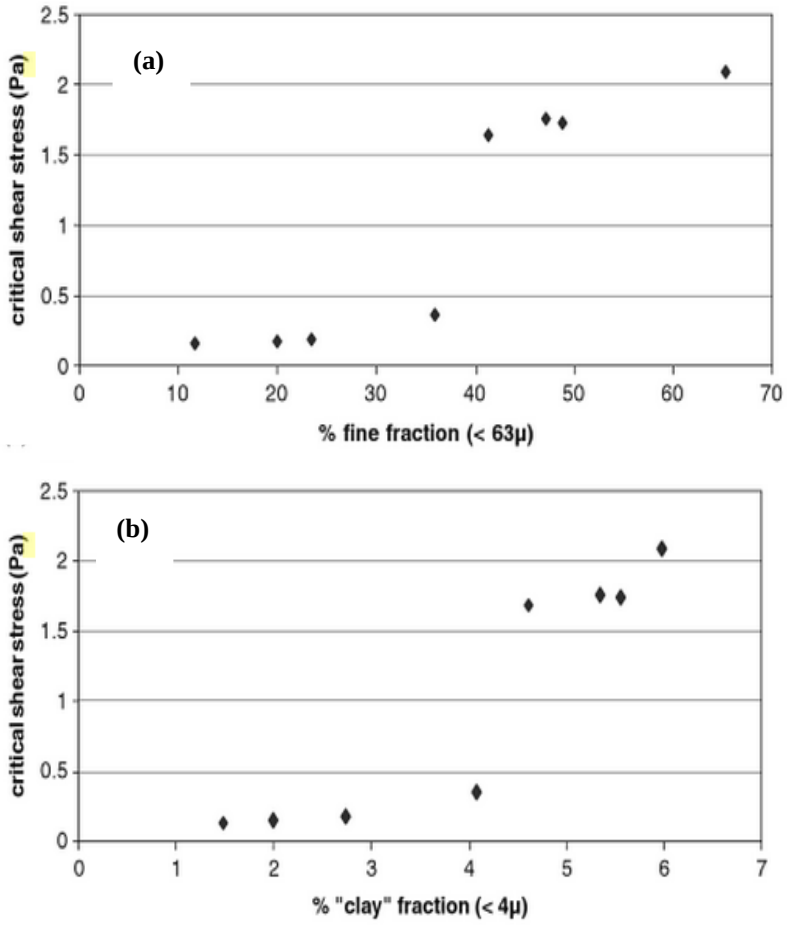

Figure 2.17 Erosion threshold of laboratory mixtures of sand (280 μm) and 'St Yves' mud against volume fraction of (a) mud and (b) clay (From Le Hir *et al.*, 2008)

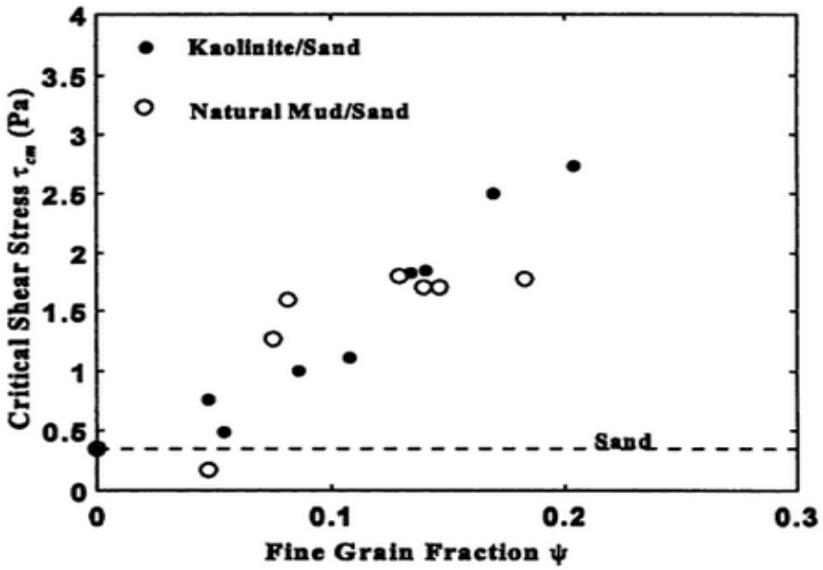

Figure 2.18 Measured critical shear stress as a function of fine grained weight fraction for mixtures of kaolinite/sand and natural mud/sand (From Torfs *et al.*, 2001)

2.5.3 Erosion behaviour of non-cohesive sediment

The mechanisms underlying the erosion processes of sand and/or silt are relatively well understood and documented. Sediments properties such as particle size, shape and packing density can be reasonably used to predict erodibility of these non-cohesive sediments (Grabowski *et al*., 2011; Mehta, 2014). In addition to the sediment properties, erosion of this class of sediments depends on the flow-induced forces. Consider the forces acting on a particle at the surface of a horizontal bed (Figure 2.19), being a cohesionless particle, it is assumed to be non-deformable, each with an identity when at rest or in motion (some authors have argued that cohesive floc can be ideally treated as sand grain based on these assumptions (e.g. Winterwerp and van Kesteren, 2004; Mehta, 2014; etc.).

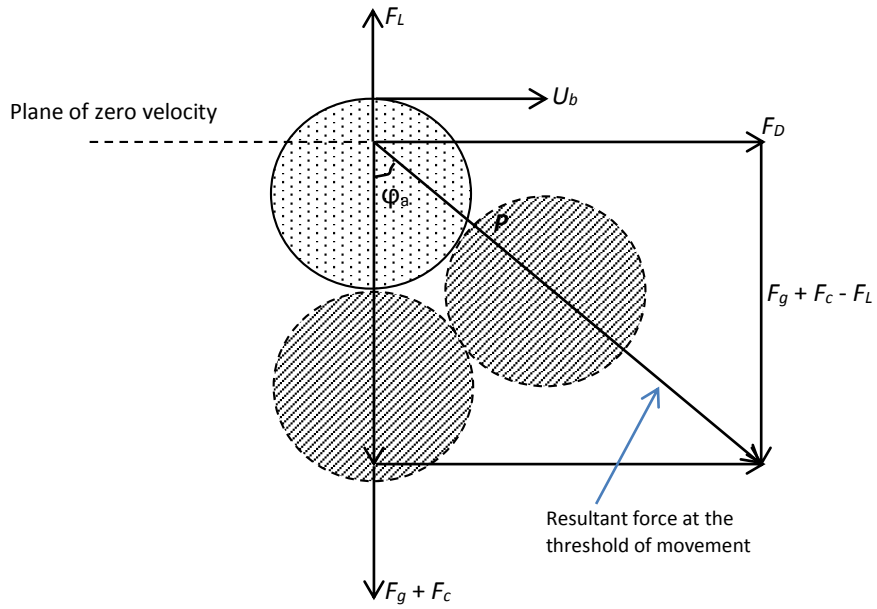

Figure 2.19 Forces on a particle at a horizontal bed surface subject to turbulent flow (Adapted from Mehta, 2014)

Above the particle (Figure 2.19), for curved streamlines, a low pressure is generated which induces a vertical lifting force F_L. The drag force is as a result of flow by means of viscous skin friction and low pressure, F_D, acting at the same level with bed surface (plane of zero-velocity). If the cohesive-adhesive force (represented by F_C), which may be assumed to be equal to inter-particle electromagnetic attraction, is considered, then the total resisting force on the particle will be particle buoyant weight (F_g) and F_C. Therefore, the net normal force on the particle can be given as: '$F_g + F_C - F_L$'. Angle φ_a is termed angle of repose, and corresponds to the threshold of movement of the first particle

anywhere on the bed surface (Mehta, 2014). F_D can be assumed to be = $c_* \, d_p \tau_c$ (where, c_* is a coefficient that takes into account the geometry and packing of the grains and the variation of the drag coefficient – it is equally expected to vary with boundary Reynolds number; d_p is the particle diameter; and τ_c is the average boundary shear stress).

Shields (1936) developed a parameter to determine the initiation of motion for cohesionless particle (sand) based on the principle of force balancing described above. The model is generally referred to as Shields' entrainment parameter θ_{cr} (Equation 2-22), but when F_C is negligible, θ_{cr} for coarse particles can be defined as a function of the particle roughness Reynolds number R_{e*} (Equation 2-23). Examples of some flume experimental data relating Equations (2-22) and (2-23) are shown in Figure 2.20 (i.e. Shields' diagram). Generally, if R_{e*} is known, θ_{cr} of the particle can be determined and by extension the critical shear stress (τ_c) of the particle. Under given flow conditions, a Shields parameter greater than the critical line (Figure 2.20) will result in motion of non-cohesive sediments, i.e. the particles start rolling and sliding as the applied shear stress is reaching critical shear stress.

$$\theta_{cr} = \frac{|\tau_c|}{(\rho_s - \rho_w) g d_p} \tag{2-22}$$

where τ_c (N/m^2) is the critical bed shear stress at the threshold of erosion, g ($m\ s^{-2}$) is the acceleration due to gravity, d_p is the particle diameter, and ρ_s and ρ_w are the particle and fluid density respectively.

$$R_{e*} = \frac{u_{*c} d_p}{v} \quad ; \; u_{*c} = \sqrt{\frac{\tau_c}{\rho_w}} \tag{2-23}$$

where v is the kinematic viscosity of water and u_{*c} is the critical value of the friction velocity.

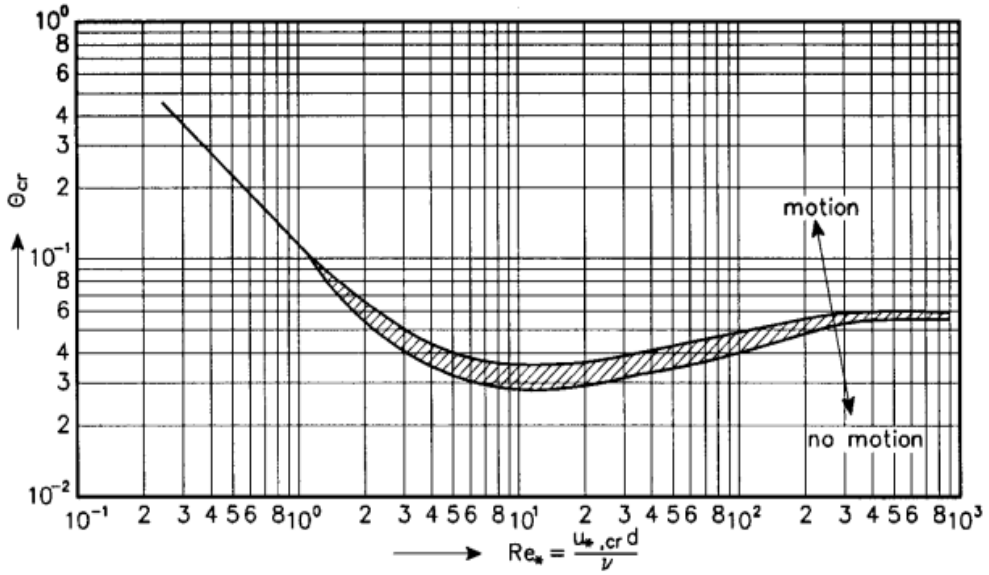

Figure 2.20 Initiation of motion according to Shields (1936) [i.e. Shields' diagram]

A wide range of flow conditions for which there is weak but noticeable sediment movement is one of reasons why determination of particle movement threshold is so challenging, which leads to the general problem of how to define the condition of incipient movement in the first place. This explains why the Shields diagram is under criticism in its application to define condition of incipient movement; for example, because τ_c and d_p both appear in the axis variables it will be impractical to use it to find the threshold shear stress that corresponds to a given sediment diameter, or to find the largest sediment diameter that is moved by a given shear stress. Van Rijn (1993) suggested that the Shields curve in terms of R_{e*} and θ_{cr} is largely not practical because τ_c value can only be obtained by iteration. Nonetheless, the Shields diagram continues to be used, because it gives good ballpark results for both engineering and sedimentological purposes. Recently various sand erosion laws (often called *pick up functions*) have been formulated to address the pitfalls of Shields diagram, although experimental validation of such laws is rare. Most of these published sand erosion laws (e.g. van Rijn, 1985; Beach and Sternberg, 1988; Nielsen, 1992; etc.) are expressed by relating erosion rate as a function of the excess-shear stress to a power, which value varies depending on the sand diameter (e.g. higher power for smaller particles) [Le Hir *et al*., 2008]:

$$E_{sa} = E_{0,sa}\left[\frac{\tau_b}{\tau_{es}} - 1\right]^{ns} \qquad \text{for } \tau_b > \tau_{es} \tag{2-24}$$

where τ_{es} is the sand particles critical stress for erosion (e.g. deduced from Shields curve, and parametrically formulated in terms of grain size and density by Soulsby, 1997); ns

is generally optimised from calibration and varies according to authors [e.g. ns = 1.5 in van Rijn (1985); ns =1 in Beach and Sternberg (1988); ns =0.5 in Waeles *et al*. (2007)].

Bed shear stress obtainable from the erosion formulae can be used to characterise the modes of sand particles transport. For example, at relatively low bed shear stress but still sufficient enough to initiate motion but incapable of suspending the particles in the overlying water body, the bed load transport regime dominates, where particles are only experiencing the first three modes of sediment transport (i.e. sliding, rolling and saltation). Bedforms in the scale of ripples can be formed in such a situation. Generally, ripples are formed when shear stresses are about 10-20% larger than critical shear stress (Julien, 1995; Soulsby, 1997). For relatively higher bed shear stress, the predominant mode of transport is suspension, although as recorded by Soulsby (1997) bedload can still occur but the quantity af sand that will be carried in suspension will often be very much greater than that carried by bedload, especially for fine sands. The transport regime is called sheet flow regime (i.e. the flow regime in which the shear stress exerted on the sediment bed by the fluid flow is strong enough to set in motion a thick layer of particles) where due to strong flows ripples are washed out.

2.5.4 Erosion behaviour of cohesive sediment

The principle of particle erosion described in the preceding section (i.e. Shields' entrainment parameter θ_{ec}) cannot be adequately used to describe erodibility of cohesive sediment because when dealing with cohesive sediment, ideally prediction of cohesion and adhesion forces should not only be based on particle size, but also on mineralogy, organic content, biogenic substances, etc. (Winterwerp and Van Kesteren, 2004; Mehta, 2014; etc.). In numerical models of cohesive sediment transport, the critical shear stress and sediment erosion rate are commonly used parameters. The first set of systematic experiments on erosion of mud beds was carried out by Parthenaides (1965); based on his results, Ariathurai (1974) proposed the following erosion equation, for erosion rate (*E*), defined as the mass of material eroded per unit time once the erosion threshold has been exceeded [i.e. at an excess shear stress ($\tau_b - \tau_e$)] (Grabowski *et al*., 2011):

$$E = M\left(\frac{\tau_b - \tau_e}{\tau_e}\right) \qquad \text{for } \tau_b > \tau_e \tag{2-26}$$

where E ($kg\ m^{-2}s^{-1}$) is the erosion rate, M ($kg\ m^{-2}s^{-1}$) is an empirical erosion parameter; τ_b (Pa) and τ_e (Pa) are the bed shear stress and erosion threshold respectively.

Winterwerp and Van Kesteren (2004) however, cautioned that care must be taken when using Equation (2-26) in establishing M from erosion experiments as it is very sensitive to small errors in τ_e thereby leading to inaccurate results. Equation (2-26) has been generalized [e.g. as Equation (2-27)] by various other researchers (e.g. Sheng, 1984; Lick, 1982; Mehta, 1981; Harrison and Owen, 1971; etc.) and it is widely used (e.g. in mathematical models) for its simplicity (Winterwerp and van Kesteren, 2004). The value of τ_e in Equation (2-27) often varies with depth and time due to consolidation and physico-chemical effects.

$$E = M\left[\frac{\tau_b - \tau_e\,(z,t)}{\tau_e(z,t)}\right]^n \qquad \text{for } \tau_b > \tau_e \qquad (2\text{-}27)$$

where n is generally unity; however, Harrison and Owen, (1971) and Kusuda *et al*. (1985) suggested that n can assume a range of other values. Various cohesive sediment erosion formulae have been proposed by other authors based on that of Partheniades (1965). For instance, Winterwerp *et al*. (2012) treated surface erosion in terms of Mohr-Coulomb failure of the drained layer of flocs exposed at the bed surface. Smerdon and Beasley (1959) presented one of the earliest models to address the issue of sediment cohesiveness, by relating erosion threshold (τ_e) to the cohesiveness of the sediment bed rather than to the clay content, by expressing cohesiveness in terms of plasticity index, *PI* (%). Additionally, Mitchener and Torfs (1996) proposed an equation to estimate critical shear stress (τ_e) by relating it to the bed bulk density.

2.5.5 Erosion of sand-mud mixtures

Section 2.5.2.1 highlights the erosion behaviour of a mixture of sand and mud. From the different experimental works reviewed, it appears that below a critical mud fraction, the mixture behaves like pure sand, whereas above this critical value the resistance to erosion increases with the mud fraction. Based on some of the observed behaviour, these researchers proposed different semi-empirical based relationships to estimate erodibility of beds with mixture of sand and mud. Although, there is still need for more investigation on the subject, van Ledden (2003) and van Ledden *et al*. (2004) undertook a thorough analysis on the various studies on this subject. On this basis, and on the textural classification provided by ternary diagrams (Figure 2.1), they proposed two heuristic

formulas. The first formula was based on the assumption that in a non-cohesive regime, sand and mud particles will behave independently and that the individual sediment component does not affect the erodibility of the other fraction (Winterwerp and Van Kesteren, 2004), hence Equation (2-31) was proposed:

$$E^{sa} - D^{sa} = \gamma W_s(C_e^{sa} - C^{sa}) \;\; ; \quad E^m = \in^m M\left(\frac{\tau_b - \tau_{e,n}}{\tau_{e,n}}\right); \;\; \text{for } \tau_b > \tau_{e,n} \qquad (2\text{-}31)$$

where E = erosion rate, D = deposition rate, W_s = settling velocity, C = suspended sediment concentration, M = erosion parameter, C_e^{sa} = sand equilibrium concentration, and γ = form coefficient, $\in^m$ = mud content, $\in^{sa}$ = sand content. Superscripts m and sa are mud and sand fractions respectively. On the other hand, in the cohesive regime, it is believed that erosion is governed by the cohesiveness of the bed, i.e. mud fraction is active while sand fraction is passive. It is equally assumed that the erosion of sand particles occurs simultaneously with the mud particles at a rate proportional to its fraction; Equation (2-32) was proposed as a result:

$$E^{sa} = \in^{sa} M\left(\frac{\tau_b - \tau_{e,c}}{\tau_{e,c}}\right) \;\; ; \quad E^m = \in^m M\left(\frac{\tau_b - \tau_{e,c}}{\tau_{e,c}}\right); \quad \text{for } \tau_b > \tau_{e,c} \qquad (2\text{-}32)$$

It should be noted that Winterwerp and Van Kesteren (2004) suggested that the erosion threshold of the cohesive bed ($\tau_{e,c}$) and that of non-cohesive bed ($\tau_{e,n}$) may be different, so also their erosion rates.

Jacobs *et al*. (2011) argued that one of the main reasons why there is currently inadequate insight into the determining processes of erosion of a sediment bed is because only highly empirical formulations describing the erosion behaviour of sand-mud mixtures rather than process-based formulations are available. They suggested that, in order to obtain more physically founded, and more generally applicable erosion formulations, a soil mechanical approach is required, such as the approach proposed by Schofield and Wroth (1968). This approach was based on the soil critical-state concept, defined as the end or ultimate state of a deformation process for saturated soils (Schofield and Wroth, 1968). The critical-state model proposed by Schofield and Wroth (1968), relates the mechanical behaviour of soils to the applied loading conditions on one side, and the cohesiveness, permeability, stress history and parking density on the other (Jacobs *et al*., 2011). Some

of the findings of Jacobs *et al*. (2011) from their experiments on surface erosion based on the soil mechanical approach are summarised below:

- Sediment bed deposits exhibits purely granular behaviour for a plasticity index (*PI*) < 2 (i.e. sand rich bed). For larger *PI*, only two types of erosion can occur: flocs and surface erosion.
- Surface erosion threshold exhibits a negative correlation with water content, which is a measure of the packing density. A clear power law relation exists between the threshold and the plasticity index which, according to them, is a bulk material parameter for the cohesiveness of a soil being a function of the clay content and mineral type and the effect of pore water chemistry. (Basis for characterising surface erosion as a drained process in their study).

2.5.6 Modes of erosion

Below critical bed shear (τ_{cs}) erosion is insignificant, whereas significant erosion occurs beyond this threshold. Depending on the flow characteristics, four different modes of erosion (Figure 2.21) have been formulated by Winterwerp and Van Kesteren (2004) based on the geotechnical approach of Schofield and Wroth (1968), and are summarised below:

1) **Entrainment** (Figure 2.21a)**:** occurs when turbulent flow causes entrainment of fluid mud from the surface of the bed into the overlying water body. [*Fluid mud is a high concentration aqueous suspension of fine grained sediment in which settling is substantially hindered* (McAnally *et al.* 2007)]
2) **Floc erosion** (Figure 2.21b): this is the case when individual flocs get disrupted from the surface of the bed by flow-induced peak bed shear stresses.
3) **Surface erosion** (Figure 2.21c): occurs in the absence of pore water pressure gradients (i.e. drained failure process) when the mean bed shear stress is greater than the mean erosion threshold. The implication is that sediment particles (sand and mud) simultaneously and continuously erode from the whole surface layer of the sediment bed, which is in contrast with the random character of floc erosion in spatial and temporal terms.
4) **Mass erosion** (Figure 2.21d): is the last erosion mode, which occurs in the presence of pore-water pressure gradient (i.e. an undrained process) characterise by erosion of lumps of material due to external fluid stresses, which largely

exceed the cohesive bed strength as well as the strength resulting from pore water pressure gradients.

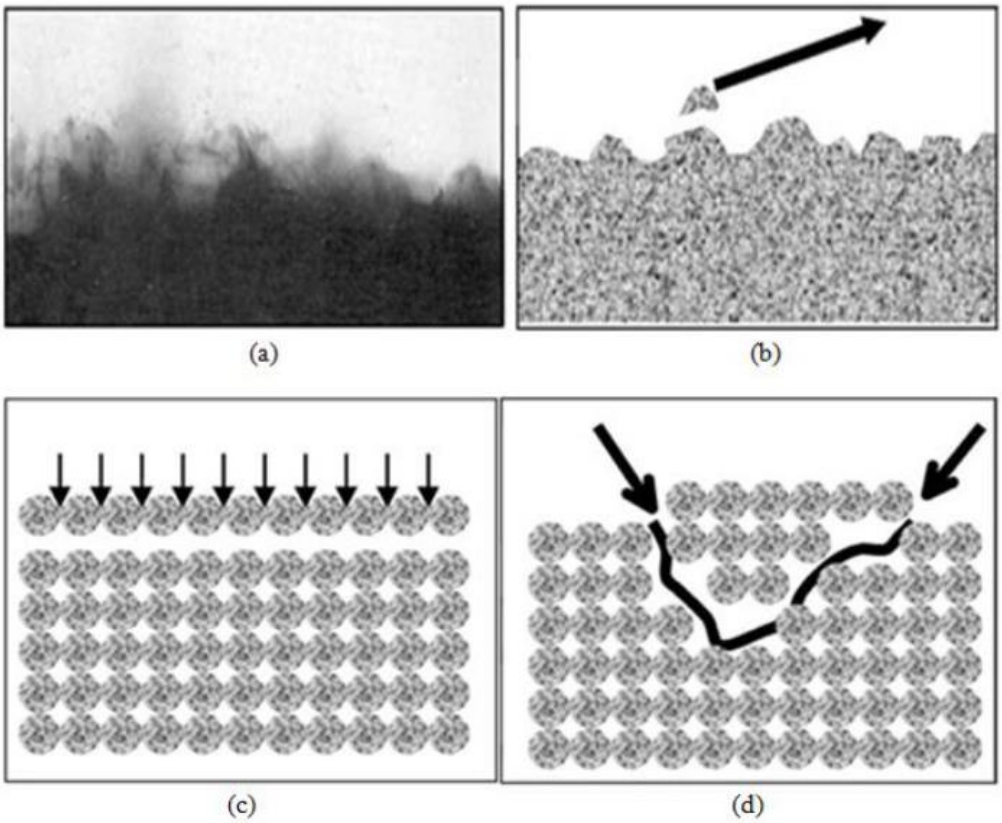

Figure 2.21 (a) Entrainment of mud layer (b) Floc erosion (c) Surface erosion (drained failure) (d) Mass erosion (undrained failure) (Winterwerp and van Kestern, 2004)

2.5.7 Bedform development in mixed (sand-mud) beds

Experimental studies in flumes, modern rivers and intertidal areas have found that, water flowing over a flat-bed will, as the flow-induced shear stress increases, develop a sequence of individual topographic elements, termed bedforms, which generally differ in terms of morphology and behaviour. As an example, Figure 2.22 presents definition of terms commonly used to describe asymmetrical bed-forms under unidirectional flows. These bedforms make up the overall bed configuration, and their geometry (and that of the bed configuration) depends on the depositional environment defined by the sediment properties and flow conditions (Menard, 1950; Ashley, 1990; Baas, 1994; etc). It is a common practice to broadly classify bedforms, based on the flow regime under which they develop (Simons and Richardson, 1961). However, bedforms development is expected to also be influenced by the presence of cohesive clay particles within the bed, as grain size, is reported to have a primary control on equilibrium bedform height and

wavelength (e.g. Baas, 1994, Raudkivi, 1997; Baas *et al*.,2013). Also, in addition, as demonstrated in previous studies (e.g. Mitchener and Torfs, 1996; Jacobs *et al*., 2011), addition of cohesive clay has been shown to increase dramatically, the erosion thresholds of sandy beds. Therefore, cohesive sediment fraction is expected to play significant role in defining the morphology and stability of sedimentary bedforms (Baas *et al*., 2013). The direct application of the information in Figure 2.22 is shown in chapter 6.

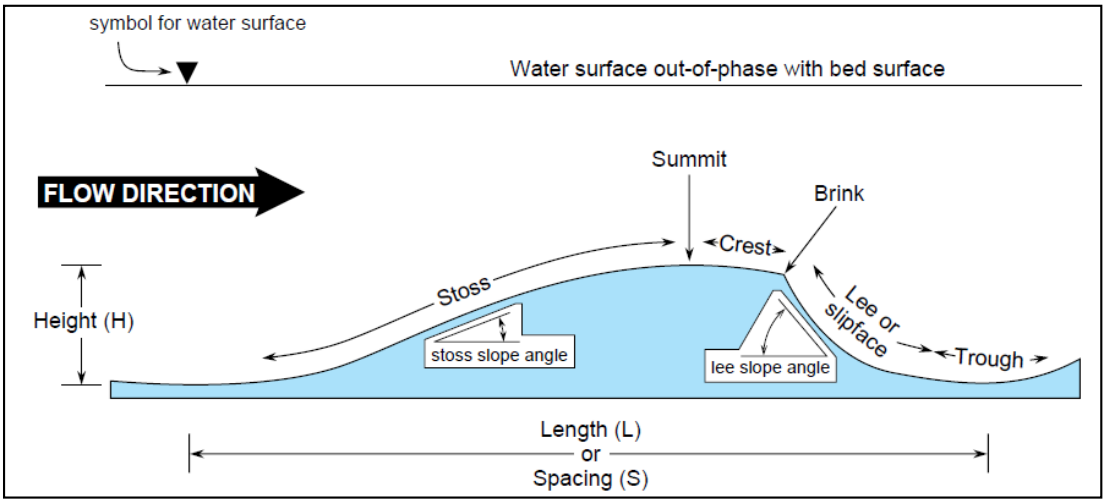

Figure 2.22 Definition of terms used to describe asymmetrical bed-forms that develop under unidirectional flows (Simons and Richardson, 1961).

2.6 Bed Characterisation: Measurement Techniques

2.6.1 General overview

Reliable bed characterisation measurement techniques are unequivocally required for accurate analysis and prediction of mixed sediment settling, deposition and bed re-structuring/consolidation which are essential to improve our understanding of coastal sediment transport and morphodynamics. However, availability of simple and non-destructive measurement techniques to achieve this (for example, characterisation of spatial and temporal variation in sediment bed structure and composition) has been identified as a major challenge [Been, 1981; Ha *et al*., 2010; etc.].

Most traditional techniques are intrusive and end up altering the structure of the bed under investigation. An example of such is *'direct coring'*, which though still regarded as the standard testing method against which to compare measurements from other characterisation methods that require elaborate calibrations for estimation of bulk density. However, density measurements based on core samples are laborious, time consuming,

unreliable, and its spatial and temporal resolution is very low for most applications especially in unconsolidated sediments where the sample is unlikely to be representative of the bulk material by the time it is tested (Ha *et al*., 2010).

Alternatively, from previous experimental studies on sedimentation process, bulk density profiles and porosities of the sediment bed deposits have been successfully obtained by passing high energy X-rays or attenuated gamma rays through the sediment bed (Been, 1981; Pane and Schiffman, 1997; Ellis, 1987; Been and Sills, 1981, Jacobs *et al*. 2009). These nuclear devices are based on the principle that an increase in sediment bulk density will cause the sediment to absorb more nuclear radiation (Hirst *et al*., 1975; Been and Sills, 1981) hence, the bulk density of the sediment can be estimated from the attenuation of nuclear radiation passing through its layers (Ha *et al*., 2010). However, although these X-ray/Y-ray techniques are non-intrusive, they are relatively inflexible, expensive, laborious and have clear health and safety implications. In addition, field loss from these radioactive materials can lead to serious contamination problems (Ha *et al*., 2010).

Recently, other non-intrusive methods such as *acoustic* and *wave attenuation (AWA)* and *turning fork (TF)* methods have been developed (Libicki and Bedford, 1989; Maa *et al*., 1997; Fontein and van der Wal, 2006). *AWA* techniques are based on the principle that acoustic echo strength is proportional to the product of the speed of sound and density (i.e. acoustic resistivity), thus analysis of the acoustic signals returned from the sediment bed can be used as a proxy to calculate corresponding bulk density (Maa and Lee, 2002; Kaya *et al*., 2008). Though they have the advantages of being relatively simple and safe to use, they are however limited to the top layer of the sediment beds and their vertical resolution is relatively too low. *AWA* based techniques have been found to be unreliable in the presence of air bubbles and organic materials; and give varying results depending on the composition of the mud (Hydramotion Ltd, 2013). In addition, the calibration of *AWA* requires direct extraction of sediment sample thereby defeating the non-intrusive goal (e.g. Ha *et al*., 2010). In *TF* devices on the other hand, the bulk density of the medium under test is derived from the vibration frequency of the exposed prongs of the tuning fork (Hydramotion Ltd, 2013). They have drawbacks of being applicable only to low-density fluid mud and require complementary methods for higher density sediment layers. Furthermore, errors in the measurements are very common in these devices because granular material can easily become trapped between the prongs of the fork. (Libicki and Bedford, 1989; Dowling, 1990; Hydramotion Ltd, 2013 and Ha, *et al*., 2010).

The drawbacks of the non-intrusive methods mentioned above emphasise the need for reliable, less cumbersome and non-intrusive sediment bed characterisation measurement techniques. Studies have shown that, although knowledge of the electrical properties of marine sediments is scant, the increasing use of electrical resistivity techniques to study soils has shown significant promise as a viable geophysical tool (Breitzke, 2006; Blewett *et al*., 2001: 2003; Lovell, 1985; Jackson, 1975; Dai *et al*., 2009; Samouelian *et al*., 2005; Schlaberg *et al*., 2006; te Slaa, *et al*., 2013). Hence, one of the main objectives of the current study is to explore and develop a non-invasive characterisation technique based on the principle of electrical resistivity to characterise the spatial and temporal variation in sediment bed structure and composition resulting from differential settling behaviour of the sediment mixtures, without most of the various limitations of other techniques highlighted above.

2.6.2 Electrical resistivity and sediments

The electrical resistivity measurement technique (ERMT) is based on the principle that, when an electric current passes through water-saturated marine sediments, the electrical resistivity of the sediments will depend on the resistivity of both the solid (sand-mud fractions) and fluid components. Hence different combinations of these components should, in theory, have different resistivities associated with them (Breitzke, 2006). As the sediment grains are insulators (or at least poor conductors), it has been concluded that the propagation of electric current takes place via the interstitial pore fluid (Jackson, 1975; Dowling, 1990; Lovell, 1985; Breitzke, 2006). Many researchers have recorded that the dominant transport mechanism for electrical current propagation in a pore fluid is by ionic (electrolytic) conduction. Therefore, current propagation within the water-saturated sediments actually occurs through the *pore spaces* and hence, the resistivity of the sediment bed has been noted to depend both on the conductivity of the pore water and the microstructure of the sediment (e.g. porosity, pore geometry, grain surface morphology and dielectric properties of the mineral grains) [Kanagy and Mann, 1994; Salem, 2001; Wildenschild *et al*., 2000; Roberts and Wildenschild, 2004; Breitzke, 2006; Metayer *et al*., 2010]. Therefore, this dependency or relationship can then be used as a proxy to estimating bulk density.

Electrical conductivity of the pore fluid is, therefore, a function of salinity, pH, dissolved ions/molecules mobility, and concentration (i.e. fluid saturation); while that of sediment microstructure is controlled by the amount and distribution of the pore space, and its

capillarity and tortuosity; common to both is sensitivity to temperature (Breitzke, 2006; te Slaa *et al*., 2013). As a consequence, the electrical resistivity of marine sediments cannot be considered as a bulk parameter solely dependent on relative amount of solid and pore fluid in the bed deposit. However, it has been successfully shown (Archie, 1942; Winsauer *et al*., 1952; Boyce, 1968; Taylor Smith, 1971; Erchul and Nacci, 1972; Jackson, 1975; Sen *et al*., 1981; Lovell, 1985; Wildenschild *et al*., 2000; Samouelian *et al*., 2005; Breitzke, 2006; Blewett *et al*.,2001; 2003; Ibikunle *et al*., 2014) that it can be correlated to bed porosity, wet bulk density and permeability, provided an adequate calibration to a typical sediment composition can be carried out. Recently, electrical conductivity measurements have been successfully correlated to sediment mass concentration [te Slaa *et al*. (2013)] and suspended sediment concentration (Dai *et al*., 2009).

2.6.3 Theory of Electrical resistivity technique: Galvanic method

There have been several models developed to describe electric flow through solid structure like rocks and water-saturated sediments theoretically (Sen *et al*., 1981; Waxman and Smits, 1968, Ruffet *et al*., 1991), but, in practice, because often only few of the required model parameters are known, these models are not very useful, and the most widely preferred model was an empirical equation proposed by Archie in 1942 (Breitzke, 2006). Conventional treatment of rock resistivity data (Archie, 1942 and Winsauer *et al*., 1952) has been to use a term known as the formation factor F to define a normalised resistivity which is the ratio of bulk deposit resistivity of the saturated rock ρ_{bulk} to the resistivity of the saturating liquid ρ_p, and relating F to the porosity φ through the following relationship (Archie, 1942),

$$F = \frac{\rho_{bulk}}{\rho_p} = a\varphi^{-m} \tag{2-33}$$

where exponent m is known as the cementation factor and is related to the tortuosity and connectivity of the pore network within the rock; a is an empirically-derived coefficient of saturation (Winsauer *et al*.,1952 and Breitzke, 2006), which is valid over a particular range of porosities φ. Similar to those of a, values of m are also determined empirically and are characteristic for a given porous rock system. A wide range of values have been reported for m and a for different rock and sediment formations, with a, typically in the range 0.4–2.5 and m ($m > 1$), typically ranging between 1.2 – 3.5 (e.g. Worthington 1993;

Bassiouni, 1994; Devarajan *et al*., 2006; Khalil and Santos 2011). It should be noted that, Archie (1942) postulated that the formation factor F is a constant independent of resistivity of the liquid and solely a function of pore geometry.

This model [i.e. Equation (2-33)] has been extended successfully to study sedimentation of clay slurries (Blewett *et al*., 2003; te Slaa *et al*., 2013), where F is defined as the ratio of the bulk resistivity of the clay-water mixture ρ_{bulk} to that of the water phase ρ_p, with a and m, again, empirical coefficients. Equation (2-33) can thus be used, provided appropriate calibration is carried out, to determine more physically-relevant properties of a porous material, example of such is solids volume concentration ϕ_s (i.e. ratio of the volume of solids to the total wet volume) expression derived by te Slaa, *et al*. (2013), i.e.

$$\phi_s = \left[1 - \frac{\sigma_m}{\sigma_w}\right] \text{å} \qquad (2\text{-}34)$$

where å is an empirically-derived coefficient, σ_w and σ_m are the conductivity of water and the sediment-water mixture respectively (note: conductivity is the reciprocal of resistivity). From Equation (2-34), the corresponding mass concentration c_s can be computed via $c_s = \phi_s.\gamma_s$, where γ_s is the density of the sediment particles.

2.7 Electrical Resistivity Measurements: Technical Issues

Past and recent studies have established the potential of electrical resistivity techniques as a viable geophysical tool to study soils (Breitzke, 2006; Blewett *et al*., 2001: 2003; Lovell, 1985; Jackson, 1975; Dai *et al*., 2009; Samouelian *et al*., 2005; Schlaberg *et al*., 2006); te Slaa *et al*., 2013; Ibikunle *et al*., 2014). However, some key technical issues have been identified which must be adequately addressed before reliable results can be obtained from the techniques, examples of such are: temperature, salinity and pH effects; electrode polarisation; electrode configuration (e.g. spacing, types), cation exchange capacity (CEC) of clay, triboelectric effect and effect of electric field on cohesive force (te Slaa *et al*., 2013; Pahtz *et al*., 2010; Metayer *et al*., 2010; Ha *et al*., 2010; Nowak *et al*., 2005; Winterwerp and van Kesteren, 2004; etc.). The significance of each technical issue differs from one to another and depends on the prevailing environmental or experimental conditions (e.g. in brackish environment, the prevailing issue is likely to be surface conduction of electrically active material, such as clay). In the following sub-

sections, literature has only been reviewed on these technical issues, whilst the methodologies for overcoming them have been extensively discussed in chapter-3.

2.7.1 Electrode configuration

Measurement of electrical resistivity usually requires four electrodes (i.e. 4-point measurement, Figure 2.23a) [Samouelian *et al*., 2005], although, a two-electrode system is also a common practice (i.e. 2-point measurement, Figure 2.23b) [Blewett *et al*., 2001; 2003]. Using a 4-point/electrode configuration (i.e. Figure 2.23a), two of the electrodes (i.e. *current electrodes*), designated by letter A & B, are used to inject current, while the other two *potential electrodes*, designated as M & N, are used to record the resulting potential difference across the sample (Figure 2.23). If the potential difference measured between the electrodes M and N is denoted by ΔV, then the electrical resistivity (ρ) can be calculated using:

$$\rho = k\frac{\Delta V}{I} \tag{2-35}$$

where k is a geometric coefficient (with the unit of length) that depends on the arrangement and geometry of the four electrodes A, B, M and N (Samouelian *et al*., 2005). Various types of electrode combinations have been proposed, each type of combination has advantages and limitations in terms of lateral resolution and vertical penetration (Bernard *et al*., 2004). One aspect of electrode configuration that has not been extensively dealt with in the literature is the effect of electrode horizontal spacing on lateral resolution of the measurements, this has been extensively investigated in the current study. 'k' in Equation (2-35) takes different forms, depending on the geometry and configuration of the electrode. For instance, if resistivity (in $\Omega\, m$), of a unit cubic volume of a specific material is measured between two opposite faces, separated by a distance L, and R is defined as the bulk resistance of the prismatic sample contained between a pair of electrodes (i.e. the two opposite faces) of surface area A (i.e. Figure 2.23c), then the bulk resistivity ρ_{bulk} can be written as:

$$\rho_{bulk} = \frac{RA}{L}\,(\Omega.\mathrm{m}) \tag{2-36}$$

This is the typical relationship for a 2-point plate electrode arrangement e.g. Blewett *et al*. (2001; 2003). However, where a 4-point pin electrode arrangement (e.g. Figure 2.23a)

has been used (i.e. equally-spaced in-line electrodes), the relationship in Equation (2-37) is appropriate.

$$\rho_{bulk} = 2\pi aR \ \ (\Omega.m) \tag{2-37}$$

where '2πa' represent the surface of a hemispherical sphere of radius a.

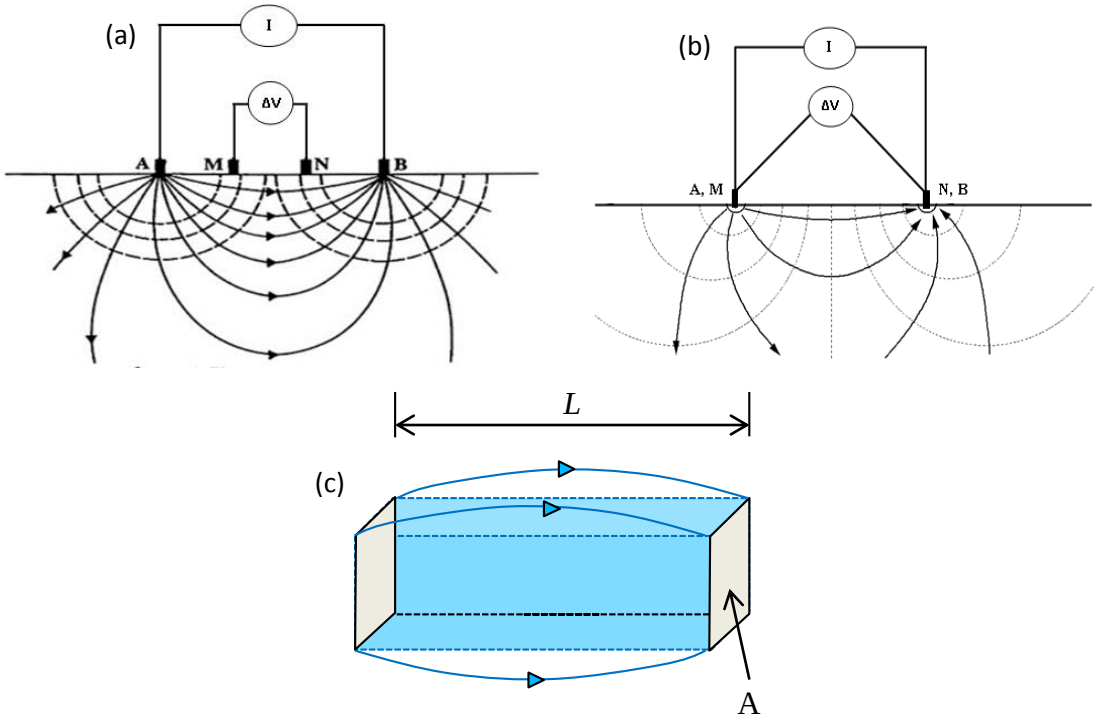

Figure 2.23 Electrode configuration for resistivity measurements showing electric field lines (solid lines) and equipotential curves (dashed lines) (a) 4–point arrangement (b) 2–point arrangement (c) 2–point plate-electrode arrangement.

2.7.2 Electrode polarisation (EP)

EP is one of the identified challenges associated with electrical resistivity techniques and it has been adequately managed in the current study (see *section 3.4.2*). It is mechanisms typically causing formation of compounds that can partly passivate the electrode surfaces thereby render the surfaces less reactive electrically. As an effect, EP can decrease the voltage required by electrolysis cells, lowering currents and increasing the output voltage. When applying electrical resistivity methods to soil or sediment samples, EP will manifest itself as resistivity at the electrode-soil interface shunted in series with the sample resistivity (McCarter and Desmazes, 1997; Carrier and Soga, 1999; and Dahlin, 2000). As shown in Figure 2.23(b & c), in some instances e.g. Blewett *et al*. (2001; 2003) and te Slaa *et al*. (2013), a 2 point-electrode measurement method can be used.

However, electrode polarisation (EP) is a major problem in such configuration especially when plate electrodes are used (Janesch, 2013).

In addition, *fringing effect* (FE) may be observed when the specimen under test is not prismatic. For example, considering the plate electrode arrangement in Figure 2.23c, the geometrical constant *A/L* (i.e. in Equation 2-36) for the pair of electrodes cannot be calculated directly due to *fringing effects* occurring in the electrical field. This fringing makes the area of the field spread, and the length of the field path greater than that obtained from the electrode geometry. Calibration of the electrode pair is required to overcome this challenge (Blewett *et al*., 2003). In 2-point/plate electrode system (Figure 2.23b & c), EP effects on soil are normally eliminated by using alternating current and by monitoring the resistivity over sufficiently wide range of frequencies. This is because EP effects reduce as the frequency of applied electrical field increases (Blewett *et al*., 2003). Obtaining an ideal frequency range at which EP effect can be minimised might however be very difficult when dealing with heterogeneous sediment samples or when the resulting sedimentary forms of the sample cannot be easily predicted, as in the case of bed deposits generated under fluvial processes and with heterogeneous sediments. Excessive EP could result in erroneous resistivity/conductivity results and/or could result in measurement system breakdown; this could possibly explain why te Slaa *et al*. (2013) experienced conductivity signal blurring during measurement in two of their columns. Employing a 4-point pin electrode measurement technique eliminates the effects of EP and fringing with the problems listed above and allows accurate measurement of the bulk resistance of the sample between each electrode pair. Samouelian *et al*. (2005) pointed out, however, that as EP is also attributed to charge build-up at the interface between the electrode and the soil, it can be avoided by not measuring the potential with the electrodes that have just been used to inject current, this is basically the principle behind a 4-point measurement.

2.7.3 Temperature effects

Electrical resistivity decreases with an increase in temperature. To avoid misinterpretation of resistivity measurements either in the laboratory or on the field, it is important that variation in temperature (especially seasonal variation for field application) and its effect on electrical resistivity are accounted for (Samouelian *et al*., 2005). The common practice both in the laboratory and in the field is to measure resistivity and temperature simultaneously and, subsequently, correct the results to an equivalent

resistivity at a reference temperature of choice e.g. 25^0C (Blewett *et al*., 2001;2003; Ibikunle *et al*., 2014).

2.7.4 Cation Exchange Capacity (CEC), Ionic double layer of clay and Surface conduction

Clays with grain less than 4μm in diameter composed of hydrous aluminium silicates and alumina (Al_2O_3), are the most electro-chemically active portion of the sediments. As a consequence, they exhibit a more complex behaviour, especially when occurring in conjunction with other sediment as in the case of shaly sands (Bassiouni, 1994; Grabowski *et al*., 2011). One such complex behaviour is the ability of clay minerals to adsorb certain ions at their surfaces which, in turn, produces an *'ionic double layer'* at the clay surface, if either of the following conditions exists: (i) ions of different valences present in the solution, or (ii) heterogeneous distribution of unbalanced charges on the clay surfaces (Winsauer and McCardell, 1953; Salem, 2001). With respect to the electric current, conductivity in porous media containing clay minerals, the overall influence of *'ionic double layer'* becomes significant as the grains and pores become smaller and smaller (Salem, 2001).

The *'ionic double layer'* has excess negative charges, therefore, for electrical neutrality, hydrated cations will be required from the pore liquid electrolyte (Devarajan *et al*., 2006). The rate and extent of exchange of these hydrated cations depend on clay mineralogy, or the clay *cation exchange capacity* (CEC). Winterwerp and van Kesteren (2004) defined CEC as the number of cations that can be exchanged in the double layer of clay particles. Therefore, in addition to other influencing parameters on the mechanism of electric-current conduction in water-saturated mixed sediments mentioned above, ionic double layer and CEC of clay minerals are also very important.

The failure of Archie's equation (Equation 2-33) to account for the CEC of clay minerals under the influence of an electric field has drawn some criticism in its application on heterogeneous sediments containing clay minerals (Waxman & Smits, 1968, Sen *et al*., 1981, Clavier *et al*., 1984, Ruffet *et al*., 1991, Bassiouni, 1994, Revil *et al*., 1998, Devarajan *et al*., 2006). As a consequence, various empirical models have been developed to address this gap, for example; Waxman-Smits model by Waxman & Smits (1968) and Dual-Water model by Clavier *et al*. (1984) were proposed to account for the dual conductive pathways formed by pore brine and clay mineral exchange cations. The

Waxman-Smith model gave the following expression to address the 'deficiency' of Equation (2-33):

$$\sigma_p = \frac{1}{F}(\sigma_{bulk} + BQ_v) \tag{2-38}$$

where σ_{bulk} *and* σ_p *are* the bulk conductivity of the saturated rock and conductivity of the saturating liquid respectively; Q_v is the cation concentration per unit pore volume (*meg/ml*); and *B* is the average mobility of the counter ions close to the grain surface (mho cm^2/meg) (Devarajan *et al*., 2006). In practice, most of these models are impractical because many of their required parameters (e.g. *B and* Q_v in Equation 2-38) are unknown or very difficult to obtain (Breitzke, 2006), which makes the empirical equation proposed by Archie (1942) still the most widely used, and despite the inherent errors due to surface conduction effects (Breitzke, 2006).

CHAPTER THREE

Methods, Materials and Equipment

"How you climb a mountain is more important than reaching the top."
— Yvon Chouinard

3.1 Introduction

Owing to large amount of uncertainties and variations associated with in-situ investigation of sediment transport processes in marine environments, laboratory studies are often the preferred option in advancing our knowledge and understanding of the mechanisms governing these complex processes. Laboratory studies enable the study of cause and effect as it allows for the deliberate and precise control of one variable, whilst keeping all other variables constant (van Leussen and Winterwerp, 1990). However, findings from laboratory studies have often been found to differ significantly from corresponding observations in natural marine environments, due to assumptions and scaling problems (Cuthbertson, 2001). Nevertheless, the data from laboratory studies have been found to be useful in advancing our understanding of physical processes that govern sediment transport dynamics and have extensively been used in the development and validation of process-based numerical models (e.g. Waeles *et al*., 2008; Le Hir, 2011; Van and Pham Van Bang, 2013, Grasso *et al*., 2015, etc.) that have been formulated to simulate mixed sediment settling and deposition processes and structural development in mixed sediment beds.

Materials, equipment and methods employed in the current laboratory studies are designed to meet the aims and objectives detailed in chapter 1. The experimental procedures described below follow, to some extent, previous settling column and annular flume experimental studies found in the literature (e.g. te Slaa *et al*., 2013; Laksanalamai, 2007; Lintern, 2003; Sills, 1998; Been & Sills, 1996; Mitchener and Torfs, 1996; Williamson and Ockenden, 1996; Villaret and Paulic, 1986; Parchure and Mehta, 1985;

etc.). However, modifications have been made on both the experimental methods and equipment to meet the specific needs of the current work.

In an attempt to ensure that experimental results are applicable to prototype conditions, a theoretical procedure termed 'scaling analysis' is usually employed to establish correct procedures for relating experimental results to the prototype conditions, thereby avoiding incorrect extrapolation of data. As such, in the current study, consideration has been given to this concept, and the 1:1 scaling has been considered appropriate and adopted for all the sediments used, in terms of their size distribution and physical properties.

3.2 Outline of Experimental Studies

The experimental programme is divided into three series, denoted: ES-1, ES-2 and ES-3 and, discussion on 'materials, methods and equipment' is presented separately for each experimental series.

3.2.1 ES-1: Electrical Resistivity Measurements Technique (ERMT)

This experimental programme was undertaken to develop an ERMT for characterisation of sand-mud deposits [i.e. mainly to achieve point (1) of the main objectives of the current study; pg. 6]. In this work, two settling columns with different electrode arrays and configurations were fabricated (*section* 3.5.1 provides a detailed description of the settling columns used in this experimental series). The experiment started with a pilot study conducted within a low resolution acrylic sedimentation column (named: Settling Column-1). The main purpose of this preliminary experiment was to test the feasibility of the electrical resistivity method for characterising mixed sediment deposition. A second acrylic sedimentation column (named: Settling Column-2) was also constructed, in order to develop, test and optimise a higher resolution electrical resistivity measurement, than that offered by the Column-1.

3.2.2 ES-2: Systematic mixed sediment slurry experiment

This series of experiments was carried out in the Settling Column-2, to conduct a parametric study on the settling/ deposition/ onset of consolidation of sand-mud mixed sediments. The purpose of this experimental work was to identify and quantify spatial and temporal variation in sediment bed structure and composition resulting from differential settling of mixed sediments over a wide range of parametric conditions, such

as: initial mixture concentration, mixing fluid salinity and sediment mixture compositions [This is synonymous to points (2) - (3) of the main objectives; pgs. 6 – 7].

3.2.3 ES-3: Mixed sediment bed erosion experiment

The purpose of this experimental work, was to generate a new set of data from time-dependent erosion and deposition processes of placed mixed sediment beds with varying sand-mud fractions [i.e. in line with point (4) of the study's objectives; pg. 7]. This was obtained over a large number of cyclic, unsteady flow events, with the aim of relating the experimental data to the nature and extent of bed restructuring, segregation and stabilisation in mixed sedimentary environments. ES-3 employed a benthic annular flume called *Voyager II* (*section* 3.8.1 gives a detailed description of the annular flume). This flume, is the only commercially available benthic annular flume in the UK and provides an ideal platform to investigate the effect of unsteady turbulent shear flows on the size-selective erosion and deposition of mixed sediments, such as those conditions typically encountered in periodically-reversing (tidally-driven) estuaries or tidal inlets.

3.3 Materials

3.3.1 Cohesive sediment: Kaolin clay

Polwhite B kaolinite (SiO_2= 47 %; Al_2O_3 = 37 %), a high quality medium particle size kaolin clay [D=~0.5–20 μm; D_{50}= 2 μm; plastic limit (PL) = 28 %; liquid limit (LL) = 54 %; SG = 2.59] supplied by IMERYS Minerals Ltd was used in all the experimental series. Typical particle size distribution for this material is shown in Figure 3.1. Kaolin has been used majorly in the current set of experiments for the following reasons, its: (1) behaviour in-situ and in the laboratory has been widely documented in the literature; (2) engineering properties (e.g. Plastic Limit, liquid limit, etc.) are well documented; (3) colour (i.e. white) will allow easy qualitative analysis of the bed deposits when in mixture with the sand, and (4) artificial clay is chosen over natural mud to eliminate influence of biological and organic factors on the experiments in line with the aims of the current study. In addition, reasons discussed in *section 3.4.3* also made kaolin the best choice.

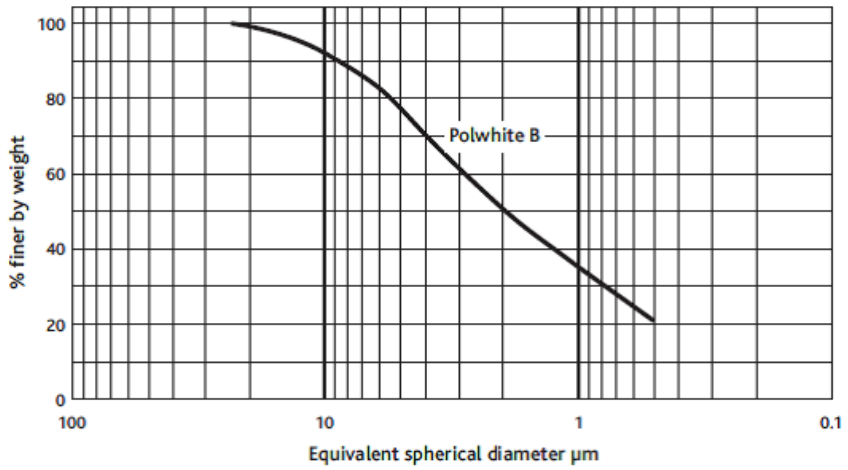

Figure 3.1 Typical particle size distribution for Polwhite-B Kaolin clay (Courtesy: IMERYS Minerals Ltd)

3.3.2 Non-cohesive sediment

The matrix grade of the two sediment types used throughout the experimental programme was a fine to medium, well graded sand. CLS33-Superfine high silica sand (SiO_2> 95 %; see Table 3-1 for particle size distribution) was one of them, the material is super fine [D = ~75–500 μm; D_{50} = 150 μm; SG = 2.64] washed light yellow high silica sand with sub-rounded and highly spherical grains supplied by *Cornish Lime Company Ltd.*

Table 3-1 Particle size distribution (PSD) of CLS33-Superfine High Silica Sand

Sieve size (mm)	% Retained
5	0
2.36	0
1.18	0
0.6	0.87
0.3	43.79
0.15	50.9
0.075	4.42
<0.075	0.02

HST-95 (rounded, light yellow, washed, surface treated and graded quartz based silica sand) sourced from Bent Farm in Congleton, Cheshire was the other fine sand used mainly for *ES-3*. A summary of the HST 95 sand properties is shown in Table 3-2 and its PSD shown in Figure 3.2. The significant advantages of using these sand grades are their (i) distinct yellowish colour, which is ideal for visual observation and qualitative analysis of the mixed bed deposits (ii) relatively finer grading will ensure their differential settling velocities are reasonably closer to that of kaolin (i.e. closer resident time for the fractions within the mixture). Further examination of these sand particles under microscope

revealed they are generally sub-rounded to rounded; this is particularly advantageous as it indicates that the influence of particle shape on the settling velocity would be insignificant.

3.3.3 Brine water

Each experiment requires that the sediments are mixed with water, as the intention was to mimic estuarine and coastal zones conditions especially in terms of salinity, appropriate salt solutions were required. Brackish waters of estuaries (where fresh river water meets salty ocean water) may have salinity levels between 1 and 17 *ppt*, which may vary from estuary to estuary and can change from one day to the next depending on the tides, weather, etc. (Levinton, 1995). For the purpose of this study, salt solutions ranging from '15 – 40 *ppt*' (plus additional controlled solution with 0 *ppt*) were used depending on test conditions. Analytical reagent grade *Sodium Chloride* (NaCl) salt and double distilled water were used to prepare the brine water samples used. The brine water samples were prepared at least 24 *hours* before use to ensure thorough dissociation of the salt.

Table 3-2 Physical properties HST 95

Soil Properties	HST 95 Silica Sand
D_{10} (μm)	100
D_{30} (μm)	120
D_{60}(μm)	140
SG	2.63
Loose bulk density (kg/m^3)	1420

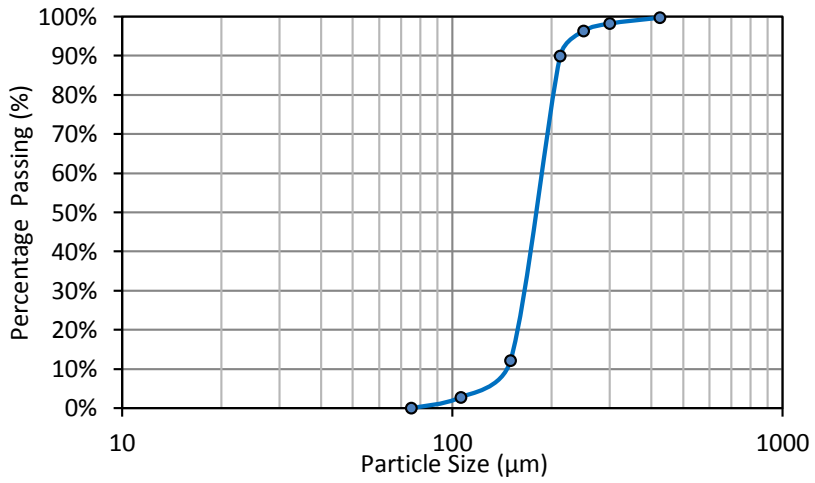

Figure 3.2 HST 95 Silica Sand PSD

3.4 ERMT: Technical Issues

In chapter-2 some technical issues associated with electrical resistivity measurements were highlighted. As a necessity, the most significant of these technical issues are addressed and discussed in the following sub-sections.

3.4.1 Temperature

For ionically conducting sediment, such as the sand-mud mixtures under investigation, bulk resistivity, ρ_{bulk}, and temperature can be linked through an Arrhenius relationship,

$$\rho_{bulk} = Ae^{\left[\frac{E_a}{\Re T}\right]} \tag{3-1}$$

where T is the absolute temperature (K); A is the pre-exponential constant (Ω-cm); $\Re$ is the gas constant (8.314 $J\ mol^{-1}\ K^{-1}$) and E_a is activation energy for the conduction process (kJ/mol).

An increase in temperature results in a corresponding increase in fluid viscosity which, by extension, increases ions agitation in the fluid, thus electrical resistivity decreases with an increase in temperature. Although the experiments for this study were undertaken in a temperature-controlled laboratory (21 ℃ ± 2 ℃), it was still considered appropriate to account for the effect of minor fluctuations in temperature on the measured resistances, as briefly mentioned in the preceding chapter. All the electrical resistivity measurements were therefore expressed at a standardised temperature (in degree Celsius). To achieve this, the temperature variation within the settling sand-clay mixtures was monitored using bead thermistors embedded in the column walls; as the thermistors measurements were in ohms, these measurements were converted to ^{0}C using the ***Steinhart-Hart*** equation (Equation 3.2):

$$T = [A + BlnR + \mathrm{C}\ (lnR)^3]^{-1} - 273.15 \tag{3-2}$$

where R is the measured resistance of the themistor ($ohms$); T is the temperature (^{0}C); A, B and C are coefficients which depend on the type of thermistor, and ln is the natural logarithm. For the thermistor used in this current work, values of A, B and C were evaluated from manufacturer's data to be: $1.288 \times 10^{-3}\ K^{-1}$; $2.357 \times 10^{-4}\ K^{-1}$ and $9.510 \times 10^{-8}\ K^{-1}$ respectively. Once the corresponding temperature measurements in ^{0}C have been obtained for all the experimental results, resistivity values were then *corrected* to an

equivalent resistivity at a predefined reference temperature which was 25 ℃ (i.e. T_{ref}) through Equation (3-3),

$$\rho_{ref} = \rho_{bulk} e^{\frac{E_a}{\Re}\left[\frac{1}{T_{ref}} - \frac{1}{T}\right]}, \quad \left(\frac{E_a}{\Re} = \beta\right) \tag{3-3}$$

Equation (3-3) allows any resistance measured at an arbitrary temperature T to be referred to a standard reference temperature T_{ref} as long as a value for β is known (β is a function of activation energy, i.e. E_a and *universal gas constant,* $\Re$). The values of β for the range of mixing fluids used throughout the test were obtained through a calibration experiments carried out in a controlled temperature chamber. This was done by steadily increasing the temperature of the mixing fluid in the chamber and recording the corresponding changes in resistance (ρ_{ref}). The slope of the graph shown in Figure 3.3 gives for example the value of β as approximately 1.7 K for 0.5M NaCl solution.

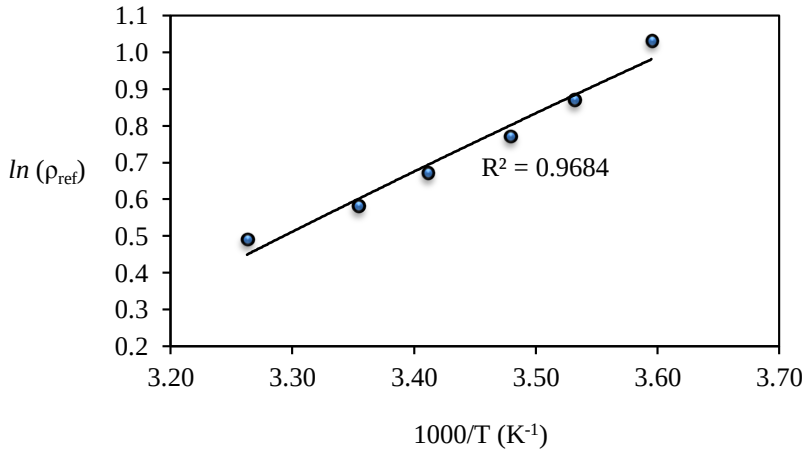

Figure 3.3 Graph of ln (ρ_{ref}) against (1000/T) K^{-1}

3.4.2 Electrode polarization and fringing effects

Figure 3.4 presents the two types of electrode configuration and arrangement, employed in the current work. As discussed in *section* 2.7, a 2-electrode point measurement method (e.g. Figure 2.23 b & c) is generally in use due to its simplicity and ease of automation. However, electrode polarisation (EP) can be a major problem in such a configuration. Throughout the current experiments, a 4-point measurement technique or arrangement (e.g. Figure 3.4) has been employed, which eliminates the effects of EP. In column-1 (i.e. Figure 3.4b) experiments, sufficiently high frequency/signal amplitude (10 *kHz*/1000*mV*) was used to overcoming EP effects from the plate electrodes. The field fringing (Figure

3.4b) was accounted for by the calibration of electrodes to obtain geometrical constant in *Equation (2-36)*.

For each set of electrodes on the array, electrical resistance measurements were taken using a 4-electrode method (see Figure 3.4) with the two outer electrodes (A&B) serving as the current input/output connections, and the two inner electrodes (M&N) served as the voltage (sensing) connections. In addition to the elimination of electrode polarization effects, as the plexiglas column walls can be regarded as a non-conducting boundary, the 4-electrode method has the added advantage that the measured resistance (R) can be converted directly to resistivity, ρ_{bulk}, through the Equations (2-36) and (2.37), (i.e. $\rho_{bulk} = \left(\frac{RA}{L}\right)$ and $\rho_{bulk} = 2\pi aR$) in the case of settling column-1 and column-2 respectively, where '*a*' is the inter-electrode spacing (e.g. 6 *mm* or 20 *mm*).

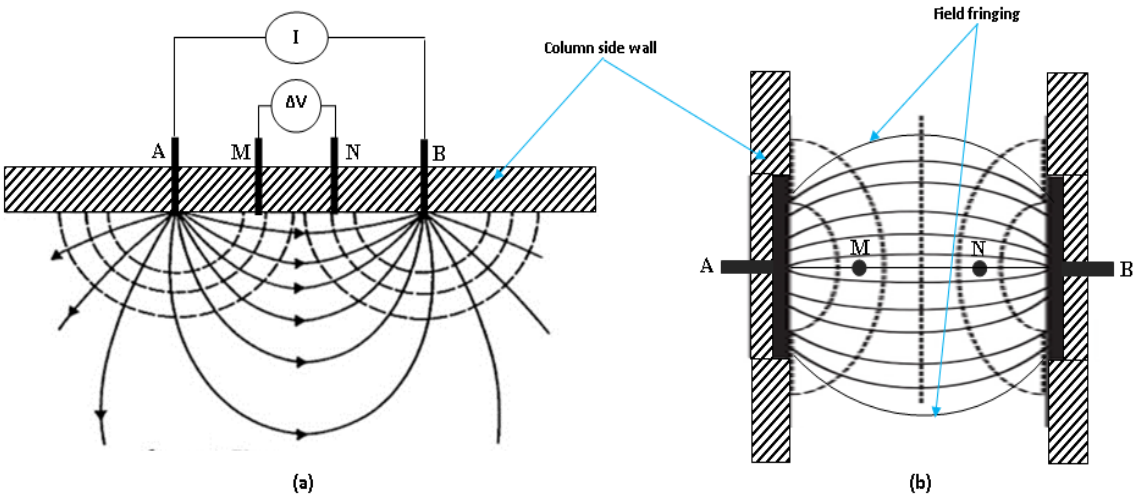

Figure 3.4 Electrode configuration employed in the current study (a) Settling Column-1 electrode array (b) Settling Column-2 electrode array

3.4.3 Ionic double-layer effect

In saturated sand-mud mixtures, the clay particles develop a diffuse, electrical double-layer. This can give rise to surface conduction processes and represents an additional, parallel current conduction path. This effect, however, is only significant in low-porosity systems and when the interstitial pore-water is of high resistivity; the contribution of surface conduction effects on the measured resistance becomes increasingly less significant as the pore-water resistivity decreases (i.e. ionic concentration within the pore water increases) [Revil *et al*, 1998; Wildenschild *et al*., 2000; Salem, 2001]. In such circumstances, conduction via the interstitial aqueous phase dominate over any

contribution from surface conduction. In the current study, the resistivity of the mixing water samples (i.e. 0.1 - 0.5M brine solution) was considered low enough to ensure that surface conduction had a negligible effect on the bulk resistance measurement.

Also, because of the likely role of clay mineralogy in influencing surface conduction, the effect of clay mineralogy was eliminated by using commercially available Kaolin clay, which has a very low CEC relative to other clay minerals (Table 3-3). In addition, the calibration samples were the actual sediments used in the experiments, so any effect (if any at all) of clay mineralogy would have been accounted for in the final results. Furthermore, after each experiment, the resistivity of the pool of water overlying the bed was determined and compared with the resistivity of the initial mixing fluid, the results show no significant difference (see Table 3-4), thereby confirming there has not been significant ionic leaching from the Kaolin clay.

Table 3-3 Important Properties of Clay Mineral Groups

Clay	Density (g/cm^3)	Hydrogen (%)	Average CEC (meq/g)
Kaolinite	2.69	1.5	0.03
Illite	2.76	0.5	0.2
Montmorillonite	2.33	0.5	1.0
Chlorite	2.77	1.2	0.0

Table 3-4 Resistivities of mixing fluid and pore fluid

Sample Composition	Mixing fluid (NaCl solution) resistivity (Ω.m)	Final Pore-fluid resistivity (R_f) (Ω.m)
100% C	0.2175	0.205
50C:50C	0.2175	0.205
75C:25S	0.2175	0.205
25C:75S	0.2175	0.206
100% S	0.2175	0.205

3.5 Experimental Series (ES- 1): Development of ERMT

The tests carried out in ES-1 below, detail experimental procedures to develop non-invasive, electrical resistivity measurements to characterize the spatial and temporal variation in sediment bed structure and composition resulting from differential settling of cohesive kaolin clay and non-cohesive sand mixtures. Two sets of tests (i.e. pilot and high-resolution) were carried out under ES-1 as described below.

3.5.1 Settling columns set-up

The pilot test

The preliminary (or pilot) study into the development of ERMT was conducted within a 50 *mm* by 50 *mm* (i.e. square plan form) by 600 *mm* high acrylic (10 *mm* thick) sedimentation column (i.e. Settling Column-1; Figure 3.5a) with pairs of square stainless steel plate electrodes (50 *mm* × 50 *mm*) at five elevations (centred at z = 25, 125, 225, 325 and 425 *mm* from the column base) embedded within two opposite walls of the column, flush with the internal wall faces. Additional pairs of 1.6 *mm* diameter stainless steel pin electrode were mounted horizontally into the column through one of the other two opposite column walls at the mid-elevations of the plate electrodes. This stainless steel plate-pin electrode arrangement allowed 4-point electrical resistivity measurements to be obtained at the different elevations within the column.

As it would be seen later in the test results (see Chapter 4), the coarse spatial resolution of the electrical measurement results, due largely to the electrode arrangement in settling column-1, meant that a detailed vertical characterisation of the settling and deposition processes was not possible. Therefore, in order to facilitate higher resolution resistivity measurements, a set of tests was further conducted in a larger, demountable settling column as described below.

The high-resolution test

The second test column was constructed with dimensions 150 *mm* by 150 *mm* (i.e. square plan form) by 500 *mm* high (Figure 3.5b). The electrode arrangement in this modified column consisted of sets of four 1.6 *mm* diameter stainless steel pin electrodes embedded through the column walls in horizontal rows, with vertical spacing between these sets ranging from 5 *mm* up to 20 *mm*. The horizontal spacing between the individual electrodes in each set was set at 6 *mm* on one column wall and 20 *mm* on the other wall, to test the influence of electrode spacing on measured electrical resistivity. In total, 35 electrode sets were embedded in both column walls (Note: the electrode sets on the opposite column walls collect electrical measurements simultaneously but independent of each other). Each column has a sealed base and top plate to prevent leakage and/or pore water evaporation. It should be noted that, the design and construction of a rectangular column over a more conventional cylindrical column was chosen for the following reasons (i) ease of embedding resistivity probes especially plate electrodes within the walls (i.e. to allow a wide range of electrode arrays and configuration to be

tested, (ii) to allow the column to be demountable (i.e. for cleaning purposes), and such that four different electrode configurations can be tested simultaneously, and (iii) the clear, flat wall surface of the column makes it easy to capture images of the settling/deposition process without curvature effects.

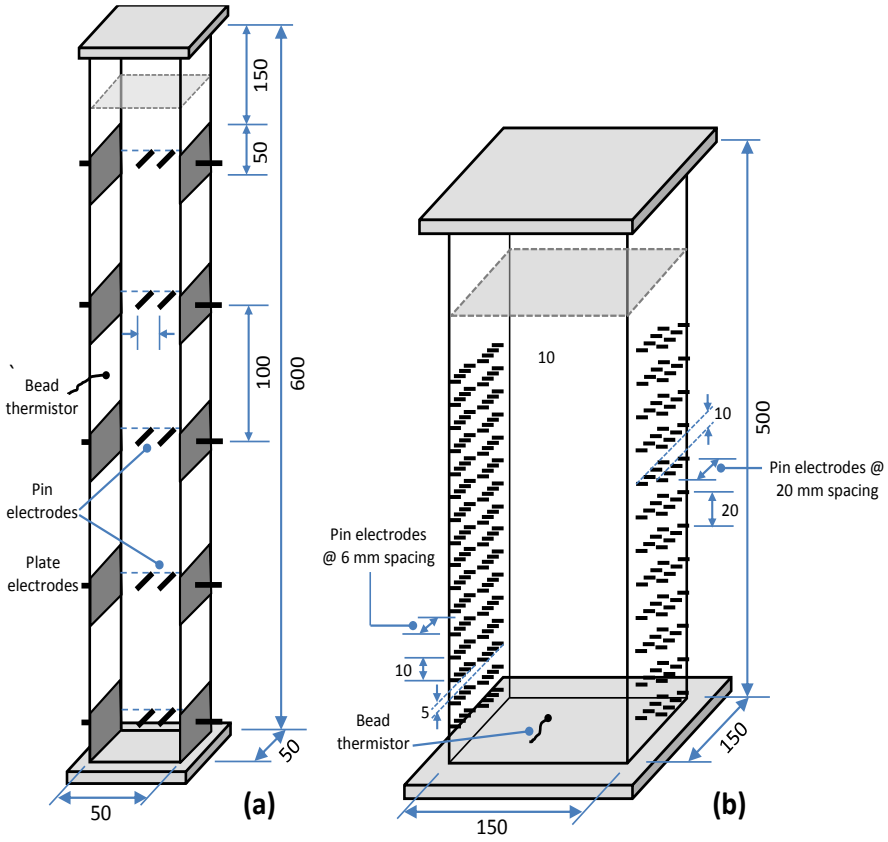

Figure 3.5 Settling column arrangements: (a) 0.6 m-high 4-point (plate-pin) electrode settling column (adapted from Blewett *et al.*, 2001); and (b) 0.5 m-high, high-resolution 4-point (pin) electrode settling column.

3.5.2 Sample preparation and experimental procedure

Prescribed sediment mixtures were generated from the Polwhite-B kaolin clay and fine-to-medium grade quartzite sand (d = 150 – 500 μm; specific gravity, SG = 2.64). The same sample preparation procedures and mixtures compositions were used for both pilot and high-resolution tests; one of the advantages of this was that it makes it more reasonable to compare the spatial and temporal characterization results from both columns. Mixtures were tested for the following sand(s): clay(c) compositions (% by dry weight): (i) 100s:0c; (ii) 75s:25c; (iii) 50s:50c; (iv) 25s:75c; and (v) 0s:100c. Sand-clay compositions were mixed into a concentrated slurry (c_s = 0.33 *g/ml*) with a brine solution (0.5 M NaCl). The concentration of brine water (i.e. 0.5M) allows assessment of the effect of salinity on the suitability of electrical measurement in a brackish environment (Ha *et*

al., 2010; Winterwerp and van Kesteren, 2004). All mixtures (sand, clay and brine solution) were homogenously mixed for minimum of 30 minutes; it is considered that this time was sufficient to achieve a thoroughly mixed sediment-water mixture (te Slaa *et al*., 2013).

Again, for both column tests (i.e. pilot and high-resolution tests), the same experimental procedures were employed; however, the homogenous sediment mixtures in the high-resolution test were designated as follow: 100s:0c = ERM-EX1; 75s:25c = ERM-EX2; 50s:50sc = ERM-EX3; 25s:75c = ERM-EX4; and 0s:100c = ERM-EX5. For each mixture composition, the homogenized sediment mixture was transferred in a *single-shot* into the test settling column [Figure 3.5 (a) or (b)], where the sediment-water mixture was further agitated thoroughly by a grid stirrer for up to 5 minutes after which the mixture is left to settle, this was necessary to prevent preferential settling during placement. For each test, the column was sealed appropriately to prevent evaporation of the pore water. The differential settling and depositional processes for each tested mixture within the columns were monitored over a period extending up to 72 hours. After the initial settling phase (within the first 1 hour), the longer term bed development was monitored at prescribed elapsed times throughout the experiment (i.e. 6, 24, 30, 48, 72 *hours*).

3.5.3 Measurement methods and equipment

In both columns, the differential settling and depositional processes of each sand-clay composition were monitored using a combination of time-lapsed photographic imaging (by Canon EOS 600D, Resolution 18.0 MP) and electrical resistivity measurements over the period of each experimental run. For ES-1, two separate electrical resistivity measurements systems were used, due to varying levels of technicality brought about by the different electrode configurations (see Figure 3.5) within each settling column (i.e. Settling Column-1 and -2). These two measurement systems are discussed separately below. Nevertheless, in combination with the photographic imaging system, both electrical resistivity measurements systems allowed the settling patterns and depositional behaviour of the different mixtures to be investigated and analysed in line with the main aim of ES-1.

The pilot test column (Column-1)

Due to having only 5 sets of electrodes (Figure 3.5a) through which electrical resistivity is measured, time-elapsed measurements were taken manually by connecting the

measurement leads to the appropriate ports on the Hewlett Packard HP4263B LCR meter (see Figure 3.6a). This LCR meter operated at a sample frequency of 10 kHz in a voltage-drive mode with signal amplitude of 1000mV (after Blewett *et al*., 2001).

The high-resolution column (Column-2)

For the high resolution test column, the measurement procedures described above were laborious and obtaining continuous time-elapsed measurements was very difficult as there were about 70 pairs of electrodes to switch through manually for every measurement regime. Therefore, the need for automated system was obvious, however, due to some technical difficulties associated with the available instruments and their limitations at the time; a semi-automatic measurement system (see Figure 3.6b) was developed with which resistance measurements were taken from all the 70 pairs of electrodes within 10-15 minutes.

The electrode sets were wired into Agilent-34970A 4-wire-multiplexer modules, allowing 4-point electrical resistivity measurements to be taken via a data acquisition switch unit (Agilent-34970A) [see Figure 3.6b]. This switch unit was in turn connected via its output ports to the input ports of Hewlett Packard HP4263B LCR meter (see Figure 3.6b). Measurement is trigged by switching through each point (representing each pair of electrodes) on the multiplexer modules with the switching control on the Agilent-34970A. The measurement system operated at frequency and signal amplitude of 1 kHz and 350mV respectively.

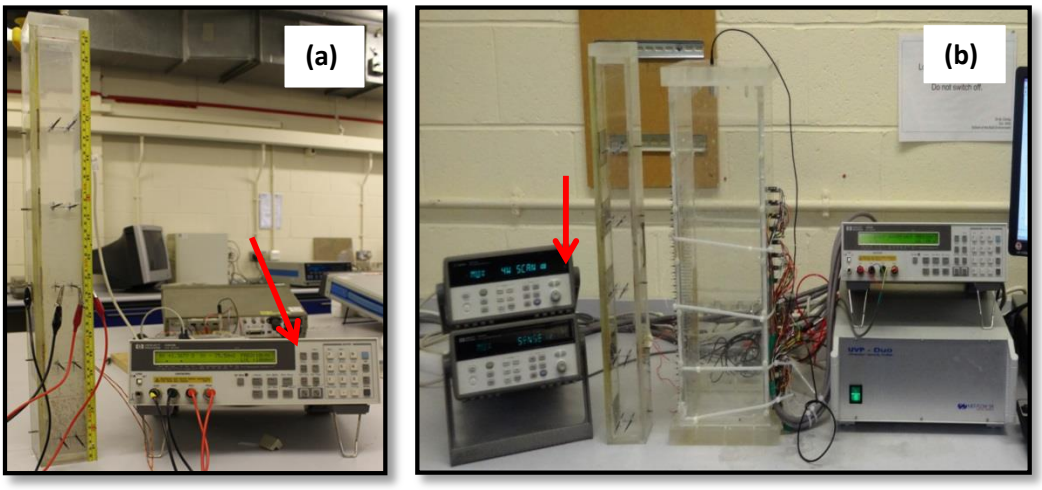

Figure 3.6 Measurement set-up: (a) Preliminary test column only
(b) High resolution settling column

Temperature fluctuations within the sand-clay mixtures were monitored as previously discussed (see *section* 3.4.1). This allowed direct comparisons between the electrical resistivity measurements obtained in all tests by expressing them to a standardised temperature of 25 ℃ (i.e. 295.15 *K*) with the *Arrhenius Equation* (i.e. Equation 3-3). For clarity, each pair of electrodes shall be referred to as (resistivity) probes.

3.6 Calibration of ERMT

Within the study, two calibration procedures were required (for ES-1 and ES-2): (i) calibration of the different electrode configurations within each column to measure bulk resistivity ρ_{bulk}, pore water resistivity ρ_p, and hence, the formation factor *F* [from Equation (2-33)]; and (ii) calibration of the acquired formation factor *F* profiles within the columns to obtain more physically-relevant properties such as bulk density (and, by extension, porosity) and volumetric composition.

3.6.1 Calibration of electrode configuration

Within settling column-1, the bulk resistance *R* of the saturated sand-clay mixture is measured at different elevations within the column between the five pairs of square plate electrodes. Due to the field fringing effects (Figure 3.4b) described earlier, the electrode system had to be calibrated in order to convert the measured resistance R (*ohms*), to resistivity, ρ_{bulk} (in *ohms.m*). Calibration of the electrodes was conducted using a standard solution of known conductivity/resistivity, in this instance, 0.1M NaCl solution, (ρ_p = 8.333 $\Omega.m$) to obtain correction factors *k* (Equation 2-35), which is equivalent to *A/L* in Equation (2-36) for each pair of plate electrodes in the column. The *k* factors for resistivity-probes 2-5 (Figure 3.5a) were 0.1835 *m*, 0.1909 *m*, 0.1888 *m* and 0.1944 *m*, respectively, whereas resistivity-probe 1 had a value of 0.1574 *m*. The significant difference in *A/L* between the resistivity-probes (i.e. 1 and 2-5) is as a result of the non-conductive boundary (i.e. the base of the column) in close proximity to resistivity-probe 1. (Note that if there were no field fringing effects, the theoretical value of the *A/L* for this configuration would be 0.125 *m*)

By contrast, for the pin electrode arrangements in settling column-2 (Figure 3.4a), fringing effect is not an issue, due to the hemispherical electrical equipotential lines generated (Figure 3.4a) (Samouelian *et al.*, 2005). The bulk resistivity ρ_{bulk} from this 4-point pin electrode arrangement is then evaluated from Equation (2-37), i.e. $\rho_{bulk} =$

$2\pi rR$. Calibration of each electrode set within this column was still necessary to account for small changes to electrodes during manufacturing, and it was also performed with 0.1M NaCl solution (i.e. ρ_p = 8.333 $\Omega.m$) initially, and following each experimental run, to check for any alteration or drift in the electrode measurements. The values of '$2\pi r$' for each probe (i.e. all the 70 probes) are presented in *Appendix 3-1*.

Recalling Equation (2-33), i.e. $F = \rho_{bulk}/\rho_p = a\varphi^{-m}$; the cementation factor (m) is related to tortuosity and continuity of the pore network within the material and, any alteration in the porosity or topography of the pore network would result in changes in the F. Therefore**,** the calibrated bulk resistivity ρ_{bulk} measurements obtained for the different sand-clay mixtures at each 4-point electrode set in both columns were then *normalised* by the resistivity of the interstitial pore fluid, ρ_p to obtain the formation factor F from Equation 2-33. In the current experimental configurations, the clear solution forming at the top of the column as the sand-clay mixture settles and deposits is assumed to have the same resistivity, ρ_p, as the interstitial pore fluid within the sand-clay deposit itself. This assumption is, to a large extent, correct as shown in *section 3.4.3* as there was no significant difference between the resistivity (0.2175 $\Omega.m$) of the initial mixing fluid (i.e. 0.5M NaCl solution) and that of the overlying clear pore-fluid resistivity (~ 0.205 $\Omega.m$) at the end of each experimental run.

3.6.2 Empirical equations for physically-relevant properties of bed deposits

As mentioned in the previous chapter, Equation (2-33) has been extended successfully to study sedimentation of clay slurries (e.g. Blewett *et al*., 2003; te Slaa *et al*., 2013). With appropriate calibration being carried out, Equation (2-33) can be used to determine other physically-relevant properties of a porous material. For instance, the solids volume concentration ϕ_s (i.e. ratio of the volume of solids to the total wet volume) of the sediment particles can be calculated as:

$$\phi_s = (1 - \varphi) = \left[1 - \left(\frac{a}{F}\right)^{\frac{1}{m}}\right] \tag{3-4}$$

Note: From Equation 2-33, $\varphi = \left(\frac{a}{F}\right)^{\frac{1}{m}}$.

From Equation (3-4), the corresponding mass concentration C_s and γ_{bulk} of pure clay-water (or sand-water) mixture can be computed via:

$$C_s = \phi_s.\gamma_s, \quad (\gamma_s \text{ is the density of the sediment particles}) \tag{3-5}$$

$$\gamma_{bulk} = (\phi_s \gamma_s + \varphi \gamma_p) \tag{3-6}$$

where γ_s and γ_p are the densities of the clay (or sand) particles and the pore fluid, respectively. For mixtures containing sand, clay and water; the solid volume concentration ϕ_s will then be expressed as:

$$\phi_s = \phi_s^{sa} + \phi_s^{cl} \tag{3-7}$$

where ϕ_s^{sa} and ϕ_s^{cl} are, respectively, the volumetric concentrations of the sand and clay fractions. Hence, the mass concentration C_s and bulk densities of the sand-clay-water mixture are given by the modified expressions,

$$C_s = \phi_s^{sa}\gamma_s^{sa} + \phi_s^{cl}\gamma_s^{cl} \tag{3-8}$$

$$\gamma_{bulk} = (\phi_s^{sa}\gamma_s^{sa} + \phi_s^{cl}\gamma_s^{cl} + \varphi\gamma_p) \tag{3-9}$$

where γ_s^{sa} and γ_s^{cl} are respectively the densities of the sand and clay particles. In the event where $\gamma_s^{sa} \approx \gamma_s^{cl}$ (i.e. = γ_s), then Equation (3-9) can be represented as follows:

$$\gamma_{bulk} = \gamma_s\left(\phi_s^{sa} + \phi_s^{cl}\right) + \varphi\gamma_p = \gamma_s(1 - \varphi) + \varphi\gamma_p = \gamma_s - \varphi\left(\gamma_p - \gamma_s\right) \tag{3-10}$$

Dividing through by the pore fluid density γ_p allows the normalised bulk density γ_{bulk}/γ_p to be determined from Equations (3-4) and (3-10), such that:

$$\frac{\gamma_{bulk}}{\gamma_p} = \frac{\gamma_s}{\gamma_p} - \left(\frac{a}{F}\right)^{\frac{1}{m}}\left(\frac{\gamma_s - \gamma_p}{\gamma_p}\right) \tag{3-11}$$

However, the general validity of Equation (3-11) requires that the Archie equation (i.e. Equation 2-33) for the formation factor F as a function of porosity to be universally valid

over a wide range of sand-clay-water mixture conditions. Specifically, from Equation (2-33), it is clear that empirical parameters *a* and *m* cannot be fitted to satisfy the condition: $F \rightarrow 1$ as $\varphi \rightarrow 1$ (i.e. very dilute suspensions, where $\gamma_{bulk} \rightarrow \gamma_p$), unless *a* is set as unity. However, as noted above, the value of *a* varies within wide limits. As a consequence, the relationship between normalised bulk density γ_{bulk}/γ_p and formation factor *F* is determined through a best-fit power law to calibration measurements on predefined sand-clay-water mixtures (see *section* 4.4.2, pg. 108 for more details). Additionally, expressing the term $(a/F)^{-m}$ as porosity φ in Equation (3-11), then, the following expression can be obtained:

$$\varphi = \frac{\gamma_s - \gamma_{bulk}}{\gamma_s - \gamma_p} \tag{3-12}$$

where, by definition, $\varphi \rightarrow 1$ when γ_{bulk}/γ_p (i.e. very dilute suspensions) and $\varphi \rightarrow 0$ as $\gamma_{bulk} \rightarrow \gamma_p$ (i.e. solid bed with no pore space).

3.6.3 Calibration tests for physically-relevant properties

Relating *F* values to more physically-relevant characteristics of the sand-clay deposits required, further calibration tests. In this case, six saturated sand-clay samples of known fractional composition (i.e. ϕ_s^{sa} and ϕ_s^{cl}) were carefully prepared with 0.1M NaCl solution (ρ_p = 8.333 $\Omega.m$) and mixed to an appropriate consistency such that particle segregation could not occur within the test samples. Each saturated mixture was transferred carefully into a specially designed test ring cell (Figure 3.7) with the embedded set of pin electrodes used to obtain 4-point resistivity measurements (these set of electrodes vary in alignment and position, the purpose for varying the alignment and position of the electrodes was to ascertain that the test sample within the test ring is isotropic). Employing the ERMT and calibration methods described in *sections* 3.5.3 and 3.6.1 respectively, three sets of resistance readings were taken on each test sample and later used to calculate formation factor, *F*.

The specific gravity (G_s) of the mixture constituents (i.e. sand, kaolin clay and brine solution) and sample compositions (e.g. 10s:90c; 40s:60c; etc.) was determined prior to the calibration test in accordance with *BS 1377: Part 2: 1990*. Immediately after each test, the water content (w_c) of the test sample was also determined in accordance with

standard protocol in *BS 1377: Part 2: 1990*. Subsequently, knowing G_s and w_c values, the bulk density (γ_{bulk}), porosity (φ) and void ratio (e) of each test sample were calculated using standard geo-mechanical equations. *Appendix 3-2* presents detailed geo-mechanical equations [i.e. *Appendix 3-2(a)*] and the table containing the results [i.e. *Appendix 3-2(b)*]. A total of three measurements were made for each sand-clay mixture composition to test repeatability and consistency of the calibration method (results of these calibration tests are discussed in chapter 4, i.e. *section 4.5.2*).

It should be noted that, the calibration and experimental series used to develop the electrical resistivity method were obtained at constant salinity and pH, while the temperature was generally kept at average of 21^0C (though all the measurements were converted to standardised temperature of 25^0C later); so, having controlled all the necessary parameters, the resistivity measurements are solely function of solid components (i.e. sand and clay).

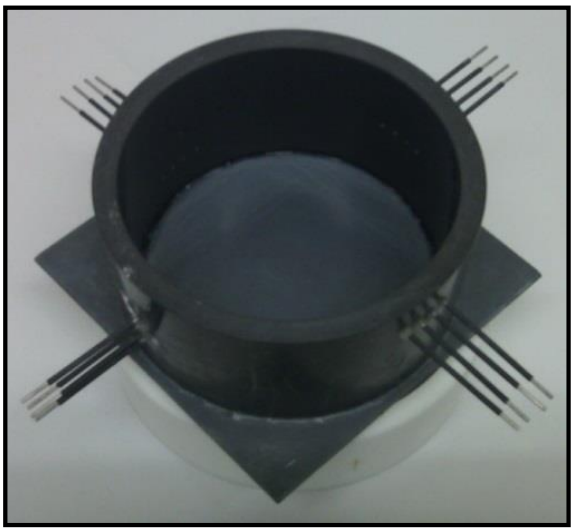

Figure 3.7 Calibration test ring with embedded resistivity probes

3.7 Experimental Series (ES-2): Sand-Clay Suspension Settling Experiment

The preceding series of tests (i.e. ES-1) have been majorly carried out to develop and test the ERMT, one of the deliverables of ES-1 was the potential of obtaining physically-relevant properties of sediment bed deposits (such as bulk density, porosity, etc.) from this non-invasive bed characterisation technique. The extensive knowledge of the applicability of ERMT from ES-1 especially in terms of characterisation of spatial and temporal variations in bed deposit has been employed in the current experimental series (i.e. ES-2), which was designed to investigate the influence of initial mixture concentration, mixing fluid salinity and sediment mixture compositions on spatial and

temporal variation in sediment bed structure and composition resulting from differential settling of mixed sediments.

The experimental set-up and procedures described in the current work are similar to those carried out on most sedimentation and consolidation column experiments performed in the literature (te Slaa *et al*., 2013; Xu *et al*., 2012; Lintern, 2003; Sills, 1998; Been & Sills, 1996; Torfs *et al*., 1996; Imai, 1981; etc.). The difference, however, is that the settling column is custom built (see Figure 3.5b) to facilitate the characterisation of the spatial and temporal variations of the resulting bed deposits within the column (see Figure 3.5b) with the ERMT. Most settling column experiments, for example, start from sediment suspensions of known initial concentration which are poured into the column. The suspension-water interface moves down with time in the column, leaving clear water above, while the bed builds up from the bottom. The resulting sedimentary structure properties are measured as it settles and consolidates. Although, this practice mainly represents events such as excavation of dredging or disposal of dredging materials, nevertheless, column tests have been found useful to study sediments deposition, bed formation and bed restructuring in laboratory environments. Also, because settling is a one-dimensional process (downward movement of sediment and upward movement of water), it can be conveniently modelled at any scale in the laboratory within vertical settling column under controlled conditions. Results from these types of laboratory tests have been extensively used to understand and model sediment dynamics in more environmental realistic conditions similar to those found in natural estuaries and coastal regions.

This section describes, the set-up and configuration of the sedimentation system, comprising the settling column used, image capturing and bulk density/porosity measurement technique employed.

3.7.1 Experimental set-up and procedures

The procedures and set-up for these tests are similar to those described in *section* 3.5.1, but the difference lies mainly to changes in (i) sample composition, (ii) initial slurry bulk density and, (iii) mixing fluid salinity. These changes were necessary to meet the set objectives of this particular experiment, aimed at investigating the development and properties of sedimentary bed structures over a range of mixed sediment compositions, mixing fluid salinity and initial mixture concentration. During settling, vertical resistivity

(see *section* 3.7.3) profiles were measured every 30 *seconds* for up to 24 *hours*. Also, the interface that formed between the supernatant liquid and the settling mixed-sediment layer were recorded manually every 30 *minutes.* Time-lapse photography and videos were equally used (see *section* 3.7.4 on image capturing).

Sample preparation and input

Sediment-water mixtures from Polwhite-B kaolin clay and fine sand were generated for a range of sand(s): clay(c) compositions (% by dry weight), mixing fluid salinity (0 - 40 *ppt*) and initial mixture concentrations (367-813 $kg.m^{-3}$) as shown in Table (3-5). This table also shows the types of measurements made in each test.

Settling column set-up

The 150 *mm* x 150 *mm* x 500 *mm* settling column (Figure 3.5b) described in *section* 3.5 has been used for these tests. A scale bar was attached to the column wall to enable the measurement of interface developments.

3.7.2 Bulk density and porosity measurements

Bulk density and porosity were obtained indirectly using non-invasive electrical resistivity measurements techniques (ERMT) described in *sections* 3.5 and 3.6. Other parameters e.g. volume concentration and void ratio, were calculated from resistivity values (see chapter 4). Calibration of the resistivity probes was carried out after each experimental run; to check for any alteration or drifting of the probes during washing and cleaning or other handling operations. Reference concentration measurement was estimated from resistivity profiles obtained from each sample of the brackish water before the start of each experimental run.

3.7.3 Instrumentation and data acquisition

Due to time dependent nature of the parameters measured in the current experimental series, a fully automated data acquisition system was used for resistivity measurements. The following items of equipment were used (Figure 3.8a-c): (a) a Stanford Research Systems (SRS) SIM900 — Mainframe, (b) SRS-SIM921 — AC resistance bridge and (c) SRS-SIM925 — 4-pole relay multiplexing unit. To get an adequate number of channels, 5 SRS-SIM925 multiplexing units were used. For the purposes of this research, an automatic real time process control programme was configured using the software *WinWedge Pro* with Excel macros, allowing communication between these multiple data

collection devices. Each pair of the electrodes was wired, with wires of negligible resistance, into each channel of SRS-SIM925 module (each SIM925 can accommodate 7 channels); the five SIM925 modules used provided 35 channels in total. The time for one measurement was approximately 1 second per channel, with a complete profile taking approximately 30 *seconds*.

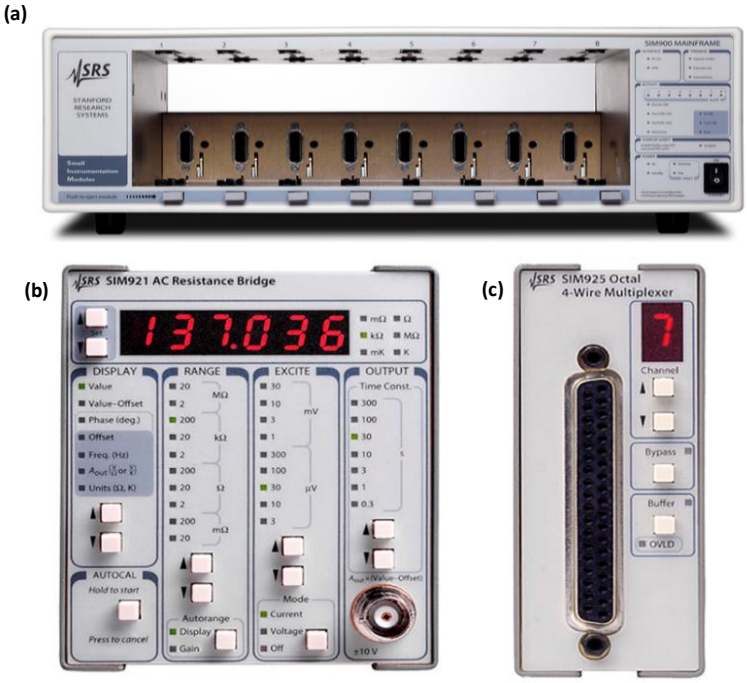

Figure 3. 8 Real-time resistivity measurement system: (a) SIM900-Mainframe (b) SIM921-AC Resistance Bridge and (c) SIM925-4-pole relay switching multiplexer

The above set of instruments within the measurement system facilitates 4-point resistivity measurements, from which bulk density, void ratio, porosity and other relevant data will then be calculated. Throughout the period of each experimental run, temperature fluctuations were monitored and recorded accordingly.

3.7.4 Video and photographic systems

To facilitate a more complete understanding of settling, deposition and bed restructuring processes, time-lapsed photographs and videos were taken at variable time intervals during each experimental run. The video recording was done with GZ-MG20 HDD-based camcorder from JVC, while for still images, a Canon EOS 600D (resolution: 18.0 MP) was used, both were mounted on stable tripods, set at different plane sides of the column (see Figure 3.9). Considering the initial density ranges of the mixed sediment slurries being tested, it was expected that the settling phase will happen very fast, so, EOS utility software, provided by Canon Inc., was used to control the camera. This allowed

continuous image capturing and post experiment editing of the captured images. For each test, the frequency of still image capturing was: 360 images in the initial 30 *minutes* (i.e. 1 image every 5 *seconds*), 12 images in the next 60 *minutes*, followed by 5 images in the following 150 *minutes* and finally 2 images in the last 2 *hours*. It should be noted that these images were mainly used for qualitative observation (see chapter 5).

Table 3-5 Details of the Slurry settling experimental conditions and types of measurements made

Experiment Name	Clay Content (%)	Initial Concentration, C_o (*g/mL*)	Salinity (*ppt*)	Settling Time (*hr*)	Self-weight Height (*mm*)	Density* Profiles (y/n)	Photographic Images (y/n)	Segregation (y/n)
SET-EX1	15	0.561	15	24	470	y	y	y
SET-EX2	15	0.561	30	24	470	y	y	y
SET-EX3	25	0.561	30	24	470	y	y	y
SET-EX4	35	0.561	0	24	470	y	y	y
SET-EX5	35	0.561	15	24	470	y	y	y
SET-EX6	35	0.561	30	24	470	y	y	y
SET-EX7	35	0.561	40	24	470	n	y	y
SET-EX8	35	0.367	30	24	470	n	y	y
SET-EX9	35	0.813	30	24	470	n	y	n

*Resistance measurements could not be obtained for SET-EX8 to EX9 due to some technical problem with the real time measurement system.

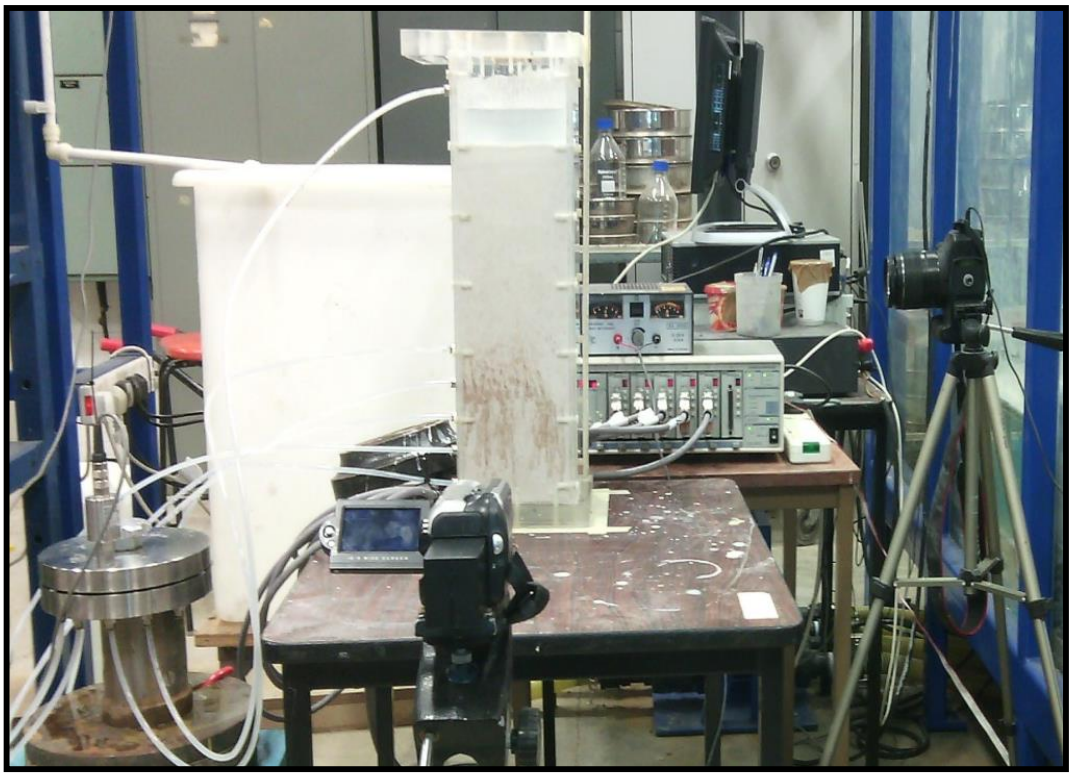

Figure 3.9 Photographic image of ES-3 experimental set-up

3.8 Experimental Series (ES-3): Mixed Sediment Bed Erosion Test

Before bed evolution can be correctly predicted, knowledge of the vertical structure of the sediment is required (Torfs *et al*., 1996; Van and Pham Van Bang, 2013). This set of experiments (i.e. ES-2) was designed to improve our understanding of the dynamics of natural sediments sedimentation and bed formation processes over a range of parametric conditions (e.g. initial mixture concentration, ambient salinity and sediment compositions), which are important to accurately assess and predict erosion and deposition processes that take place in estuarine and near-shore coastal marine environments. The settling column experiment, such as the one described above, is a one-dimensional process which may not fully capture the dynamic physical processes common in sedimentary environments. The sedimentation of fine-grained sediment in estuaries is largely governed by accelerating and decelerating tidal flows (van Leussen and Winterwerp, 1990). This process, and the subsequent erosion and deposition of the fine-grained sediments within estuaries is further influenced and/or complicated by a number of factors, such as river discharge, wind-driven flows, waves, salinity and the fine-grained sediments' properties (Scott, 1984; van Leussen and Winterwerp, 1990; Cheng, 1997; Dankers, 2006; Le Hir *et al*., 2011; etc.).

The specifications and geometry of the benthic annular flume used in the study are detailed; the challenges faced, and considerations made in respect of some important aspects when using this facility in the laboratory, are discussed. Details of how the flume was adapted for the laboratory-based study are described, e.g. design and construction of housing tank for the flume. The bed composition, preparation and placing are also outlined. Finally, a comprehensive description of the instrumentation and measurement techniques used to obtain parameters such as bulk density, 3D flow profiles and suspended sediment concentrations is provided.

3.8.1 Description and operation of the annular flume

The use of an annular flume permits monitoring of cohesive and mixed sediment transport processes in an infinite length channel under fully-developed turbulent flow conditions generated above the erodible sediment bed, with no disturbance or interruption from pumps, etc. The annular flume employed for the erosion tests was a 'Voyager II Benthic Flume' supplied by Partrac Consulting Ltd (Figure 3.10). The use of benthic annular flume in the current study, is unique as it provides a link between field and laboratory-based experiments.

The Benthic annular flume, which was based on the designs and dimensions of Amos *et al*. (1992), consists of an aluminium channel 0.3 *m* high (*H*) and 0.15 *m* wide (*W*), with a total diameter (*D*) of 2.2 *m* (Figure 3.10). Eight equidistantly spaced paddles (Figure 3.11a) induce a current via a train drive, driven by a 0.6 *hp*, 24 V DC submarine motor and gearbox. The lower tip of the set of paddles is ~200 *mm* above the nominal bed level. Eight lid sections, each equipped with a lid which can open to allow flushing of water during flume deployment, are arranged on top of the channel (one section is transparent which allows the paddle drive train to be easily seen). A 0.07 *m* wide and 0.005 *m* thick skirt around the outer channel wall allows the flume to sink ~45 *mm* into the bed evenly, and ensures a constant channel depth. An on-board computer ensures accurate control of the flow conditions within the enclosed flume by driving the eight equidistantly-spaced paddles (Figure 3.11a) at a specified rotation rate. This allows either steady or pre-programmed cyclic and reversing flows to be simulated. The flume itself is equipped with state-of-the-art instrumentation including a Nortek-Vectrino velocimeter for measuring flow velocities and turbulence characteristics (at 0.15 *m* above the nominal bed level) [Figure 3.11b] and optical backscatter sensors (OBS) for turbidity measurements at three different heights (centres at 85, 145 and 200 *mm* above the nominal bed level) [Figure

3.11c]. A Perspex™ window on the internal channel wall allows for submarine video imagery to be recorded while the flume is in operation.

3.8.2 Setup and bed configuration

In order to adapt the Benthic annular flume to this laboratory based study, it was housed within a custom-built 2.5 *m* x 2.5 *m* x 1.5 *m* tank, 3 sides of the tank are glass-walled while the last side is made up of waterproof marine plywood (see *Appendix* 3-3). Figures 3.13a & b respectively show the schematic diagram and plan view of the set-up. The tank has four hoses (50 *mm* diameter) connected close to the corners of the tank at the base; these are for filling and draining of the tank accordingly. For easy drainage and prevention of loss of materials, from the base, the tank was layered with 200 *mm* gravel, followed by 0.5 *mm* geotextile filter fabric and finally, 1 *mm* perforated stainless steel sheet (Figure 3.13).

Figure 3.10 Voyager II in-situ benthic annular flume (Courtesy: Partrac Consulting Ltd)

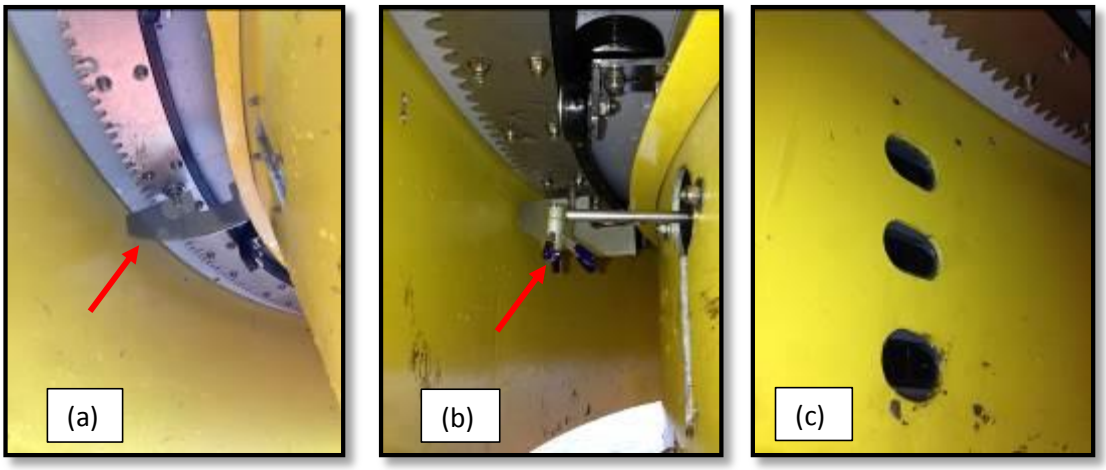

Figure 3.11 Images showing (a) the paddle (b) ADV probe (c) the vertical OBS array (Red arrows point to the paddle and ADV probe respectively) [Courtesy: Partrac Consulting Ltd]

The sediment bed was placed on the perforated sheet. In order to have platforms to stand on for any adjustment or inspection, platforms were made with bricks and wooden boxes at the centre of the tank and sides close to the walls. These platforms also served as supports for the flume (Figure 3.12b).

3.8.3 Bed preparation and placing

Artificially generated sediment beds have been used; the beds are homogeneous and unconsolidated, such beds normally have nearly-uniform density from top to bottom. Although sediment beds in estuaries and tidal lagoons often consist of a mixture of sand and mud, their mode of occurrence could be such that sand and mud fractions can be homogeneously mixed, form alternating layers or occur in patches (Jacobs *et al*., 2007). Research has shown that the erosion and deposition processes are not only dependent on sediment mixtures but also on the mode of their occurrence (Winterwerp and van Kesteren, 2004; Jacobs *et al*., 2007; Mehta, 2014). However, the current study is aimed at investigating the effect of varying clay content within sandy beds on the erosion and deposition characteristics of such artificially generated sand-clay mixtures. The occurrence of sediment beds with these properties is highly unlikely; it is, however, believed that the artificially generated sand-clay mixtures used in this study can form a reference for mixtures with more natural properties.

To generate the artificial beds, it is assumed that the generated sediment beds are isotropic (i.e. their vertical and horizontal properties are the same) and that the following requirements are met in order to obtain reproducible bed samples:

1) The sediment samples should be fully saturated; this is important as clay particles need to be saturated to exhibit cohesive behaviour; and,
2) The sediments samples should be homogeneously mixed in order to avoid segregation during placement and, as an effect, result in non-uniform erosion behaviour
3) The sediment samples should be adequately plastic for ease of placement within the holding tank.

For a 100% sand-bed, the tank was filled with dry sand to the designated height (see Figure 3.14) which was then flooded with tap water (note, all the tests under this section was conducted with tap water). For each experimental run with mixed sediments bed, the approach was different. The measured fractions (i.e. sand, kaolin and water) were firstly mixed in a '15W-40' rotary mixer (The Creteangle Multi-Flow Mixer; Type ME/CL) (see *Appendix 3-4)* for up to 30 *minutes* before being transferred into the tank. The quantity of water added in each case was sufficient to ensure proper mixing but not enough to cause segregation of particle fractions.

For the current test, the following sand(s): clay(c) bed compositions (% by dry weight) were used: (i) 100(s):0(c) [EDT-EX1]; (ii) 98(s):2(c) [EDT-EX2]; (iii) 95(s):5(c) [EDT-EX3]; and (iv) 90(s):10(c) [EDT-EX4]. These sediment compositions were chosen, such that the effect of low clay fractional contents, on the erosional behaviour of predominantly sandy beds could be studied. Previous studies (e.g. Raudkivi, 1998; Dade and Nowell, 1992; Mitchener and Torfs, 1996; Panagiotopoulos *et al*., 1997; Whitehouse *et al*., 2000; Baas *et al*.,2013) observed that, once the cohesive fraction (i.e. mud) within a sediment bed exceeds 5 - 10 % by weight, the bed cohesion becomes the dominant control on erosion rate.

3.8.4 Instrumentation and visualization techniques

This section describes the techniques and instruments employed within the experimental set-up to measure flow turbulent characteristics, suspended sediment concentration (SSC) and real time bed bulk density/ porosity. Visualisation and image capturing devises are also discussed.

3.8.4.1 Acoustic Doppler Velocimeter (ADV)

A Vectrino®, 3-D ADV manufactured by Nortek-AS™ was used to measure mean and turbulent flow characteristics within the flume. The measurement technology of ADV probe is based on the principles of Doppler processing. This particular Vectrino has a side looking probe (Figure 3.15) but because of the way it is fitted within the flume it operates as a vertically oriented probe, i.e. down-looking, this orientation is ideal for measuring turbulence characteristics close to a bed surface. The ADV probe measures the 3-D instantaneous velocities and turbulence characteristics in tangential (x), radial (y) and vertical (z) directions of the flow within a sampling volume located at a known distance below the tip of the probe.

The ADV probe was mounted within the flow, 0.15 *m* above the nominal bed level, through an opening on the side of the flume wall (Figure 3.11b). The sampling rate chosen was between 20-25 *Hz*, and other relevant user-defined specifications were appropriately set (e.g. sampling volume was set at ca 240 mm^3), to ensure detailed measurement of turbulence characteristics. Simplicity of set-up and operations is the main attraction of this device, it requires no probe calibration and detailed time series data of the turbulent characteristics can be obtained and viewed on the go. Post-processing of large ADV data has also been made easier with *WinADV* software.

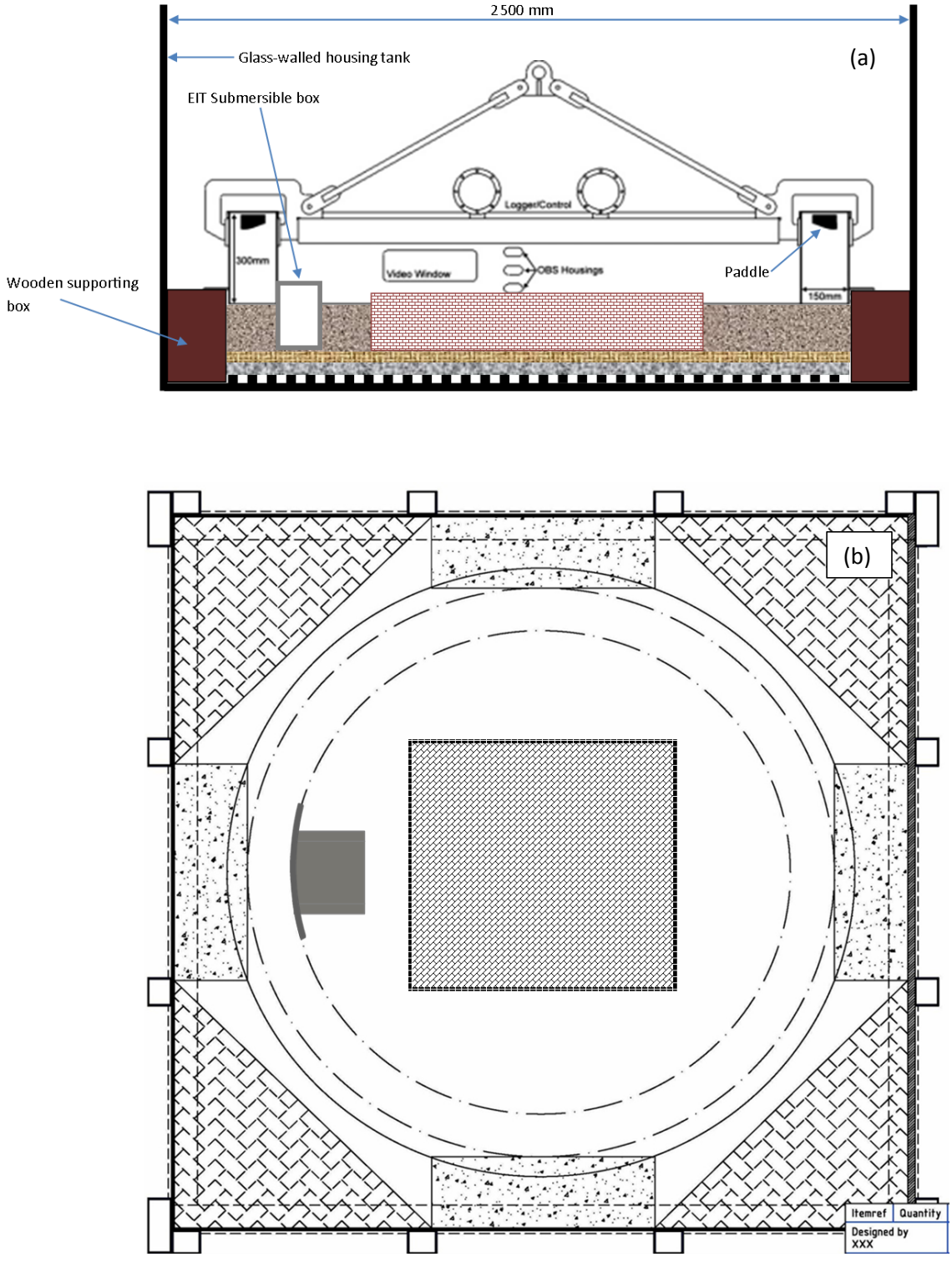

Figure 3.12 (a) Schematic diagram of experimental set-up (b) Plan view of the set-up

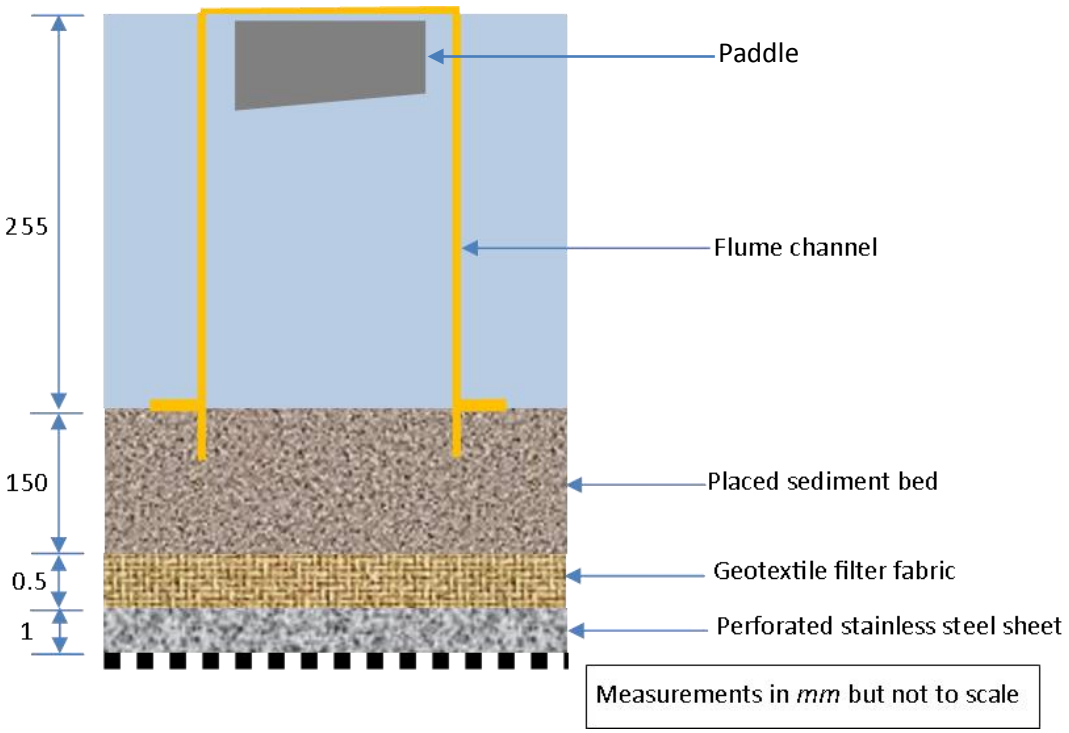

Figure 3.13 Artificial bed configuration for ES-3

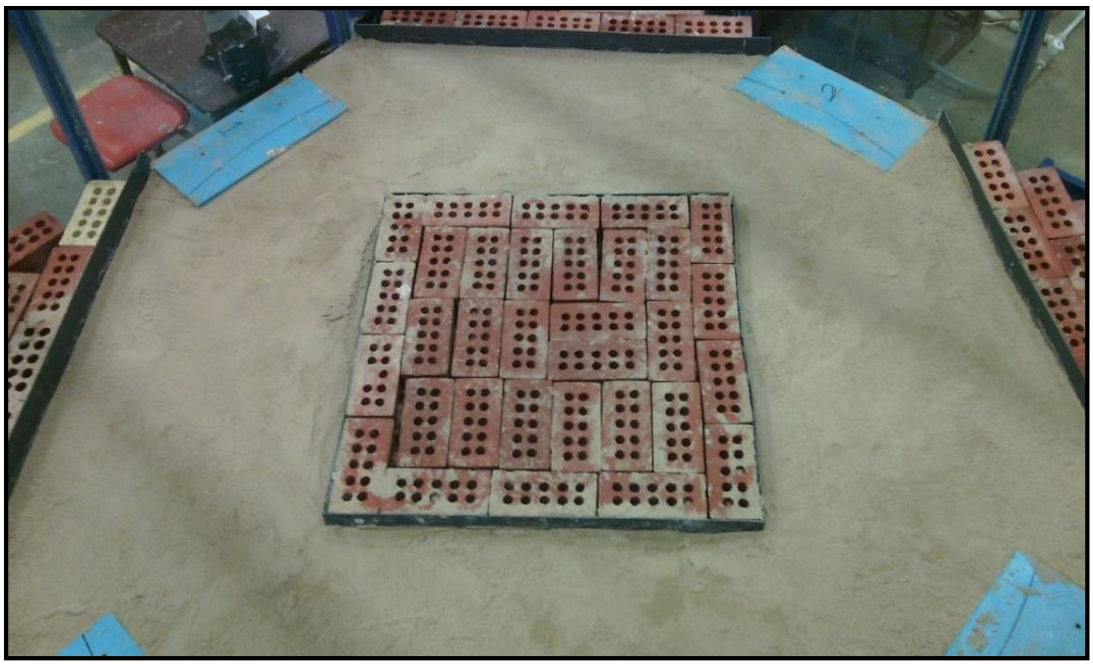

Figure 3.14 Image showing 100% sand bed prior to wetting and placing of annular flume

Figure 3.15 3-D Side-looking ADV probe (from: www.nortek-as.com)

3.8.4.2 Optical backscatter sensor (OBS)

A special on-board OBS measurement system was required to obtain the SSC due of the nature of this experimental set-up. The system employed two devices: a 'XR-420CT+Tu data logger' manufactured by RBR® and an auto-ranging *Seapoint Turbidity Meter* by Seapoint Sensors Inc (Figure 3.16). RBR's 'XR-420CT+Tu' is a small, autonomous data logger powered by four 3V CR123A cells. It is designed to monitor (1*Hz* sampling rate) and store recorded data on its inbuilt internal memory (8MB Flash). The turbidity meter comes in *delrin polymer* pressure case making it rugged and water-tight. Two of the major advantages which made the *Seapoint Turbidity sensor* very suitable for the current study are: (i) ability to sense scattered light from a small volume within 5cm of the sensor windows, which allows the sensor to be calibrated in relatively small water containers without errors from surface and wall reflections; and (ii) the small sampling distance (i.e. 5 *cm* from the sensor windows) allows the sensor to be used in confined spaces and where limited volumes of water exist, such as it is with the Benthic annular flume.

For the current study, three of the measurement systems described above were used to measure turbidity in *NTU* within the flume's channel at three different heights (centres at 85, 145 and 200 *mm* above the nominal bel level, see Figure 3.11c) during erosion and deposition processes. Prior to deployment of the OBS measurement system, they were locally connected to a computer to be configured, scheduled and enabled [i.e. set measurement parameters, set frequency/time scales (3*Hz* over 5 *hours* was used), and initiate measurement respectively] in *Ruskin*® which is a software package that provides

a graphical user interface to manage and control the loggers. When already deployed or during operation, data sets were graphically viewed in *Ruskin*®. Finally, after each experimental run, the data were downloaded and exported in a range of formats with the same software. Figure 3.17 shows an example of turbidity-time series plot obtained during one of the erosion tests.

To obtain SSC (*g/l*) from the OBS Turbidity measurements (in *NTU*), the OBS was calibrated. The best way to do this would be to take water samples immediately adjacent to the sensor and develop a *numerical relationship* between the signals and the SSC values of the samples; however, this was found impractical because of limited access. An alternative approach was to calibrate the OBS sensors with the sediments used for the study. This was done by incrementally adding a known quantity of the sediment to a fixed volume of water. A small submersible pump was placed in the container to ensure uniform mixing of the suspension. Figure 3.18 shows the calibration curve from which a numerical relationship between the sensor's signals (in *NTU*) and the SSC values (in *g/l*) was obtained. One major problem with the OBS measurement system however, was that output was non-linear above 750 *NTU* (see Figure 3.18); the implications of this were further discussed in chapter 6.

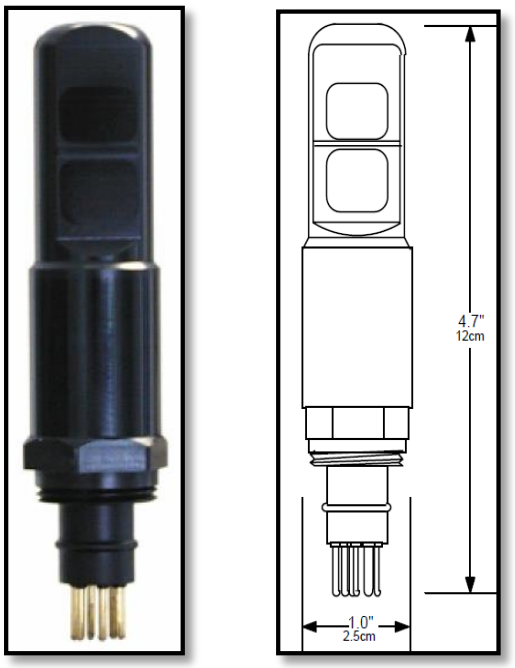

Figure 3.16 The Seapoint Turbidity Meter (adapted from the users' manual)

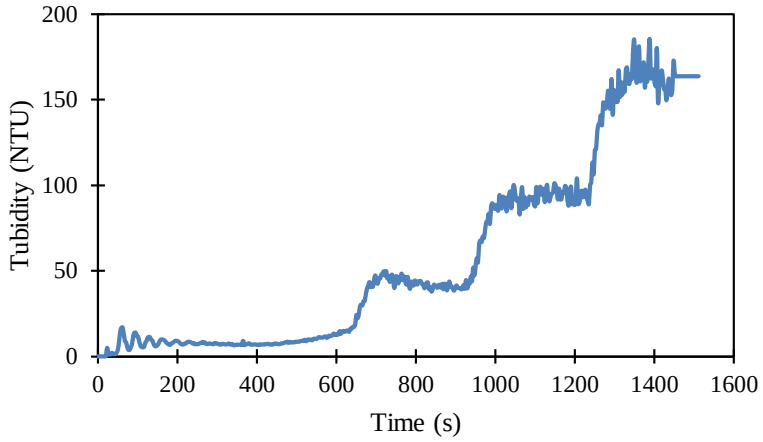

Figure 3.17 Example of turbidity-time series plot

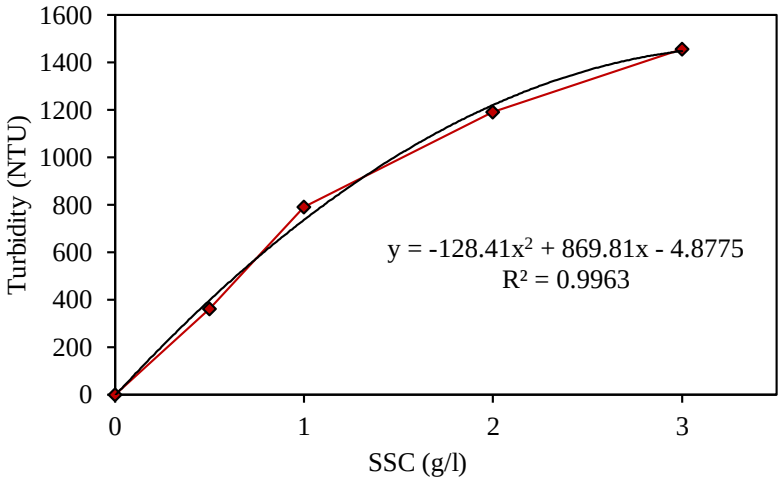

Figure 3.18 SSC versus Turbidity calibration curve

3.8.4.3 Novel submersible resistivity measurement box

Exploration of the electrical resistivity technique described in *sections (3.4)* and *(3.5)* was further extended to capture evolution and restructuring of sediment bed under turbulent flow conditions. This application meant that the measurement set-up had to be water proof (i.e. the wiring has to be adequately concealed) and capable of being adapted to the benthic annular flume. These requirements necessitated the design and development of a *novel custom built submersible 4-point resistivity measurement box*. The box (165 *mm* x 165 *mm* x 210 *mm*) was fabricated from 10 *mm* thick clear acrylic Perspex (Figure 3.19a). 30 pairs (each pair containing four 1.6 *mm* diameter stainless steel pins) of electrodes were embedded into the side in contact with the bed [i.e. the (50*mm* x 10*mm* x 210*mm*) rectangular plate firmly glued to the main face of the box] (see Figure 3.19b for the schematic diagram of the electrode arrangement). Due to the nature of its deployment, and to compensate for any gap between the bed and the box during placement, the tips of

the electrodes protruded by 1*mm* from the plate. The vertical and horizontal distances between and within each pair of electrodes were approximately 5mm and 6mm, respectively. To ensure stability, lead plates were sealed within the box, although once implanted in the bed, additional load was always placed on the box. These electrodes were wired-up accordingly to work with the data acquisition techniques described in *section 3.7.3*. Calibration of each set of the electrodes was performed similarly to the method previously described in *section 3.6.* The box was immersed in a tank full of 0.1 M NaCl solution and 5 sets of resistance measurements of the fluid were taken for onward calculation of the values of '$2\pi r$' (i.e. geometrical constant) for each of the electrode pair (see values of '$2\pi r$' for each pair of electrodes in *Appendix* 3-1). The resistivity data obtained for each erosion test were converted to bulk density following the procedures described in *section* 3.6.

3.8.4.4 Video and photographic systems

To facilitate better understanding of suspension, deposition and bed restructuring processes, video recording was done with 12*MP Professional Grade HERO3+ Black edition of GoPro camera* with ultra-sharp $f/2.8$ - 6 element aspherical glass lens and ultra-wide angle with reduced distortion. The main reasons for using this camera are (i) up to 30 frames per second achievable (ii) built-in Wi-fi making it possible to control remotely (iii) most importantly, waterproof to 131'/40 *m*.

A Perspex™ window on the internal channel wall of the annular flume allows for submarine video imagery to be recorded. The GoPro camera was fixed to look through the window at an angle to provide an oblique view across the sediment surface within the channel. A sealed submarine lamp (*Aquabeam*) was used to illuminate the bed surface through the Perspex window. Unfortunately, the video images recorded were not useable because of the poor quality of the video imagery resulting from excessive turbidity generated within the flume during the test. On the other hand, still images of the resulting bed after each experimental run were taken with 18.0 *MP* Canon EOS 600D camera. Extreme care was taken when lifting up the flume after each experimental run, this was to ensure no or minimal disruption to the bed before post experimental analysis.

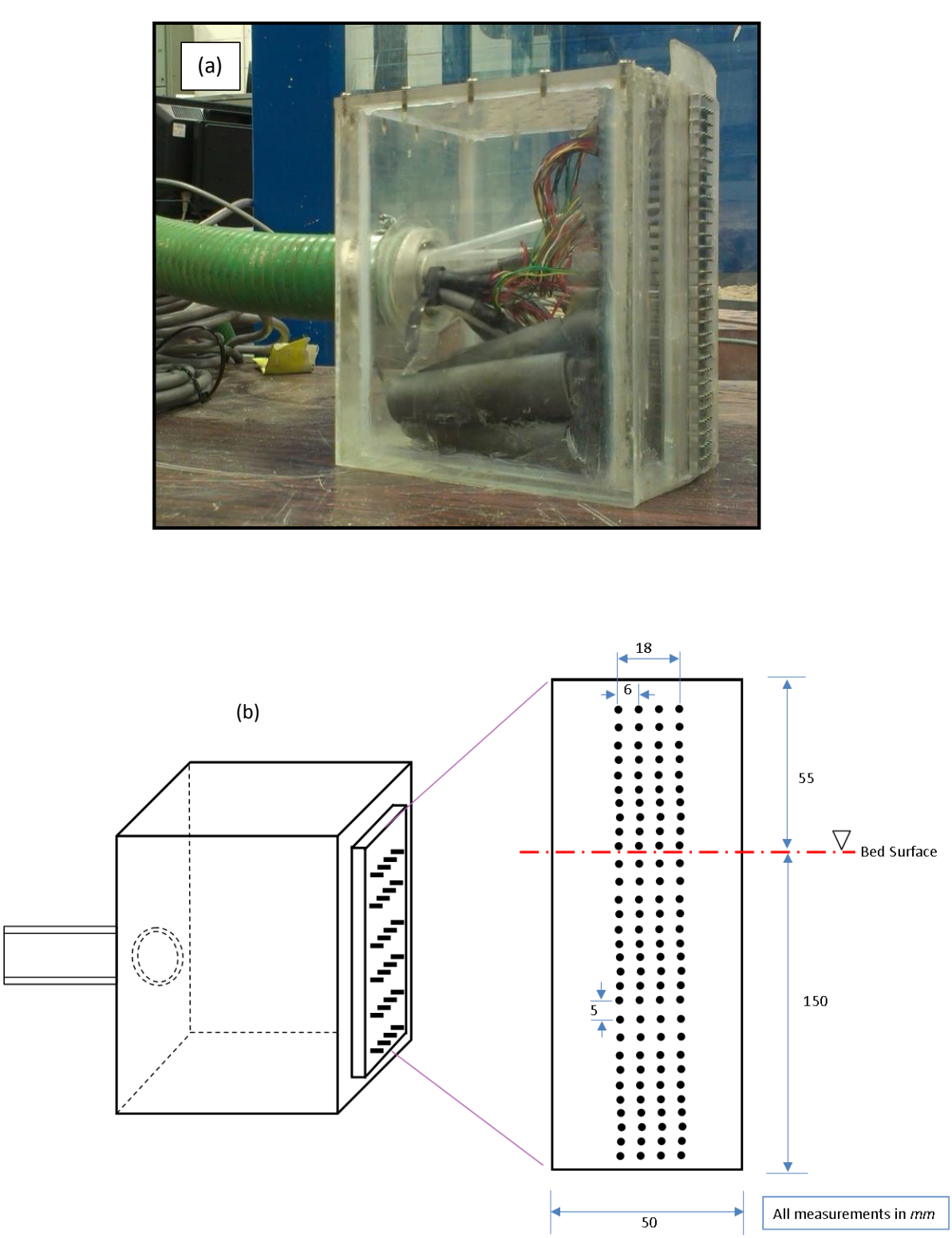

Figure 3.19 (a) Novel custom built submersible 4-point resistivity measurement cell (b) Schematic diagram of the electrode arrangement

Figure 3.20 Images showing the Resistivity box being buried and fitted into the bed and flume prior to the erosion test.

3.8.5 Experimental procedures

The beds were placed and levelled within the test tank before lowering the flume into the tank with overhead electrically operated crane, after it has been properly aligned and fitted in place, the *custom built submersible resistivity measurement box* (see Figure 3.19 & 3.20) was implanted appropriately into the bed, this was possible as the flume had been modified (i.e. a groove created for it on the flume internal wall) to accommodate this box (see *section* 3.8.4.3). To enhance firmness of the box to the flume's wall, transparent silica gel was applied appropriately. The tank was then filled with water to the level of the bed and left to stand till the following day in order to further meet requirement (i) mentioned in *section* 3.8.3. On the following day, all other measurement devices (e.g. OBS, ADV, Go-Pro camera, see *section* 3.8.4) were then configured and programmed as required before fitting them into appropriate positions on the flume and ready to take measurements. Once this has been completed, the tank was finally filled with water to a level that completely covered the flume's motor. This was necessary to prevent the motor becoming overheated.

Hydrodynamic conditions were generated within the flume by increasing the paddle rotation speed for a set period of time (10 *mins*) in a stepwise fashion as shown in Figure (3.21). This was designed to sequentially re-suspend and erode the bed. The discrete power settings applied to achieve the changes in paddle's speed were: 2, 6, 8, 10, 12, 14, 16 and 17 *volts*. It should be noted that the voltage levels and experimental conditions employed here, were decided after series of preliminary tests. Following the completion

of each experimental run, the water is the tank was drained very slowly overnight. Prior to the draining process, a waiting time of 20 *minutes* was introduced to allow for any remaining suspended particles within the flume to settle. On the following day, the measurement devices were removed to retrieve the stored data from the OBS and Go-Pro camera, as ADV data was logging directly of the on-board computer. The flume was then lifted up with extreme care so as not to disturb the bed. Photographic images of the bed were taken at various positions (with Canon EOS 600D); the bed profiles (height and geometry of bed-forms) were measured using a meter rule, after which, sediment cores from the resulting sediment bed were taken with a PVC tube to examine any vertical stratification. A trial run was carried out with 100% sand bed to ensure that the experimental set-up work as expected.

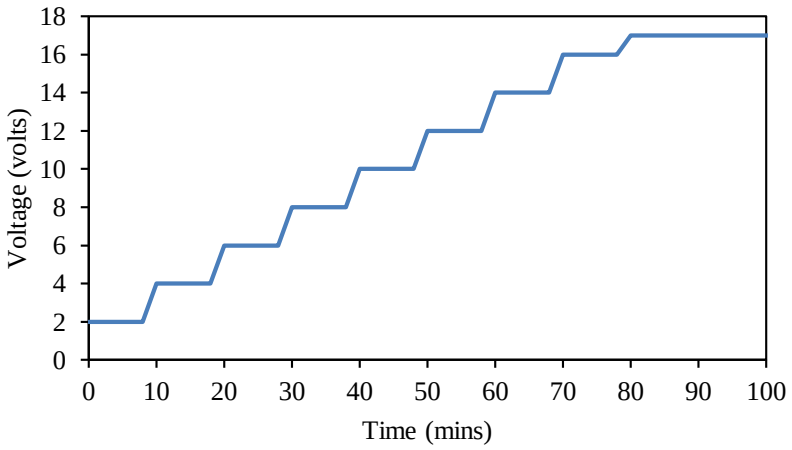

Figure 3.21 Time series of the motor voltage for generation of hydrodynamic conditions

CHAPTER FOUR

Experimental Results: ERMT (ES-1)

"Great design is not just a solution; it is the elimination of the problem"
—M. Cobanli

4.1 Introduction

This chapter presents the development and application of the electrical resistivity technique (EMRT), designed to characterise both the spatial and temporal variation in bed structure and composition resulting from the differential settling of mixed (sand-clay) sediments. Technical issues associated with the electrical resistivity measurements are identified and the technique is trialled using a specially designed acrylic sedimentation column described in the previous chapter. The intention is to highlight the potential for the methodology to provide an additional, non-invasive and sensitive characterization technique to study sand-mud mixture sedimentation processes both within the laboratory and in the field. The hypothesis for this study is that when an electric current passes through water-saturated marine sediments, the measured electrical resistivity will depend on the resistivity of both the solid (sand-mud fractions) and fluid components, hence different combinations of these components should, in theory, have different resistivities associated with them. The set of experiments is carried out in three phases:

1) The pilot test (i.e. preliminary study) conducted within a 50x50x600 mm (high) acrylic sedimentation column (Figure 3.5a);
2) Further developmental study (i.e. high-resolution test) conducted within a 150x150x500 *mm* (high) column (Figure 3.5b), for improved spatial resolution and to evaluate the influence of electrode configuration on measured electrical resistivity. This was necessary due to limitations of the column mentioned in 1 above;
3) Calibration experiments carried out to achieve the following:
    - to evaluate the values of geometric constant (*A/L* and '$2\pi r$') for each pair of electrodes within the settling columns. This allows the bulk resistivity ρ_{bulk}

together with the pore water resistivity ρ_p to be obtained, and hence formation factor F can be calculated from Equation (2-33); and,

- to obtain more physically-relevant properties such as bulk density (and, by extension, porosity) and volumetric composition from Formation Factor, F, values within the columns.

For ease, the preliminary study will be, henceforth, referred to as *Column-1* experiments and the high-resolution tests as *Column-2* experiments. The electrical resistivity measurements presented in the current work are complemented by time lapsed photography of the developing deposits, which allowed both qualitative aspects of the bed formation to be observed and discussed.

All the experimental runs in the current chapter was run at constant salinity and pH while the temperature variations were controlled and corrected as discuss in *section* 3.4.1. Having controlled these parameters, the resistivity measurements are solely function of solid components (i.e. sand and clay).

4.2 Qualitative Observations on Sand-Clay Deposition

It is informative, at this point, to briefly obtain a qualitative understanding of the typical formation of these mixed sand-clay deposits, as well as variations in their vertical structures and composition. This is important to evaluate how the electrical resistivity technique has performed in characterising the observed temporal and spatial variations in the structure of the bed deposits.

Clearly, differential settling effects between the sand and clay fractions - due to variations in the densities and sizes of particle and flocs, respectively - would suggest that sand particles should settle out first, followed by the clay particles/flocs leading to segregation layers within the bed deposit (e.g. Williamson, 1991; Torfs *et al*., 1996). However, the complexity of the interaction between the sand and clay fractions, together with the influence of the pore water salinity, means that the resulting deposit structure is likely to be complex and, to some extent, depends on the sand and clay proportions in the initial mixture. This is thought to be controlled by the initial mixture concentration ϕ_s and relative volumetric concentration of the sand ϕ_s^{sa} and clay ϕ_s^{cl} fractions in the initial sediment mixture (Cuthbertson *et al*., 2008). The parametric influence of ϕ_s, ϕ_s^{sa} & ϕ_s^{cl} on a wider range of resulting sand-clay deposits will be discussed in detail later in chapter 5.

4.2.1 Preliminary test: sand-clay deposition

As indicated previously, time-lapsed images were obtained with a digital camera to observe the settling and deposition characteristics for the different sand-clay mixture compositions used for the development experiments. Figure 4.1 shows the typical temporal development and evolution of the deposit structure for the 50s:50c mixture within the column-1. Assuming each graduation mark on the scale shown in Figure 4.1 is 10 *mm*, the rapid settling of a large proportion of the sand fraction appears to result in the formation of a sand-rich bottom deposit layer ~ 30 *mm* thick [Figure 4.1(i)], with near-vertical dewatering channels formed in this layer during the rapid settlement phase. Above this initial sand-rich deposit, a patchier mixed sand-clay layer ~ 25 *mm* thick [Figure 4.1(iv)] is deposited over a specific time period [i.e. $\Delta t \approx 90$ *minutes*; Figure 4.1(i)-(iv)]. Subsequent to this, a thicker clay-rich layer containing discrete sand patches or clusters [i.e. ~ 100 *mm* thick, up to $z \approx 160$ *mm* mark, Figure 4.1(vi)] forms over a relatively longer time period [i.e. $\Delta t \approx 150$ *minutes*, Figure 4.1(iv)-(vi)]. It is particularly interesting to note the presence of the sand patches within this clay-rich layer as this suggests the remaining sand becomes trapped as the concentration of the clay reaches the gelling point (e.g. Winterwerp and Van Kesteren, 2004), although subsequent settlement of these patches is observed [Figure 4.1(vi) $\rightarrow$ (viii)] as the clay-rich layer becomes denser through on-going settlement. Finally, the remaining clay appears to form a relatively sand-free surface layer in the bed deposit [i.e. $z > 160$ *mm* mark; Figure 4.1(viii)].

4.2.2 High-resolution test: sand-clay deposition

A similar final deposition structure as discussed above for 50s:50c in the preliminary test column was observed to occur also for the 50s:50c mixture (i.e. run ERT-EX3) within the column-2 (see Figure 4.2b). In comparison, the final deposition structures of the sand-rich mixture (ERT-EX2; 75s:25c) is shown (Figure 4.2c) to result in a more clearly defined segregation interface between the sand-dominated layer at the column base and overlying clay-dominated layer, with discrete trapped sand patches again shown especially close to the interface. By contrast, the clay-rich mixture (run ERT-EX4; 25s:75c) is shown (Figure 4.2a) to result in no clear segregated layers forming within the resulting deposition.

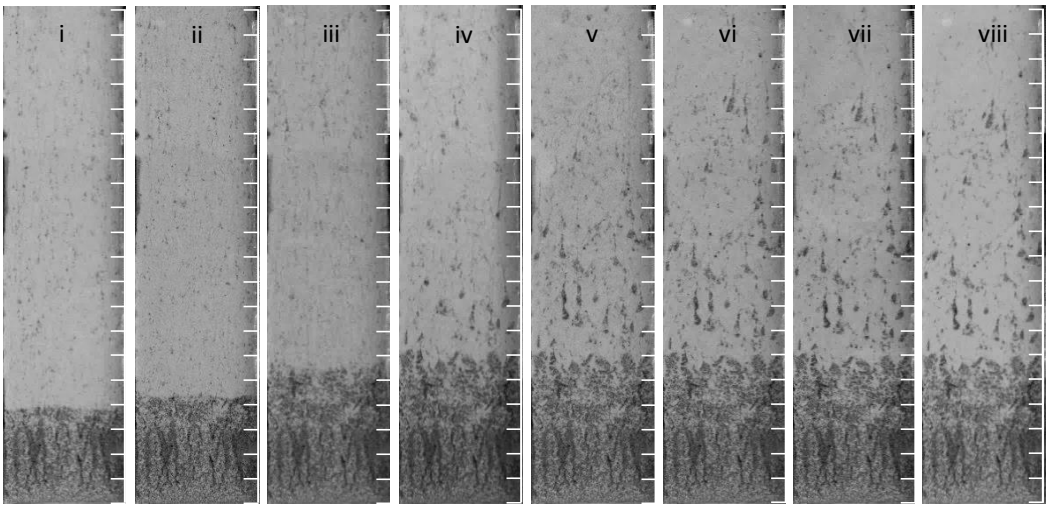

Figure 4.1 Time-lapsed images showing the development of sand-mud deposit layer in the preliminary column design for 50s:50c mixture at elapsed times (hrs) of (i) 0.25, (ii) 0.5, (iii) 1.0, (iv) 1.5, (v) 2.0, (vi) 4.0, (vii) 5.0 and (viii) 6.0. (Each graduation mark on the scale is equivalent to 10 *mm*)

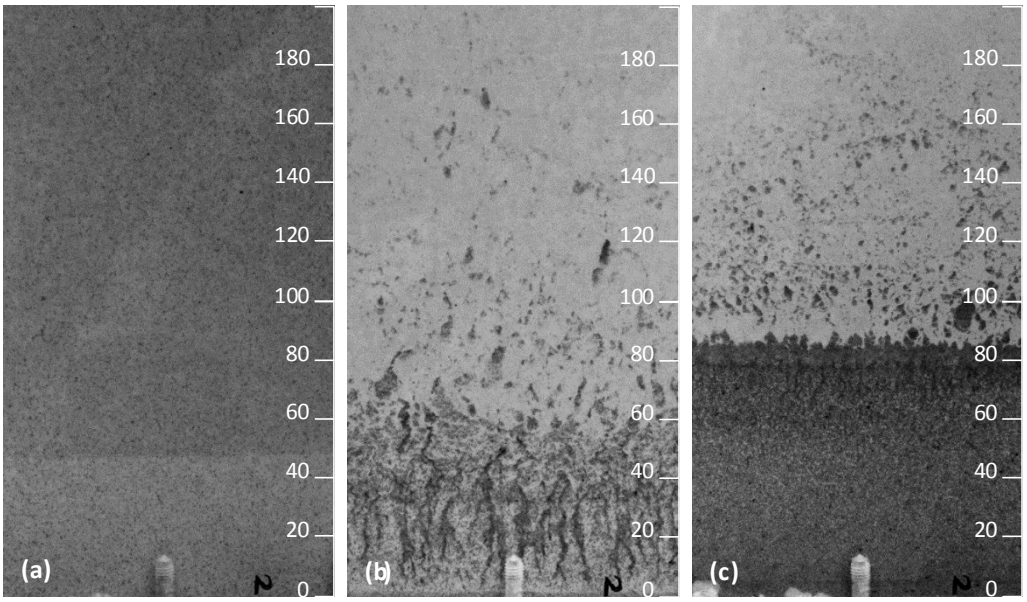

Figure 4.2 Final deposition patterns in the high-resolution column for (a) ERT-EX4 (25s:75c), (b) ERT-EX3 (50s:50c) and (c) ERT-EX2 (75s:25c)

4.3 Electrical Measurements

As previously indicated, measurements of formation factor *F* profiles were obtained in both columns (i.e. column-1 and -2) to investigate the settling and depositional behaviour of the different sand-clay mixtures tested. Where appropriate, these profiles were transformed into more physically-relevant properties (e.g. bulk density γ_{bulk}, porosity φ) to

characterise structural features, such as segregated bed layers and transitions in solid volumetric composition within the resulting bed deposits.

4.3.1 Preliminary sedimentation tests (Column-1)

For the tests conducted in column-1, these measurements focused primarily on proving the viability of the ERMT for determining spatial and temporal variations in the sand-clay deposit formation and resulting composition. In this regard, Figure 4.3 shows comparisons of the measured formation factor F profiles at discrete elapsed times during these preliminary runs. These results show the pure-sand deposit forms almost immediately with a reference F value of 4.6 – 5 (Figure 4.3a). A high F value is also measured at the base of the column (i.e. $z = 25$ *mm*) for the sand-rich (i.e. 75s:25c) mixture (i.e. $F \approx 4$, Figure 4.3a), reflecting the initial formation of a base layer composed predominantly of deposited sand. By contrast, initial F values for the other sand-clay mixtures and pure-clay runs appear to be relatively consistent over depth, with only a slight increase in F observed for the 50s:50c mixture (i.e. $F \approx 1.9$, Figure 4.3a), which reflects the initial development of a sand-clay deposited layer at the column base. After 6 hours, the F value at the column base for the 75s:25c mixture has further increased (i.e. $F \approx 4.2$, Figure 4.3b) to approach that of the pure-sand deposit. The corresponding F value for the 50s:50c mixture has also increased significantly (i.e. $F \approx 3.14$, Figure 4.3b), reflecting the formation of a mixed sand-clay deposit layer. Evidence of sand deposition in a clay-rich base layer is also indicated by the slight increase in F for the 25s:75c mixture (i.e. $F \approx 1.95$, Figure 4.3b). Higher up the column (i.e. $z = 125$, 225, 325 and 425 *mm*), F values appear to have less variation for all sand-clay mixtures, suggesting the dominance of the clay fraction in the deposition characteristics away from the column base. For the measurements taken at 24 and 72 *hours* (i.e. Figure 4.3c & d, respectively), there appears to be no significant changes to the overall F profiles with respect to the 6-hour measurement. However, all F values continue to increase as the resulting sand-clay deposits continue to compact over this time scale.

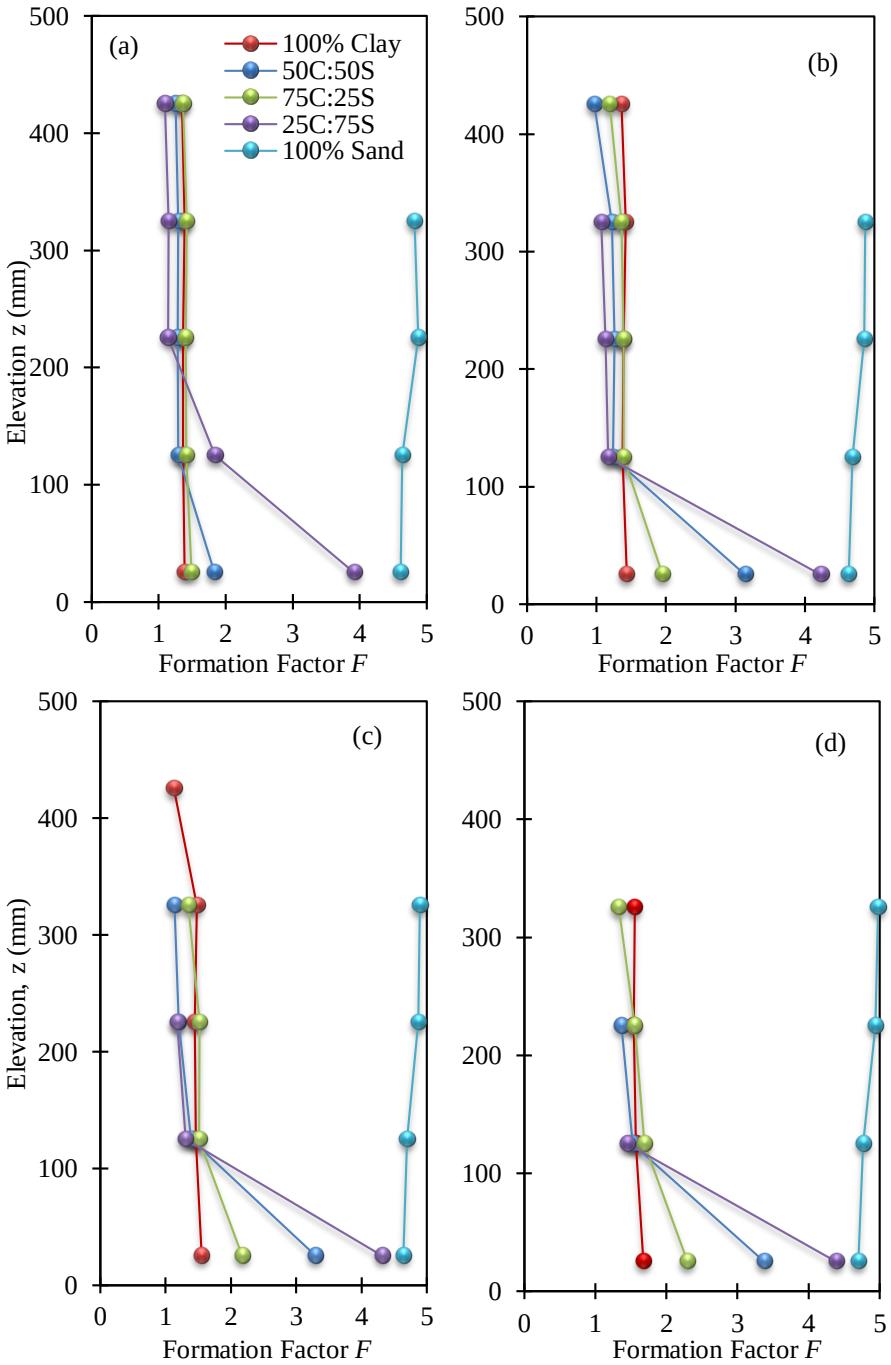

Figure 4.3 Measured formation factor F profiles in preliminary column-1 for 0(S):100(C); 25(S):75(C); 50(S):50(C); 75(S):25(C) and 100(S):0(C) at elapsed times of (a) 0 hrs; (b) 6 hrs; (c) 24 hrs; and (d) 72 hrs.

4.4 High-resolution Settling Column Tests (Column-2)

Clearly, the results of the preceding section demonstrate that distinct variations in measured *F* profiles are obtained for different compositions of sand-clay mixtures and their resulting deposits for the tests within the settling column-1. These results undoubtedly establish the potential of ERMT in characterising spatial and temporal variations in mixed sediment deposits. However, the low-resolution of electrical

measurements associated with the settling column-1 design, meant that detailed information on the vertical variations in structure and composition of the mixed deposits were not possible. Therefore, the potential of this technique was further investigated in a specially designed high resolution column (see *section* 3.5 and Figure 3.5b). One of the main advantages of this column over column-1 was that it was designed to investigate the influence of electrode geometry and horizontal spacing on the electrical measurement. The remainder of this chapter will focus, therefore, on the high-resolution electrical measurement results obtained in this specially built sedimentation column and their physical interpretation. The use of electrical measurements method to obtain physical properties of mixed sediment deposits is discussed below and also in chapters 5 and 6 of this thesis.

4.4.1 Influence of electrode geometry and configuration

Initial electrical measurements in the high-resolution settling column were designed to test the influence of pin electrode spacing within each four-point set on the ability of the ERMT to identify structural features (e.g. changes in layer composition) within the sand-clay deposits. In this respect, two sand-clay settling test runs were completed in which simultaneous measurements were taken in the high-resolution column with the 6 *mm* and 20 *mm* spaced pin electrode sets (with vertical spacing fixed at 10 *mm* between sets). Figures 4.4a & b show comparisons of the formation factor *F* profiles for the 50s:50c (ERT-EX3) and 75s:25c (ERT-EX2) mixtures, respectively, obtained with the 6 *mm* and 20 *mm* pin arrangements after 6 *hours*. These plots appear to indicate that a reduction in the horizontal electrode resolution (i.e. 20 *mm* $\rightarrow$ 6 *mm*) results in reduced vertical gradients (i.e. *dF/dz*) observed at transitions between sand-rich layers (with high *F* values) and clay rich layers (with lower *F* values). This is particularly noticeable in the 75s:25c mixture, which was shown (Figure 4.2c) to have a sharp segregation between the sand-rich and clay-rich deposition layers. A final test using an artificially-generated deposit consisting of alternate layers of pure-sand and pure-clay clearly demonstrates this effect. The resulting formation factor *F* profiles (Figure 4.4c) confirm that horizontal pin electrode spacing (together obviously with the vertical spacing of electrode sets) affects significantly ability of the electrical resistivity technique to pick up sharp transitions in segregated beds.

The influence of electrode geometry, in particular, was also evaluated by comparing the results obtained after 6 hours for tests consisting of 25c:75s within both columns. From the results (Figure 4.5), it is obvious that there is no significant difference from the profiles obtained by 6 *mm* spaced pin-electrodes, 20 *mm* spaced pin-electrodes and square plate-electrodes, in the region of the beds with little or no segregation (i.e. $z \geq 120$ *mm*), but significant differences exist in the segregated region (i.e. $z < 120$ *mm*) of the bed; with the least resolution result from the plate electrodes. In general, these findings suggest that spatial resolution of the EMRT is affected by electrode configuration (horizontal spacing) and geometry especially when characterising segregated bed deposits or settling processes where segregation is likely to occur. It was therefore decided to use the 6 *mm* electrode spacing to more clearly identify these transitions, hence, subsequent experimental results in the current study are based on measurements made with a 6 *mm* electrode spacing.

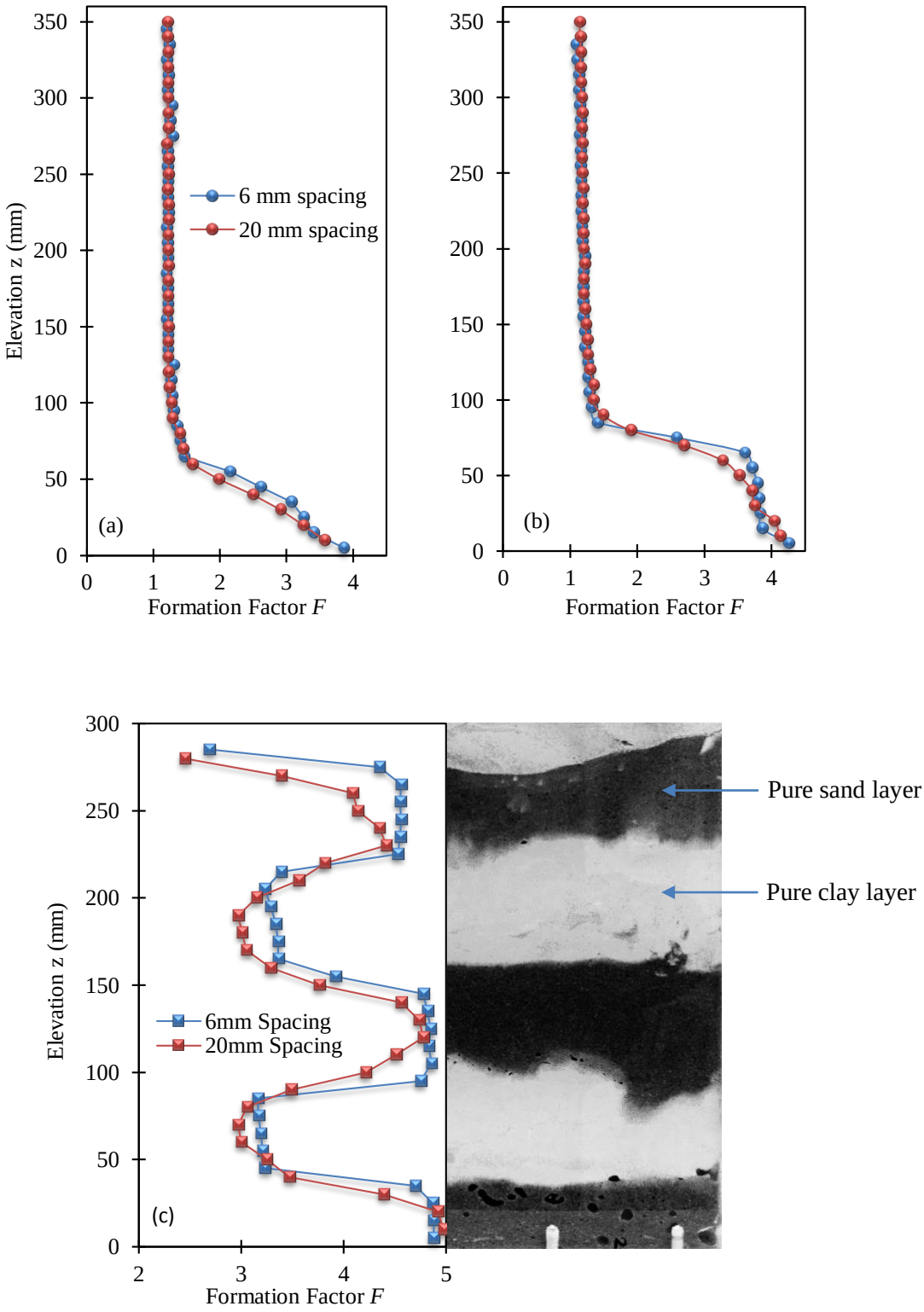

Figure 4.4 Development of formation factor F profiles at 6 hours for runs with (a) ERT-EX3 (50s:50c); (b) ERT-EX2 (75s:25c); and (c) placed deposits (with alternating pure-sand and clay layers) to compare the 4-Pin electrode horizontal resolutions (i.e. pin-pin spacing; 6mm and 20mm).

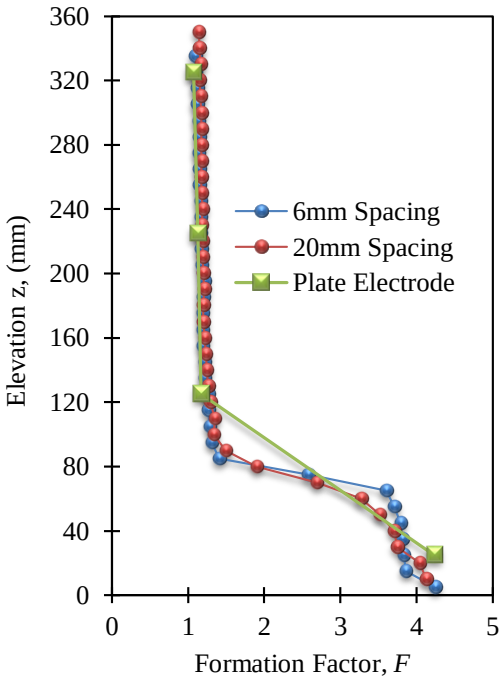

Figure 4.5 Profiles showing the influence of electrode configuration and geometry on spatial resolution of ER.

4.4.2 Calibration Measurements: physically-relevant properties of bed deposits

The physical properties, i.e. bulk density (γ_{bulk} /γ_p) and porosity (φ), obtained from calibration tests described in *section* 3.6.3 (pg. 77), were related to the formation factor *F* for each test sample (Figures 4.6 and 4.7). From Figure 4.6, *F* versus φ for the range of sand-clay mixtures tested, the values of the empirical coefficients *a* and *m* in Equation (2-33) can be obtained as *a* = 1.575 and *m* = 1.135 from the best-fit power relationship through this calibration data, which has been shown to have the same form as the Archie (1942) relationship (Equation 2-33), such that:

$$F = \frac{\rho_{bulk}}{\rho_p} = 1.575\varphi^{-1.135} \qquad (4\text{-}1)$$

Interestingly, coefficients *a* and *m* in Equation (4-1) are in general agreement with values obtained from other studies in unconsolidated, saturated soil [a = 0.62–1.97 (e.g. Boyce 1968 and Bassiouni, 1994) and *m* = 1.0–1.5 (e.g. Archie, 1942; Schon, 1996 ; Worthington, 1993 and McCarter *et al*. 2005)].

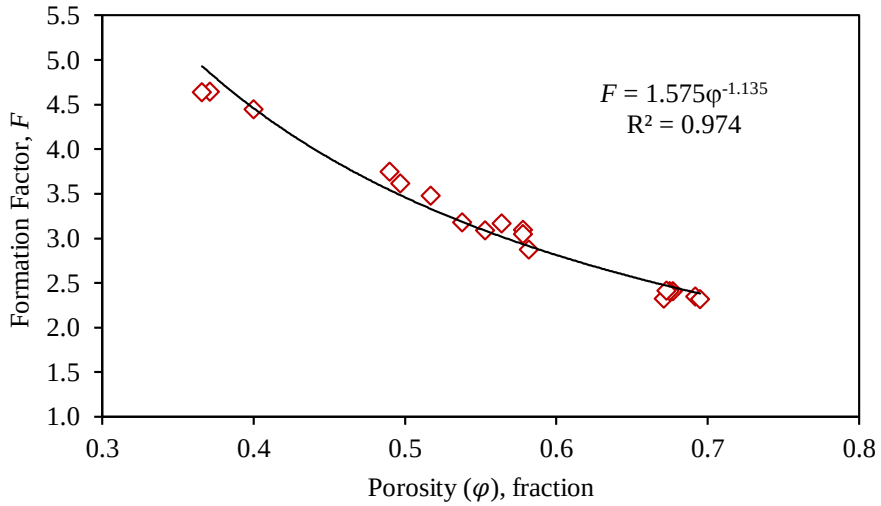

Figure 4.6 Derived Archie (1942) relationship between Formation Factor, *F* and Porosity, φ

It is reemphasised here that the range of applicability of Equation (4-1) (and, hence, Equation 2-33 in general) is limited as the condition: $F \rightarrow 1$ as $\varphi \rightarrow 1$ is not satisfied (i.e. pore fluid only). Therefore, Equation (4-1) can only be considered valid over the range of porosities ($\varphi = 0.35 - 0.92$) for the calibration mixtures tested. As indicated previously, these limiting conditions also have implications for general validity of Equation (3-11), which relates normalised bulk density γ_{bulk}/γ_p with formation factor *F*. Indeed, this relationship is shown in Figure 4.7a (red line) and, while reasonable fit is demonstrated within the calibration data range, the required condition that $\gamma_{bulk}/\gamma_p \rightarrow 1$ as $F \rightarrow 1$ is clearly not satisfied. Hence, an improved fit to the calibration data (i.e. blue line in Figure 4.7a) is proposed ($R^2 = 0.9948$), which as it can be seen satisfies the imposed condition, such that:

$$\frac{\gamma_{bulk}}{\gamma_p} = 1.016\, F^{\,0.455} \tag{4-2}$$

In the same vein, the improved fit to the calibration data is proposed for the relationship between Porosity (φ) and Formation Factor *F*, as shown by the *black solid line* in Figure 4.7(b). This proposed fit apparently satisfies better the required condition (i.e. $\varphi \rightarrow 1$ as $F \rightarrow 1$), therefore the following equation is proposed ($R^2 = 0.994$):

$$\varphi = 1.284\, e^{-\,0.265\,F} \tag{4-3}$$

Equations (4-2) and (4-3) can therefore be used to predict evolving normalised density (γ_{bulk}/γ_p) and porosity (φ) profiles within the sand-clay deposits directly from electrical resistivity measurements as it has been demonstrated in the current study. It should be borne in mind that, the calibration plots in Figures 4.6 and 4.7 have been derived from tests on unconsolidated, saturated sand-clay mixtures and hence are more representative of freshly deposited bed conditions. Hence, the coefficients in these equations (i.e. 4-2 and 4-3), are therefore valid for the range of sand-clay mixtures tested here or for sediment mixtures of similar characteristics and compositions. As such, the electrical properties of sand-clay suspensions (i.e. prior to bed layer formation) or heavily consolidated sand-clay bed layers would be expected to vary from the range of formation factors (e.g. $F \approx 2.0$–5.0) as measured in the calibration tests. However, the physical properties (e.g. bulk density and porosity) of the former can clearly be estimated from Equations (4-2) and (4-3) when extrapolated back to the required condition γ_{bulk}/γ_p and $\varphi = 1$ when $F = 1$.

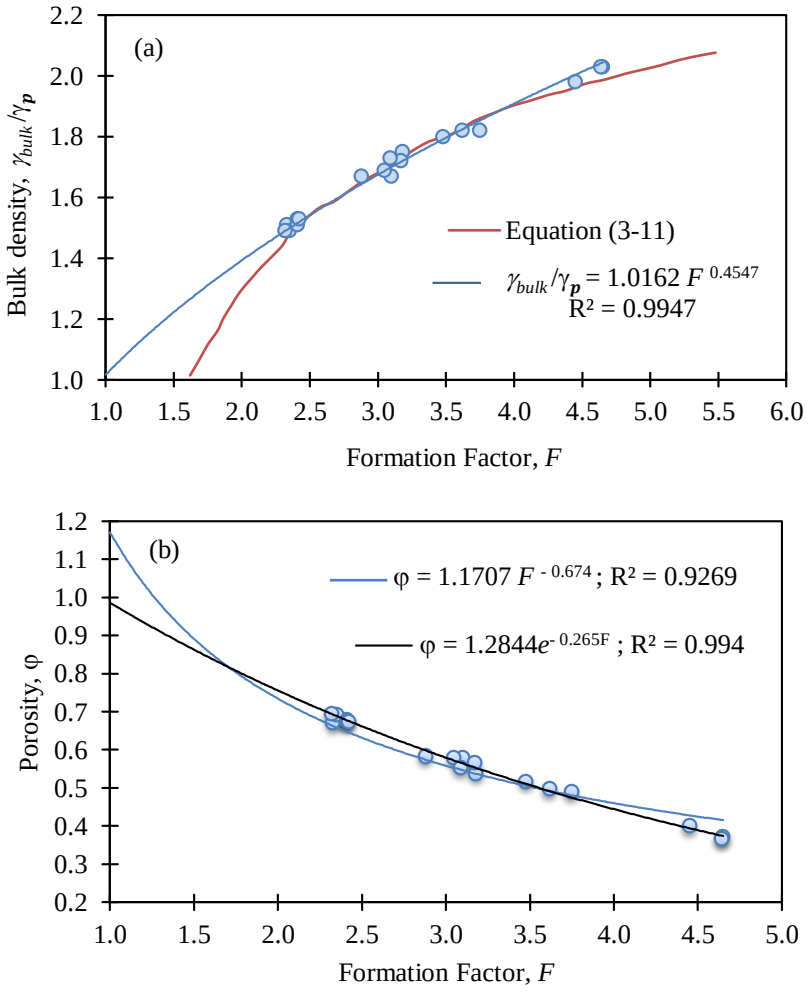

Figure 4.7 Calibration plots showing the derived relationships between (a) normalised bulk density γ_{bulk}/γ_p and formation factor F; (b) porosity φ and formation factor F within sand-clay test samples

4.4.3 Formation factor (F) profiles

As the effects of pore solution salinity and temperature are constant; and using the sand-clay mixture calibrations outlined above, a time series of measured formation factor *F* profiles (e.g. colour maps of measured formation factor *F* profiles shown in Figure 4.8) can be obtained (see *sectio*n 2.6.3, pg. 54 for more details). Visual observation of the photographic images in Figures 4.2(b-c) and 4.8 clearly shows that, in both cases, although segregation occurred, the degree of clarity of the interfaces between these segregated layers in the bed deposits differ significantly depending on granular material concentration. The colour maps in Figure 4.8 clearly present these differences. In both Figures 4.8a & b, different layers can be identified in the bed deposits with the magnitude of each largely dependent on sand concentration. In the corresponding colour map, at z = 80 *mm*, a sharp transition can be seen between the clay rich layer and sand rich layer in 75s:25c mixture (Figure 4.8b) but at the corresponding height (z = 40 *mm*) in 50s:50c mixture (Figure 4.8a) the transition is not distinctly clear as it can be seen in the bed deposit image.

In general, Figure 4.8 appears to allow more quantitative analyses of different settling conditions, segregation/stratification mechanisms and structural differences of the resulting bed deposits. For instance, information on settling regimes can be clearly picked from Figure 4.8, in both runs ERT-EX3 (50s:50c) and ERT-EX2 (75s:25c), 't_0-t_1' represents a period where the granular materials rapidly settled; and 't_1-t_2' shows the phase where clay particles concentration dominate thereby causing hindered settling of the granular materials. However, in run ERT-EX3, 't_2-t_3' regime denotes phase with settling clay particles in a consolidating bed while this regime extends to 't_4' in run ERT-EX2.

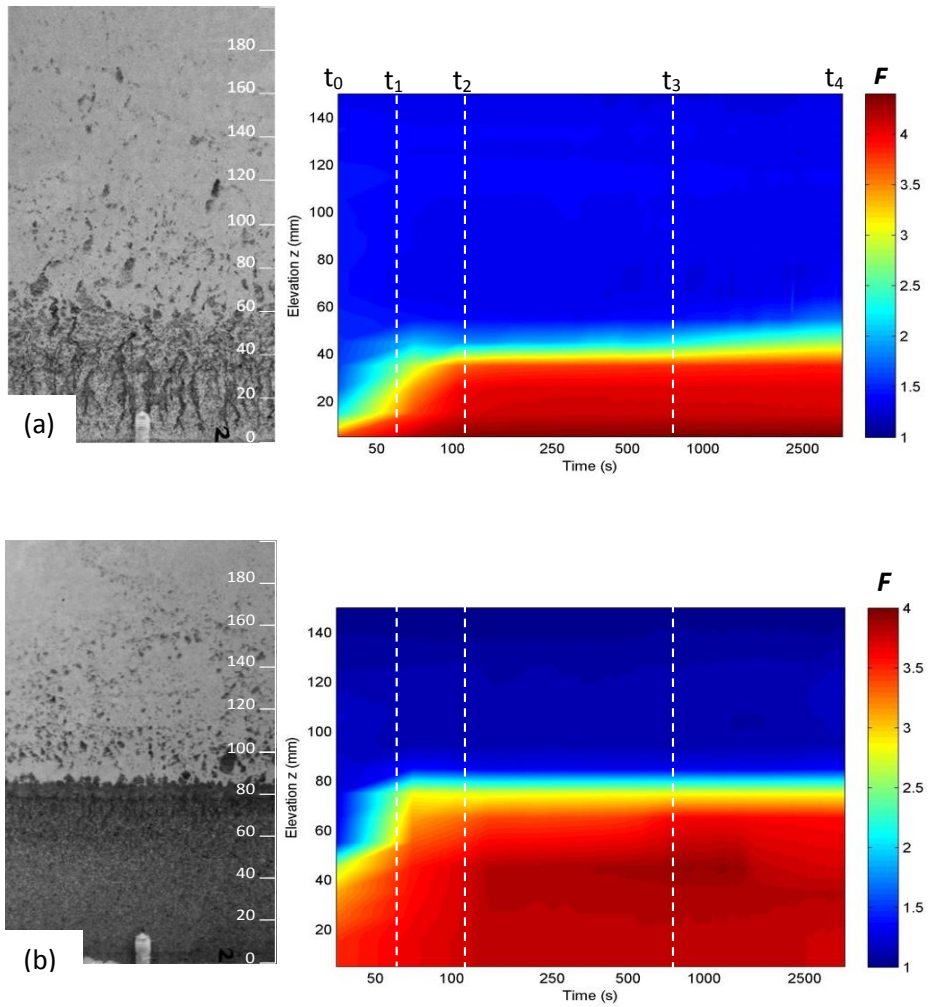

Figure 4.8 Time series colour map plots showing variation in measured formation factor *F* profiles for (a) ERT-EX3 and (b) ERT-EX2. (Corresponding images show bed deposit structure after 48 hours)

4.4.4 Bulk density and porosity profiles

In terms of characterising variations in the vertical composition of sand-clay deposits, it is more informative to convert the measured electrical properties into more physically-relevant properties such as bulk density and porosity. These can then be easily associated with specific bed structural feature at different elevations within the deposits. The formation factor *(F)* profiles (e.g. Figure 4.8) can be transformed into normalised bulk density γ_{bulk}/γ_p and porosity φ profiles using Equations (4-2) and (4-3) respectively. Figure 4.9 presents typical results of the temporal variation in normalised bulk density γ_{bulk}/γ_p for the majority of the mixtures (i.e. ERT-EX2 to EX5) tested in the high-resolution column with the 6 *mm*-spaced pin electrodes while Figure 4.10 presents their corresponding vertical porosity (φ) profiles (i.e. from Equation 4-3).

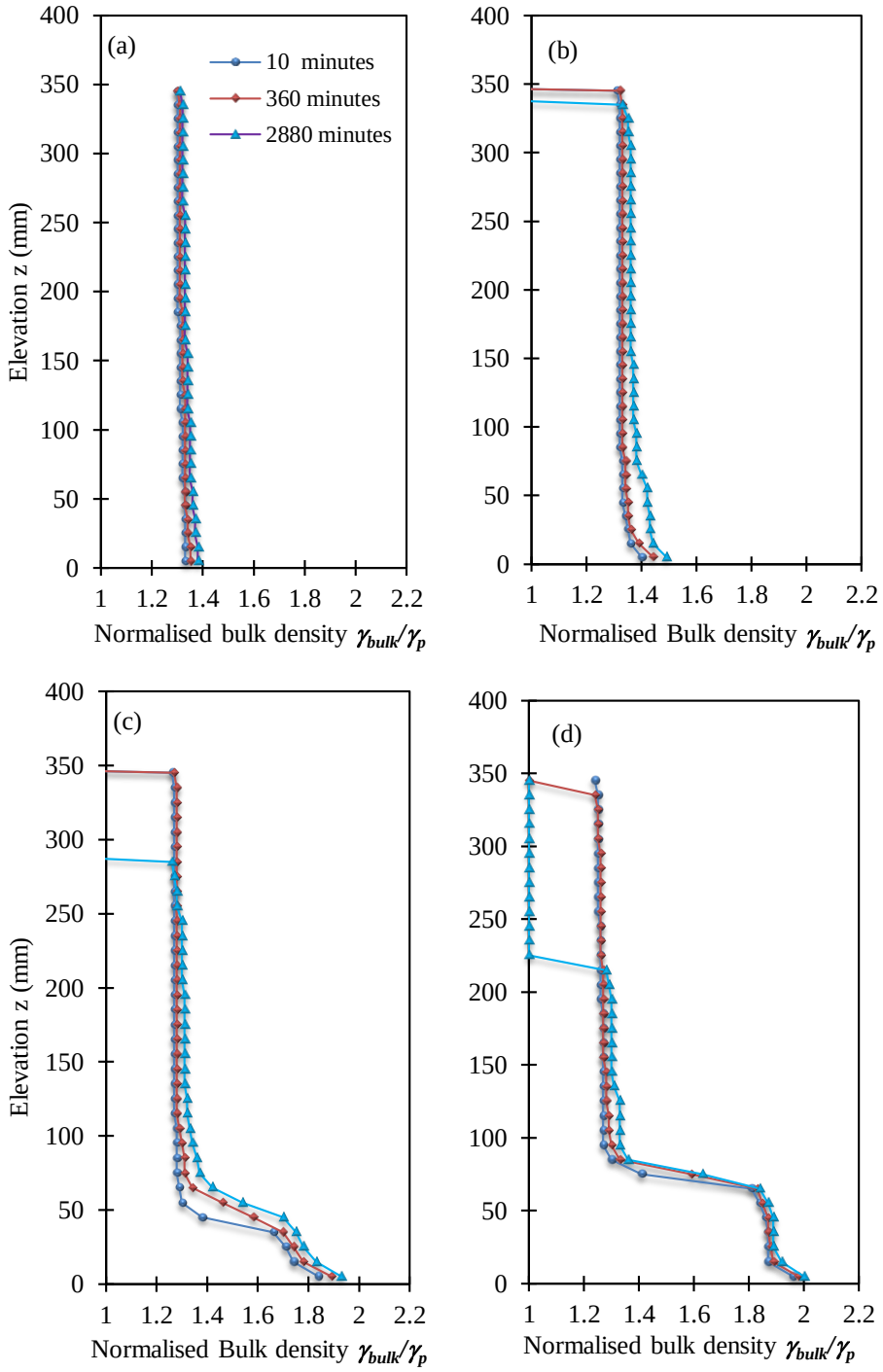

Figure 4.9 Vertical profiles of normalised bulk density γ_{bulk}/γ_p at elapsed time shown for run (a) ERT-EX5 (0s:100c; i.e. pure-clay); (b) ERT-EX4 (25s:75c; i.e. clay-rich); (c) 50s:50c (ERT-EX3); and (d) ERT-EX2 (75s:25c; i.e. sand-rich).

For the pure-clay deposit (i.e. ERT-EX5) the γ_{bulk}/γ_p values increase slightly (γ_{bulk}/γ_p = 1.3 $\rightarrow$ 1.4) with both increasing deposit depth (i.e. reducing z values) and increasing elapsed time (0 $\rightarrow$ 6 $\rightarrow$ 48 hours), due primarily to compaction effects within the pure-clay deposit (Figure 4.9a). The porosity of the (i.e. ERT-EX5) final bed structure appears to be uniform across the bed (i.e. z = 0 $\rightarrow$ 200 *mm*), with the average indicative values of bed porosity, φ (Figure 4.10a) $\approx$ 0.85.

For the clay-rich mixture (ERT-EX4; Figure 4.9b), bulk density profiles are found to be similar to that for the pure-clay deposit, except in the near-base region (i.e. $z < 75$ *mm*) of the deposit, at greater elapsed times (i.e. at 48 *hours*), where the average γ_{bulk}/γ_p values are increased slightly (γ_{bulk}/γ_p = 1.4 – 1.5) by the presence of trapped sand within the dominant clay matrix. The indicative values of the bed porosity in this region of the bed (i.e. $z = 0 \rightarrow 75$ *mm*) vary from $\varphi \approx 0.73$ to 0.81; but for $z > 75$ *mm*, the average value of φ is 0.84 (see Figure 4.10b), which is similar to average porosity in 100% clay sample.

For run ERT-EX3 (50s:50c; Figure 4.9c), the bulk density profiles show three distinct changes in gradients within the near-base region (i.e. $z < 100$ *mm*), representing the transitions between layers of different composition [see Figure 4.2(b)]. Above this region appears to be predominantly clay deposit. From the bulk density profile at 48 hours elapsed time, the slight increase in γ_{bulk}/γ_p values (1.3 $\rightarrow$ 1.5) between $z = 100 \rightarrow 65$ *mm* appears to be associated with the formation of the clay-rich layer with trapped sand patches (see Figure 4.2b and Figure 4.11a); the corresponding porosity values between $z = 100 \rightarrow 65$ *mm*, vary from $\varphi \approx 0.82$ to 0.86 (Figure 4.10c). A transition in gradient is then observed at $z = 65$ *mm*, indicating the presence of the sand-rich layer with clay patches, which extends down to $z = 45$ *mm* with γ_{bulk}/γ_p values increasing from about 1.4 $\rightarrow$ 1.7 and φ varying from $\approx$ 0.60 to 0.82 over this layer. A second gradient transition is observed around $z = 45$ *mm*, indicating the presence of the near-base, sand-dominated layer (with de-watering channels and some clay present, Figure 4.2b and Figure 4.11a). In this layer of the bed, the values of γ_{bulk}/γ_p increase from about 1.7 $\rightarrow$ 1.93 with the corresponding porosity values range from $\varphi \approx 0.44$ to 0.60 (Figure 4.10c).

Finally, for the sand-rich mixture (ERT-EX2; Figure 4.9d) there is a relatively sharp transition between the sand-dominated base layer (with γ_{bulk}/γ_p between 1.8 – 2.0 and $\varphi \approx 0.44 – 0.48$ for $z < 65$ *mm*) and the clay-dominated upper layer (with γ_{bulk}/γ_p = 1.2 – 1.3 and $\varphi \approx 0.84 – 0.91$ for $z > 85$ *mm*). This sharp transition was evident from the final deposit of the 75s:25c (i.e. ERT-EX2 after 48 hours; see Figure 4.2c and Figure 4.11b). Interestingly, a layer [i.e. $z = 65 \rightarrow 85$ *mm*; region (ii) in Figure 4.11b] is sandwiched in between the sand-dominated base layer and clay-dominated upper layer with γ_{bulk}/γ_p = 1.36 – 1.84 and $\varphi \approx 0.48 – 0.84$ (Figure 4.10d and Figure 4.11b), this layer (i.e. $z = 65 \rightarrow 85$ *mm*) is however sand rich as shown in Figure 4.10d. Comparison of near-base

variations in normalised bulk density γ_{bulk}/γ_p at 48 *hours* was shown in Figure 4.12 for all mixtures tested.

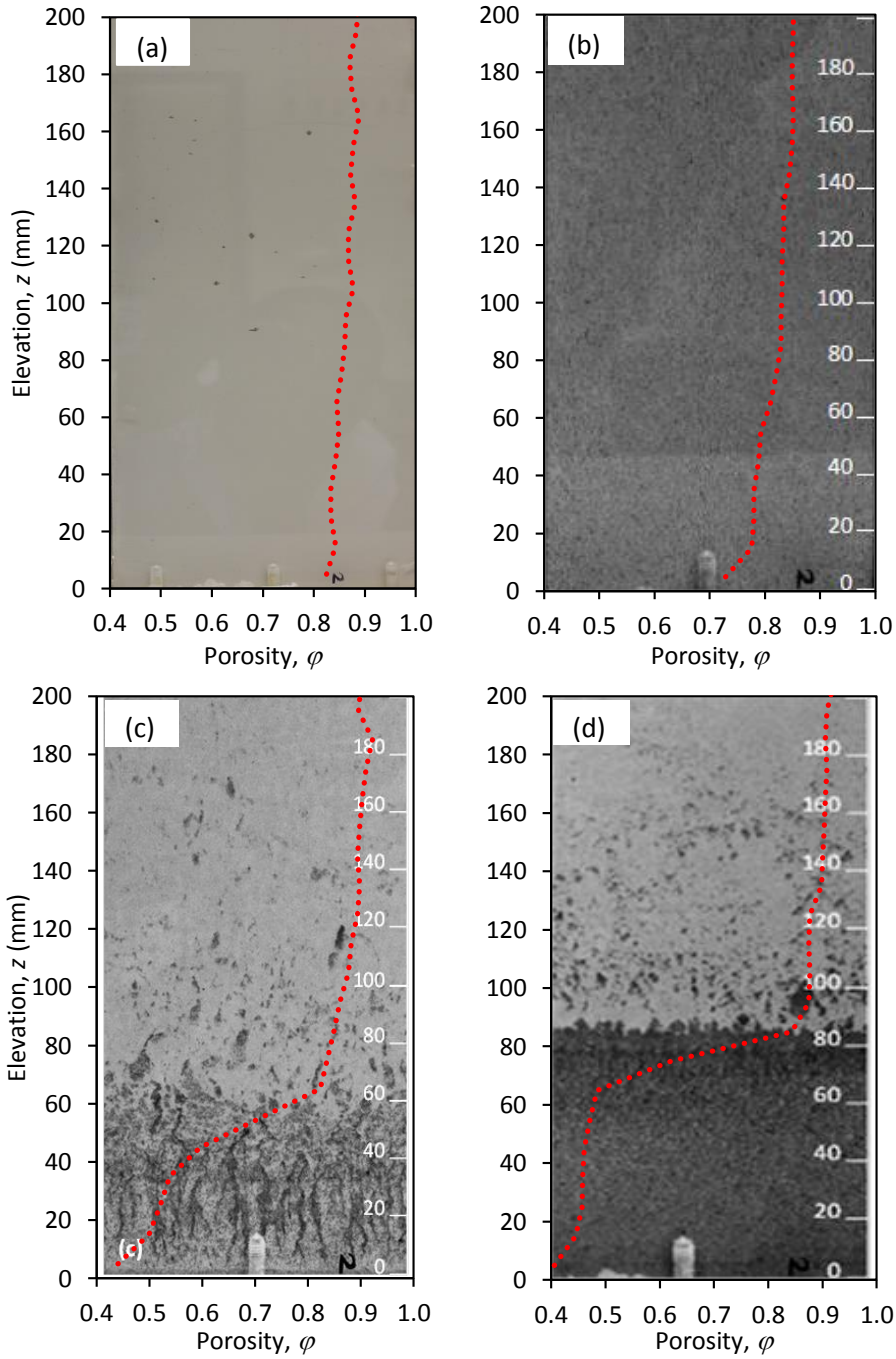

Figure 4.10 Vertical profiles of Porosity, φ at 48th hour for run (a) ERT-EX5 (0s:100c; i.e. pure-clay); (b) ERT-EX4 (25s:75c); (c) 50s:50c (ERT-EX3); and (d) ERT-EX2 (75s:25c).

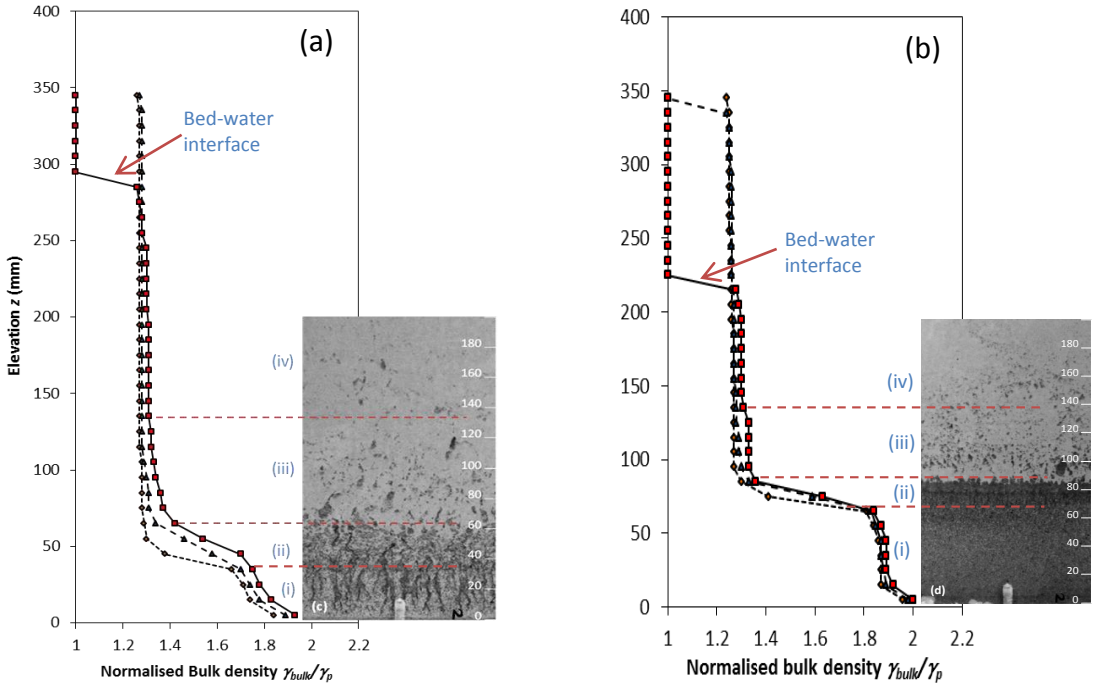

Figure 4.11 Normalised bulk density profiles and images of sand(s)-clay(c) deposits obtained for run (a) ERT-EX3 (50s:50c) and (b) ERT-EX2 (75s:25c). Zones (i) – (iv) show sand-rich (>60% sand); sand-clay mix; sandy-clay (<10% sand) and clay layers, respectively.

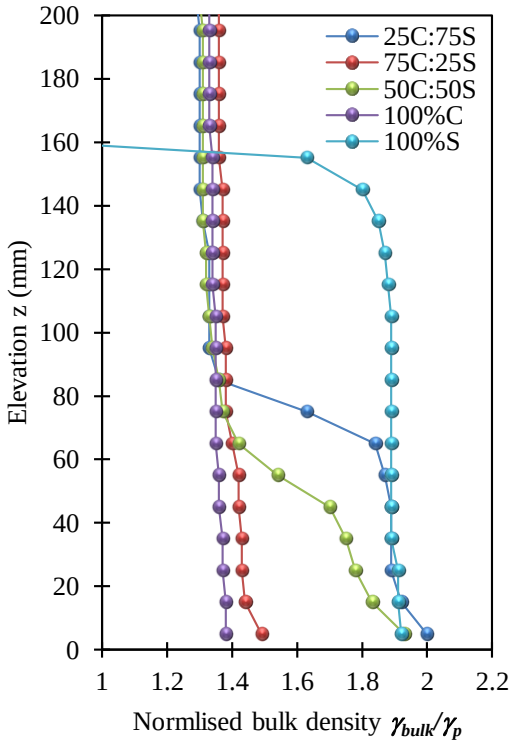

Figure 4.12 Comparison of near-base variations in normalised bulk density γ_{bulk}/γ_p at 48 *hours* for mixtures of composition: 0s:100c (pure-clay); 25s:75c (clay-rich); 50s:50c (sand-clay); 75s:25c (sand-rich); and 100s:0c (pure-sand)

From the vertical porosity (φ) profiles of the bed deposits shown in Figure 4.10, qualitative analysis of the granular material distribution in the resulting bed deposits is possible which may complement further analysis such as particle size distribution (further calibration tests may be required). From Figure 4.10, it is apparent that sand fraction significantly decreases vertically upward through the bed deposit with corresponding increase in porosity; an opposite trend is observed in the case of clay fraction. In terms of bulk density of the sediment bed deposits, bed samples with little or no sand particles will have relatively high porosity (Figure 4.10a & b), meaning porosity increases with decreasing sand content. A similar trend was reported by te Slaa *et al*. (2013). Furthermore, Figure 4.13 indicates how the normalised bulk density of the prepared sand-clay calibration samples increases (though non-linearly) [i.e. γ_{bulk}/γ_p= ~1.5→~2.0] with sand content (i.e. 0→100 %); and decreases [i.e. γ_{bulk}/γ_p= ~2.0→~1.5] with clay content (i.e. 0→100 %).

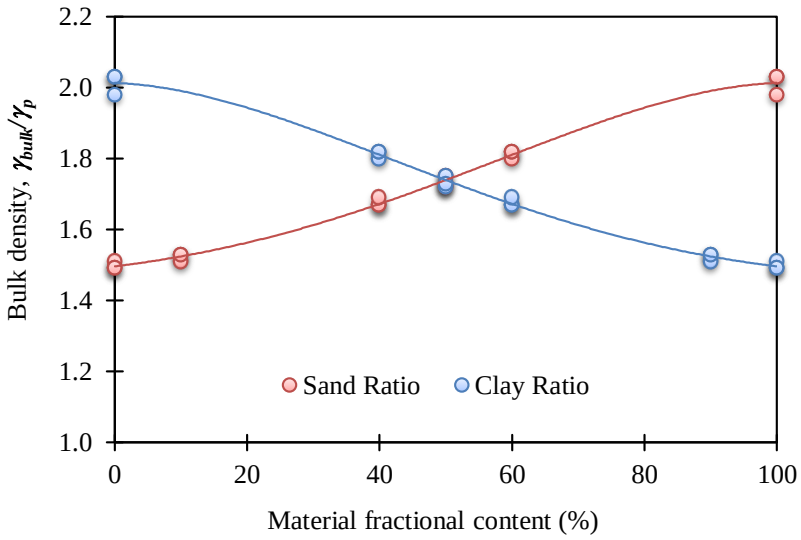

Figure 4.13 The relationship between γ_{bulk}/γ_p and material fractional content within sand-clay test samples

In summary, the formation factor colour map plots (Figure 4.8); bulk density profiles (Figure 4.9) and porosity profiles (Figure 4.10) have clearly shown the initial stages of the bed layer development for different sand-clay mixture compositions and indicate quantitatively how the individual deposit layer forms over time, as well as providing an indication of their composition and structure (i.e. through corresponding γ_{bulk}/γ_p and porosity φ values in the different bed regions).

4.5 Main Conclusion

This chapter has extensively described results of an experimental study exploring the potential of non-intrusive electrical resistivity techniques to characterize the spatial and temporal variation in sediment bed structure and composition, resulting from the differential settling of cohesive clay and non-cohesive sand mixtures. Various associated technicalities have been identified and finally, continuous bulk density profiles and an expression for porosity profiles have been successfully obtained for these sand-clay mixtures with ERMT. In addition, the time series profiles of these physically relevant properties (e.g. bulk density, porosity and material ratio) obtained from formation factor *F* have been demonstrated to allow quantitative analyses of different settling conditions, segregation/stratification mechanisms and structural densities of the resulting bed deposits from sand-mud mixtures.

The bulk density profiles obtained for the different sand-clay mixtures in the current work demonstrate, to a large extent, the influence of the non-cohesive sand fraction, in particular, on the spatial and temporal variation of the resulting composition and structure of mixed sediment bed deposits (e.g. Torfs *et al*. 1996; Manning *et al*., 2010; Xu *et al*., 2012; etc.). Generally, considerable care should be taken when comparing results from different devices for characterisation of bed deposits as variation in results could be technically linked to various factors such as scale of deployment, environmental conditions, etc., nevertheless, the bulk density values obtained from the current study are broadly in agreement with values obtained by other authors utilizing other non-invasive techniques for similar sand-mud compositions. For example, Torfs *et al*. (1996) recorded bulk densities ranging from 1.0 to 1.4 $g\ cm^{-3}$ for single shot experiments on Scheldt mud with sand additions of 0%, 5%, 10% and 20%. Similarly, Been and Sills (1981) obtained bulk densities ranging from 1.02 to 1.53 $g\ cm^{-3}$ for various consolidating soft soils, (see *Table 4-1*).

Table 4-1 Comparison of ER with other common non-invasive techniques

Author	Bulk density ranges (g cm^{-3})	Technique Used	Sediment Compositions	Accuracy (+/-)
Current study	1.2 – 2.0	ERMT	0-75% Sand	0.025-0.04 g cm^{-3}
Torfs, *et al*. (1996)	1.0 – 1.4	Gamma-ray (MAST-G6M, 1992)	0-32% Sand	0.01 g cm^{-3}
Been and Sills (1981)	1.02 – 1.53	X-ray	75µm sieved Silt + 30%Clay	0.01 g cm^{-3}

Therefore, in spite of identifying some technical issues that must be given consideration when using EMRT, such as *electrode polarization*, *temperature effects*, *electrode configuration* and *CEC of clay* (or surface conduction effects), the results presented in this chapter have established that, ERMT is an extremely useful non-invasive characterization methodology to study sand-mud mixture sedimentation and bed formation processes, and, provided a suitable calibration is carried out, it is anticipated that this methodology can be deployed on variety of samples both at laboratory and field scales.

Finally, based on the findings of the current work, the following general relationship is proposed between the normalized bulk density of the sediment bed deposit and corresponding formation factor *F* value:

$$\frac{\gamma_{bulk}}{\gamma_p} = a.F^b \tag{4-4}$$

Also, to capture the relationship between porosity, φ and formation factor *F*, the following equation is equally proposed:

$$\varphi = \hat{a}e^{-\hat{b}.F} \tag{4-5}$$

The coefficients in Equations (4-4) and (4-5) are experimentally-derived [e.g. the coefficients in Equations (4-2) and (4-3) respectively, have been derived for sand-clay mixtures tested in this study]. The require condition for the proposed relationships is such that γ_{bulk}/γ_p and $\varphi \rightarrow 1$ as $F \rightarrow 1$. As an extension of the application of ERMT in settling column experiment, use of this technique in *quasi-field environment* has been demonstrated by adapting it to a benthic annular flume to study bed entrainment and erosion processes (see *chapter 6* for further details).

CHAPTER FIVE

Experimental Results: Sand-Clay Suspension Settling Experiment (ES-2)

"There are three principal means of acquiring knowledge…observation of nature, reflection and experimentation…"
—Denis Diderot

5.1 Introduction

The experimental findings from chapter 4 have served to demonstrate the ERMT to be suitable for the non-intrusive characterisation of spatial and temporal changes in mixed (sand-clay) sediment bed deposits forming as a consequence of sedimentation (i.e. settling and deposition) and subsequent consolidation behaviour for mixed sediment slurries in settling column tests. This will help improve fundamental understanding of the dynamic behaviour of mixed sediment beds within estuaries.

The current chapter details a parametric study on the spatial and temporal variations in sediment bed structure and composition resulting from the differential settling of cohesive clay and non-cohesive sand mixtures for a range of different mixture compositions, initial mixture mass concentrations and ambient fluid salinities (see Table 5-1). The main objectives of these experiments are as follows:

- To study the influence of these parametric conditions on the spatial and temporal variation of sediment bed layer composition and structure (i.e. mixed or segregated) resulting from the differential settling of mixed sediments. This is investigated in terms of settling and consolidation rates, depth dependent bulk densities, and bed porosities.
- To provide a significant dataset on sand-clay sedimentation processes, over a wide range of initial mixture concentrations and compositions required to (i) investigate further the parametric dependence of mixed and segregated bed deposit formation and (ii) test the polydisperse hindered settling formulation proposed by Cuthbertson *et al*. (2008) in terms of its predictive capabilities for the generation of these mixed and segregated bed deposits.

- To derive appropriate parametric criteria to describe the conditions under which well mixed or segregated bed layers will form in mixed sedimentary environments.

To achieve these objectives, an experimental programme and methods have been designed, as described in *sections* 3.6 (pg. 74) and 3.7 (pg. 78) of Chapter 3, a summary of which is provided in the following section.

5.2 Summary of Experimental Set-up and Conditions

The experiments were carried out in the custom-built settling column (Figure 3.5b) with embedded electrical resistivity probes to facilitate electrical resistance measurements of the evolving sand-clay deposit formation. Nine settling experiments (SET-EX1 to -EX9, Table 5-1) were carried out in addition to the five (i.e. ERT-EX1 to EX5) test runs carried out during the development stage of the test column (see Table 5-1).

Prescribed sand-clay mixture compositions were generated from the Polwhite-B kaolin clay and fine-to-medium grade quartzite sand (see *section* 3.7.1, pg. 79). For this set of experimental runs (i.e. SET-EX1 to EX9), the following sand(s): clay(c) compositions (% by dry weight) were tested: (i) 85(s):15(c); (ii) 75(s):25(c); (iii) 65(s):35(c). These sand-clay proportions extend the range of mixture from those tested in past studies on sand-mud sedimentation processes, which have typically considered mixtures with low to medium sand contents (i.e. > 10-20%) [e.g. Toorman 1996, 1999; Merckelbach and Kranenburg 2004b; Le Hir *et al*., 2011; Grasso *et al*., 2015; etc.]. Hence, the current tests are expected to provide additional data sets to validate existing analytical and numerical models (e.g. Cuthberston *et al*., 2008; Grasso *et al*., 2015; etc.), for hindered settling, sedimentation and consolidation processes, particularly those defining parametric conditions that lead to bed segregation. Previous research has revealed a correlation exists between the final structure of mixed sediment bed deposits and the initial sediment mixture concentration (Torfs *et al*., 1996; Been & Sills, 1996 and Sills, 1998). As such, three single-shot input concentrations have been tested in the run, i.e. 367 $kg\ m^{-3}$, 561 $kg\ m^{-3}$ and 813 $kg\ m^{-3}$.

The ambient fluid salinity was also varied between runs, with the mixed sediment slurries prepared using brine solutions with the following salinities: 0 *pp*t (i.e. fresh water),

15 *ppt*, 30 *ppt* and 40 *ppt*. Brackish estuarine waters may have salinity levels between 1 and 17 *ppt*; while on average, seawater in the world's oceans has a salinity of approximately 35 *ppt* (Levinton, 1995). Thus, the range of salinities tested covers the majority on aquatic environment and allows direct comparison with results from other experimental studies in the literature (e.g. Owen 1970; Sutherland *et al*., 2014; Mehta, 2014; etc.).

A summary of the main experimental parameters and test conditions for all the experiments is presented in Table (5-1). In each experimental run, the sand-clay mixture was transferred into the column as a single shot and mixed thoroughly with a porous grid mixer to prevent initial deposition prior to the start of the test. During the settling phase, vertical resistivity (see *section* 3.7.3, pg. 80) profiles were measured at 30 *second* intervals for up to 24 *hours*. The interface that developed between the supernatant pore liquid and the settling sediment layer was recorded at every 30 minutes for the first 6 hours and every hour subsequently from photographs and video recordings of the settling process (see *section* 3.7.4 on image capturing, pg. 81). These time-lapsed photographic and video images were used essentially to observe and measure (i) the developing bed layer structure and, in particular, segregation between the depositing sand and clay fractions, and (ii) the vertical displacement of the interface formed between the developing bed deposit layer and supernatant pore water.

5.3 Qualitative Observation on Sand-Clay Sedimentation

This section provides a qualitative description of the physical observations made during the sedimentation experiments. Within the settling column arrangement employed in the current study, the typical sedimentation and bed formation processes displayed by different sand-clay mixtures are essentially one-dimensional, with upward pore water flow and downward movement of sediment (Torfs *et al*., 1996). Clearly, it is anticipated that due to differential settling effects, sand particles in the initial mixture will settle out faster than the clay particles/flocs. These processes have been reported to be largely responsible for the observed segregation layers forming within sand-mud bed deposits (e.g. Migniot, 1968; Ockenden and Delo, 1988; Williamson, 1991; Williamson and Ockenden, 1993; Torfs *et al*., 1996; etc.). However, the specific parametric influence of initial mixture concentration, sand and clay proportion and fluid salinity means that the resulting bed deposit structure and layer composition are likely to be more complex.

Table 5-1 Main experimental parameters and conditions for ES-2

Experiment Name [(1)]	%Sand: %Clay	Initial mixture Concentration, $C_{o,s}$ (kg/m^3)	Pore-water Salinity (ppt)	Pore-water density ρ_w (kg/m^3) [(2)]	Initial clay concentration $C_{o,s}^{cl}$ (kg/m^3)	Initial sand concentration $C_{o,s}^{sa}$ (kg/m^3)	Initial vol. mix. conc. $Ø_s$	Initial vol. clay conc. $Ø_s^{cl}$	Initial vol. sand conc. $Ø_s^{sa}$	Deposit segregation (Y/N)
SET-EX1	85S:15C	561	15.0	1009.10	84	477	0.2131	0.0324	0.1807	Y
SET-EX2	85S:15C	561	30.0	1020.50	84	477	0.2131	0.0324	0.1807	Y
SET-EX3	75S:25C	561	30.0	1020.50	140	421	0.2136	0.0541	0.1595	Y
SET-EX4	65S:35C	561	0.0	997.80	196	365	0.2140	0.0757	0.1383	Y
SET-EX5	65S:35C	561	15.0	1009.10	196	365	0.2140	0.0757	0.1383	Y
SET-EX6	65S:35C	561	30.0	1020.50	196	365	0.2140	0.0757	0.1383	Y
SET-EX7	65S:35C	561	40.0	1028.10	196	365	0.2140	0.0757	0.1383	Y
SET-EX8	65S:35C	367	30.0	1020.45	128	239	0.1399	0.0494	0.0905	Y
SET-EX9	65S:35C	813	30.0	1020.45	285	528	0.3100	0.1100	0.2000	N
ERT-EX1	100S:0C	330	29.2	1019.90	0	330	0.1250	0	0.1250	-
ERT-EX2	75S:25C	330	29.2	1019.90	83	247	0.1256	0.0320	0.0936	Y
ERT-EX3	50S:50C	330	29.2	1019.90	165	165	0.1262	0.0637	0.0625	Y
ERT-EX4	25S:75C	330	29.2	1019.90	247	83	0.1268	0.0954	0.0314	N
ERT-EX5	0S:100C	330	29.2	1019.90	330	0	0.1274	0.1274	0	-

[(1)] SET-EX1-9 - shorter term tests (up to 24 hours); EIT-EX1-5 - longer term tests (up to 72 hours)

[(2)] Pore-water densities ρ_w calculated at 22^{0}C

For the vast majority of the sediment mixtures tested (SET-EX1 to EX8 and ERT-EX2 to EX3, see Table 5.1), following the onset of the settling phase, the sand particles tend to settle to the bottom of the column, resulting in the formation of two distinct interfaces in the settling column by the end of the experimental run. The top interface occurs between the overlying supernatant pore fluid and the settling clay-rich sediment layer, while the lower interface forms as a result of segregation between the sand and clay proportions in the mixture. Additionally, within the final bed deposits, distinct regions or segments with different composition and structure can be identified, particularly for all the segregated bed deposits. This is discussed in greater detail below.

5.3.1 Segregation in bed deposits

The settling characteristics of the tested sand-clay mixtures were largely responsible for the observed variability in the final structure and composition of the bed deposits, defined parametrically by initial sediment mixture concentration, composition and pore fluid salinity. For clarity, all the experimental runs have been grouped as shown in Table (5-2) to facilitate comparison of parametric dependencies.

Table 5-2 Classification of experimental runs into parametric groupings

Group	Elements	Descriptions
A	SET-EX1 & EX5	Constant salinity (15ppt) with varying clay contents (15 & 35%)
B	SET-EX2, EX3 & EX6	Constant salinity (30ppt) with varying clay contents (15, 25 &35%)
C	SET-EX1 & EX2	Lower clay content (15%) with varying salinity (15 & 30ppt)
D	SET-EX4, EX5, EX6 & EX7	Higher clay content (35%) with varying salinity (0, 15, 30 & 40ppt)
E	SET-EX6, EX8 & EX9	Constant salinity (30ppt) and clay content (35%) with varying initial mixture concentrations (367, 561 and 813 kg/m^3)

Figures 5.1 – 5.3 (and *Appendices* 5-1 – 5-2) show the time-lapsed images of the formation of bed deposits from run SET-EX1 to EX9. These figures reveal that a large proportion of the sand particles settle out of the mixtures between t = 0 and t = 3 *hours*. It is clear that the time of initiation of segregations vary among the tested mixtures. For examples, the 85s:15c mixtures (run SET-EX1 and EX2; Group C, Table 5.1), begin to segregate almost immediately following the initiation of the settling phase of the test (i.e.

elapsed time t = 10 *s*, Figure 5.1a & *Appendix* 5-1), with a sand-dominated deposit layer forming at the base of the column over an elapsed time t = 2 *mins* (Figure 5.1a & Appendix 5-1). Above these sand-dominated bottom deposit layers, a sharp interface forms with the overlying clay-rich bed layer that develops over a significantly longer period of time (i.e. $t \rightarrow 6$ *hrs*, Figure 5.1a & Appendix 5-1), as indicated by the vertical displacement of the upper interface with the supernatant pore fluid. From Figure 5.1b, the 75s:25c mixture (run SET-EX3) appears to follow similar trend, the initial formation of sand-dominated deposit layer at the base of the column occurring over t = 15-30 *mins* (Figure 5.1b).

Time-lapsed images of sedimentation process shown in Figure 5.2 & *Appendix* 5-2(a-c) respectively for four of the mixtures with 65s:35c (i.e. run SET-EX4, SET-EX5, SET-EX6 and SET-EX7, Group D; Table 5.1), also reveal a similar segregation trends to the 85s:15c and 75s:25c mixtures discussed above, but with the sand-dominated layers forming at the base of the column over a longer time period t = 60 *mins* [Figure 5.2 & *Appendix* 5-2(a-c)]. Here also the interfaces between the overlying clay-rich and sand-rich layers are shown to be less well-defined.

Another experimental run which exhibited strong sand-clay segregation was SET-EX8 (i.e. Figure 5.3a), immediately after initiation of the settling phase (i.e. similar to SET-EX1 and SET-EX2). The formation of the sand-rich base layer is formed over a similar time scale (t = 60 *mins*) to the 65s:35c mixtures (e.g. SET-EX4, SET-EX5, SET-EX6 and SET-EX7) [Figure 5.2 & Appendix 5-2(a-c)]. Only two experimental runs with sand-clay mixtures did not indicate the development of segregation in the settling column test: SET-EX9 [65s:35c, Figure 5.3(b)] and ERT-EX4 (25s:75c; Figure 4.2a). This was due to the high clay concentration (i.e. $C_{o,s}^{cl}$ = 285 $kg\ m^{-3}$ and 247 $kg.m^{-3}$ respectively; Table 5.1) in the sand-clay mixtures, irrespective of the corresponding sand content in the mixture (i.e. $C_{o,s}^{sa}$ = 528 $kg\ m^{-3}$ and 83 $kg\ m^{-3}$ in SET-EX9 and EIT-EX4 respectively). Interestingly, images from the resulting deposit from run SET-EX9 (i.e. Figure 5.3b) indicate that although no sand-dominated bottom layer is shown to form, the high sand content in the mixture becomes trapped in distinct patches within the clay-dominated layer, i.e. for $z < 200$ *mm* at t = 6 and 24 *hours*.

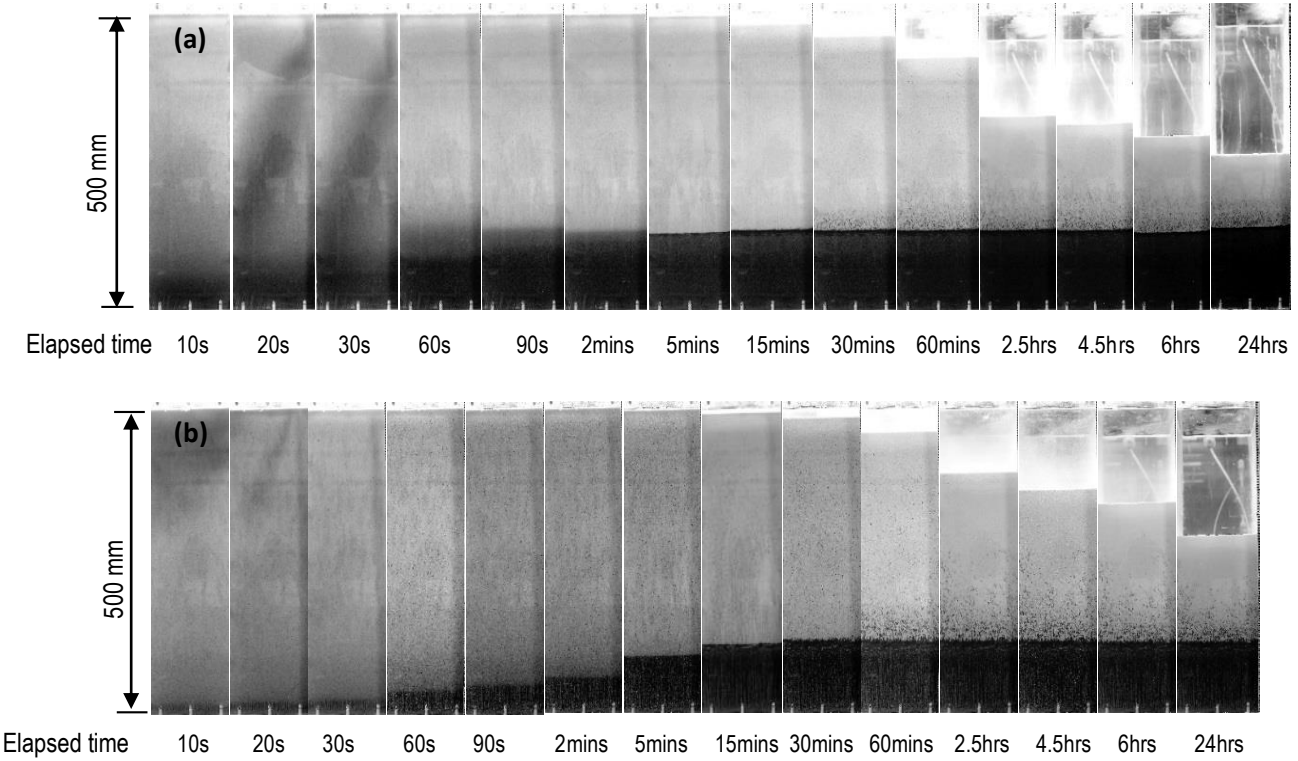

Figure 5.1 Time-lapsed images of sand-clay sedimentation process at *t* shown for (a) 85s:15c mixture, run SET-EX1 and (b) 75s:25c mixture, SET-EX3 (see Table 5.1)

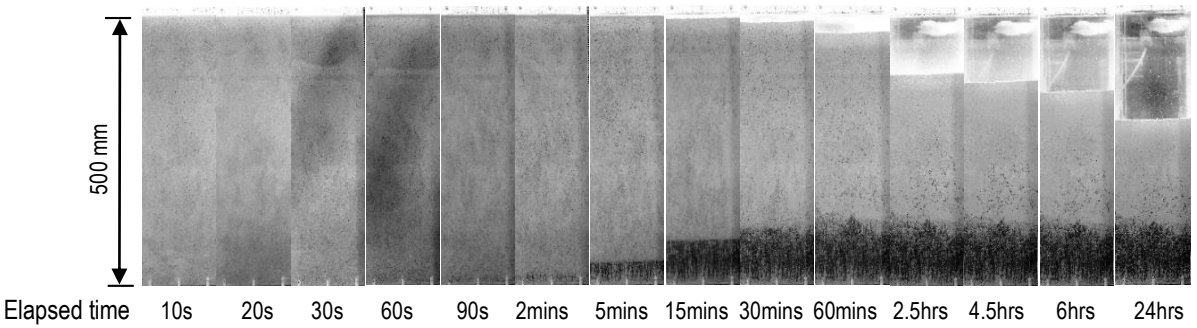

Figure 5.2 Time-lapsed images of sand-clay sedimentation process at times t shown for run SET-EX4 (65s:35c) [see Table 5.1]

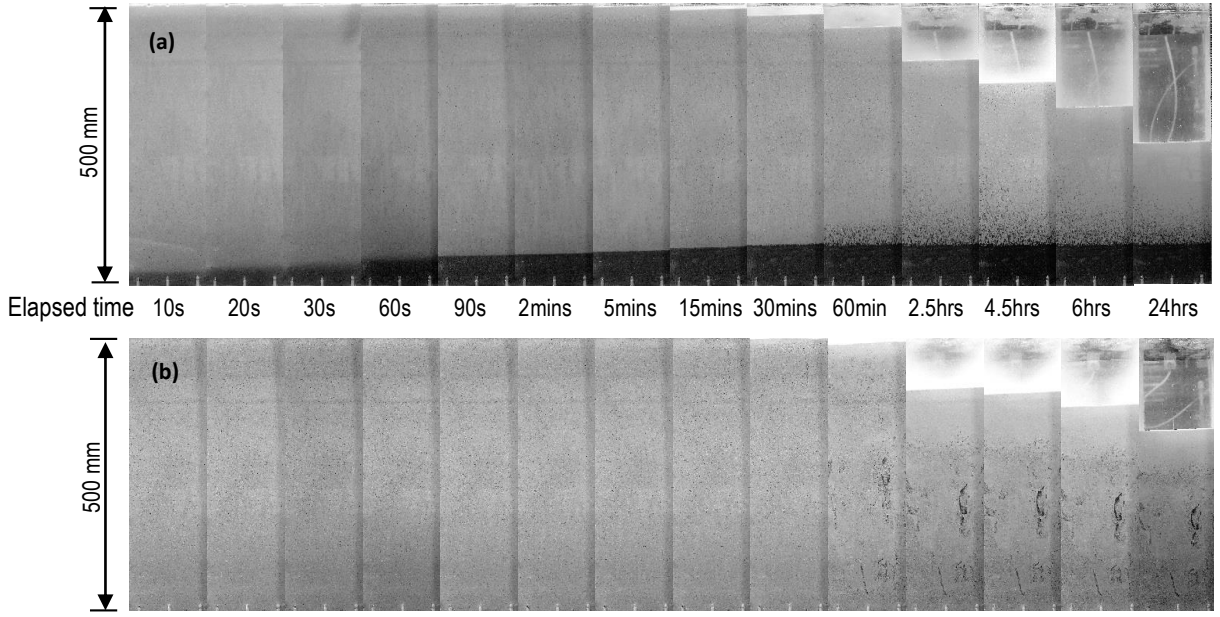

Figure 5.3 Time-lapsed images of sand-clay sedimentation process at times t shown for 65s:35c mixtures (a) run SET-EX8 (C_s = 367 kg.m^{-3}) and (b) SET-EX9 (C_s = 813 kg.m^{-3}) [see Table 5.1]

In terms of the classification of experimental runs into parametric groupings (Table 5-2), comparison of SET-EX1 and SET-EX2 [i.e. for otherwise similar 85s:15c mixture conditions; Figure 5.1a & *Appendix* 5-1), shows the influence of salinity to have no significant effect on the formation of segregation in sand-clay sedimentation process, particularly in the presence of high volumetric sand concentration ($Ø_s^{sa}$). Similarly, comparing experiments SET-EX4 (0 ppt), SET-EX5 (15 ppt), SET-EX6 (30 ppt) and SET-EX7 (40 *ppt*), for equivalent 65s:35c mixture conditions [Figure 5.2 & Appendix 5-2(a-c)], shows the formation of segregation within their resulting bed deposits to be temporally and spatially similar. As such, the differences in ambient pore fluid salinity between runs appears to have no significance influence on the bed deposit formation or the degree of sand-clay segregation observed.

The parametric influence of initial clay concentration (C_s^{cl}) within the mixtures (for otherwise similar mixture conditions) can be investigated by comparing experimental runs SET-EX1 and SET-EX5, conducted at a salinity of 15 *ppt*, and runs SET-EX2, SET-EX3 and SET-EX6, conducted at a higher salinity of 30 *ppt*. Comparing the time-lapsed images of SET-EX1 (Figure 5.1a) and SET-EX5 (*Appendix* 5-2a) shows that the lower clay concentration in SET-EX1 resulted in strong segregation with a well-defined interface between the sand-dominated base layer and the overlying clay-dominated layer, which developed over a short time period t = 2 *mins* (Figure 5.1a). By contrast, an increase in the clay content in the run SET-EX5, resulted in a more transitional segregation with a less well defined sand-clay interface forming over a longer time period t = 60 *mins* (*Appendix* 5-2a). Similarly, for runs SET-EX2, SET-EX3 and SET-EX6 (i.e. *Appendix* 5-1, Figure 5.1b & *Appendix* 5-2b respectively), it is clear that the degree of segregation observed in each bed deposit appears to become more transitional with a less well defined interface with increasing initial clay concentration.

The findings highlighted above, clearly indicate that the most highly segregated bed conditions tend to occur for sand-mud mixtures with higher sand $Ø_s^{sa}$ and lower clay $Ø_s^{cl}$ concentrations, respectively, while salinity was shown to have negligible effect. It is also interesting to note that the two sand-clay mixtures for which no segregation was observed had the highest volumetric clay concentrations [i.e. $Ø_s^{cl}$ = 0.095 (ERT-EX4) and $Ø_s^{cl}$ = 0.110 (SET-EX9), Table 5.1], irrespective of the corresponding volumetric sand content [i.e. $Ø_s^{sa}$ = 0.0314 (ERT-EX4) and $Ø_s^{sa}$ = 0.20 (SET-EX9), Table 5.1]. This latter finding suggests that a critical value of clay concentration $Ø_s^{cl}$ exists where sand particles in the

mixture become trapped within the overlying clay-dominated layer and prevented from settling to form a segregated sand dominated layer at the bottom of the settling column. This would appear to be analogous to a gelling concentration condition forming in the clay-dominated layer (e.g. Winterwerp and van Kesteren 2004) at which point the clay flocs will form a space-filling network within the evolving bed layer, which represents the onset of primary consolidation (Winterwerp, 2001).

5.3.2 Bed deposits compositional and structural variations

Qualitative analysis of photographic and video images for all the tests show clearly that the segregation behaviours within the bed deposits display different compositional and structural features and transitions with depth. A schematic representation of the compositional and structural transitions observed within the bed deposits is shown schematically in Figure 5.4. At the initiation of the settling phase in all the tests, all mixtures were uniformly distributed, mixed slurries (Figure 5.4a), and they settled to form distinct bed deposits with vertical changes in composition and structure. In general, deposit regions (or segments) with four distinct and different composition and structure have been identified for all the segregated bed deposits. These are presented as *Segment Type I – IV* in Figure 5.4b, with corresponding brief descriptions of each observed segment given. It is interesting to observe that some experimental runs exhibit all the four segment types during the settling phase while others show only some regions/segments to be present. It is also noted that the time of formation of the different segments differs between sand-clay mixtures. The number and nature of segments exhibited in each deposit and the corresponding time of formation are controlled largely by the parametric conditions in each run (e.g. solid volumetric concentration of mixture, sand-clay composition and pore fluid salinity).

In all tests, after the initiation of hindered settling phase and prior to the onset of primary consolidation stage, near-vertical drainage paths (i.e. *dewatering* channels), were formed within the predominantly clay suspensions in Segment Type III and IV. Pore fluid was seen being expelled through these *dewatering* channels ($\sim \leq 3.0$ *mm* in diameter). After the onset of primary consolidation phase, they later became smaller or even disappeared completely. It was also observed that these dewatering channels not only allowed the upward expulsion of water, but sand grains were also shown to settle through the dewatering channels; an observation also recorded by Merckelbach (2000). When the *dewatering* channels have significantly diminished or disappeared (analogous to the clay

matrix reaching the gelling concentration, e.g. Winterwerp and van Kesteren, 2004), the remaining sand grains were trapped within the clay matrix, thereby contributing to the development of sand clusters or patches (e.g. Segment Type II and III).

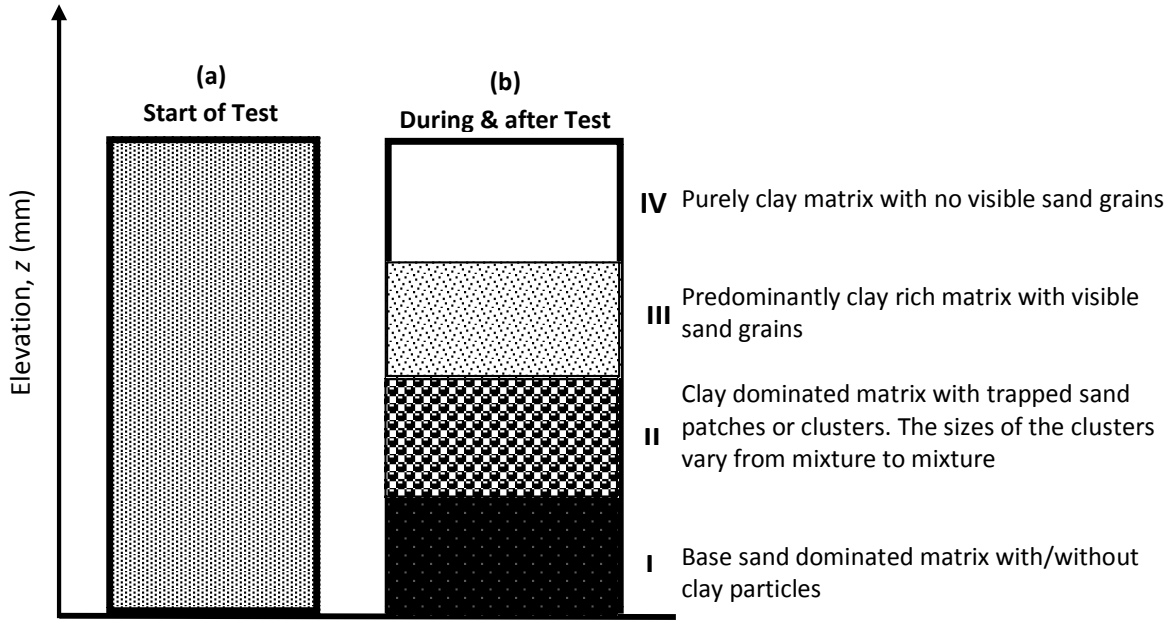

Figure 5.4 Schematic representation of the compositional and structural features observed in the sand-clay bed deposits over the range of parametric conditions tested (a) at the start of the test (b) of the final bed deposit formed

Figures 5.5 & 5.6 present time-lapsed images of the developing bed deposits for all the mixtures tested to investigate closer, the structure and composition of the segregated sand-clay regions/segments that occurred within these deposits in line with schematic representation in Figure 5.4. For the majority of the experimental runs, it is apparent that a proportion of the clay fraction is trapped in the sand-dominated base layer; while some sand particles become trapped as clusters in the upper clay-dominated layer during the bed formation process, resulting in segment types discussed above (Figure 5.4).

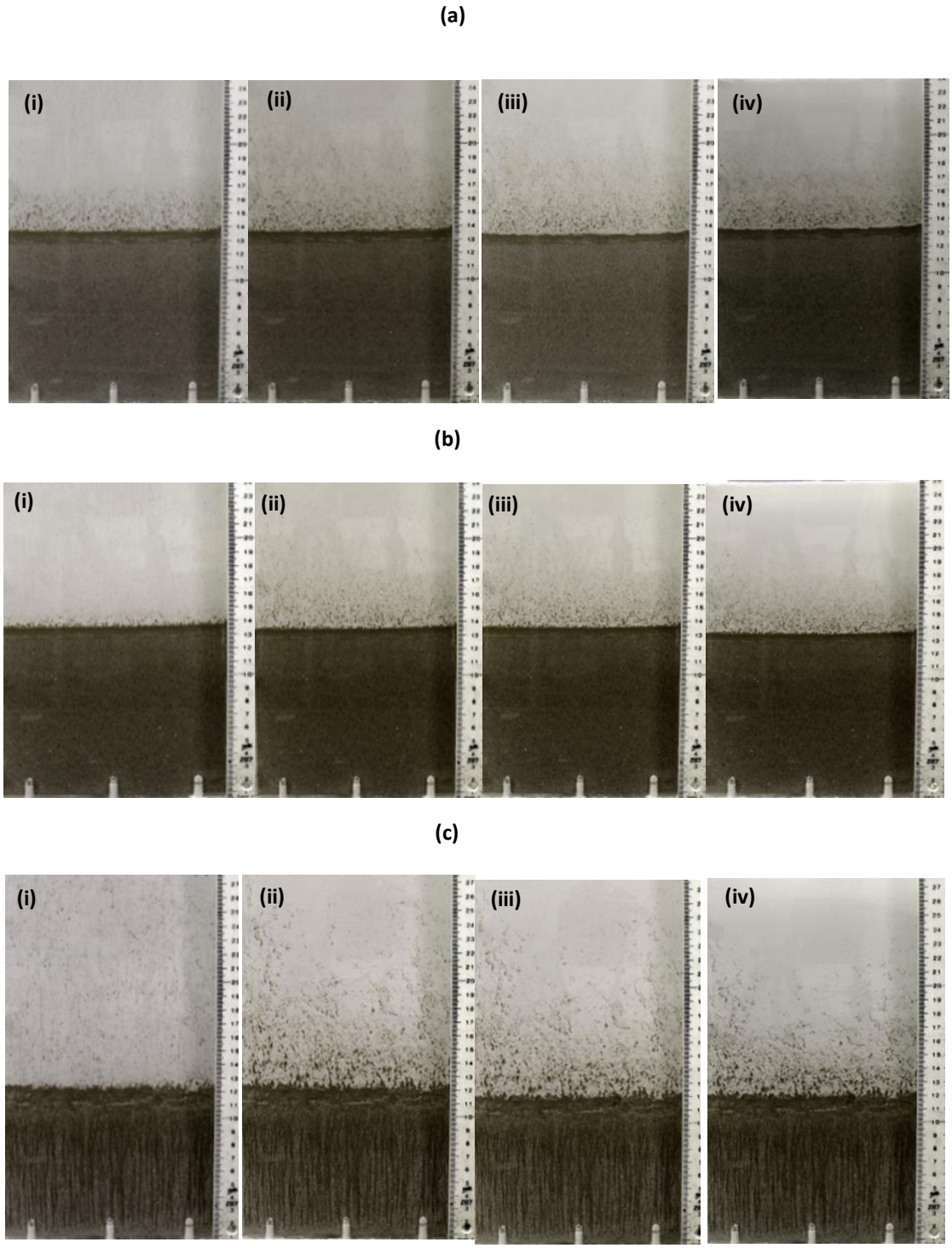

Figure 5.5 Time-lapsed images showing segregated deposit formation at elapsed times t shown for run (a) SET-EX1 (85s:15c) (b) SET-EX2 (85s:15c) and (c) SET-EX3 (75s:25c) (see Table 5.1); Elapsed times of (i)→(iv) = 30, 180, 360,1440 minutes respectively.

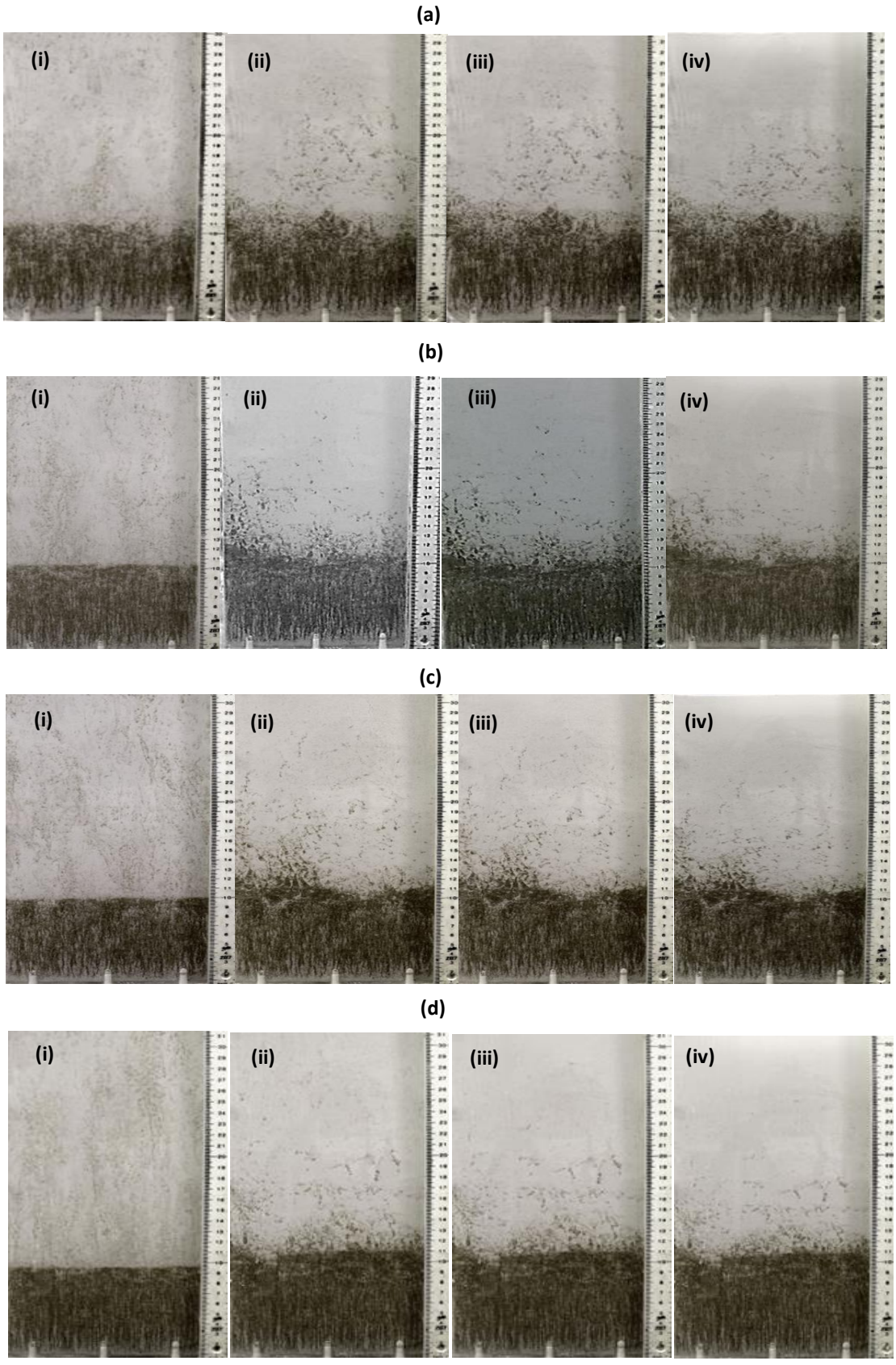

Figure 5.6 Time-lapsed images showing segregated deposit formation at elapsed times *t* shown for runs with 65s:35c mixtures (a) SET-EX4 (b) SET-EX5 (c) SET-EX6 and (d) SET-EX7 (see Table 5.1); Elapsed times of (i)→(iv) = 30, 180, 360,1440 minutes respectively.

Comparison between Figures 5.5b & 5.6c, show the temporal development of strongly segregated bed deposits for the 85s:15c mixture (run SET-EX2, Table 5.1) and the transitionally segregated deposit arising from the 65s:35c mixture (i.e. run SET-EX6 (Table 5.1), respectively. These images again highlight the rapid formation of sand-dominated layer (i.e. Segment Type I, Figure 5.4) at the base of the column (i.e. z = ∼140 *mm* thick and ∼100 *mm* thick at t = 30 *mins* for SET-EX2 and SET-EX6, respectively). The layer in SET-EX6 is characterised by near-vertical banding indicative of the development of clay-pore water "dewatering" channels during this initial settlement phase. However, this is not visible in the thicker sand-dominated bottom layer of SET-EX2. For both mixtures, this bottom layer (Figure 5.4) appears to be overlain by a thicker clay-dominated layers containing discrete sand patches and grains [i.e. z =140∼200 *mm* and 110∼260 *mm* after t = 180 *mins* for SET-EX2 (Figure 5.5b) and SET-EX6 (Figure 5.6c)]. The discrete sand patches appear to be large in SET-EX6 and smaller in SET-EX2. With increasing duration (i.e. for t = 360→1440 *mins*), this layer (i.e. Segment Type II) is shown to slightly compact, as indicated by the downward displacement of the trapped sand patches (Figures 5.5b & 5.6c), although, this is less obvious in SET-EX2 than observed in SET-EX6 due mainly to (i) the lower volumetric clay concentration in run SET-EX2, compared to SET-EX6, and/or (ii) the formation of a sharp segregational interface between the incompressible base sand layer and overlying clay-rich deposit.

The presence of discrete sand patches within the clay-dominated layers of the two mixtures is particularly interesting when considering the time at which trapping occurs. The significant difference in the mixture composition for SET-EX2 and SET-EX6 (see Table 5-1) appears to indicate that a proportion of the sand fraction becomes trapped at elapsed times $t \geq 150$ *mins* (see also *Appendices* 5-1 and 5.2b), most probably, as the clay concentration $\emptyset_s^{cl}$ reaches the gelling concentration. Above segment type II layer, the remainder of the overlying clay suspension deposits to form a (relatively) sand-free surface layer (i.e. Segment Type IV) within the bed deposit (i.e. z > 200 *mm* and 260 *mm* for SET-EX2 and SET-EX6 respectively; Figures 5.5b & 5.6c).

A similar comparison is carried out on runs within parametric classification *Group-D* in Table 5.2 (i.e. runs SET-EX4 to -EX7), to identify any significant influence that the pore fluid salinity may have on the temporal and spatial development of the resulting bed deposit composition and structure in particular in the presence of high % clay content (i.e. 35%). From the images in Figure 5.6, the development of transitional segregated deposits

is shown for all the mixtures considered in classification *Group-D* (Table 5.2). Indeed, the temporal and spatial evolution of the bed deposits are similar to the descriptions given above for the bed deposit formation from the 65s:35c mixture (i.e. SET-EX6). This is obvious as they all have the following parametric conditions in common: initial mixture concentration and sand and clay contents (Table 5.1). In summary, these runs appear to have similar segment types (Figure 5.4) of approximately the same vertical extent (see Figure 5.6), with each final bed deposit having all the four distinct segment types as defined in Figure 5.4. In other words, salinity has little or no influence on the formation and structure of the final segregated (sand-clay) bed deposits in comparison to the strong influence of initial mixture concentration and fractional sand and clay concentration. However, further analysis of a large number of their photographic and video images, indicates that the appearance of segment type-II is delayed in mixture with the highest salinity concentration i.e. SET-EX7 (40 *ppt*) [at t = 150 *mins*; Appendix 5-2c], compared to SET-EX4 (0 *ppt*) [at t = 60 *mins*; Figures 5.2]. Similar trend was equally observed in SET-EX2 (30 ppt) [Appendix 5-1] and SET-EX1 (15 *ppt*) [Figure 5.1a], where Segment Type II appeared at t = 60 *mins* and 30 *mins* respectively. Further analysis on the parametric influence of pore fluid salinity on for example differential settling behaviour of sediment mixtures shall be discussed later in the chapter.

5.4 Hindered Settling and Consolidation Rates

The vertical displacement of the upper bed interface with the supernatant pore fluid for different sand-clay mixtures was measured from the time-lapsed photographic and video images (e.g. Figures 5.1-5.3). Previous studies (e.g. Torfs *et al*., 1996; Xu *et al*., 2012, Sutherland *et al*., 2014, etc.) used the temporal change in this fluid-sediment interface elevation to determine the variation in sedimentation rates for sand-mud mixtures over the experimental duration. As such, the settling and consolidation rates (w_s, *mm* s^{-1}) of the depositing sediment mixtures tested here are also estimated directly from measurement of the temporal variation in the interface elevation over the duration of each experimental test.

Graphical representation of this temporal change in the upper interface elevation for the different sand-clay mixtures tested is shown in Figure 5.7a, while Figure 5.7b, is the plots of the corresponding settling/consolidation rates (*mm* s^{-1}) against elapsed time t (*s*). From Figure 5.7a, an initially high vertical displacement in the interface elevation which

reduces as the elapsed time increases, can be seen for all the sand-clay mixtures (i.e. SET-EX1 to SET-EX9) between t = 0 and 3 *hrs.* It is clear from this plot that, an inflection point exists on the temporal evolution of these interfacial settling profiles, that delineates the transition between hindered settling behaviour and the onset of the so-called phase I consolidation (Imai, 1981; Merckelbach and Kranenburg, 2004a) [see *section* 2.4]. Figure 5.7b shows that the time at which this transition occurs between the settling phase and the onset of phase I consolidation lies between t = 9,000 s and 18,000 *s*, depending on the sand-clay mixture tested. As these upper interfaces occur between the clay-rich sediment and the overlying supernatant pore fluid, these inflections points are thought to be initiated when the gelling concentration (e.g. Danker, 2006; te Slaa *et al*., 2013) or structural density (e.g. Sills, 1998; Been and Sills, 1981) in the overlying clay-rich sediment is reached.

During the so-called hindered settling regime (Figures 5.7), it is clear that, for sand-clay mixtures with relatively high volumetric clay concentrations $Ø_s^{cl}$ and/or pore water salinity, the downward interfacial displacement reduces and occurs over a longer period of time. This corresponds to a general reduction in the hindered settling rate (Figures 5.7b), compared to runs with a lower clay content and lower salinity. These findings, are expected considering the form of the hindered settling velocity formula proposed by Winterwerp (2002) for a mono-dispersed suspension of cohesive sediment flocs (see *section* 2.3.4; pg. 25):

$$w_s^{cl} = \frac{\left(1-\emptyset_{floc}^{cl}\right)\left(1-\emptyset_s^{cl}\right)}{1+2.5\emptyset_{floc}^{cl}}\, w_{s,0}^{cl} \tag{5-1}$$

where $\emptyset_{floc}^{cl}$ is the volumetric concentration of clay flocs within the suspension and $w_{s,0}^{cl}$ is the fall velocity of a single clay floc. It has been demonstrated in Figure 5.7 that, higher clay concentrations $\emptyset_s^{cl}$ result in larger hindering effect on sedimentation rates. This is due to increased buoyancy, which acts against the weight of settling flocs [i.e. accounted for by the hindered settling factor $(1-\emptyset_s^{cl})$, Equation 5-1]. More speculatively, higher salinities may result in the formation of larger clay flocs (and, hence, larger volumetric clay floc concentration $\emptyset_{floc}^{cl}$) at least over a range of salinity values tested. The result would be an increase in return flow, and increased viscosity effects [i.e. accounted for by

the hindered settling factors $\left(1 - \emptyset_{floc}^{cl}\right)$ and $(1 + 2.5\emptyset_{floc}^{cl})$, respectively, Equation 5-1].

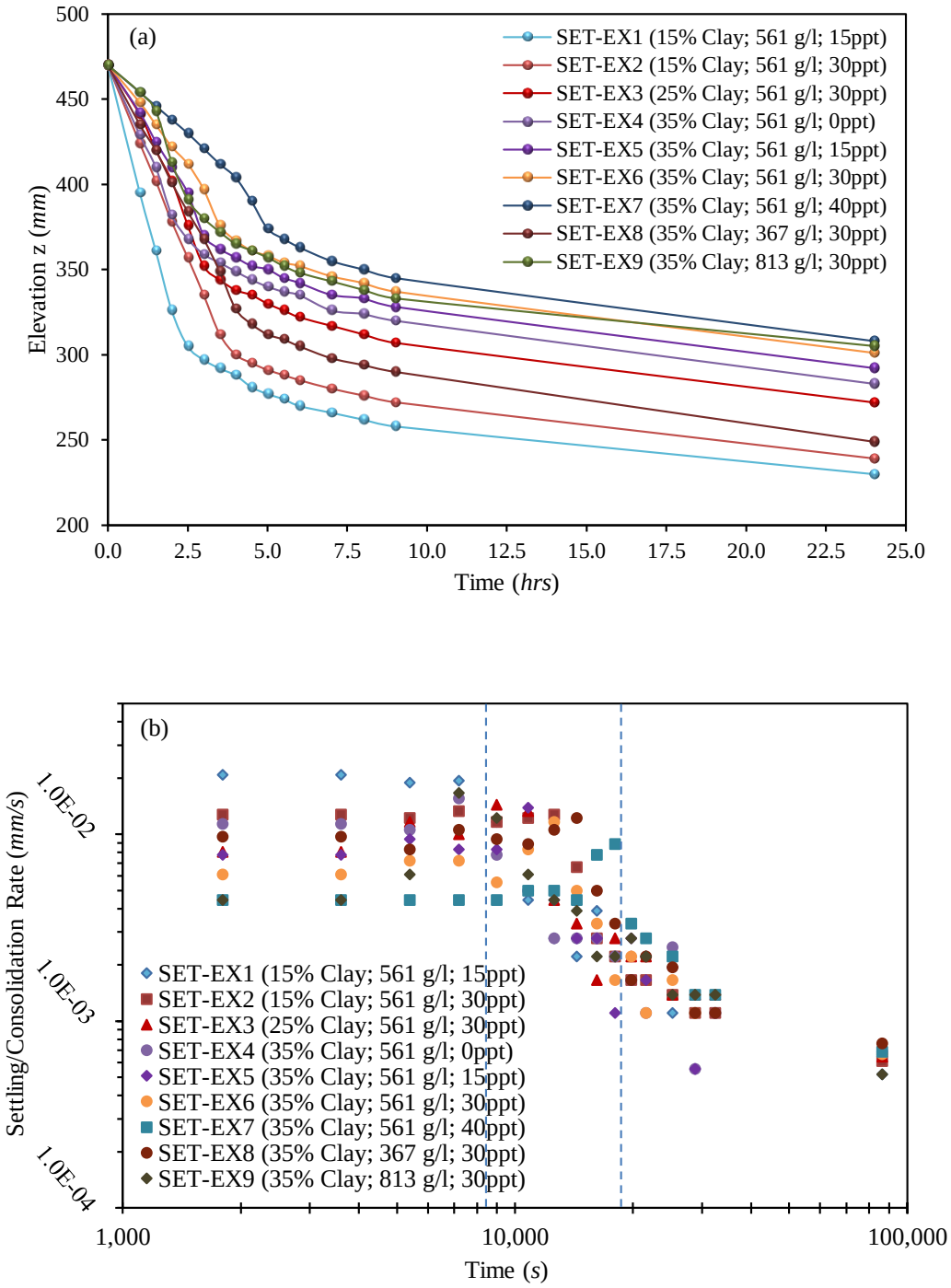

Figure 5.7 Temporal variation in upper clay layer interface with supernatant pore water for SET-EX1 to EX9 (b) corresponding temporal variation in settling/consolidation rates for all the experimental runs

Furthermore, Figure 5.7b, indicates that, the hindered settling rates vary in the order O $(10^{-3}–10^{-2})$ $mm\ s^{-1}$, depending on the initial mixture fractional composition (and particularly clay concentration $\emptyset_s^{cl}$ values), while consolidation rates decrease from O

(10^{-3}) *mm* s^{-1} to *O* (10^{-4}) *mm* s^{-1} with increasing elapsed time. These results are also broadly in agreement with the findings of other researchers, e.g. Torfs *et al*. (1996), te Slaa *et al*. (2013), etc. In addition, the settling patterns exhibited by sand-mud mixtures with high sand concentrations $Ø_s^{sa}$, suggest that settling rates of the sand-clay mixtures generally increase with increasing sand content, a finding also in agreement with Torfs *et al*. (1996).

5.5 Parametric Dependency of Sedimentation Rates

The parametric dependency of the sedimentation process on initial fractional composition of sand-clay mixtures (i.e. relative sand and clay concentrations) was investigated under two levels of salinity (15 and 30 *ppt*). As anticipated, Figures 5.8a(i) & b(i), show that immediately after the start of the experiments, the vertical interfacial displacement during the hindered settling stage is much slower in SET-EX5 (15 *ppt*) and SET-EX6 (30 *ppt*) [both with C_s^{cl} = 196 *kg* m^{-3}] when compared with SET-EX1 (15 *ppt*) and SET-EX2 (30 *ppt*) [i.e. with C_s^{cl} = 84 *kg* m^{-3}]. Figure 5.8a(ii) indicates that the initial hindered settling rates for SET-EX1 (C_s^{cl} = 84 *kg* m^{-3}) and SET-EX5 (C_s^{cl} = 196 *kg* m^{-3}) [i.e. Group A, Table 5-2] are on the average of 66 *mm/hr* and 33 mm/hr respectively, with corresponding initial consolidation rates of 8 *mm/hr* and 6 *mm/hr* respectively [Note: these average settling rates were estimated by finding the average of sedimentation rates from the initiation of hindered settling regime up until *t* = 10,000 *s*, for hindered settling phase; where *t* = 10,000 *s* was arbitrarily taken as the inflection point that delineates the transition between hindered settling behaviour and the onset of the phase I consolidation, see *section* 5.4].

On the other hand, Figure 5.8b (ii) shows for SET-EX2 and SET-EX6 (Group B, Table 5-2), average initial hindered settling rates of 45 *mm/hr* and 25 *mm/hr* respectively, with both mixtures having similar consolidation rates of 6 mm/hr [Figure 5.8b (ii)]. These results appear to suggest that, at the consolidation stage, the sedimentation behaviour of the sand-clay mixtures under consideration are very similar. This is expected, as the clay-dominated bed deposit layer is expected to be fully formed and subsequent vertical variation in the sediment-fluid interface elevation will result primarily from consolidation effects in the clay-dominated layer (see Figures 5.1 & 5.2). Nevertheless, the significant differences between the average settling rates of these sand-clay mixtures at hindered settling phase, indicate again, that higher clay mass concentration within the initial sand-

clay mixture inhibit both the initial hindered settling phase and subsequent formation of the mixed bed deposit, broadly in agreement with the findings of Torfs et al. (1996).

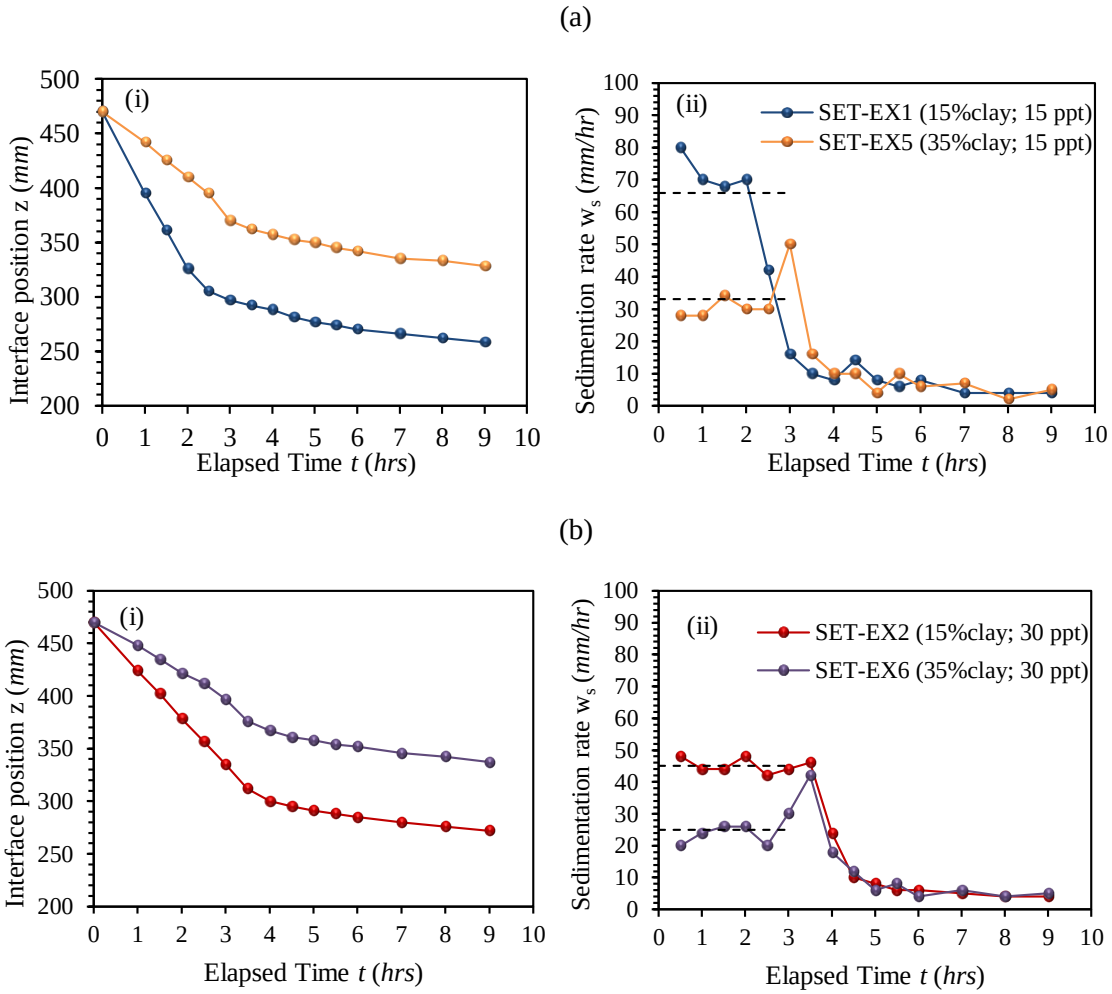

Figure 5.8 Sedimentation rates showing parametric influence of clay mass concentrations C_s^{cl} for (a) SET-EX1 and SET-EX2 (b) SET-EX2 and SET-EX6; [a(i) and b(i) being comparison of their corresponding upper interface displacement profiles respectively; with dashed lines in a(ii) and b(ii) showing corresponding average settling rates at hindered settling phase]

Figure 5.9 shows the parametric influence on sedimentation rates of salinity for identical sand-clay mixture compositions. Generally, for the two groups (i.e. Group C and D; Table 5.2), the results in Figures 5.9a(i) and b(i), clearly demonstrate that, there appears to be a systematic dependency of the temporal displacement of the upper interface on the pore water salinity. Specifically, higher initial settling rates are measured for sand-mud mixtures with lower pore water salinities [Figures 5.9a(ii) & b(ii)]. This trend is also clearly demonstrated from the calculated sedimentation rates [i.e. Figure 5.9b(ii)], which indicate larger and earlier peak settling rates occur for sand-clay mixtures with lower pore water salinities.

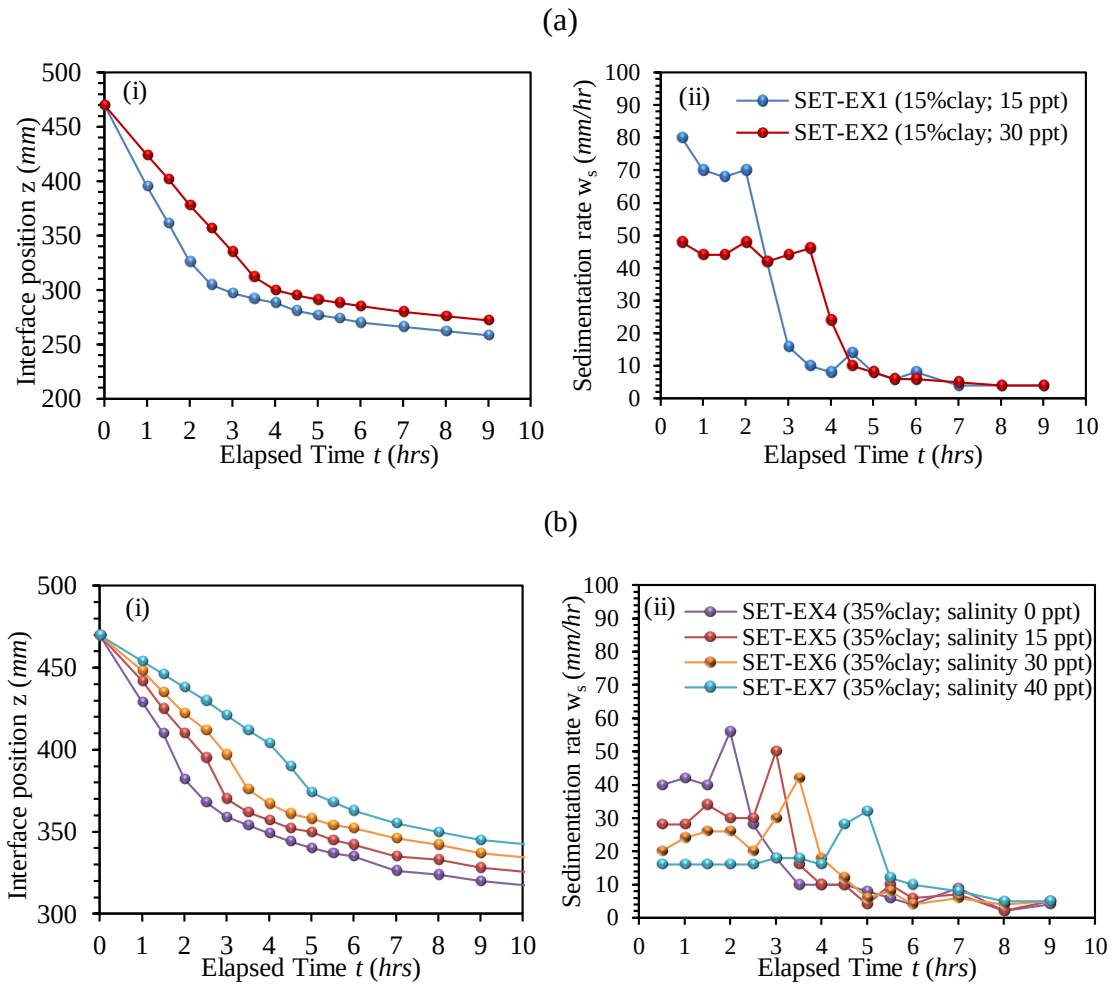

Figure 5.9 Sedimentation rates showing parametric influence of salinity concentrations for mixtures with (a) low C_s^{cl} (b) high C_s^{cl}; [a(i) and b(i) being comparison of their corresponding upper interface displacement profiles respectively]

Results in the current chapter along with previous studies (e.g. Torfs *et al.*, 1996; te Slaa *et al.*, 2013; Grasso *et al.*, 2014; Grasso *et al.*, 2015), have established that initial clay concentration has a strong parametric influence on sedimentation characteristics of sand-mud mixtures. However, from Figure 5.9, it is apparent that ambient salinity equally, has significant effect on settling characteristics of sand-clay mixtures. These results (Figures 5.9) specifically reveal that, if the salinity of sand-clay mixture is sufficiently large (e.g. > 15 *ppt*), and the proportion of clay in the initial mixture is relatively high (e.g. ≥ 15%), the settling/consolidation rate will be significantly inhibited. These findings on the parametric influence of salinity on sedimentation rates are somewhat surprising, considering the general consensus (see *section* 2.3.5; pg. 30) that settling velocity would be expected to increase with increasing ambient salinity up to about 30 *ppt* (e.g. Owen, 1970; Grabowski *et al.*, 2011; Mehta, 2014; etc.). Also there is an expectation that, to some degree, salinity would be expected to promote flocculation within clay

suspensions (e.g. as occurs in brackish estuarine waters; ~15 *ppt*) [Guan *et al*., 2005; Hauck *et al*., 2009; etc.], and would result in increased sedimentation rates compared to those obtained in freshwater (Sutherland *et al*., 2014). It should be equally noted that, the parametric influence of salinity on mud flocculation processes is also known to diminish for salinity values above 20 *ppt* (e.g. Al-Ani *et al*., 1991; Allen and Posamentier, 1993; etc.). The parametric inconsistency identified here, may be attributed to the significant differences in the mixture composition (in particular, range of high clay mass concentration, i.e. $C_s^{cl} = 84–285\ kg\ m^{-3}$ in mixtures tested here, Table 5.1) compared with those of other studies. As a comparison, Sutherland *et al*. (2014) investigated the settling of kaolinite clay suspensions within a mass concentration range, up to one order of magnitude lower than the current study, i.e. $C_s^{cl} = 14.7–39.3\ kg\ m^{-3}$; while within turbidity maximum zone of estuaries, suspended sediment concentrations can typically reach up to ~10 to ~15 $kg\ m^{-3}$. Thus, the sand-clay mixtures tested in the current study are more representative of hyper-concentrated, near-bed, fluid-mud layers and, consequently, are expected to display significantly different settling characteristics compared to these more dilute suspensions.

Figure 5.10 compares runs SET-EX6 and EX9 (i.e. Group E, Table 5-2) which shows the parametric influence of initial mixture concentration (561 and 813 $kg\ m^{-3}$, respectively) for the same sand-clay mixture proportion (i.e. 65s:35c) and pore fluid salinity (i.e. 30 *ppt*). It is noted here that the developing bed conditions for SET-EX9 do not show segregation while SET-EX6 does (Figure 5.3b and Appendix 5-2b respectively). Although, the first 90 *mins* of the sedimentation process indicate similar initial downward interface displacement over this time period, albeit noticeably lower for SET-EX9 (Figure 5.10). After this initial settlement, the rate of downward displacement increases sharply in SET-EX9 compared to SET-EX6, which remains approximately at the same rate over the period $t = 1.5 \rightarrow 3$ *hrs* (Figure 5.10a). This is reflected in the corresponding sedimentation rates (Figure 5.10b), which show an earlier and higher peak value in SET-EX9 compared to SET-EX6.

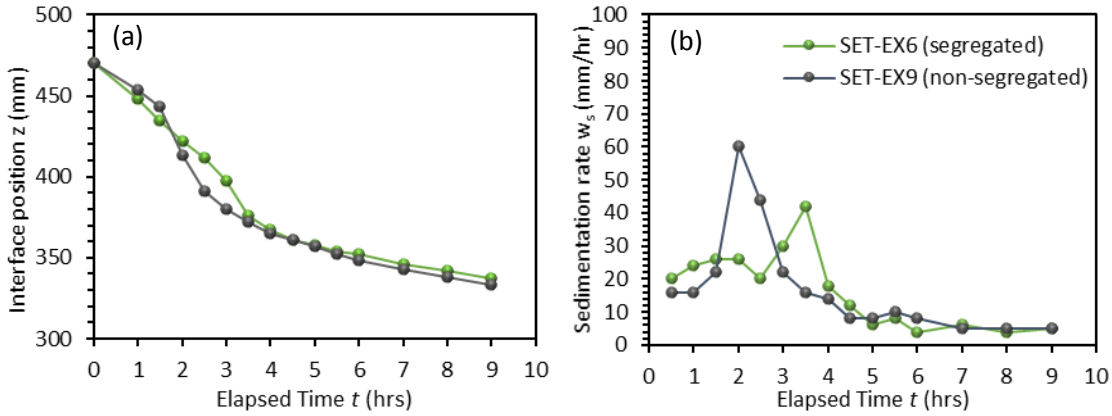

Figure 5.10 (a) Comparison of upper interface displacement profiles and (b) Corresponding sedimentation rates of segregating/non-segregating sand-clay mixtures.

It is interesting to note here that in the sand-clay mixtures demonstrating bed segregation (i.e. through sand deposition to the base of the column), the subsequent hindered settling characteristics and transition to phase I consolidation is expected to behave similar to a clay only suspension in the absence of sand after this initial segregation (e.g. Figures 5.1-5.3). However, it is unclear what influence the trapped sand fraction has on the sedimentation rate of sand-clay mixtures, in which segregation is inhibited (e.g. Figure 5.3b) or how it affects the transition between the settling regime and the onset of phase I consolidation. It can be hypothesised therefore that, the initial settling regime may not exist or at least be of a sufficiently short duration within non-segregating sand-clay mixtures, as the fact that the sand fraction does not segregate suggests that the clay fraction has reached the gelling concentration rapidly before segregation can occur. As such, this condition cannot be accounted for in many polydisperse hindered settling models (e.g. Cuthbertson *et al*., 2008) for hindered settling of sand-clay mixtures, which is considered in chapter 7 (Discussion and Analysis).

5.6 Electrical Resistivity Measurements of Bed Deposit Formation

5.6.1 Electrical resistivity profiles

Temporal changes in the formation factor *F* profiles during both the hindered settling and bed formation (i.e. phase I consolidation) phases of the sand-clay sedimentation process were measured in line with the experimental procedures described in the preceding chapter. Figure 5.11 (see Appendix 5-3 also) presents colour maps of the temporal change in formation factor *F* profiles over the first hour of the sedimentation process for the majority of the sand-clay mixtures tested. These electrical resistivity time series profiles show rapid development of a strongly segregated bed over $t = 0 \rightarrow \sim 150$ *s* for the 85S:15c

mixture in SET-EX2 (Figure 5.11a), with high formation factors F ranging from 3.5 – 4.2, recorded for its segment type I (Figure 5.4b) at the column base (z = 0 – ~130 *mm*). Above this base layer (i.e. segment types II – IV; Figure 5.4b), a range of lower formation factor F values was recorded (i.e. F = 1 – 1.5). Clearly from Figure 5.11a, the sharp transition between high and low F values delineates the rapidly forming sand-dominated base layer (i.e. segment type I; Figure 5.4b) and the overlying clay-dominated layer (i.e. segment types II – IV). The elevation of this transition is consistent, with the interface elevation (z ~125 *mm*) shown in the time-lapsed image of the bed development (Figure 5.1b). For the 75s:25c mixture tested on SET-EX3 (Figure 5.11b), the time-series colour map of F profiles shows similar trend to that observed in SET-EX2, but with a reduction in formation factor values (i.e. F = 3.2 – 3.8) at its segment type I (i.e. the sand-dominated base layer; z = 0 – 110 mm), which also develops over a longer time period (t = 0→~350 *s*).

The observed reduction in the F values of SET-EX3 compared to those of SET-EX2, at their corresponding segment type I (Figure 5.4b), reflects the influence of increased clay concentration, C_s^{cl}, both on the hindered settling characteristics of sand fraction and the increased presence of trapped clay in the sand-dominated layer at the column base (indicated by the presence of vertical clay bandings in the corresponding time-lapse image in Figure 5.11b). By contrast, the formation factor colour map (Figure 5.11c) for SET-EX6 (65s:35c; Table 5.1), shows a less well defined interface between the base sand-rich (i.e. segment type I; Figure 5.4b) and upper clay-rich layers (i.e. segment types II – IV), which reflects the more gradual transition in formation factor F values between these two layers. The resulting sand-rich layer in this mixture, is relatively thinner (z = 0 - 85 *mm*) with lower F values (i.e. F = 2.4 - 3.6) and develops over a significantly longer period of time (t = 0→~1300 *s*). Finally, comparison between SET-EX4 (65s:35c; 0 ppt; Figure 5.11d) and SET-EX6 (65s:35c; 30 *ppt*; Figure 5.11c), reveals that the key bed layer development characteristics for these mixtures (i.e. layer thicknesses and development time; range of F values) are very similar despite variations in their ambient pore fluid salinity.

In summary, the formation factor colour maps highlight key differences in the nature and extent of segregation that occurs in the bed deposits of different sand-clay-water suspensions. These are associated particularly with (i) the sharpness of the interfacial transition between the sand-dominated base layer and overlying clay-dominated layer and

(ii) the quantity of clay trapped in the sand-dominated base layer and vice versa. It is interesting to note, however, that the pore water salinity appears to have little influence on the key characteristics of this initial bed layer formation phase, at least, as shown by the electrical resistivity results (i.e. Figure 5.11 and Appendix 5-3).

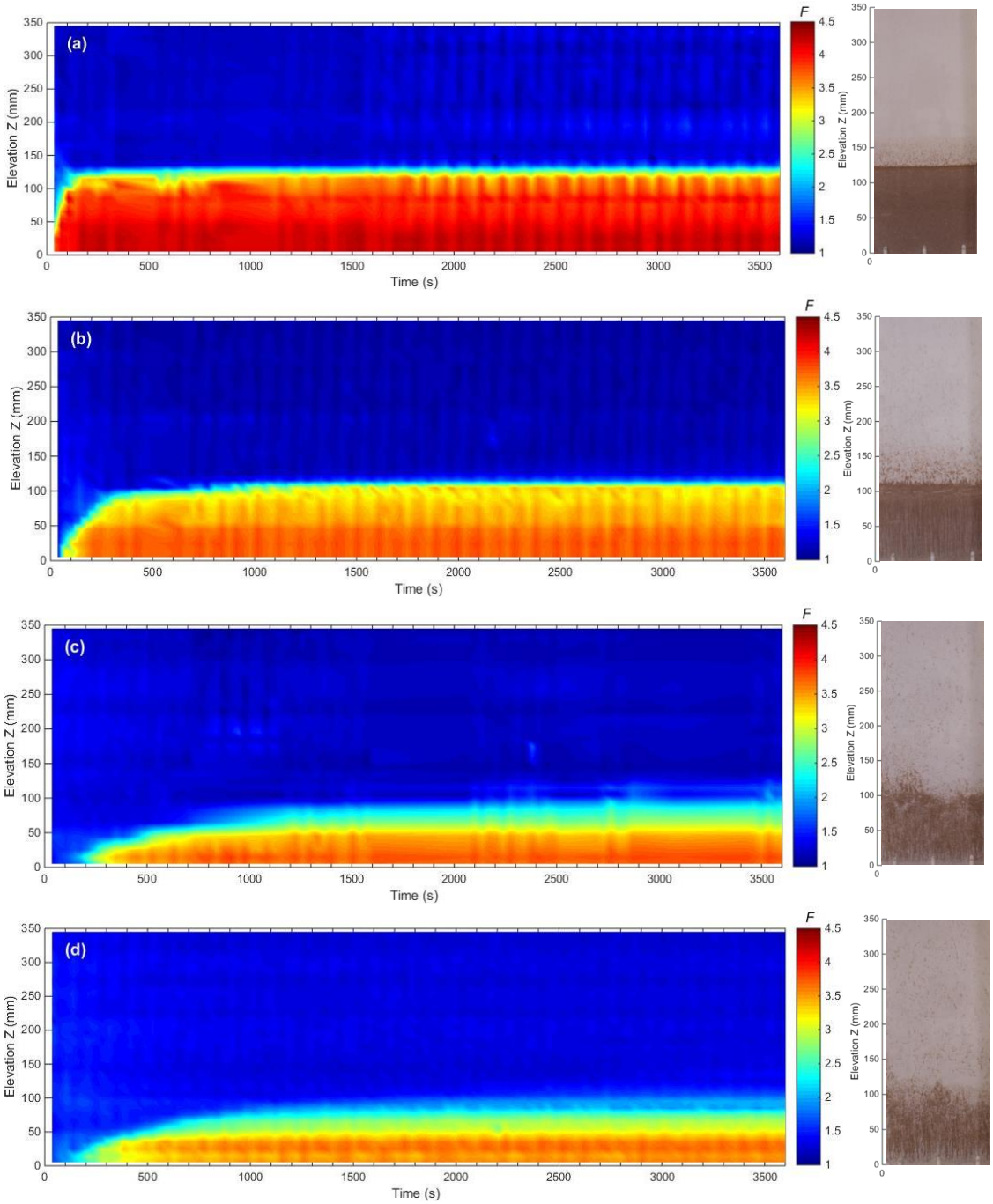

Figure 5. 11 Time series colour map plots of the variation in measure formation factor F profiles during the first hour of the sand-clay sedimentation process for (a) SET-EX2 (b) SET-EX3 (c) SET-EX6 and (d) SET-EX4 (see Table 5.1). Corresponding images show bed deposit layer formation at t = 1hr

5.6.2 Bulk Density Profiles

In terms of characterising variations in the vertical composition of sand-clay deposits, it is more informative to convert the measured electrical properties (i.e. formation factor *F*) into more physically-relevant properties such as bulk density and porosity. These can then be more easily associated with specific composition at different elevations within the deposits. The measured formation factor *F* profiles obtained for most of the experimental runs are thus transformed into normalised bulk density and porosity profiles using Equations 4.2 and 4.3 respectively, with the aid of sand-clay mixture calibrations, detailed in *section* 4.4.2; pg. 108. In this context, Figure 5.12 presents equivalent contour plots of the temporal change in the normalised bulk density γ_{bulk}/γ_p profiles over the initial sedimentation period for the same sand-clay mixtures previously considered in Figure 5.11 (for SET-EX2, EX3, EX4 and EX6) and Appendix 5-4 (for SET-EX1 and EX5).

5.6.2.1 Initial sedimentation stage

In terms of the influence of salinity, the contour plots of normalised bulk density γ_{bulk}/γ_p profiles over the initial sedimentation period for 85s:15c mixtures in SET-EX2 (Figures 5.12a) and SET-EX1 (*Appendix* 5-4a), show similar development of the segregated (i.e. sand $\rightarrow$ clay-dominated) layers in the resulting deposits. In addition, calculated layer densities γ_{bulk}/γ_p and porosities ϕ values appear to be largely similar at this initial stage of the sedimentation process. For example, Figure 5.12a shows that γ_{bulk}/γ_p values vary initially (i.e. t = 30 *s*) from ~ 1.23 at z = 200 *mm* to ~1.59 at z = 5 *mm*. This is representative of the differential (sand-clay) settling and layer segregation process that occurs immediately following the start of the test (see *section* 5.1). The γ_{bulk}/γ_p values of the lower sand-dominated layer (i.e. segment type I; Figure 5.4b), that develops as a consequence of this segregation of sand particles over ~120 *s*, vary from ~1.80 to ~1.90 in the column region z = 0 $\rightarrow$ ~125 *mm*. The segregation interface was shown to form at $z \approx$ 135 *mm*. For this segment type I, the estimated sand content was > ~60 % (i.e. from Figure 4.13). The corresponding indicative values of bed porosity ϕ (from Equation 4-3) are shown to vary from ϕ = 0.45 for lower sand layer up to ϕ = 0.94 in the upper segment type IV (i.e. clay-water suspension).

By contrast, the initial formation of the sand dominated base layer (i.e. segment type I) for 75s:25c mixture in SET-EX3, was shown (Figure 5.12b) to develop (i.e. z = 0 $\rightarrow$ ~105 *mm*) over a longer period of time (i.e. t = 0$\rightarrow$ ~360 *s*), with $\gamma_{bulk}/\gamma_p \approx$ 1.84 and ϕ = ~0.51.

Overlaying this segment type I (i.e. sand-dominated base layer) was a mixed sand-clay deposit layer (segment types II; Figure 5.4b), with γ_{bulk}/γ_p = ~1.40 to ~1.71; ϕ = 0.57–0.63), while the elevation of the sand-clay transition to the upper clay-water suspension (i.e. segment type IV) [γ_{bulk}/γ_p < ~1.20, ϕ = 0.94] was shown to increase gradually with time (i.e. z ≈ 105 → 120 *mm* as *t* =350→1000 *s*).

Figures 5.12c-d (and *Appendix* 5-4b) indicate a more transitional structure in the resulting deposit (sand → clay-dominated), as well as in the layer densities γ_{bulk}/γ_p and porosity ϕ values. The initial bed development for run SET-EX4 (65s:35c; 0 ppt) is shown to be very similar to other sand-clay mixtures of similar composition but with varying salinity concentrations (Figures 5.12c–d and *Appendix* 5-4b). Figures 5.12c-d also show that, the time required for the segment type I (i.e. Figure 5.4b) to develop for 65s:35c mixtures is significantly longer (i.e. *t* = 0→ > ~1200 *s*) than for 85s:15c and 75s:25c mixtures (Figures 5.12a-b). It is also evident that significant differences in physical bed properties occur between different mixtures with more transitional changes found in 65s:35c bed deposits, from the segment type I layer at the column base (i.e. γ_{bulk}/γ_p = ~1.7→~1.8; ϕ = 0.51) to an upper clay-dominated layer (segment types III-IV) [i.e. γ_{bulk}/γ_p = ~1.2→~1.5; ϕ = 0.68–0.87]. In summary, these contour plots of γ_{bulk}/γ_p show the initial stages of the bed layer development for different sand-clay mixture compositions and indicate quantitatively how the individual deposit layer forms over time, as well as providing an indication of their composition and structure (i.e. through corresponding γ_{bulk}/γ_p and porosity ϕ values in the different bed regions).

5.6.2.2 Longer term sedimentation period

Figures 5.13, 5.14 and *Appendix* 5-5 present the longer term development of normalised density γ_{bulk}/γ_p profiles over the first 24 *hrs* for the range of sand-clay mixtures tested. Figure 5.13a and Appendix 5-5a, respectively show the comparison of changes in the normalised bulk density profiles for runs within parametric classification *Group-C* in Table 5.2 (i.e. 85s:15c mixtures: SET-EX1 and SET-EX2), while Figure 5.13b shows similar comparison for 75s:25c mixture (i.e. SET-EX3) at elapsed times of 1 *min*, 10 *mins*, 1 *hr*, 6 *hrs* and 24 *hrs*. It is apparently from these profiles (i.e. Figure 5.13a and *Appendix* 5-5a) that, the vertical elevation of the density interface between the sand-dominated base layer (i.e. segment type I; z < 125 *mm*) and clay dominated upper layer

(i.e. segment types II – IV; $z > 125\ mm$) is established at a relatively early stage in the sedimentation process (i.e. $t < \sim 10\ min$).

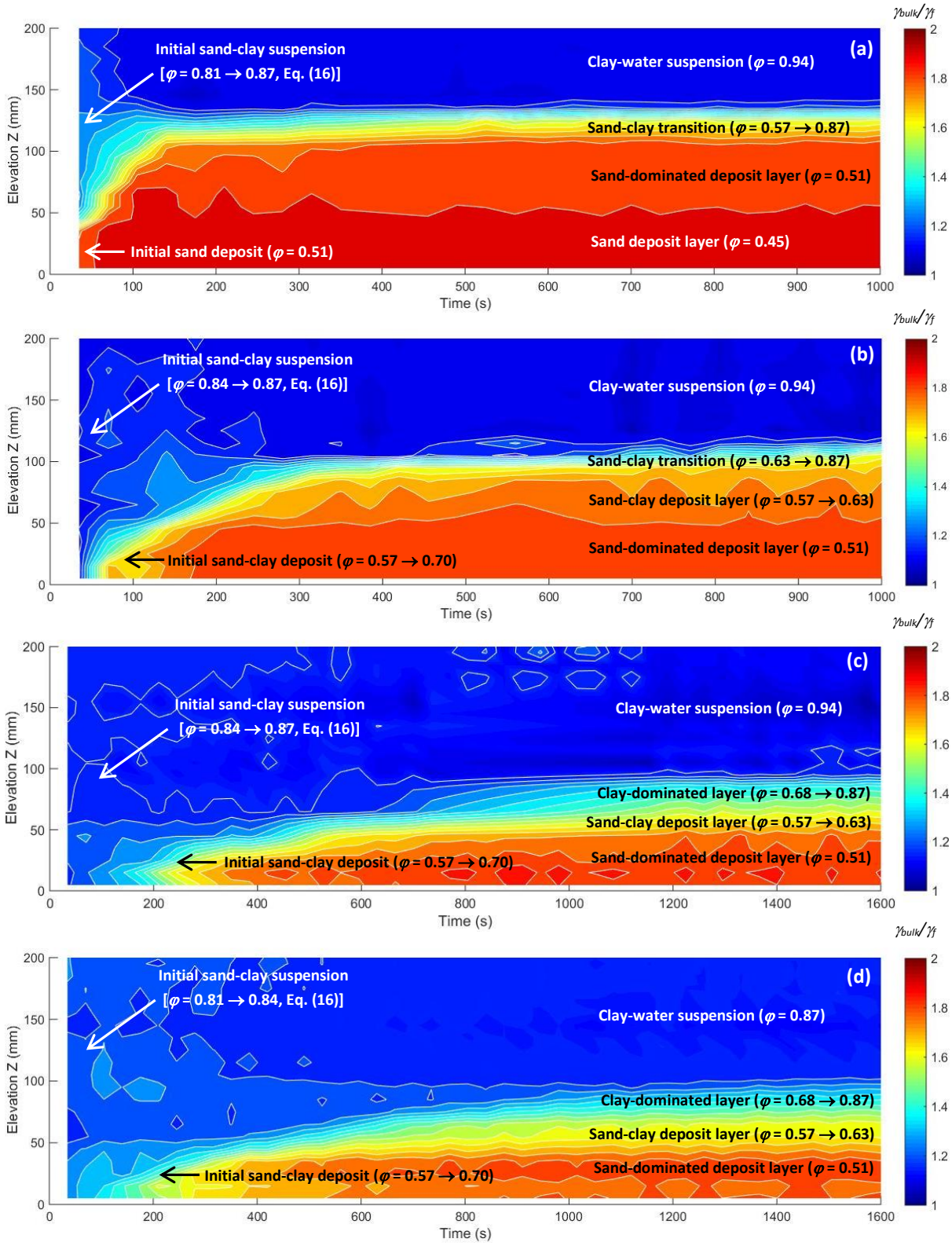

Figure 5.12 Initial temporal development of normalised bulk density γ_{bulk}/γ_p within sand-clay bed deposit layers for (a) SET-EX2 (85s:15c; 30 ppt), (b) SET-EX3 (75s:25c; 30ppt), (c) SET-EX6 (65s:35c; 30ppt) and (d) SET-EX4 (65s:35c) [see Table 5.1]. Values of porosity ϕ shown are indicative (based on Equation 3-12)

Over the 24 *hr* experiment duration, this interface elevation remains largely unchanged, with the sand-rich bottom shown to develop a uniform γ_{bulk}/γ_p profiles below this interface at all elapsed times (Figure 5.13a). It is interesting to note that, the average γ_{bulk}/γ_p values in this sand-dominated layer increase slightly over the experiment duration (i.e. γ_{bulk}/γ_p = ∼1.65 → ∼2.00). This is thought to indicate that some degree of compaction or structural re-organisation occurs during this period, similar to self-weight consolidation process (e.g. Terzaghi, 1943 and Sills, 1998; see *section* 2.4 for detailed discussion on this process).

Above the sand-rich bottom layer there is a sharp transition in gradient observed at z = ∼125 *mm* for both 85*s*:15c mixtures (i.e. Figures 5.13a and *Appendix* 5-5a), to the clay dominated upper layer. These layers are characterised by the presence of trapped sand patches (i.e. segments II-III) close to the interface, which visibly extend up to z = ∼210 *mm* for both tests (see Figures 5.5a(iv) & b(iv)]. It is noted that a significant increase in density within this upper clay-dominated layer (i.e. z = 130 – 235 *mm*) is also observed over the experiment duration with γ_{bulk}/γ_p values increasing; γ_{bulk}/γ_p = 1.19→1.36 and 1.28→1.40 for runs SET-EX1 and SET-EX2 respectively. In general, this is clearly indicative of the settling and initial consolidation regimes in the clay-dominated bed layer above the deposited sand-dominant base layer. This is also suggested by the reduction in γ_{bulk}/γ_p values at higher elevations within the column (i.e. z > 245 *mm*) due to differential settling effects or reduction in sand concentration at these locations.

Figure 5.13b shows the temporal development of the γ_{bulk}/γ_p profiles for the 75s:25c mixture (i.e. SET-EX3, Table 5.1), to be largely similar to SET-EX1 and EX2 runs; but with a more notable difference in their sand-clay interface elevation within the first 10 *mins*. Figure 5.13b shows that, the position of the sharp density interface between the sand-dominated base layer (i.e. z < ∼100 *mm*) and clay dominated upper layer (i.e. z > ∼105 *mm*) is established over t = ∼60 *mins*, with the interface remaining virtually unchanged for the remainder of the experiment duration. This is consistent with the results presented in (Figures 5.1b and 5.12c), which indicates that the transitional interface elevation is developed over a longer time (i.e. t > 600 *s*). The bulk density γ_{bulk}/γ_p in the base sand-dominated layer (i.e. segment type I) also increases over time but is generally lower [i.e. γ_{bulk}/γ_p = ∼1.44→1.88 (on average) as t = 1 *min* → 24 *hrs*] in the SET-EX3

(compared to SET-EX1 and EX2), due to the increased presence of clay in the lower sand-dominated layer.

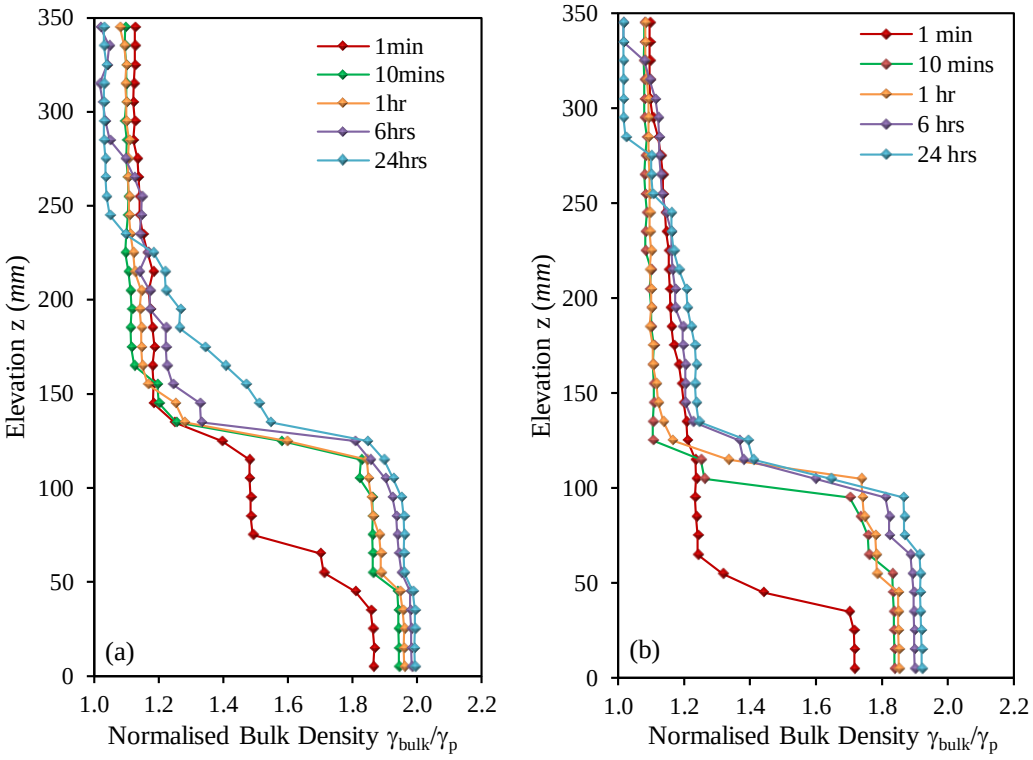

Figure 5.13 Longer term temporal development in normalised bulk density γ_{bulk}/γ_p profiles at elapsed times shown for (a) SET-EX1 (85s:15c) and (b) SET-EX3 (75s:25c). [See Table 5.1]

The longer term development of normalised bulk density γ_{bulk}/γ_p profiles over 24 *hrs* for 65s:35c mixtures (i.e. SET-EX4 → -EX6, Group D; Table 5.1) are presented in Figure 5.14 (for SET-EX4 and EX6) and *Appendix* 5-5b (for SET-EX5). Significant differences can be seen in their γ_{bulk}/γ_p profiles, compared to the results presented in Figure 5.13. Specifically, the density profiles for these 65s:35c mixtures, indicate significant changes continue to occur up to t = 6 *hrs* (Figures 5.14). Again, similar to the trend in SET-EX3, the results in Figure 5.14, show that a longer elapsed time is required for development of the transitional interface between the sand-dominated and clay dominated layer due to the increased clay content. The normalised bulk densities of the sand-dominated layers (i.e. z < 45 *mm*) for these mixtures, increase with elapsed time [i.e. γ_{bulk}/γ_p = ~1.25 → ~1.87 as t = 1 *min*→24 *hrs*]. Again generally lower, when compared to SET-EX1 and EX2 (e.g. Figure 5.13a), due to the increased presence of clay in these layers, evident by more near-vertical clay bandings (see Figure 5.6). Directly above the sand-dominated base layers in these mixtures (i.e. SET-EX4 to -EX6), a notable deviation from the well-defined sand-clay interface observed in the 85s:15c and 75s:25c mixtures (i.e. Figure 5.13) is shown,

to an approximately linear density reduction within a sand-clay transition [i.e. γ_{bulk}/γ_p = 1.48→ 1.57 (SET-EX4); = 1.62→ 1.71 (SET-EX5) = 1.59→ 1.81 (SET-EX6) as t = 1 and 24 *hrs*]. This is clearly indicative of the more transitional segregation (e.g. Figure 5.3) that occurs in mixed sediment bed deposits for sand-clay mixtures containing higher clay contents C_s^{cl}, as discussed in previous sections.

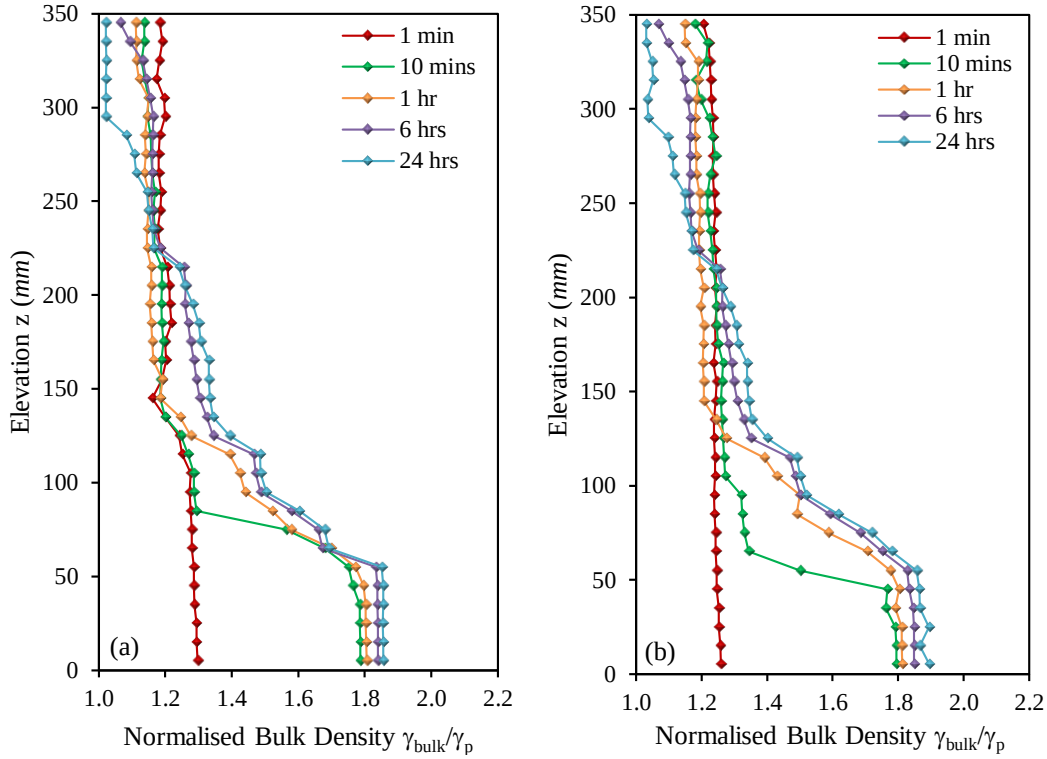

Figure 5.14 Longer term temporal development in normalised bulk density γ_{bulk}/γ_p profiles at elapsed times shown for mixtures with 65s:35c (a) SET-EX4 (0 *ppt*) and (c) SET-EX6 (30ppt). [See Table 5.1]

5.7 Conclusion of Main Findings

The following brief conclusions have been drawn out of the findings of this chapter, whilst detailed conclusions are provided in chapter 8:

- The sedimentation behaviours of the tested sediment mixtures were generally as expected (e.g. Imai, 1981; Torfs *et al.*, 1996; Winterwerp, 2002; Danker, 2006; Xu *et al.*, 2012; te Slaa *et al.*, 2013; Sutherland *et al.*, 2014; Grasso *et al.*, 2014; etc.). Within the resulting upper clay-rich bed layer, the time evolution of the upper clay-water interface (i.e. via time-lapsed images) provides information on the transition from hindered settling regime to phase I consolidation regime (e.g. Merckelbach, 2000).

- The findings, have generally shown to hold, the anticipated parametric dependence of decreasing settling rates for sand-clay mixtures with higher initial mass concentration (and, specifically, higher clay mass concentration) [e.g. Cheng, 1997; Danker, 2006; Xu *et al*., 2012; te Slaa et al., 2013; Grasso *et al*., 2014; 2015; etc.)].
- The formation of segregated (sand-clay) bed layers has equally been shown, to be largely controlled by relative sand and clay concentration within the initial mixture. Specifically, mixtures with low clay contents are shown to form well-defined (sand-clay) layer segregation within the resulting deposits, while higher clay contents result in more transitional segregation patterns or no layer segregation (for very high clay concentrations).
- Specifically, if the salinity concentration of sand-clay mixture is sufficiently large (e.g. > 15-ppt), and in addition, the ratio of clay particles in the initial mixture is relatively high (e.g. ≥ 15%), the settling/consolidation rate will be significantly inhibited. Revealing a more significant hindrance to the particles settling rates under conditions with high clay content and salinity concentration.
- Higher clay mass concentrations C_s^{cl}, plays a more significant role in defining particles settling rates in sand-mud mixtures. However, comparison between SET-EX6 (segregated bed; 65s:35c; C_s^{cl} = 196 $kg\ m^{-3}$; salinity = 30 *ppt*) and SET-EX9 (non-segregated bed; 65s:35c; C_s^{cl} = 285 $kg\ m^{-3}$; salinity = 30 *ppt*) revealed an opposite trend, with distinct differences in the transition behaviour of the two mixtures. It can therefore be hypothesised, whether or not the initial settling regime exists for non-segregating sand-clay mixtures, as the fact that the sand fraction has not segregated clearly suggests that the clay fraction has already reached the gelling concentration.

Lastly, the temporal changes in deposition characteristics of the sand-clay suspensions investigated here, are successfully identified by the time series electrical resistivity profile measurements taken throughout the duration of each experimental run. Indeed, the experimental results clearly demonstrate the potential and success of this new non-invasive characterisation technique (i.e. ERMT) in the fine resolution measurement of mixed sedimentation processes and (dis)continuities within the resulting bed layer deposits (i.e. density, porosity and composition), following appropriate calibrations.

CHAPTER SIX

Experimental Results: Mixed Sediment Bed Erosion Experiment (ES-3)

"…like the tossing sea…whose waves cast up mire and mud (cohesive sediment) …"
— (Isaiah 57:20 NIV)

6.1 Introduction

The set of experimental runs described in the preceding chapter (i.e. ES-2) was based on identifying and quantifying spatial and temporal variations in sediment bed composition and structure resulting from the differential settling of mixed (sand-clay) sediments over a wide range of parametric conditions. The main findings from ES-2 suggest that, the formation of segregated (sand-clay) bed deposits is largely controlled by the initial fractional composition (i.e. relative sand and clay concentrations). Specifically, mixtures with low clay contents are shown to form well-defined (sand-clay) layer segregation within the resulting deposits, while higher clay contents result in more transitional segregation patterns or no layer segregation (for very high clay concentrations).

The current chapter reports on experimental results for the observed erosion and deposition behaviour of prescribed mixed sediment beds (predominantly sandy beds). This experimental study employed a 2 *m* diameter benthic annular flume (Voyager II, Figures 3.10 and 3.11), which is typically deployed in the field within marine benthic environments to measure erodibility of natural sea-beds. This testing facility was supplied by PARTRAC Ltd and utilised in an idealised laboratory setting, to investigate the effect of cyclic, flow-induced shear stresses, on the size-selective erosion and deposition of mixed sediments, such as those conditions typically encountered in periodically-reversing (tidally-driven) estuaries or tidal inlets.

6.2 Summary of Experimental Set-up and Conditions

As described in *section 3.8*, the following mixed sand(s): clay(c) bed compositions (% by dry weight) were used for the erosion and deposition experiments: (i) 100(s):0(c); (ii) 98(s):2(c); (iii) 95(s):5(c); and (iv) 90(s):10(c), namely: EDT-EX1 to EX4 respectively [see Table (6-1)]. These sediment compositions were chosen, such that the effect of low clay fractional contents, on the erosional behaviour of predominantly sandy beds could be studied. Raudkivi (1998) observed that, once the cohesive fraction (i.e. mud) within a sediment bed exceeds 10 % by weight, the bed cohesion becomes the dominant control on erosion rate. Other laboratory studies on mixed-sediment bed erosion, however, put this critical clay fraction at 5% to 15% (Dade and Nowell, 1992; Mitchener and Torfs, 1996; Panagiotopoulos *et al*., 1997; Whitehouse *et al*., 2000; Baas *et al*., 2013). Therefore, in line with the aims of the current erosion tests, 10% clay by dry weight was used as the maximum. Furthermore, this range of sediment compositions tested, ultimately provides results that can be compared directly with previous studies (e.g. Lyle and Smerdon, 1965; Panagiotopolos *et al*., 1997; Torfs, 1994; Whitehouse *et al*., 2000; Baas *et al*., 2013; etc.).

Hydrodynamic conditions were generated within the annular flume by incrementally increasing the paddle rotation speeds during each experimental run (see Figure 3.21). Each paddle rotation speed increment was 10 *minutes* in duration; the exception being at the highest rotation speed, where a 2-*hour* duration was applied. The durations were determined a priori based on the results from series of trial experimental runs, and on the methodologies reported for similar erosion tests in the literature. Generally, it was expected that, for each rotational speed, erosion would occur, followed by deposition, and a state of dynamic equilibrium will then be expected to be reached within the duration of each speed. In an annular flume experiment (at any given shear stress), a dynamic equilibrium, is thought to be reached when the bed erosion rate is equal to the deposition rate (Lick, 2009; *De* Pinto *et al*., 2011). Hence, a longer duration was chosen for the maximum paddle speed, with the expectation that, this state of equilibrium will be reached at a longer duration. The fact however, is that in natural tidal environments, due to variability of flow conditions (i.e. from waves and current actions), it is unlikely for bed deposits to actually attain equilibrium state. Therefore, Lintern (2003) suggested that it is acceptable to change the turbulent condition before the bed reach such equilibrium state, provided the measuring procedure is consistent throughout the experimental runs to be compared. The complete experimental flow cycle was repeated two more times in sequence for the resulting bed from run ERT-EX4, namely; ERT-EX5 and ERT-EX6

respectively. The aim was to investigate the susceptivity (in terms of erosion and redistribution) of the previously eroded sediment bed, to further flow cycles.

The Vectrino® vertically oriented Acoustic Doppler Velocimeter (ADV) probe was used to measure the 3-D mean flow velocities within the annular flume channel throughout each test, while the suspended sediment concentration (SSC) was measured by three optical backscatter sensor (OBS) probes (see *section* 3.8.4.2; pg. 92). The OBS probes were placed at varying heights above the bed surface (i.e. at 85, 145 and 200 *mm* above the nominal bed level; Figure 3.11c), allowing the vertical variation in suspended sediment concentration (SSC) within the annular flume column to be measured.

During each experimental run, the restructuring of the sediment beds, was measured by an in-situ *4-point resistivity measurement system* (Figures 3.19 and 3.20). In this system, 30 sets of electrodes, each consisting of four 1.6 *mm* diameter stainless steel pins, were embedded into the outer wall of the annular flume in contact with the sediment bed (see *section* 3.8.4.3 for details). The resistivity profile data generated over a 30 *second* interval for the duration of each run, were processed and analysed as described in Chapter-4.

Table 6-1 Experimental parameters and conditions for ES-3

Experimental Parameters	**EDT-EX1**	**EDT-EX2**	**EDT-EX3**	**EDT-EX4**	**EDT-EX5**	**EDT-EX6**
[1]Sand [%]	100	98	95	90	90	90
[2]Clay [%]	0	2	5	10	10	10
No. of Cycle	1	1	1	3	-	-

(1) HST 95-Silica sand (SG = 2.63, see Table 3-2)
(2) Polwhite-B kaolin clay (Plastic Limit = 28%; Liquid limit = 54%; SG = 2.59)

6.3 Measurement of Flow Velocity

As described in *section 3.8.4.1*, the flow velocities ($m\ s^{-1}$) in tangential (x), radial (y) and vertical (z) directions at 0.15 *m* above the bed were measured within the annular flume with a single point ADV. The supporting software package WinADV was used to process the generated raw velocity data, following the data quality and filtering procedures recommended by Nortek (i.e. data with SNR < 15 and/or a correlation less than 85% were discarded). The flow velocity time series obtained from WinADV (Figure 6.1a) were averaged over a 5 *second* interval (i.e. Figure 6.1b). As expected, Figure 6.1 shows that, there is a corresponding increase in the tangential mean flow velocity with increase in

paddle speed. These tangential flow velocities, are shown to remain constant over the duration of each paddle speed (Figure 6.1b), showing the absence of spinning-up effects within the annular flume when the paddle rotation speed is step-wisely increased.

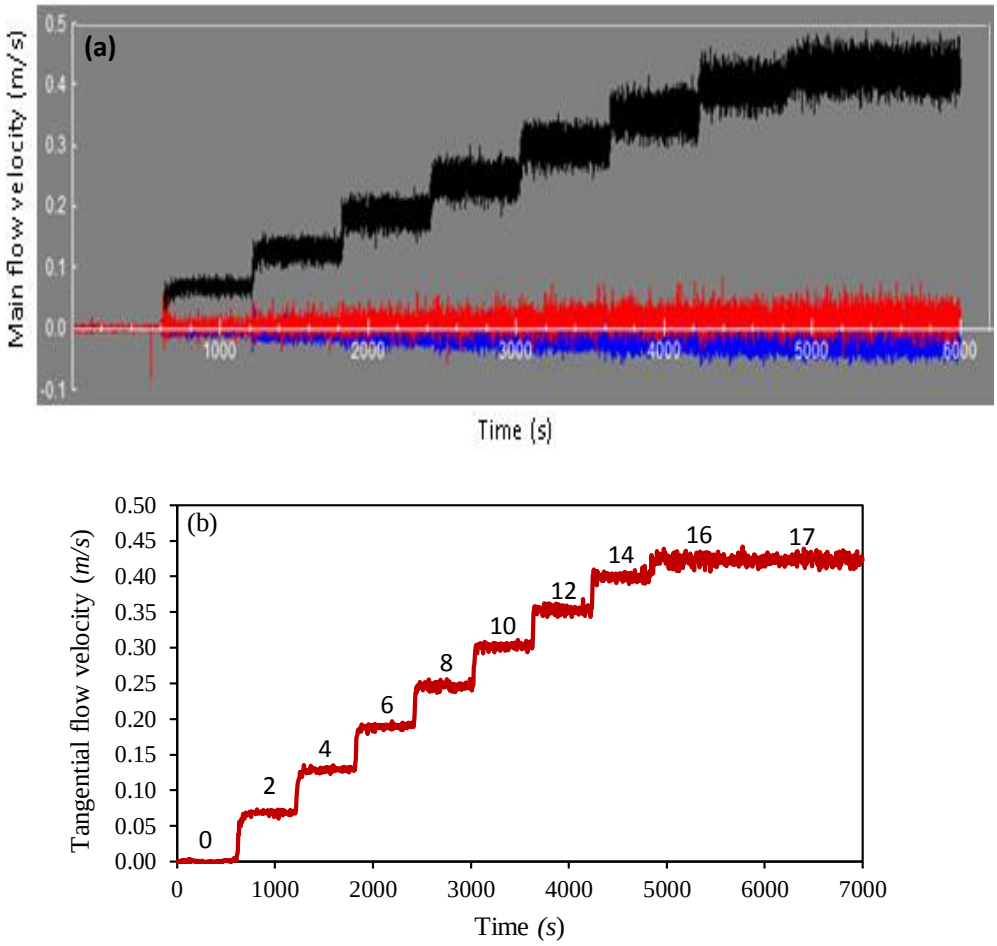

Figure 6.1 (a) Typical output of ADV-measurements showing the tangential (black), radial (blue) and vertical (red) flow velocities within annular flume column (b)Tangential flow-velocity magnitude averaged every 5 seconds (Numbers denote applied voltage)

6.4 Determination of the Bed-shear Stress

Erosion processes are driven by changes in fluid hydrodynamic conditions, as demonstrated by the correlation between applied shear stress and the threshold of bed erosion. However, other factors such as bed composition are also known to influence erosion processes, especially in mixed sediment environments. It is therefore appropriate to present the experimental results in terms of measured shear stresses and sediment mass eroded from the bed. This is in accordance with general approach being used in laboratory and field-based studies on the erosion behaviour of marine sediment beds (e.g. Williamson and Ockenden, 1996; Parchure and Mehta, 1985; Villaret and Paulic, 1986; Feates *et al*., 1999; Lintern, 2003; Laksanalamai, 2007; etc.).

For the current study, the bed shear stress (τ_b) was determined by methodologies provided by PARTRAC for the Voyager II annular flume, following empirical calibrations for different mean flow velocities, after Amos, *et al*. (1992), Thompson and Amos (2002) and Thompson *et al*. (2011). The resulting empirical relationship between shear velocity (u_{*s}, *ms^{-1})* and the mean flow velocity measurements ($\bar{u}$, *ms^{-1}*) is given as:

$$u_{*s} = 0.0167 + 0.097\,\bar{u} \tag{6-1}$$

Clearly, the estimated shear velocity (u_{*s}, *ms^{-1}*) from Equation (6-1) will result in underestimation of τ_b, as it was derived under clear water conditions. The presence of sediment in suspension is known to reduce bed shear stress (due to drag reduction), especially at sediment concentrations above 200 *mg l^{-1}*, which are very common within annular flumes during in situ sediment bed erosion measurements (e.g. Gust, 1976; Cloutier *et al*., 2006; Amos *et al*., 1992; and Thompson *et al*., 2006; etc.). Thus, it is necessary to correct bed shear stresses to account for the evolution of high suspended sediment concentrations during erosion runs. As such, the change in bed shear stress, as the erosion test progresses, is a function of both the paddle rotation speed and the increase in suspended sediment concentration. However, it will also be dependent on bed surface changes (e.g. bed forms; Baas *et al*., 2013). In view of this, Amos *et al*. (1992) proposed a correction to Equation (6-1) that has been employed to account for the effect of turbidity on the derived bed shear stresses. It should be noted here that the Voyager II annular flume was based on the design and dimensions of the annular flume used by Amos *et al*. (1992). From the corrected shear velocity values, the corresponding values for bed shear stress were derived from the expression in Equation (6-3). Table (6-2) presents the mean values of u_{*s} and τ_b obtained over the range of applied paddle rotation speeds used for all the experimental runs.

$$u_{*s} = u_{*0} - 10^{[-1.76E-4(S)]} \tag{6.2}$$

where S is the suspended sediment mass concentration (SSC).

$$\tau_b = \rho u_{*s}{}^2 \tag{6.3}$$

where ρ is the density of water within the test tank (i.e. = 1030 *kg m^{-3}*, is the estimated density of the water within the tank prior to each experimental run)

Table 6-2 Mean values of Shear velocity and bed shear stress for corresponding applied voltage Levels

Applied voltage (*Volts*)	**2**	**4**	**6**	**8**	**10**	**12**	**14**	**16**	**17**
Horizontal Flow Velocity ($m\ s^{-1}$)	0.026	0.068	0.120	0.213	0.276	0.332	0.375	0.409	0.457
Corrected Shear Velocity, u_{*S} ($m\ s^{-1}$)	0.0005	0.0065	0.0135	0.0211	0.0264	0.0325	0.0376	0.0433	0.0449
Bed Shear stress, τ_b (*Pa*)	0.0003	0.0425	0.1816	0.4464	0.6997	1.0601	1.4186	1.8808	2.0205

6.5 Erosion Test Results

The results of the current set of experiments (Table 6-1) are discussed in relation to the nature and extent of bed erosion and deposition processes in mixed sedimentary environments, through analysis of: concentration-time profile measurements, bed shear strength and erosion rate calculations and observed structural changes in the bed.

It is necessary to highlight at this point, some of the challenges encountered in the current experimental runs. Several issues arose that unavoidably limited the data collection within the annular flume and consequently, constrained the parametric extent of the experimental results presented herein. Firstly, high resolution video recorded with a *GoPro camera* with the expectation of having an indication of the dynamics of the erosion and deposition processes, was unfortunately not clear for observation, due to severe erosion, resulting in the water body in the tank being too cloudy. Hence, the description of the erosion processes in the current study, was mainly inferred from OBS and ADV data, and the images of the resulting bed structures at the end of each experimental run. In addition, while electrical resistivity data were also used, reliable data from ERMT were only possible for EDT-EX1 and EDT-EX2. The reason for this was not particularly known, however, the limitation of the technique in characterising suspended sediment is a likely cause. Finally, there were issues relating to saturation of the OBS probes at high concentrations exceeding the measurement limit of the probes (i.e. 4000 *NTU*; with non-linear output above 750 *NTU*). However, as the erosion characteristics of the sediments are not known in advance and the maximum gain of the sensors had already been utilised, this saturation effect was unavoidable. Consequently, in general, some datasets were of poor quality and not amenable to analysis.

The issue of saturation within the flume channel water body, also meant that only the datasets (i.e. before the threshold of the probe was reached) for the topmost OBS probe were considered in the analysis (see *section* 3.8.4.2; pg. 92, on OBS probe calibration). With these limitations, the discussion on the investigation into the nature and extent of bed erosion and deposition processes in the current study, is based on the assumption that (i) the available datasets are sufficient to at least indicate the inception of the erosion processes, and (ii) the bed shear stress (and erosion rate), required for the determination of the bed erosion thresholds, can be sufficiently estimated from the available experimental data.

6.5.1 Time series data analysis

The total surface area of the bed exposed to the hydrodynamic actions within the flume was estimated as 0.872 m^2, while the total volume of water in the flume at any given time was 0.262 m^3 (262 L) (i.e. from Figure 6.2). To achieve the calculations discussed below, the following additional assumptions were made; (i) no material escaped from the flume channel to the surrounding water body in the tank, and (ii) the concentration was uniform with vertical elevation in the flume. The condition assumed here (i.e. second assumption) is clearly untypical of flume erosion tests (or conditions in natural environments), where concentration gradient above the bed has been reported (e.g. Parchure and Mehta, 1985; Laksanalamai, 2007; Thompson *et al*.,2011; Mehta, 2014; etc.). However, in general, these assumptions have been found to be reasonable for determination of the erosion thresholds of the sediment beds tested here (see last paragraph of *section* 6.5.3; pg. 162).

The generated time series datasets (in *NTU*) from the OBS probe were converted to suspended sediment concentration (SSC) in $g\ l^{-1}$ following the calibration procedures outlined in *section* 3.8.4.2 (pg. 92). These SSC datasets were visually inspected for quality and outliers were deleted. The resulting dataset was then time-averaged every 2 mins, after Widdows *et al*. (2007), to eliminate high frequency, short-term variability in the SSC measurements. The mass of eroded sediments (in g) per each time step, was estimated by multiplying the estimated SSC by the water volume in the channel (262 L). The local rate of change of the averaged SSC is required to calculate the erosion rate ($g\ m^{-2}\ min^{-1}$), however, this depends on the duration over which the original concentration time-series is averaged. Hence, optimum duration (Δt) of a rotational speed is required. Using too large Δt will result in the initial increase in the concentration being averaged out. Therefore, $\Delta t = 0.2T$ (where T is the duration of each rotational speed, i.e. 10 *mins*)

was used, with the assumption that any sudden increase in SSC is well represented within this period. This agrees well with $\Delta t \leq 0.2T$, that has been used in similar annular flume tests (e.g. Laksanalamai, 2007; Thompson *et al*.,2011). The sediment erosion rate at each applied shear stress was then determined, by dividing the mass eroded per unit bed surface area ($g\ m^{-2}$) by T (10 *mins*). [Note: mass eroded per unit bed surface area is obtained by dividing mass of eroded sediment per each time step by total surface area (i.e. 0.872 m^2)]. These methods described above, are based on the methodologies provided by PARTRAC; and same as used by Thompson, *et al*. (2011) when the Voyage II benthic annular flume (i.e. Voyager II) was used to study in-situ erodibility of seabeds in the North sea seabed. Jacobs *et al*. (2011) also used similar methodologies for determination of erosion threshold of sand-mud mixtures. In addition, the methods are consistent with the approach employed by Laksanalamai (2007), with the TU Delft annular flume used for investigation of mixed sediment beds erosion characteristics.

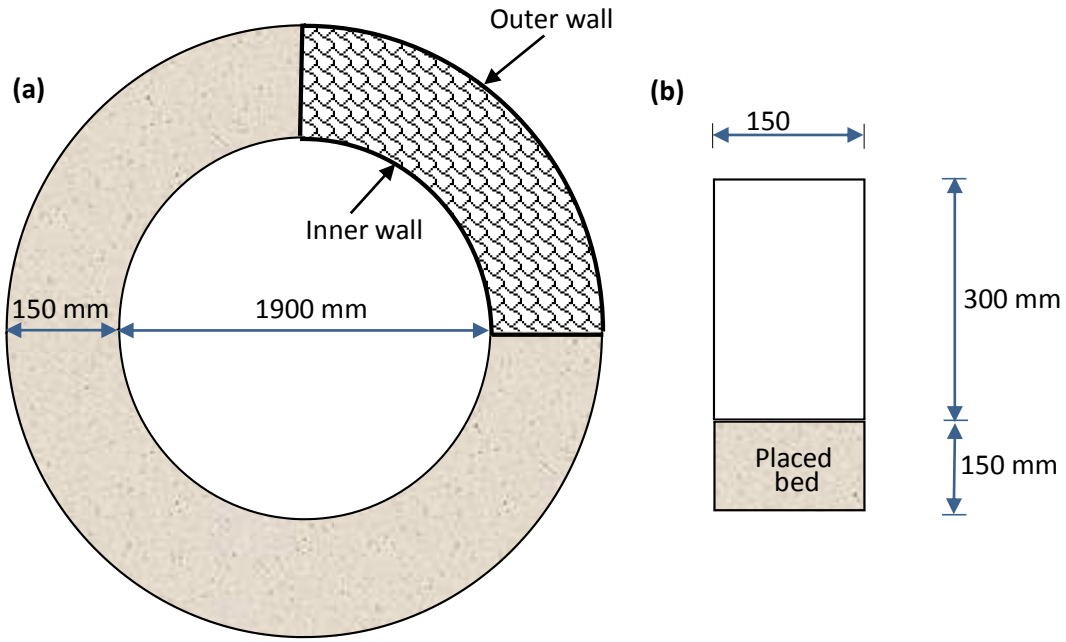

Figure 6.2 Schematic illustration of (a) the total surface area of the bed exposed to hydrodynamic actions within the flume (b) cross-section of the flume. (Bed-forms measurements and image capturing were carried out from the patterned section of (a), see *section* 6.5.4).

In the current study, Tables (6-3), (6-4) and *Appendices* (6-1), (6-2) respectively present results for (i) measured suspended sediment concentrations (SSC) ($g\ l^{-1}$); (ii) erosion rates ($g\ m^{-2}\ mins^{-1}$); (iii) total mass sediment eroded (g); and (iv) mass eroded per unit bed surface area ($g\ m^{-2}$). These calculated values are clearly estimates and should therefore be treated with same uncertainty due to the highlighted limitations. In the current chapter,

the main findings from these experimental runs and some discussions of their implications for mixed sediment transport dynamics shall be reported. However, further discussion on wider implications of the results is presented in chapter 7.

Table 6-3 Maximum suspended sediment concentration (SSC) in gl^{-1} per applied bed shear stress (Pa)

	Mean Bed Shear stress, τ_b (Pa)								
Erosion Tests	0.0003	0.0425	0.1816	0.4464	0.6997	1.0601	1.4186	1.8808	2.0205
EDT-EX1	0.00	0.050	0.932	saturated	saturated	saturated	saturated	saturated	saturated
EDT-EX2	0.00	0.065	0.876	1.866	2.026	saturated	saturated	saturated	saturated
EDT-EX3	0.00	0.006	0.007	0.008	0.033	0.114	0.201	0.383	0.624
EDT-EX4	0.00	0.001	0.001	0.001	0.001	0.001	0.011	0.075	0.269
EDT-EX5	0.00	0.002	0.002	0.002	0.002	0.002	0.020	0.125	0.405
EDT-EX6	0.00	0.002	0.003	0.003	0.003	0.107	0.121	0.233	0.439

Table 6-4 Erosion rate, E ($g\ m^{-2}\ mins^{-1}$) per applied bed shear stress (Pa)

	Mean Bed Shear stress, τ_b (Pa)								
Erosion Tests	0.0003	0.0425	0.1816	0.4464	0.6997	1.0601	1.4186	1.8808	2.0205
EDT-EX1	0.00	1.49	28.01	saturated	saturated	saturated	saturated	saturated	saturated
EDT-EX2	0.00	1.95	26.32	56.07	60.87	saturated	saturated	saturated	saturated
EDT-EX3	0.00	0.18	0.21	0.24	0.99	3.43	6.04	11.51	18.75
EDT-EX4	0.00	0.03	0.03	0.03	0.03	0.03	0.32	2.23	8.08
EDT-EX5	0.00	0.06	0.06	0.06	0.06	0.06	1.01	3.76	12.17
EDT-EX6	0.00	0.06	0.09	0.09	0.09	3.21	3.64	7.00	13.19

6.5.2 Time series of concentration measurements

The temporal changes in SSC for all the tests are presented in Figures 6.3 and 6.4. Clearly, from these results, SSC is shown to increase with increasing bed shear stress, as expected. The results also reveal that sediment entrainment was initiated at significantly different times (i.e. different shear stress conditions) for each run; i.e. at t = ~8 *mins* (at τ_b = 0.043 *Pa*); t = ~15 *mins* (at τ_b= 0.043 *Pa*); t =~40 *mins* (at τ_b = 0.700 *Pa*) and t = ~68 *mins* (at τ_b = 1.419 *Pa*) for EDT-EX1, EX2, EX3 and EX4 respectively (Figure 6.3). After the initiation of sediment entrainment (Figures 6.3 & 6.4), especially at higher shear stresses, it is shown that SSC exhibits time-increasing behaviour (Figure 6.3). This indicates that, the applied bed shear stresses had exceeded the maximum bed shear strength of each tested sediment bed (Parchure and Mehta, 1985; Villaret and Paulic, 1986). At the same corresponding bed shear stress, higher SSC values are obtained in mixed sediment beds with lower clay fractions (Figure 6.3; see also Table 6-3).

Comparison of runs EDT-EX4, EX5 and EX6 (i.e. for otherwise similar 90s:10c mixture conditions; Table 6-1), shows differences in the sediment entrainment initiation time for these runs. For EDT-EX5, sediment entrainment was shown to be initiated ~8 *mins* earlier (i.e. *t* = ~60 *mins*) than for EDT-EX4; while in EDT-EX6, it was initiated ~16 *mins* earlier (i.e. *t* = ~52 *mins*) [Figures 6.3 & 6.4].

The initiation of sediment entrainment, though at different time, occurs at the same level of applied bed shear stress for both EDT-EX4 and EX5 (i.e. τ_b = 1.419 *Pa*; Figures 6.3 & 6.4). Interestingly, in EDT-EX6, it occurs at relatively lower bed shear stress (i.e. τ_b = 1.06 *Pa*; Figure 6.4). In addition, for these runs, the corresponding total sediment mass eroded at these bed shear stresses are shown to differ significantly; i.e. 2.79, 8.81 and 28.0 *g* for EDT-EX4, EDT-EX5 and EDT-EX6 respectively (*Appendix* 6-1). These highlighted variabilities in the erosion characteristics of these runs, suggest that, mixed-sediment beds that have been exposed to repeated cyclic erosion and deposition processes, are subsequently more susceptible to rapid erosion. Decrease in the bed shear strength due probably to cyclic hydrodynamic conditions is most likely to be responsible for this observed behaviour; this is similar to enhanced erosion due to bed softening reported by Villaret and Paulic (1986).

Generally, erosion is thought to occur when the erosive forces (i.e. hydrodynamic forces) are larger than the resistive forces within the sediment (e.g. gravity, friction, cohesion and adhesion) [Grabowski *et al*., 2011]. Therefore, the observed variabilities in the erosion characteristics of runs EDT-EX4 to EX6, suggest that, antecedent conditions of the bed affect its subsequent resistance to erosion. In other words, this result clearly shows that a bed that has been previously disturbed is likely to be unstable. Therefore, it can be argued that, owing to the continuous activity of tidal current and waves, sediment beds in intertidal zones are most likely to be more unstable, i.e. having low erodibility. Ockelford and Haynes (2013) reported a similar scenario, where floods with short recurrence intervals indicated bed material being comparatively loose and less resistant to subsequent entrainment. Although, sediment beds stability in the marine environment is also defined by the aspects of the near-bed environment (e.g. increased bed roughness, present of organic components, etc.) that controls the potential of these hydrodynamic (or erosive) forces (Jumars and Nowell, 1984; Madsen and Warncke, 1983; etc.).

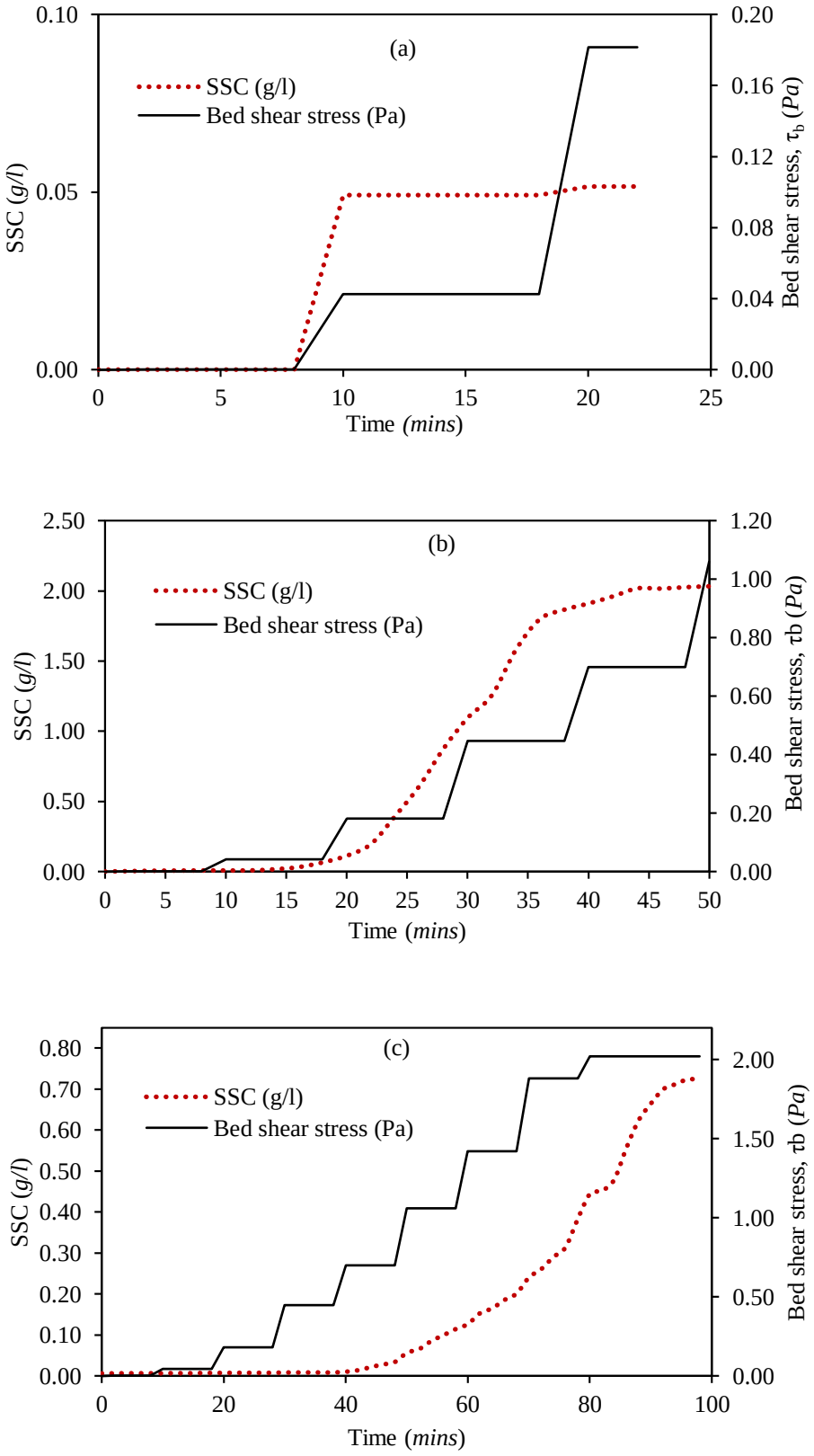

Figure 6.3 Averaged instantaneous SSC (g/l) and Bed shear stress (Pa) as function of Time (minutes): (a) EDT-EX1; (b) EDT-EX2 and (c) EDT-EX3.

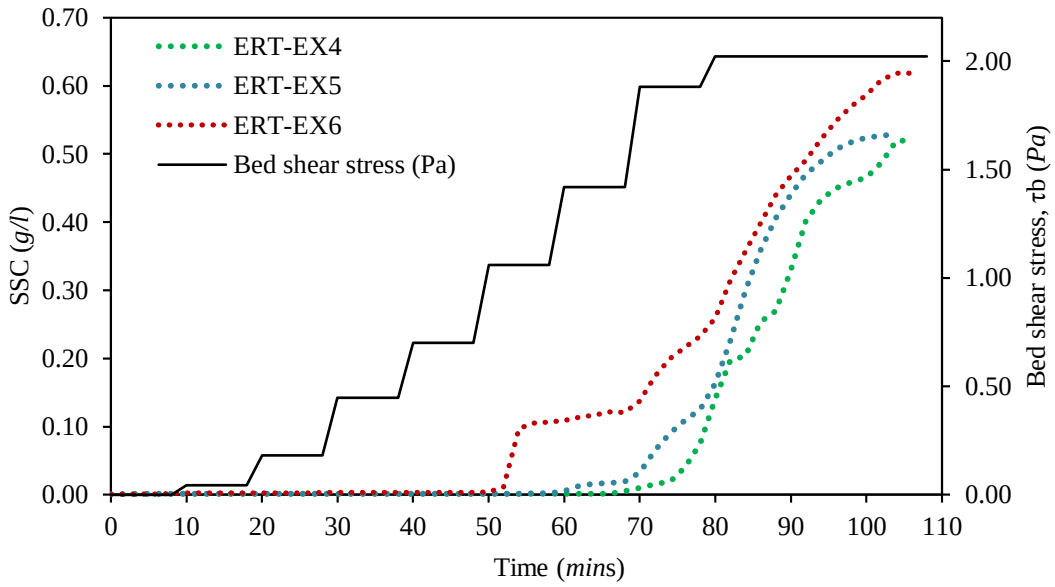

Figure 6.4 Averaged instantaneous SSC (*g/l*) and Bed shear stress (Pa) as function of Time (*mins*) for EDT-EX4, EDT-EX5 and EDT-EX6

6.5.3 Erosion rate, erosion threshold and bed shear strength

Figure 6.5, plots the corresponding erosion rates (in $g\ m^{-2}\ mins^{-1}$) for all the runs, against applied bed shear stress (τ_b, *Pa*). As expected, the results reveal that, at low τ_b, erosion of material from the bed surface is insignificant or non-existent, especially for the runs with higher clay fractions (i.e. EDT-EX3 to EX4; Figures 6.5c & d, Table 6-1). With increasing τ_b however, a certain erosion threshold (see erodibility in *section* 2.5) occurs in each run, above which sediments are randomly eroded from the exposed bed surface area, with a monotonic increase in the rate of erosion *E* (Figure 6.5). This threshold is assumed to be linked to onset of material (sand and clay particle) transport, based on the SSC data obtained from the calibration procedures (Figures 6.3 & 6.4). Once this threshold is reached, an increase in τ_b results in time-independent and unlimited supply erosion. Time-independent erosion generally occurs when τ_b exceeds bed characteristic shear strength (τ_{sc}), which is similar to Type-II erosion defined by Parchure and Mehta (1985) and also Sanford (2006). This is equally in agreement with surface mode of erosion (Winterwerp and van Kesteren, 2004; Jacobs *et al*., 2011). Therefore, the current study focuses on the threshold of this mode of erosion (i.e. surface erosion), which has been found to depend on sediment bed characteristics (e.g. bed shear strength), rather than the stochastic (or random) character of the flow as in the case of floc erosion (Winterwerp and van Kesteren, 2004 and Jacobs *et al*.,2011) [Note: all natural events (which includes waves and current actions) are stochastic phenomenon].

In Figure 6.5, if fit lines are plotted for data points between B and C, the bed characteristic shear strength (τ_{sc}) [i.e. the so-called erosion threshold] can be obtained by extrapolating the fit lines to the *x*-axis (see *Appendix* 6-3 for more details). Similarly, the shear stress value at point A, can be taken as the representative value of the corresponding bed surface shear strength (τ_{so}) for each experimental run. These methodologies are in line with those employed in previous studies on erosion and deposition processes of sediment beds, as reported in the literature (e.g. Parchure and Mehta, 1985; Villaret and Paulic, 1986; Winterwerp and van Kesteren, 2004; Laksanalamai, 2007; Jacobs *et al*., 2011; Mehta, 2014; etc.), and are based on the assumption that quasi-linear relationship exists between erosion rate (E) and applied bed shear stress (τ_b) [Jacobs *et al*., 2011]. Examples of the use of these methodologies in determining erosion thresholds are shown in *Appendix* 6-4 (pg. 230) [i.e. plots from previous studies showing this linear extrapolation process, e.g. Laksanalamai, 2007; Jacobs *et al*., 2011].

Comparison between the results of runs EDT-EX1 to EX4 (Figure 6.5), shows that, increase in clay fraction, increases sediment bed initial resistance to erosion (i.e. bed surface shear strength, τ_{so}). The τ_{so} value of EDT-EX3 (5% clay content) is shown to be 1 and 2 order of magnitude more than that of EDT-EX2 (2% clay) and EDT-EX1 (0% clay) respectively (Figures 6.5a-c and 6.6). Also, τ_{so} = 1.12 *Pa* was obtained for EDT-EX4 (10% clay), which was more than double that of EDT-EX3 (i.e. τ_{so}= 0.50 *Pa*) [Figure 6.6]. For all runs, even after the initiation of erosion, their bed characteristic shear strengths (τ_{sc}) are shown to increase with the increase in percentage of cohesive fraction in the bed (Figure 6.6).

In terms of the multiple cycle run (EDT-EX4 to EX6), Figure 6.6, shows noticeable reductions in both τ_{so} and τ_{sc} values (i.e. reduction in initial bed resistance to erosion), for each subsequent flow cycle. Specifically, τ_{so} of 1.12 *Pa* for EDT-EX4 was shown to reduce to 0.7 *Pa* in EDT-EX6 (Figure 6.6); i.e. ~37.5% reduction. In addition, this observed reduction in τ_{so}, may possibly be due to the likelihood of topmost part of the bed after the two successive flow cycles, having similar characteristics to deposited bed layer as opposed to the initial placed bed in run EDT-EX4. The shear and structural strength of deposited beds generally increase with increasing depth into the bed (i.e. weaker topmost layer), while that of placed bed is expected to be uniform across the bed (Villaret and Paulic, 1986; Winterwerp and van Kesteren, 2004; and Mehta, 2014).

Therefore, speculatively, the lower τ_{so} (i.e. 0.7 *Pa*) recorded for EDT-EX6 compared to 1.12 *Pa* for EDT-EX4 may be due to this effect as well.

It is expected that, highly erodible sediment beds would have a low erosion threshold and/or high erosion rates at a lower excess shear stress, i.e. $(\tau_b - \tau_{sc})$ (Grabowski *et al*., 2011), and vice versa. Therefore, to demonstrate this expected relationship, the rate of erosion (E) was plotted against excess shear stress $(\tau_b - \tau_{sc})$ for all the runs and $(\tau_b - \tau_{sc}) > 0$ (Figure 6.7). From the results, EDT-EX1 (0% clay) and EDT-EX2 (2% clay) have higher erosion rates at lower excess shear stresses, suggesting they are relatively more erodible than other mixtures with higher clay contents. On the other hand, EDT-EX3 (5%clay) and EDT-EX4 to –EX6 (10%clay) demonstrated significant lower erosion rates at higher excess shear stresses, thus having relatively higher erosion thresholds (i.e. higher resistance to erosion). This again re-emphasizes the role of cohesive sediment fraction in mixed bed stability (e.g. Mitchener and Torfs, 1996; Panagiotopoulos *et al*., 1997; Grabowski *et al*., 2010; etc.).

The limitations highlighted in the current study notwithstanding, the results in Figures 6.5 and 6.6, show surface erosion thresholds that vary from 0.08 to 1.45 *Pa*, this range is in good agreement with reported data for low-cohesive sediment samples (e.g. Winterwerp and van Kesteren, 2004; Le Hir *et al*., 2008; Jacobs *et al*., 2011). Specifically, Jacobs *et al*. (2011) reported erosion thresholds (τ_{sc}) that varied between 0.1 and 1.5 *Pa* for low-cohesive sand-mud mixtures in their experiments. Furthermore, Laksanalamai (2007) obtained erosion thresholds that varied between 0.75 and 1.10 *Pa*, for mixed sediment beds with 70-90% sand contents (see *Appendix* 6-4), again in broad agreement with the results from the current study.

The additional two assumptions made in *section* 6.5.1 are herein shown to be reasonable by this good agreement observed between the estimated erosion thresholds (i.e. 0.08 to 1.45 *Pa*) and those reported in the literature for similar low-cohesive sediment beds. As it has been shown (see *sections* 2.5.1 and 6.5.1), these erosion thresholds are obtained in relation to the changes in erosion rates.

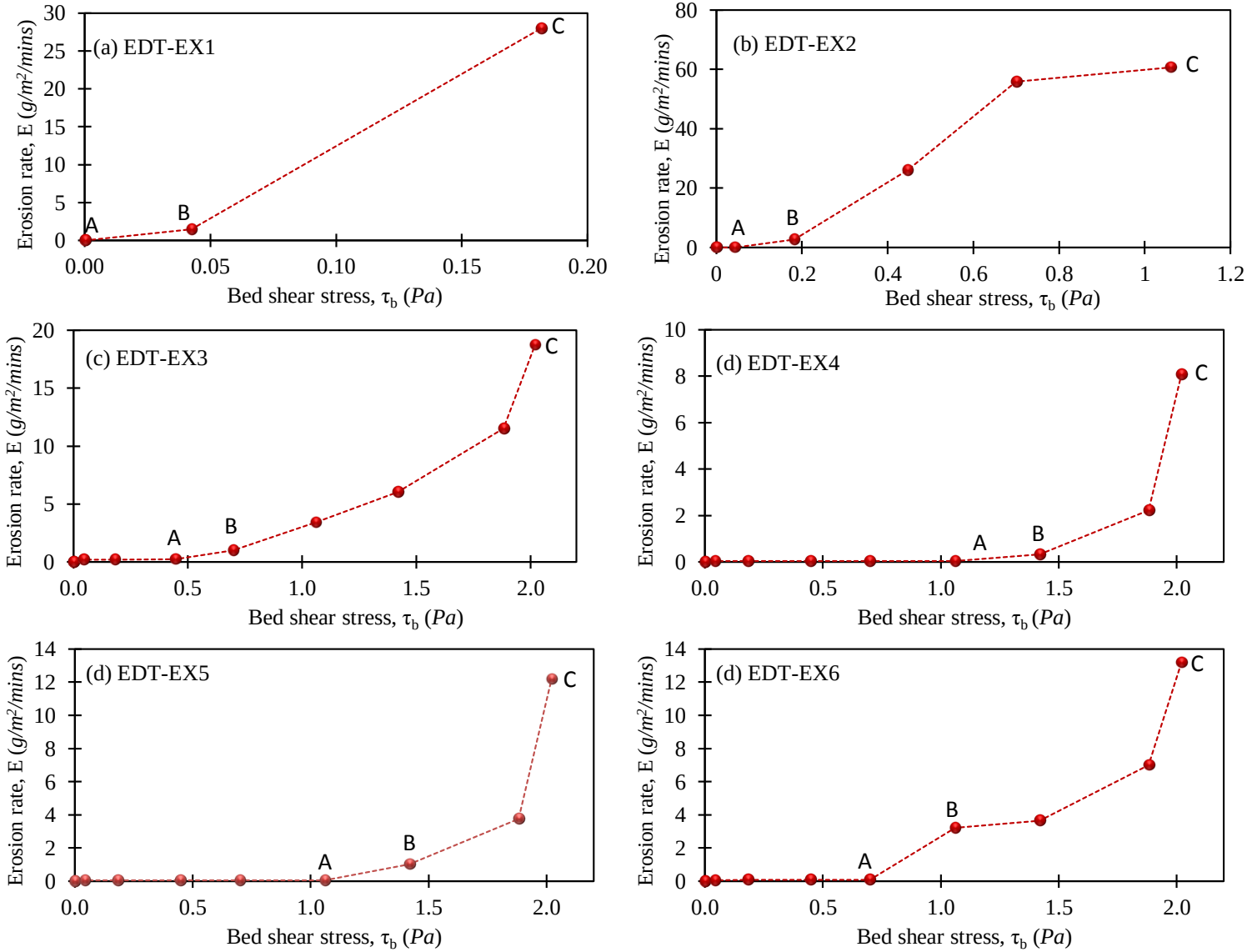

Figure 6.5 Erosion rates of materials as function of Bed shear stress: (a) EDT-EX1 (b) EDT-EX2 (c) EDT-EX3 (d) EDT-EX4 (e) EDT-EX5 & (f) EDT-EX6.

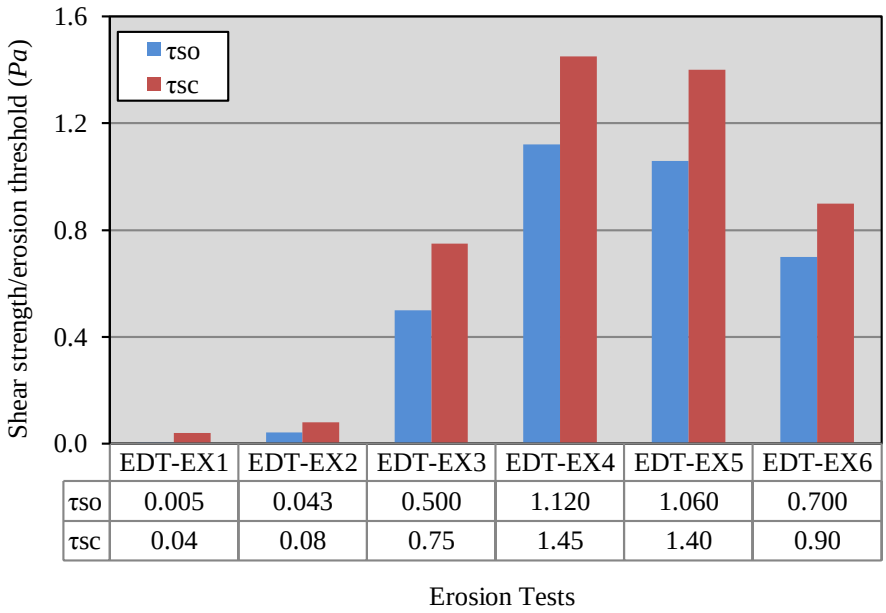

	EDT-EX1	EDT-EX2	EDT-EX3	EDT-EX4	EDT-EX5	EDT-EX6
τso	0.005	0.043	0.500	1.120	1.060	0.700
τsc	0.04	0.08	0.75	1.45	1.40	0.90

Figure 6.6 Comparison of bed shear strengths and erosion thresholds across all the erosion tests

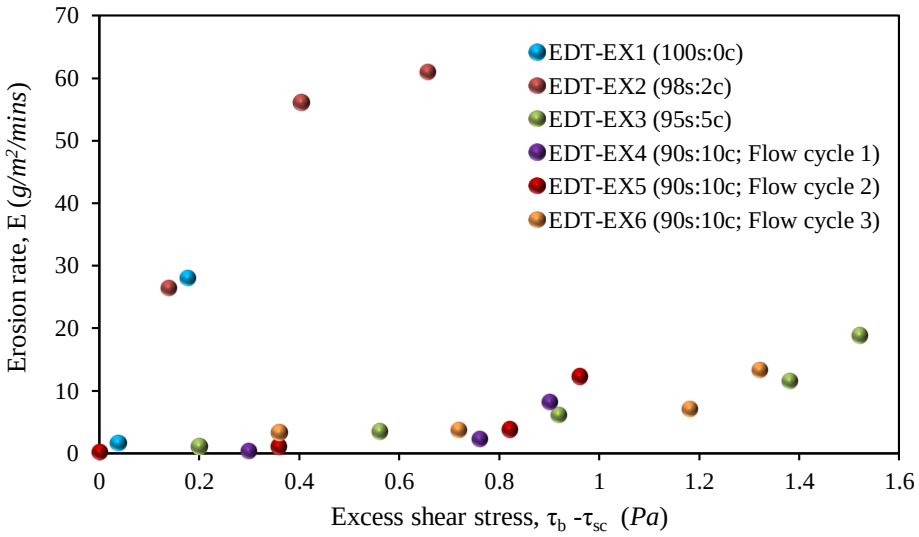

Figure 6.7 The rate of erosion (E) plotted against excess shear stress $(\boldsymbol{\tau_b - \tau_{sc}})$ for all the runs; $(\boldsymbol{\tau_b - \tau_{sc}}) > 0$

6.6 Erosion and Deposition of Bed Materials

A quadrant of the whole bed surface (i.e. ~1200 *mm* span length, see the patterned quadrant in Figure 6.2) was considered for capturing the characteristics of the resulting bed-forms and bed deposits from each experimental run. One of the closest quadrants to the electrical resistivity measurement box (see Figure 3.6) was chosen to reduce variability in the datasets. The plot of the bed deposit height against this span length for each run is shown in Figure 6.8, while the corresponding aerial view of each bed deposit

is presented in Figure 6.9. Images of these final bed deposits, reveal that, deposition of eroded materials, predominantly sand, was along the inner wall of the flume (Figure 6.9), due probably to the occurrence of secondary currents. Interestingly, Laksanalamai (2007) observed similar trends in annular flume erosion tests on mixed sediment beds.

It is clear from the results that, EDT–EX1 and EDT–EX2 have the highest average bed deposit heights across the span, i.e. ∼63 *mm* and ∼55 *mm* respectively (Figure 6.8a-b), due to large layers of sediments continuously and severely eroded and mobilised in these runs (i.e. supported by the results in Figures 6.3 & 6.4). On the contrary, EDT-EX4 (10% clay) has the lowest average bed deposit height (Figure 6.8d); suggesting, it is the bed with highest erosion resistance. This again, as expected shows the parametric influence of clay fraction on erosion and deposition processes of mixed (sand-clay) sediment beds, this is consistent with the results in Figures 6.3 - 6.7.

Bed deposits for runs EDT-EX3 to EX6 (Figures 6.8c-e & 6.9c-e) are spatially different from those of EDT-EX1 & EX2 (Figures 6.8a-b & 6.9a-b) discussed above. The deposition of eroded sand materials observed in these runs (i.e. EDT-EX3 to EX6) are relatively smaller in height and width when compared to those from runs EDT-EX1 and EX2. Sand deposit with height of ∼15 *mm* and width of ∼20 *mm* (Figures 6.8d & 6.9d), is observed for EDT-EX4 (with the highest τ_{sc} value = 1.45 *Pa*; Figure 6.6); while height of ∼45 *mm* and width of ∼80 *mm* (Figures 6.8c & 6.9c) were recorded for EDT-EX3 (τ_{sc} = 0.75 *Pa*). Lastly, significant spatial differences can be seen in the final bed deposits from EDT-EX4 and EX6. Final sand deposit from EDT-EX4 increased by an average of 70% (both in height and width) after it was subjected to further two flow cycles (i.e. in EDT-EX6; Figures 6.8e & 6.9e). Again, this is clearly indicative of reduction in the bed shear strength.

In general, the spatial extent of the sand deposit or the nature and extent of bed restructuring observed from the final sediment beds of all the experimental runs, is shown to be influenced by the fractional content of the cohesive clay within the initial mixed-sediment bed. Also, in addition, within mixed-sediment beds with highest clay fraction (i.e. runs EDT-EX4 to EX6; 90s:10c), the history and antecedent conditions of the bed, is shown to contribute significantly to the definition of their sediment transport characteristics.

6.6.1 Generated bedforms

In this study, the generated bedforms (refer to *section* 2.5.7; pg. 50, for brief description of sedimentary bedforms), have been described solely to highlight the parametric influence of cohesive sediment fraction (i.e. clay) on bedforms development in mixed (sand-clay) beds. Using the description in Figure 2.22, the characteristics of the generated bedforms were estimated from Figures 6.8 and 6.9, and Table 6.5 presents the results. The results show bedforms with length (L) ranging from 180 to 600 *mm* and height (H) of 4 to 48 *mm*. These are in good agreement with typical sand ripples dimensions of L = ~ 50 – 600 *mm* and H = ~5 – 50 *mm* (Ashley 1990). Across all the experimental runs, slightly straight-crested plan morphology of bedforms are observed on the final bed deposits (Figures 6.8 & 6.9). The sides of the final beds along the outter wall of the flume channel (Figure 6.2) are shown to have deep and wide (~100-160 *mm*) erosional scour holes (see the red oval curves in Figure 6.9) mainly in beds with clay content < 5 % (i.e. runs EDT-EX1 and EX2). However, these are completely absent in run EDT-EX4 (10 % clay; Figure 6.9d), although, a couple of such scour holes was seen across the total surface area of the final bed from run EDT-EX6 (10 % clay; e.g. Figure 6.9e), again suggesting run EDT-EX6 relative to EDT-EX4, has lower bed shear strength (Figure 6.6).

Table 6-5 Characteristics of the bedforms generated from the experimental runs

Tests	**% Clay**	**Height (H) (*mm*)**	**Length (L) (*mm*)**
EDT-EX1	0	48	360
EDT-EX2	2	32	600
EDT-EX3	5	28	440
EDT-EX4	10	4	180
EDT-EX6	10	10	220

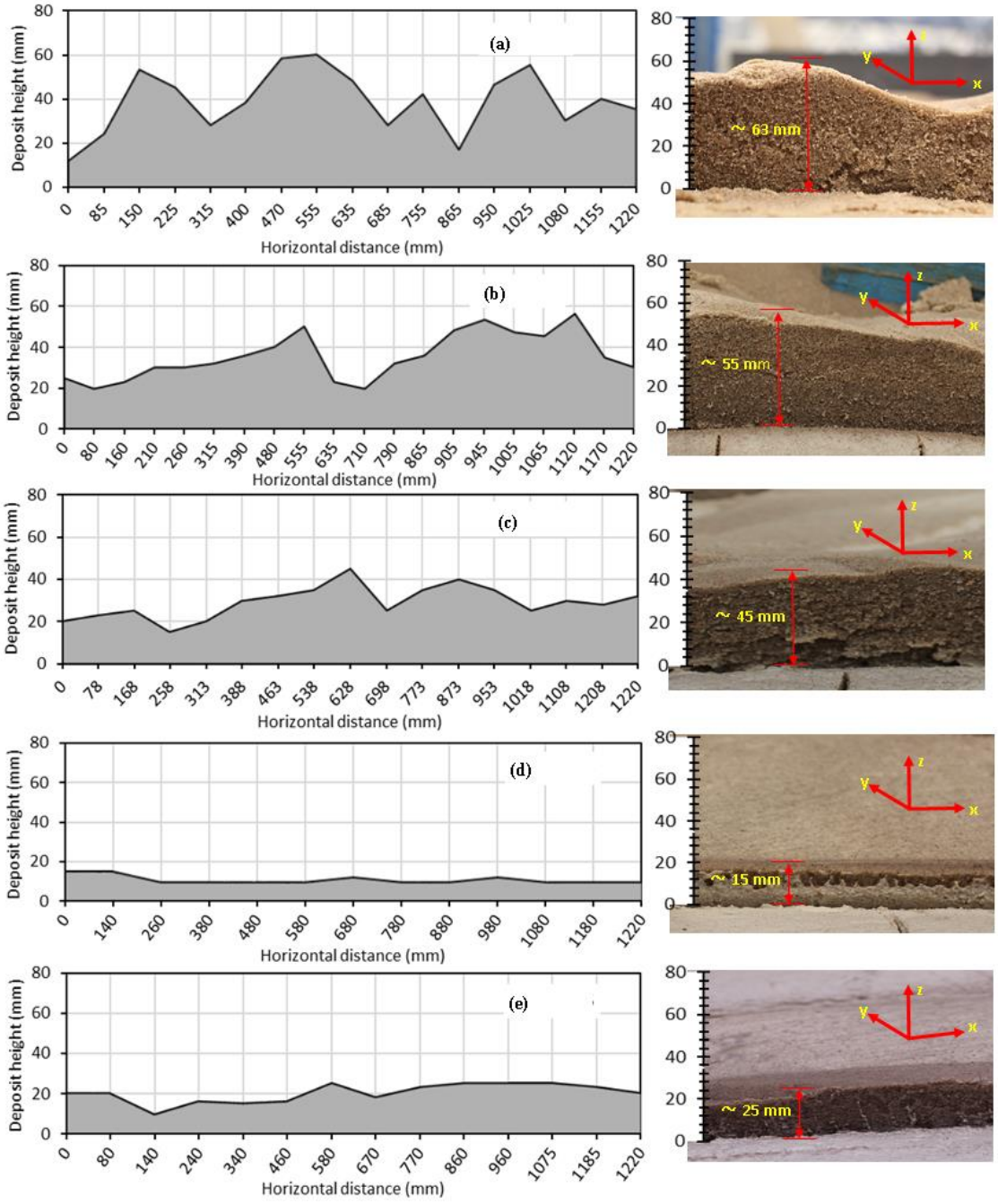

Figure 6.8 Bed deposits heights measured over the span length of the selected quadrant (Figure 6.2) for: (a) EDT-EX1 (b) EDT-EX2 (c) EDT-EX3 (d) EDT-EX4 and (e) EDT-EX6. (Corresponding photographic images show the heights of the sand deposits).

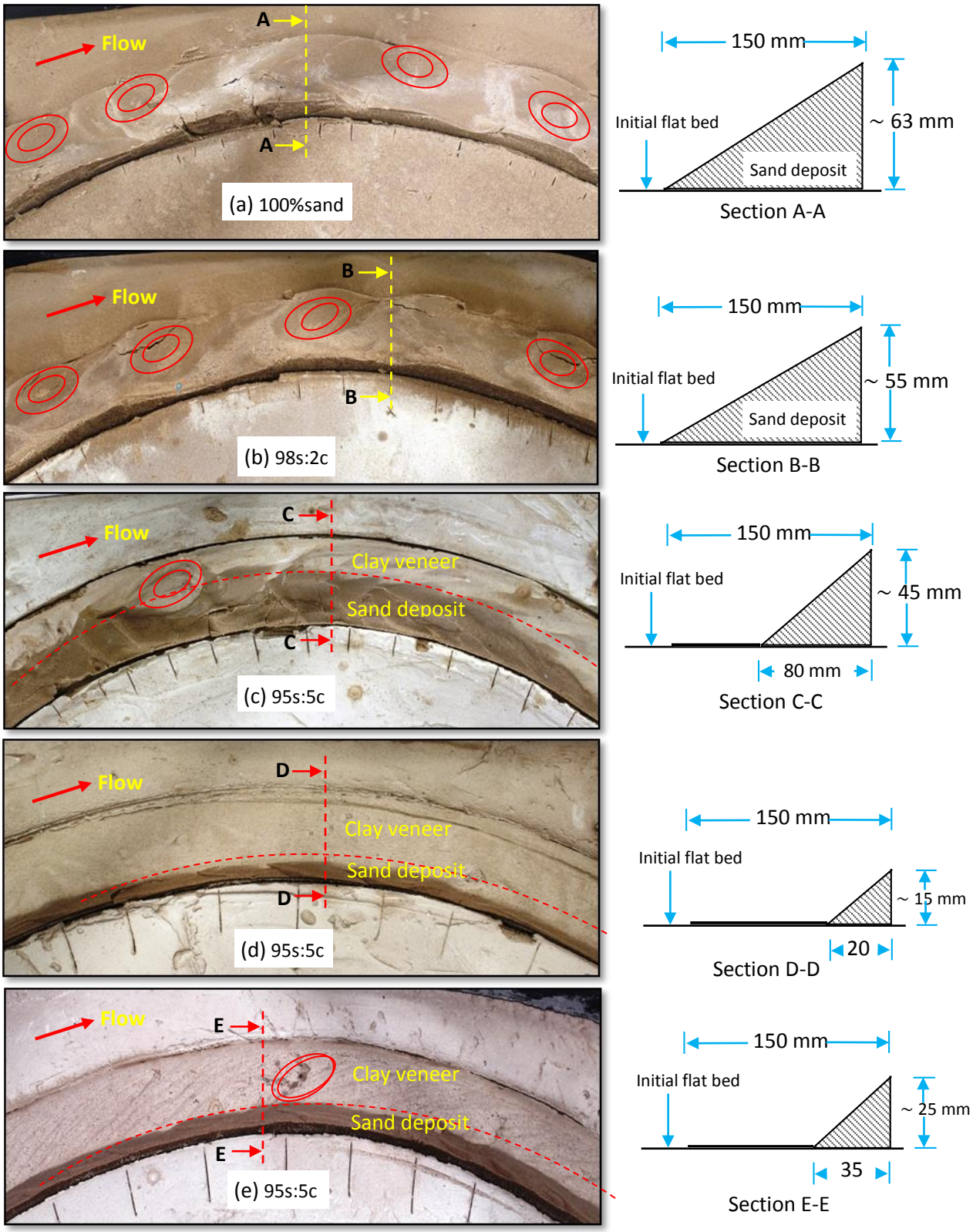

Figure 6.9 Photographic images of the aerial view of the final beds within the selected quadrant (Figure 6.2) of the flume, showing sand deposit and clay veneer parts, and red oval curves show the scour holes for: (a) EDT-EX1 (b) EDT-EX2 (c) EDT-EX3 (d) EDT-EX4 and (e) EDT-EX6. Corresponding schematic diagrams are representatives of deposits features when cut through designated sections.

The spatial-temporal development of the bedforms has not been quantified in the current study, due to some of the previously highlighted limitations. Hence the analysis is based on the characteristics of the bedforms developed on the final bed deposits for all the runs. These have been compared with the recent results from Baas *et al*. (2013) on experimental study of bedform development in mixed sand-clay sediment beds under steady flow conditions, where the influence of initial clay fraction ranging from 0 – 18% was tested. For comparison, from Baas *et al*. (2013), the characteristics of bedforms (in terms of height and length) developed at equilibrium conditions (i.e. after $t > 1$ *hr*) have been considered. The schematic representation of changes in bed morphology at $t = 0$ and 5*hrs* for the current experiment is shown in Figure 6.10. Similar to Baas *et al*. (2013), the crests of the bedforms are shown to mainly comprise clean sand (Figures 6.8, 6.9 & 6.10).

Specifically, results from Baas *et al*. (2013) suggest, a strong inversely proportional relationship between bedform height (*H*) and the initial mud fraction and a weak inversely proportional relationship between bedform length (*L*) and the initial mud fraction. These findings are in good agreement with the findings from the current study as shown in Table (6-5) and Figure 6.8. For the bedforms generated, a strong negative correlation can be consistently seen between *H* or *L* and percentage (%) initial clay fraction. Although for *L*, run EDT-EX1 appears to deviate from this relationship (see Table 6-5). Similar deviation in bedform length, was equally observed by Baas *et al*. (2013), where they found some tests with relatively lower clay fraction having shorter equilibrium-lengths compared to other runs with higher clay fractions. It may be inferred therefore, that, supply of sand material, from the initial mixed bed, needed for the development of bedforms has been limited by the increased cohesive bed strength with the increase in clay fraction (see Table 6-5), thereby forming what Allen (1968) described as sediment-starved bedforms. Thus, these findings suggest that, high cohesive bed strengths (i.e. as initial % clay fraction increases), relative to the flow-induced bed shear stresses, are to large extent responsible for the observed decrease in bedform heights and lengths (Figures 6.9 & 6.10).

Furthermore, images in Figure 6.9 show a clear banding occurring in the channel, where sand is deposited at the inner wall (darker strip in Figure 6.9c-e) and clay veneer over the remainder of the bed surface. Thus, run EDT-EX3 (5% clay; Figure 6.9c) clearly appears to be a transitional bed between sand dominated and clay dominated conditions, due to the nearly even delineation between the deposited sand part (i.e. inside the channel) and

clay veneer part (i.e. at the outer part of the channel). This is also supported by the erosion results (e.g. Figure 6.6) already discussed above, where this run has been shown to represent the transition from non-cohesive behaviour of the mixed bed (i.e. in terms of resistance to erosion) to the cohesive behaviour. Interestingly, Baas *et al*. (2013) show specifically that cohesive bed forces had a more significant influence on bedform development at clay content > 5.4 %. This is clearly consistent with the findings of the current study (i.e. run EDT-EX3 has 5% clay fraction). Le Hir *et al*. (2008) also, from the erosion experiment on mixture of 280 μm sand and 'St Yves' mud (see Figure 2.17b; pg. 42), found this critical clay fraction to occur at 4.5%.

Finally, it is informative to investigate whether stratification occurs within the resulting bed after the erosion and deposition processes. As such, cores were taken, close to the inner wall of the channel, from the final bed deposits in some of the runs (e.g. EDT-EX2 & EX3). Figure 6.11 shows two core samples from runs EDT-EX2 and EDT-EX3. In both runs, the upper parts of the cores appear to consist of relatively clean sand deposit, which may have been formed by a process similar to a phenomenon described as '*winnowing* of clay particles' by Baas *et al.* (2013). Clay *winnowing* describes a process where clay particles are selectively removed from the active part of the mixed (sand-clay) bed. It is clear that the thickness of the clean sand layer is ~20 *mm* in EDT-EX3 (5% clay) and ~50 *mm* in EDT-EX2 (2% clay). This suggests that, increase in fractional composition of clay within the mixed (sand-clay) beds (which has already been established to increase bed stability, i.e. resistance to erosion), appears to limit clay *winnowing*. Similar to these findings, Baas *et al.* (2013) equally observed that, the degree of *winnowing* tends to decrease with increasing clay fraction, with lowest degree of *winnowing* observed in runs with the smallest bedforms heights and lengths. These findings critically suggest that, *winnowing* of fine sediments from their compositional base, appears to be an important sediment transport process in the development of bedforms and also, in erosion and deposition processes of mixed (sand-mud) beds.

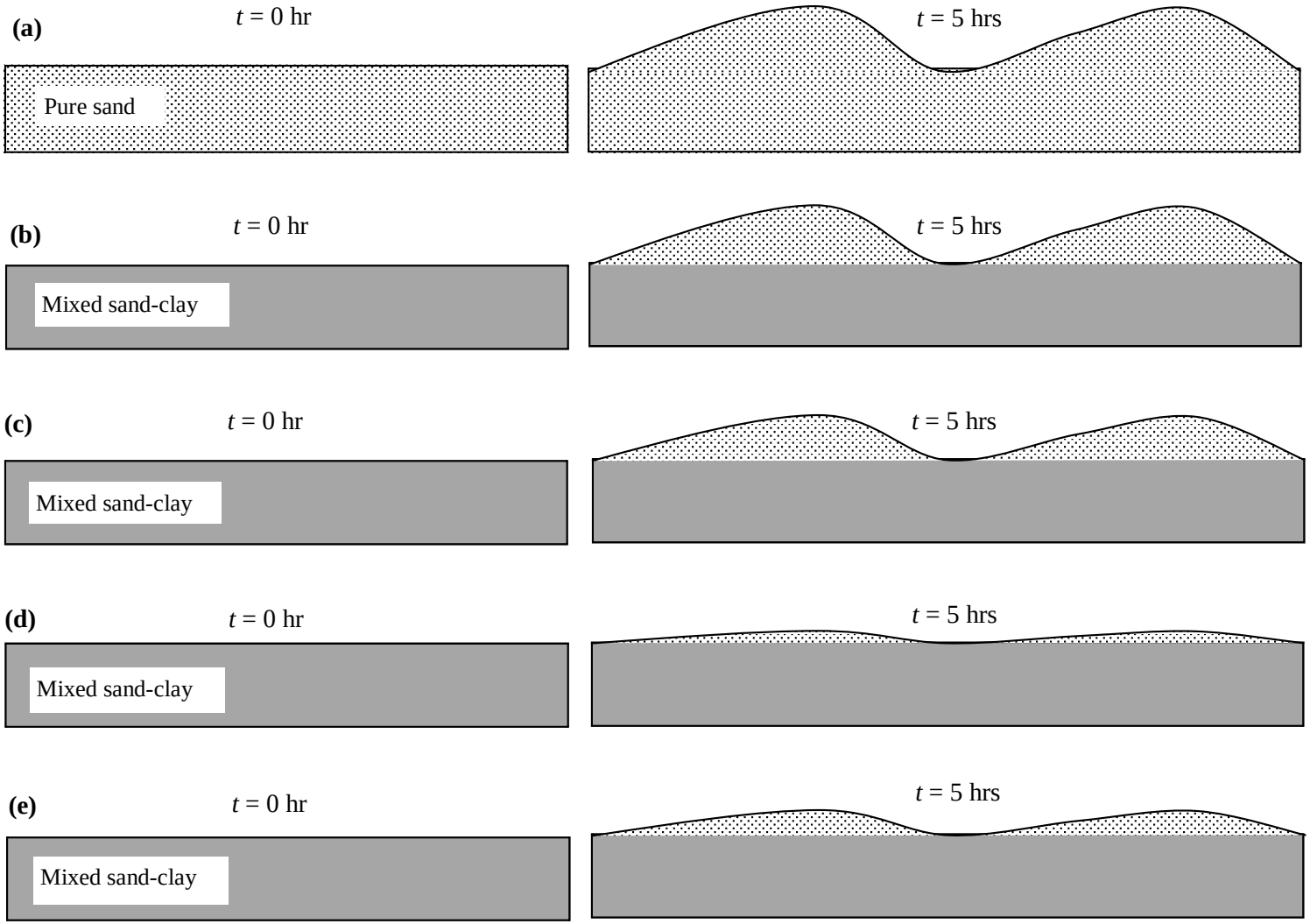

Figure 6.10 Schematic representation of changes in bed morphology at t = 0 & 5 *hrs* for (a) EDT-EX1 (100% sand) (b) EDT-EX2 (98% sand) (c) EDT-EX3 (95% sand) (d) EDT-EX4 (90% sand) and (e) EDT-EX6 (90% sand after 3rd flow cycle). [Note the pure sand bedforms overlying the mixed sand–clay beds]

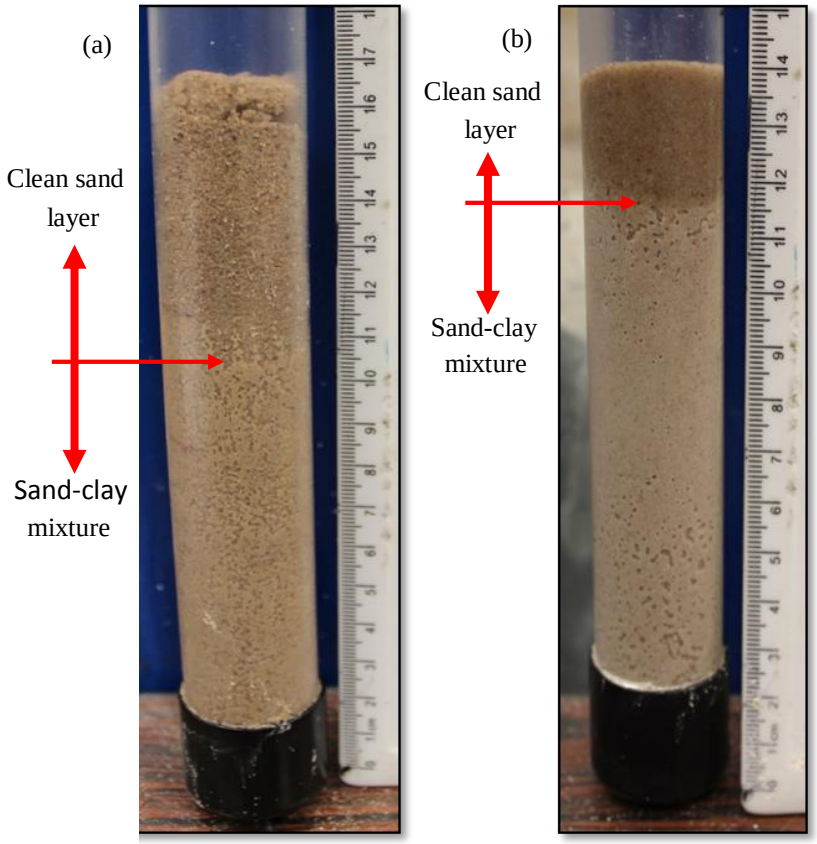

Figure 6.11 Final sediment bed core (a) EDT-EX2; (b) EDT-EX3

6.7 Electrical Resistivity Measurement Results

The real time bed restructuring, resulting from continuous erosion and deposition processes, was captured with the ERMT (at the inner wall location only, see Figure 3.12; pg. 91). Figure 6.12 shows the temporal development of normalised density (γ_{bulk}/γ_p) profiles for runs EDT-EX1 and EDT–EX2, at elapsed times ranging from t = 30 *s* and 5 *hrs*. Figure 6.13, on the other hand, presents time series colour maps of the variation in the measured formation factor F profiles over the whole period of erosion and deposition processes.

It is apparent from Figure 6.12 that, there is no significant temporal changes in the vertical position of γ_{bulk}/γ_p profiles above the initial bed height (i.e. $z > \sim 140$ *mm*) for up to t = 1 *hr*. This is also shown in Figure 6.13, where the measured formation factor F profiles remain virtually constant at the interface between the placed bed and overlying water column for up to t = 3600 *s* (1 *hr*). This suggests that, there was virtually no material deposition during this time period. However, results in Figure 6.3a-b, show that in these

runs, erosion of bed materials started within the first 20 mins. Therefore, it can be inferred that, the eroded materials within this period of time were transported mainly as suspended load (i.e. part of the total load that is moving in suspension without continuous contact with the bed as a result of agitation of fluid turbulence). From $t \geq 1$ *hr*, above the bed-water interface, continuous changes (both horizontally and vertically) in γ_{bulk}/γ_p profiles are shown for up to $t = 3$ *hrs*, with γ_{bulk}/γ_p values ranging from $\sim 1.16 \rightarrow 1.92$ for EDT-EX1 and $1.15 \rightarrow 1.89$ for EDT-EX2 (Figure 6.12). The colour maps of the F profiles in Figure 6.13 show this effect more clearly with temporal changes in F ranging from 3.5 $\rightarrow$ 5.5 for both runs. Apparently, these results indicate continuous erosion and deposition of sediment with increasing bed shear stress over this period of time (i.e. $t \geq 1$ to ~ 3 *hrs*). Results in Figures 6.12 & 6.13, show that this period of time was characterised by intermittent increase and decrease in γ_{bulk}/γ_p and F values respectively.

It should be noted also, that from $t \geq 1$ *hr*, temporal increase in interface height (i.e. from $z = \sim 140$ to ~ 200 *mm*) between the placed bed and overlying water column is shown for the two runs (Figures 6.12 & 6.13), suggesting deposition of eroded materials. Specifically, after $t \geq 3$ *hrs* and to the end of the experiment (i.e. the final 60 *minutes* during the period of ramping down of the flume paddles speed), the spatial and temporal γ_{bulk}/γ_p and F profiles appear to be steady with little or no significant changes (Figures 6.12 & 6.13). This clearly indicates that, the bed deposits are stable, with this stability shown for both tests by the similarity in γ_{bulk}/γ_p profiles obtained at $t = 4$ *hrs* and t = 5 *hrs*. In general, the observed spatial-temporal changes in γ_{bulk}/γ_p and F values across the entire duration of each experimental run, are thought to be initiated by the changes in bed shear stresses within the flume channel, and are indicative of erosion, mobilisation and deposition of bed materials.

From Figures 6.12 & 6.13, it is particularly interesting to observe that over $t \geq 1$ *hr*, the spatial-temporal rise and fall in γ_{bulk}/γ_p and F values respectively, indicates that the final bed deposits were not steadily built up, and/or suggests the migration of bedforms (i.e. local changes in bed elevation). This is similar to a scenario common in sediment transport, where bed-forms (e.g. ripples) earlier formed at relatively lower bed shear stress (τ_b) are subsequently eroded at higher τ_b, indicating a transition in the sediment transport mode from the bed load to the sheet flow regime (Hanes and Bowen, 1985; Van Rijn, 1993; Soulsby, 1997 and Winterwerp & Kesteren, 2004, etc.).

Figure 6.13b shows a clear interface (i.e. at z = ~150 *mm*) between the base sand-mud bed (*F* values = ~3.5 → 3.75) and the overlying clean sand deposit (*F* values = ~4.5 → 5.5) for run EDT-EX2, similar to schematic representation of changes in bed morphology shown in Figure 6.10b. As expected, the range of *F* values obtained for this overlying clean sand deposit is similar to the *F* values observed in sand only bed of run EDT-EX1 (Figure 6.13a). This effect is equally shown in Figure 6.12b (i.e. the area of the plot in red circle), the average value of γ_{bulk}/γ_p profile (at t = 5 *hrs*; z ≥ 150 *mm*) for instance, is ~2.15, which is approximately the same as that observed across the bed deposit in run EDT-EX1 (Figure 6.12a). This is clearly an important effect, showing the 'cleaned sand deposit' layer over the surface of the initial mixed bed (similar to diagram in Figure 6.10b). Furthermore, from Figures 6.12 & 6.13, the final height of the deposits can be estimated; i.e. ~65 *mm* and ~56 *mm* for EDT-EX1 and EX2 respectively. These measurements are interestingly similar to those measured directly from their bed deposits, i.e. ~63 *mm* and ~55 *mm* respectively (Figure 6.8). This close similarity in measurements is again highlighting the potential of ERMT to characterise bed evolution in confined sedimentary environments not readily accessible to human beings.

Lastly, from the colour maps in Figure 6.13, the spatial-temporal changes in *F* profiles seen immediately after t = ~4000 *s* is quite interesting, as they show evidence of erosion and deposition of bed materials over the period of each experimental run (especially up to t = ~14000 *s*). Particularly, the deposition processes are shown to occur even at higher bed shear stresses (τ_b), (i.e. as τ_b is increased with time, see *section* 6.2). Therefore, explaining these results in the light of '*exchange paradigms of erosion with deposition*' (e.g. Krone, 1963; Mehta, 2014; etc.), highlights the shortfalls of the '*exclusive bed exchange model'* (i.e. the model's inability to allow simultaneous occurrence of erosion and deposition). Therefore, the implication of this finding, especially as it affects erosion laws of mixed sediments, is that the laws obviously need more investigation. Conclusively, it is particularly very interesting (and informative) to see the resistivity profiles (i.e. Figures 6.12 and 6.13), identifying the simultaneous occurrence of erosion and deposition (i.e. *simultaneous bed exchange*) within these runs.

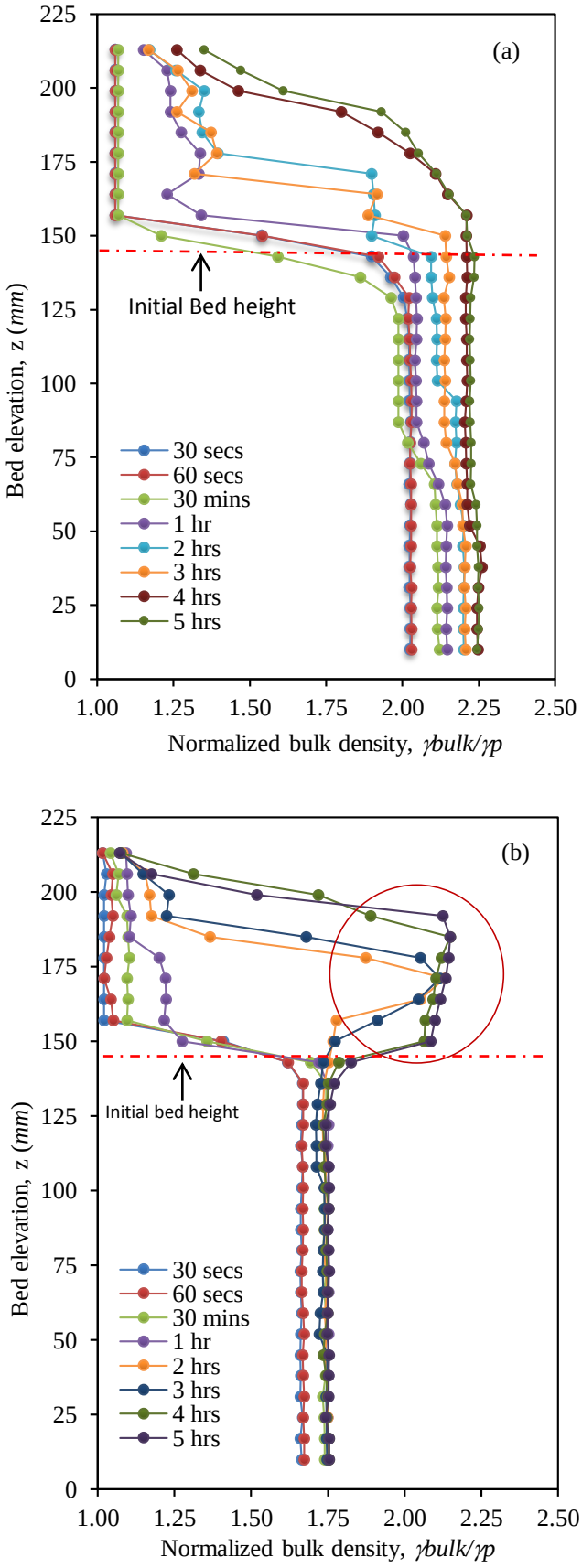

Figure 6.12 Vertical profiles of normalised bulk density $\gamma bulk/\gamma p$ at elapsed times shown for EDT-EX1 (b) EDT-EX2. Red circle in (b) highlights the deposition of clean sand layer at the surface of mixed bed of EDT-EX2.

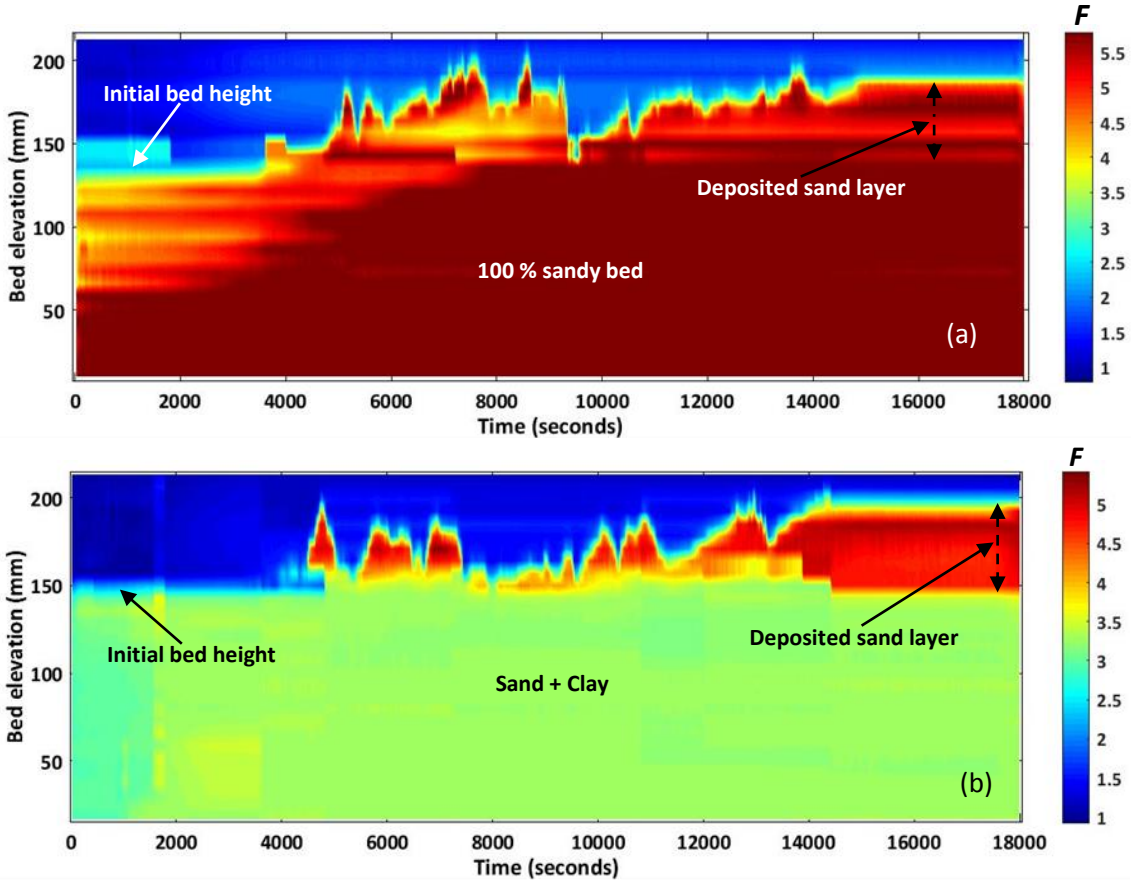

Figure 6.13 Time series colour map plots of the variation in measure formation factor F profiles during erosion and deposition processes for (a) EDT-EX1 (0% clay) and (b) EDT-EX2 (2% clay).

It is important to make reference to the unexpected variability observed in γ_{bulk}/γ_p values within the bed (i.e. z = 0 -150 *mm*; Figure 6.12). Clearly, from t = ~30 *s and* 5 *hrs*, γ_{bulk}/γ_p increases from 2.0 to 2.25 particularly for EDT-EX1 (100s:0c). This increase in γ_{bulk}/γ_p technically suggests that, in addition to erosion and deposition processes being initiated at the topmost layer of the bed, there was a form of compaction going on within the bed. The reason for this is not particularly known, however, considering the size and weight of the benthic annular flume used, plus other factors, this observation may have been due to the artefact of the experimental set-up or procedures.

6.8 Conclusions from ES-3 Experiments

The main findings of the experimental series reported in the current chapter, are summarised below:

- In agreement with previous studies (e.g. Parchure and Mehta, 1985; Villaret and Paulic, 1986, etc.), after the initiation of erosion, quasi-linear relationship was

found to exist between suspended sediment concentration (SSC) and applied bed shear stress (τ_b). Also, over the range of sediment proportions considered, a quasi-linear relationship was also found to exist between erosion rate (*E*) and applied bed shear stress (τ_b), once the erosion threshold is exceeded (e.g. Jacobs *et al*., 2011; etc.),

- A strong positive correlation between mixed sediment bed resistance to erosion and the proportion of cohesive fraction in the bed was further established.
- The results reveal that mixed sediment bed's initial resistance to erosion may be significantly reduced with further exposure to subsequent erosion cycles.
- The use of erosion rate (*E*), bed surface shear strength (τ_{so}) and bed characteristic shear strength (τ_{sc}) as measures of bed erosion in isolation may give misleading information as they are not only largely affected by bed materials' properties and compositions; but also significantly by the antecedent conditions of the sediment beds. Therefore, in this context, prediction of sediment beds erosion characteristics in marine environments is best supported by adequate understanding of the sedimentary regimes, probably gained by observational measurements rather than a priori determination.
- Surface and mass erosion processes (e.g. Winterwerp and van Kesteren, 2004) have been inferred to be most likely common in mixed beds with clay content ≤ 2% by dry weight.
- Similar to the finding of Baas *et al*. (2013), clay dry weight fraction of ≥ 5.0 % within mixed (sand-clay) beds, will result in cohesive bed forces having more significant influence on bedform development and morphology.
- *Winnowing* of fine sediments from their compositional base, appears to be an important sediment transport process in the development of bedforms and also, in erosion and deposition processes of mixed (sand-mud) beds. Baas *et al*. (2013) reported similar findings.
- The transition from the bed load to the sheet flow regime during sediment transport, (e.g. Hanes and Bowen, 1985; Van Rijn, 1993; Soulsby, 1997 and Winterwerp & Kesteren, 2004, etc.), was established by the electrical resistivity results.
- The results from the resistivity profiles, also support the adoption of *simultaneous bed exchange* model (e.g. Krone 1963; Mehta, 2014; etc.).

CHAPTER SEVEN

Analysis and Discussion

"There will come a time when our descendants will be amazed that we did not know things that are so plain to them" —Lucius Annaeus Seneca

7.1 Introduction

Physical processes associated with mixed sediments are generally known to be influenced by occurrence of time-dependent flow conditions (i.e. tidal currents and/or waves), mixed sediment characteristics (e.g. cohesive and non-cohesive sediment types, proportions and initial concentrations), water chemistry (e.g. salinity, pH, temperature) and concentration gradients generated by unsteady flow conditions. Extensive research has been conducted on the interactions between fluid and sediment within mixed sediment suspensions and, the structural characteristics of the resulting bed deposits. However, these linkages are not yet completely understood due to the complex interplay between sediment transport processes such as flocculation, settling, deposition, erosion and consolidation (e.g. Grasso *et al.*, 2015). In this context, attempts were made in the current study to address some of the current knowledge gaps and uncertainties associated with these processes in mixed sedimentary environments, through idealised experimental investigations. Some of the findings of this study, will undoubtedly provide new insight into fundamental mechanisms of mixed sediment processes in estuaries and coastal regions, as required by practitioners involved in management, planning and the implementation of legislations in these dynamic and complex ecosystems.

The main aims of the current chapter are therefore to (i) analyse and discuss the main findings from the experimental results presented in Chapters 4, 5 and 6, especially in relation to equivalent findings from previous investigations; (ii) investigate further the parametric influences on the formation of mixed and segregated bed deposits and (iii) test the polydisperse hindered settling formation proposed by Cuthbertson *et al.* (2008) in

terms of its predictive capabilities for the conditions under which mixed and segregated bed deposits are generated.

7.2 Bed Characterisation: Electrical Resistivity Measurement Techniques

Like other similar non-destructive measurement techniques [e.g. *X-ray/gamma* ray techniques (Been, 1981; Pane and Schiffman, 1997; Ellis, 1987; Been and Sills, 1981); *Acoustic & Wave attenuation* techniques and *Turning fork* methods (Libicki and Bedford, 1989; Maa *et al*., 1997; Ha *et al*., 2010; Fontein and van der Wal, 2006)], it has been established that the electrical resistivity profiling technique can be used to characterise the structure of mixed sediment deposits at laboratory, provided an accurate calibration is carried out. In addition, unlike the other techniques, the electrical resistivity measurements do not have inherent limitation such as inflexibility, health and safety implications, etc.

The major doubt in the applicability of this technique, however, is its suitability for field measurements in brackish water environments, where ambient salinity can vary in space and time (Winterwerp and van Kesteren, 2004; Ha, *et al*., 2010). The current work has demonstrated this to be trivial, although it was difficult to capture electrical resistivity measurement for mixtures with salinity greater than 30 *ppt*, this was mainly due to the limitation of the instrumentation used (see *section 3.7.3*) rather that its applicability (i.e. SIM921 — AC resistance bridge, could not accommodate higher range of resistance measurements required at salinity greater than 30 ppt). It is therefore, believed that, if this difficulty (i.e. relating to instrumentation) can be overcome, this technique can be successfully applied in high salinity environments.

Based on the findings of the current work, empirical relationships [i.e. Equations (4-4) and (4-5) respectively] are proposed between the normalized bulk density (γ_{bulk}/γ_p) and the porosity (φ) of the sediment bed deposit, as well as between the corresponding formation factor F and φ. These expressions require the following condition to be satisfied: γ_{bulk}/γ_p and $\varphi \rightarrow 1$ as $F \rightarrow 1$.

$$\frac{\gamma_{bulk}}{\gamma_p} = a.F^b \quad \text{(i.e. Equation 4-4)} \quad ; \quad \varphi = \hat{a}e^{-\hat{b}F} \quad \text{(i.e. Equation 4-5)}$$

The above empirical relationships have been used to define the temporal and spatial changes in the density, porosity and composition within bed deposits resulting from the differential settling of sand-clay mixtures tested in the current work. Specifically, the density and porosity profiles obtained have highlighted the influence of initial fractional composition (i.e. relative sand and clay concentrations) on the formation of segregated (sand-dominated and clay-dominated) bed layers within the deposits, and also on the erodibility of mixed sediment beds. These are similar to previous findings, where presence of sand in sand-mud sedimentation processes, has been shown to have a strong influence on hindered settling (e.g. Cuthbertson *et al*., 2008; Van and Pham Van Bang, 2013; etc.) and consolidation (e.g. Torfs *et al*., 1996; Xu *et al*., 2012; Grasso *et al*., 2014; etc.) processes that can lead to the formation of segregated, layered structures within the resulting bed deposits. These mixed sediment processes, and their role in defining the nature of the developing bed structure, are also shown to be crucial for determining its subsequent resistance to erosions (e.g. Torfs *et al*. 1996; te Slaa *et al*., 2013).

7.3 Sedimentation Behaviour of Sand-Clay Mixtures

In the current study, an attempt was made to differentiate between the hindered settling and phase I consolidation stages during the sedimentation processes of different sand-clay mixtures. The calculated sedimentation rates (w_s), for each experimental run (i.e. SET-EX1 to EX9), were thus divided into these stages, before their averages were computed. The results for mean settling rates, w_{s-mean} over the duration of the experiment have been expressed as function of (i) ambient salinity for runs with similar mixture conditions (i.e. SET-EX4 to EX7) [Figure 7.1], and (ii) initial clay concentration C_s^{cl}, to synthesise the influence of higher clay mass concentration for all the runs (Figure 7.2).

7.3.1 Mixed-sediment settling rate and ambient salinity

Figure 7.1 shows that ambient salinity influences the settling characteristic of the particles differently at each identified sedimentation stage. At the hindered settling stage, it is apparent that, an increase in ambient salinity up to 15 *ppt* brings about slight increase in w_{s-mean}. However, w_{s-mean} slightly decreases as the salinity increases beyond 15 *ppt*. From 0 *ppt* to 40 *ppt*, the corresponding w_{s-mean} value decreases by ~ 20% at this stage. As discussed in *section* 5.5, for a more diluted suspended sediment concentration, such as found within turbidity maximum zone of estuaries (i.e. up to ~10 to ~15 $kg\ m^{-3}$,

Manning *et al*.,2007; Dyer *et al*.,2002; Sutherland *et al*., 2014), it is generally expected that, to some degree, salinity will promote flocculation and, hence, leads to an increased sedimentation rates, compared to those obtained in freshwater (e.g. Sutherland *et al*., 2014). Interestingly, Figure 7.1 appears to suggest that this general consensus may also hold for suspensions with very high clay mass concentrations, more representative of hyper-concentrated, near-bed, fluid-mud layers (such as tested in the current study, where C_s^{cl} = 84–285 $kg\ m^{-3}$). However, this increased sedimentation rate is shown, in the current study, to peak at salinity around 15 *ppt*. It should also be noted that, the parametric influence of salinity on mud flocculation processes is also known to diminish for salinity values above ~20 *ppt* (e.g. Al-Ani *et al*., 1991; He *et al*., 2008; Sutherland *et al*., 2014). The result appears to suggest that; higher salinities above ~15 *ppt* do not increasingly boost sedimentation (similar to findings of Sutherland *et al*., 2014). Therefore, it can be hypothesised that, sediment distribution (in terms of bed deposit structure and composition) patterns in marine environment with higher ambient salinity (e.g. higher salinity basins) will be similar in certain degrees to those observed in marine environments with lower salinity (e.g. estuaries). At phase I consolidation stage on the other hand, increase in ambient salinity appears to have no significant effect on w_{s-mean} (Figure 7.1). This is understandable, because any subsequent variation in the sediment-fluid interface at this stage, will principally be due to creeping (i.e. particles framework deformation) and consolidation effects within the bed.

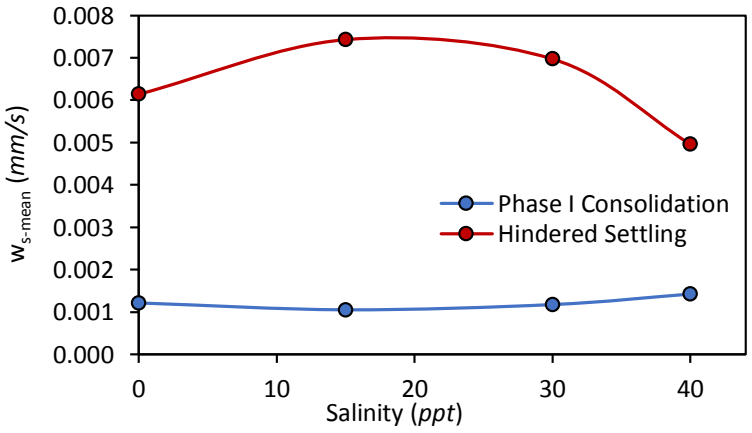

Figure 7.1 Plot of mean settling rates at each settling regime as a function of ambient salinity

7.3.2 Mixed-sediment settling rate and clay concentration

The parametric dependence of decreasing settling rates with increasing clay mass concentrations (C_s^{cl}) [or volumetric clay concentration, $\emptyset_s^{cl}$] has been observed in the

current study, and is also well documented in previous studies for different sediment suspensions (e.g. Imai, 1980; Been & Sills, 1981; Torfs *et al*., 1996; Sutherland *et al*., 2014; Amy *et al*., 2006; etc.). From Figure 7.2, during the hindered settling phase, the decrease in w_{s-mean} with increasing volumetric clay concentration ($\emptyset_s^{cl}$) is apparent, showing the hindered settling effects, as described by te Slaa *et al*. (2013). Again, clay concentration (i.e. $\emptyset_s^{cl}$) is shown to have no significant parametric influence on the w_{s-mean} at phase I consolidation stage (Figure 7.2), for reason described above.

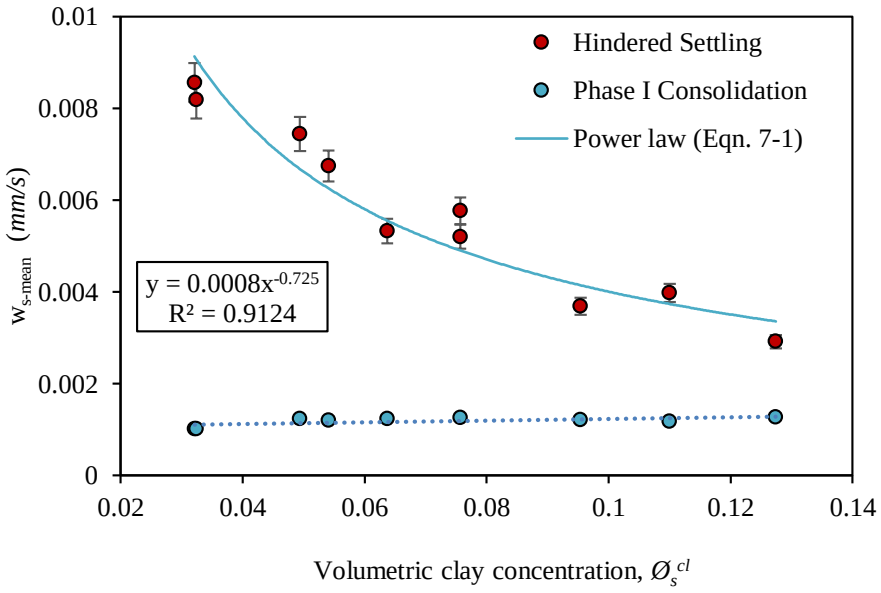

Figure 7.2 Calculated mean settling rate as a function of volumetric clay concentration

The results show a negative correlation between w_{s-mean} and $\emptyset_s^{cl}$ according to a power law (Figure 7.2). Hence, from this relationship, Equation 7-1(a) has been obtained; this provides an empirical measurement of the w_{s-mean} for the sediment mixtures under consideration:

$$w_{s-mean} = \phi\ (\emptyset_s^{cl})^{-0.725} \tag{7-1a}$$

in which, somewhat arbitrarily, ϕ is defined as:

$$\phi = {w_{s,0-mean}}\Big/{(\emptyset_{s,0}^{cl})^{-0.725}} = 0.0008 \tag{7-1b}$$

Therefore, for Equation (7-1b) to hold, the coefficients $\emptyset_{s,0}^{cl}$ and $w_{s,0-mean}$ are set as 0.1274 and 0.0036 *mm s*$^{-1}$ respectively. Thus, Equation (7-1a) takes the following new form:

$$w_{s-mean} = w_{s,0-mean} \left(\emptyset_s^{cl} \Big/ \emptyset_{s,0}^{cl} \right)^{-0.725} \tag{7-2}$$

7.4 Onset of Consolidation

From Figure 5.7 (pg. 132), after the initial hindered settling phase, the subsequent temporal evolution of the clay-water interface represents the onset of the primary consolidation [generally known as Phase I consolidation or permeability regime, e.g. Imai, 1981; Merckelbach and Kranenburg, 2004a; Winterwerp and van Kesteren, 2004; see *sections* 2.4 (pg. 32) and 5.4 (pg. 134)]. Prediction of this Phase I consolidation has been described through the adoption of a fractal approach, typically used to model aggregation processes in cohesive sediment suspensions, during formation of bed deposit. During this initial consolidation stage, the effective bed stresses are expected to be low, with the consolidation process governed largely by the deposit permeability (Been and Sills, 1981; Sills, 1998). Merckelbach (2000) and Merckelbach *et al*. (2002) derived a model to investigate initial consolidation processes under this assumption, based on the observations of the evolving interface elevation $h(t)$ alone, such that:

$$h(t) = \left(\frac{2-n}{1-n}\ \zeta_m\right)^{\frac{1-n}{2-n}} \left((n-2)\ K_k\ \frac{\rho_s - \rho_w}{\rho_w} \right)^{\frac{1}{2-n}} t^{\frac{1}{2-1}} \tag{7-3}$$

The material height, also called Gibson height (ζ_m), at any time t is given by (Winterwerp and van Kesteren, 2004):

$$\zeta_m = \frac{h.\emptyset_s^{cl}}{(1-\emptyset_s^{sa})} \tag{7-4}$$

where volumetric concentrations $\emptyset_s^{cl}$ and $\emptyset_s^{sa}$ are assumed initially to be uniformly distributed in the column of height h. Since the total mass of the sediment in the column does not change, the Gibson height (ζ_m) is said to be independent of t. ζ_m is used to

account for the total solids (i.e. clay and sand) based on the assumption that the sand particles only fill space in the clay-water mixture, and do not affect the network of the structure.

Equations (7-3) and (7-4) are applicable when the behaviour of soft sediment is dominated by clay, but the sediment may also contain small fractions of sand or silt (te Slaa et al., 2013). Hence run ERT-EX1 (100s:0c) was exempted from this analysis, however, for the other sand-clay mixtures, the equations are applicable, if restricted to the upper part of the bed, i.e. predominantly clay layers (Merckelbach, 2000). In the Phase-I consolidation stage, as soon as most of the sand particles settled to the base of the column, it was generally observed that the settlement of the interface versus time follows a power law. Therefore, the permeability parameter K_k (which accounts for effects due to viscosity, pore water density and shape) and fractal dimension n_f [i.e. $n = 2/(3 - n_f)$] can thus be determined by fitting Equation (7-3) to temporal variation of the measured upper clay-water interface (when plotted on double log scales, e.g. Figure 7.3a & b). These model predictions are shown by the dashed lines in Figure 7.3, with the corresponding fitted values of K_k and n_f shown in Table (7-1).

The measurement of the rate at which pore water pressure gradients can be dissipated within sediment deposit or soil is termed its permeability, which generally ranges from 10^{-12} to 10^{-10} $m\ s^{-1}$ for clayey soils (e.g. te Slaa *et al*., 2013). This however, corresponds with the general range of density for mud layer i.e. $1100 < \underline{\rho_s} < 1400\ kg\ m^{-3}$ (Merckelbach, 2000). Therefore, from material functions (i.e. K_k and n_f) obtained from the fits on the Equation (7-3), the permeability (k) of the upper clay-rich mixture of the deposits, can be determined as function of the solid content (Merckelbach, 2000), through the relationship shown in Equation (7-5), if fractional sediment contents of that layer of the bed are known (Winterwerp and van Kesteren, 2004; te Slaa *et al*., 2013).

$$k_{clay\ layer} = K_k \left(\frac{\emptyset_s^{cl}}{1 - \emptyset_s^{sa}}\right)^{\frac{2}{3-n_f}} \tag{7-5}$$

where $\emptyset_s^{cl}$ is the combined solid content of clay and $\emptyset_s^{sa}$ is a correction for the solid content of the sand fraction in the mixture.

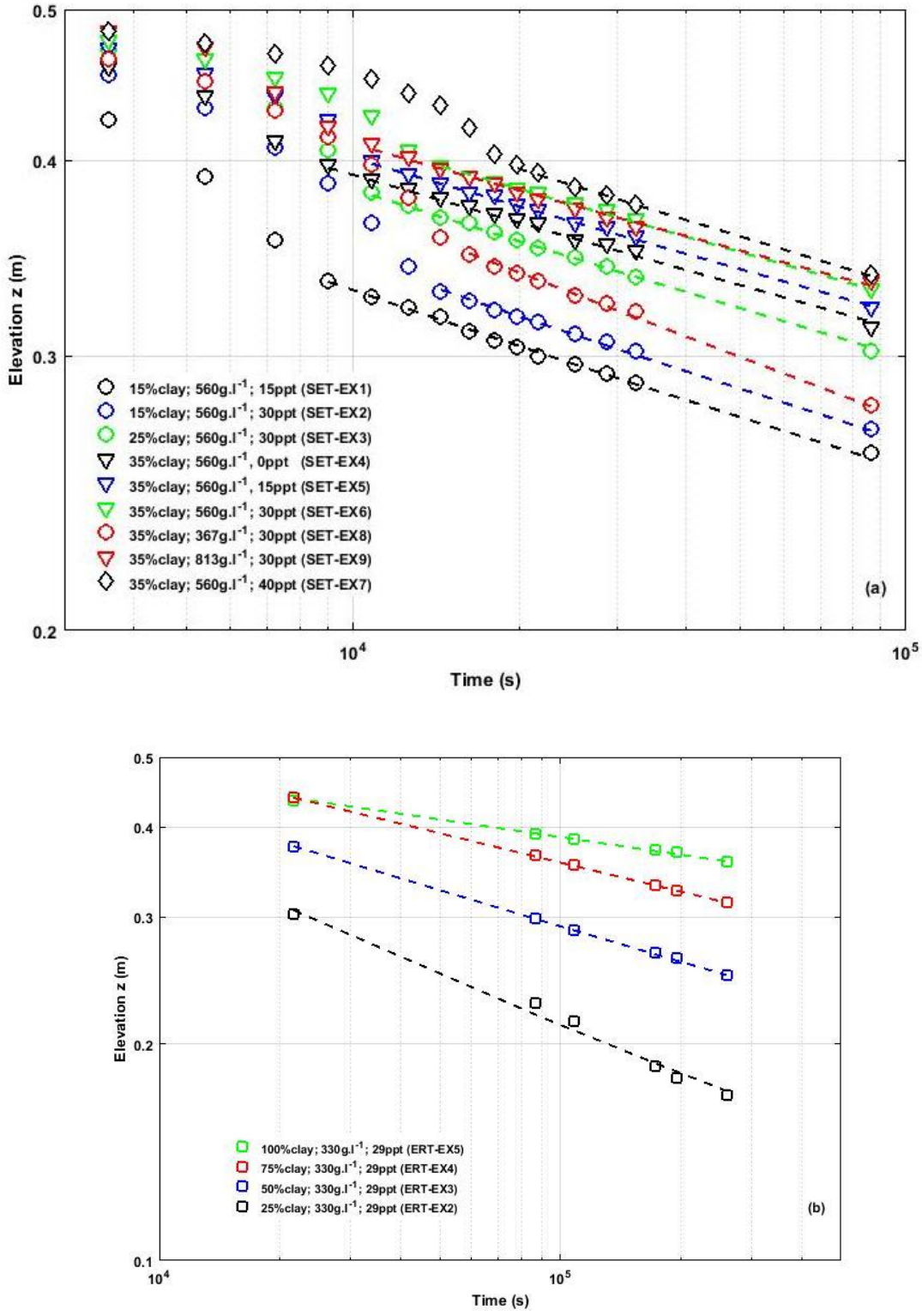

Figure 7.3 Temporal variation in upper clay layer interface with supernatant pore water showing the fit (i.e. dashed lines) of Equation (7-3) for (a) SET-EX1 to EX9 and (b) ERT-EX2 to EX5.

Table 7-1 Initial experimental conditions and sand segregation occurrence with constitutive relationship parameters

Tests	**%Sand: %Clay**	**Salinity (*ppt*)**	**Initial mass concentration C_s ($Kg\ m^{-3}$)**	C_s^{cl} ($Kg\ m^{-3}$)	C_s^{sa} ($Kg\ m^{-3}$)	$Ø_s^{sa}$	$Ø_s^{cl}$	C_{relmud} (++) ($Kg\ m^{-3}$)	**Segregation Yes/No**	n_f (+)	K_k (+) ($m\ s^{-1}$)
ERT-EX1	100s:0c	29.2	330	0	330	0.1250	0	-	-	-	-
ERT-EX2	75s:25c	29.2	330	83	247	0.0936	0.032	92	Yes	2.70	3.03×10^{-12}
SET-EX1	85s:15c	15.0	561	84	477	0.1807	0.0324	103	Yes	2.76	4.72×10^{-15}
SET-EX2	85s:15c	30.0	561	84	477	0.1807	0.0324	103	Yes	2.76	3.32×10^{-15}
SET-EX8	65s:35c	30.0	367	128	239	0.0905	0.0494	141	Yes	2.75	5.71×10^{-15}
SET-EX3	75s:25c	30.0	561	140	421	0.1595	0.0541	167	Yes	2.79	2.51×10^{-15}
ERT-EX3	50s:50c	29.2	330	165	165	0.0625	0.0637	176	Yes	2.75	1.31×10^{-13}
SET-EX4	65s:35c	0.0	561	196	365	0.1383	0.0757	227	Yes	2.80	3.01×10^{-15}
SET-EX5	65s:35c	15.0	561	196	365	0.1383	0.0757	227	Yes	2.81	2.41×10^{-15}
SET-EX6	65s:35c	30.0	561	196	365	0.1383	0.0757	227	Yes	2.81	1.92×10^{-15}
SET-EX7	65s:35c	40.0	561	196	365	0.1383	0.0757	227	Yes	2.80	4.32×10^{-15}
ERT-EX4	25s:75c	29.9	330	247	83	0.0314	0.0954	255	No	2.80	1.11×10^{-14}
ERT-EX5	0s:100c	29.9	330	330	0	0	0.1274	330	No	2.89	2.12×10^{-13}
SET-EX9	65s:35c	30.0	813	285	528	0.2000	0.1100	356	No	2.79	3.08×10^{-13}

(+) Fractal dimension n_f and permeability coefficient K_k obtained from fit to Equation 7-3.
(++) See *section* 7.5 for more details

Generally, it is expected that the consolidation characteristics of the clay dominated upper layers in the current sand-clay bed deposits will be similar to that of fully cohesive sediment deposits, which therefore allows a comparison with consolidation characteristics from previous studies investigating the sedimentation of cohesive sediments (e.g. Merckelbach and Kranenburg, 2004a; Winterwerp and van Kesteren, 2004; Merckelbach, 2000; te Slaa *et al.*, 2013; Merckelbach, 2000; Townsend and McVay, 1990). It is interesting to note that the fractal dimension n_f for the structure formation of the clay-dominated bed layer, is significantly higher than the expected fractal dimension for cohesive flocs in suspension, where the fractal dimension might be expected to be around $n_f \approx 2$ (Winterwerp and van Kesteren, 2004). Therefore, in consolidating cohesively behaving sediment, n_f is likely to increase to values close to 3 (Mehta, 2014; te Slaa *et al.*, 2013; Winterwerp and van Kesteren, 2004), indicating significant reduction in interstitial pore spaces within the flocs and the consolidating sediment matrix.

Consolidation characteristics from previous sedimentation experiments have been analysed and described, for (i) sand-mud mixtures (e.g. Merckelbach and Kranenburg, 2004a; Winterwerp and van Kesteren, 2004; and Merckelbach, 2000), (ii) silt-rich sediment (e.g. te Slaa *et al*., 2013) and (iii) soft muds (e.g. Merckelbach and Kranenburg, 2004b; Merckelbach, 2000; Townsend and McVay, 1990; and Been, 1980). Their findings show a range of values for K_k and n_f, which have been compared with those obtained in the current study [see Table (7-2); pg. 193]. In general, Winterwerp and van Kesteren (2004) noted that the fractal dimension (n_f) varies between 2.61 and 2.75; all the results (including current results) compared in Table (7-2) broadly agreed with this range. Although, the range obtained (i.e. n_f = 2.70 – 2.89) in the current study appears to be slightly higher. It should be noted that, the range of initial clay mass concentration (i.e. 83-330 $kg\ m^{-3}$) used in the current study is relatively higher than those of the studies mentioned above (see Table 7-2).

Furthermore, the predicted values of permeability coefficient K_k (= 10^{-15} to 10^{-12} m s^{-1}; Table 7-1) are equally in broad agreement with representative values obtained from these studies [see Table (7-2)]. Therefore, the measured interface height profiles at phase I consolidation phase in the current study are reasonably predicted by this model (i.e. Equation 7-3).

In a simple term (e.g. as described in *fractal geometry*), a fractal dimension of a set is a number that shows how 'densely' the set occupies the metric space in which it lies (Mahmood, 2006). The concept of *fractal geometry* is applied to describe the structure of the clay network. This structure of clay network is regarded as self-similar fractal, meaning its geometrical properties are truly scale invariant under various stretching and squeezing of the underlying space (Mandelbrot, 1982). Analogous to this definition, Winterwerp and van Kesteren (2004) described fractal dimension (n_f) as an expression that describes the extent of structure formation of clay-dominated bed layer under consolidation. They suggested that, n_f increases to values close to 3 as the degree of squeezing of the flocs (which results in expulsion of pore water) in the bed increases under self-weight consolidation (see *section* 2.4.2; pg. 32). Therefore, the higher range of n_f values predicted for the sand-clay mixtures tested in the current study relative to previous studies (see Table 7-2), suggest that, the higher sediment concentration (and specifically fractional composition of clay) mean that the clay dominated deposit layers in the current study will consolidate faster than the sediment compositions tested by these authors. This is also partly supported by the predicted range of permeability coefficient K_k values. These K_k values [see Table (7-2)] are approximately one order of magnitude larger than most of those predicted by the authors under consideration here. Similar conclusion was made by te Slaa *et al*. (2013), when they found range of K_k values (i.e. 10^{-13} to 10^{-15}) for Yangtze Estuary fresh clay deposits, that was one order of magnitude larger than those predicted (i.e. 10^{-14} to 10^{-16}) by Merckelbach (2000) for Ems-Dollar sediment [see Table (7-2)]. Hence, they concluded that, Yangtze Estuary clay deposits consolidate faster than Ems-Dollar sediment deposits.

Furthermore, te Slaa *et al*. (2013), Van and Pham Van Bang (2013) and Merckelbach (2000) specifically reported that fractal dimension (n_f) increases with increasing initial sediment concentration, i.e. for a given sediment, n_f varies with the initial sediment concentration. Increase in fractal dimension with increase in initial concentration was also indicated by numerical simulation of Vicsek (1989). However, relating n_f values from the current and previous studies as function of clay concentration (C_s^{cl}) within the initial mixed (sand-mud) sediment mass concentration (C_s) (Figure 7.4), interestingly shows that irrespective of the initial sand content (C_s^{sa}) (see Table 7-2), n_f appears to linearly increased with C_s^{cl}. Figure 7.4 indicates a good positive correlation ($R^2 = 0.90$) between n_f and C_s^{cl}. Grasso *et al.* (2015) reported similar correlation between n_f and

initial relative mud concentration (i.e. C_{relmud}; see *section* 7.5 for details), with initial sand content showing no significant influence. In support of submissions made by Grasso *et al.* (2015), these findings have significant implication on 3D estuarine transport modelling (e.g. Le Hir *et al.*, 2011; Waeles *et al.*, 2008), where overlying water column and sediment bed are usually treated as two compartments and the initial sediment concentration of the deposit always taken arbitrarily as having a constant value. It will therefore mean that consolidation processes prediction from such models will obviously be less accurate as it may be difficult to consider dependency of these parameters on this arbitrary initial sediment concentration.

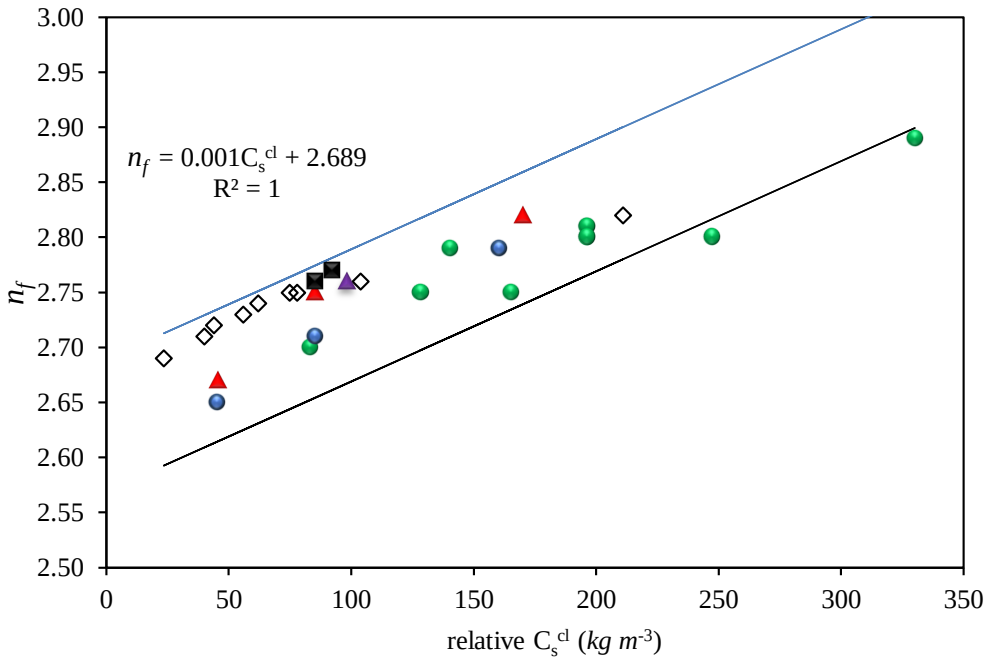

Figure 7.4 Relation between the fractal dimension (n_f) and the relative initial clay concentration for the current and previous studies: Current study (green circles); Grasso et al. (2014) (MSMB – Cancale, red triangles); Grasso et al. (2014) (MSMB – Hirel, blue circles); (te Slaa *et al.* (2013) (diamonds); Grasso *et al.* (2014) (SE-Mel, black squares); and Merckelbach and Kranenburg (2004b) (purple triangle). The solid blue-line (R^2 = 1) is the Least Square Regression Line for the data and solid black-line represents -0.12 Standard Deviation data).

In conclusion, as expected, the experimental evidence presented in this study, shows that the fractal dimension (n_f) of bed structure undergoing phase I consolidation (i.e. permeability regime) is significantly higher than that of mud flocs in suspension. Also, the predicted material functions (i.e. K_k and n_f) in the current study relative to others, suggest that the predominantly clay deposits tested here compact more efficiently or faster, evidenced by relatively higher range of predicted material functions. The specific reason for this as highlighted above, is the relatively high clay fractional composition

within the initial mixed sediment mass concentration. It can be argued also that, this will result in higher concentration of aggregates during hindered settling phase, thereby results in a higher fractal dimension.

Lastly, the current findings [e.g. Tables (7-1) & (7-2); Figure 7.4], have further established the strong dependence of material functions (e.g. K_k and n_f) or the so-called constitutive relationship parameters in permeability regime (i.e. phase I consolidation regime), largely on initial fractional composition of clay (e.g. Grasso *et al*., 2015), and less on the initial mixed sediment mass concentration (e.g. Van and Pham Van Bang, 2013; te Slaa *et al*., 2013; etc.). Therefore, the implication of this is that, in addition to the significant role of initial fractional composition of clay in controlling formation of segregated (sand-clay) bed layers within bed deposits (see *chapter* 5); its observed influence on constitutive relationship parameters in the permeability regime, suggests that the efficiency of phase I consolidation process is also largely depends on it.

7.5 Parametric Conditions for Segregation in Sand-Clay Mixtures

Partial and full segregation was observed in the resulting bed deposits for the majority of the sand-clay mixtures tested within the settling column experiments. The exceptions to this are SET-EX9 and ERT-EX4, which were shown to result in the formation of a mixed bed deposit layer. Recent analysis of Grasso *et al*. (2014) on a number of previous settling column studies revealed that sand segregation is not always observed within the deposits of sand-mud mixtures and appears to be prevented at a threshold level of the initial relative mud concentration C_{relmud} (e.g. Waeles *et al*. 2008). Based on these findings, Grasso *et al*. (2014), proposed that the initial relative mud concentration C_{relmud} in relation to the initial volumetric sand content $\emptyset_{sand}$ (i.e. grain diameter > 63 μm) in the mixture could be used as a potential segregation indicator in the resulting deposit, such that:

$$C_{relmud} = \frac{C_{mud}}{1-\emptyset_{sand}} \tag{7-6}$$

where C_{mud}, is the initial mass concentration of mud (clay and silt) fraction. Note that the C_{relmud} is directly related to the relative volume fraction of fine particles defined by Marckelbach and Kranenburg (2004b).

Table 7-2 n_f and K_k: Comparison between current study and other studies

Authors	Initial clay concentration C_s^{cl} ($kg\ m^{-3}$)	Initial sand concentration C_s^{sa} ($kg\ m^{-3}$)	Initial silt concentration C_s^{silt} ($kg\ m^{-3}$)	Fractal Dimension n_f	Permeability Coefficient K_k ($m\ s^{-1}$)
Townsend and McVay (1990)	167.4	-	-	2.62	4.12×10^{-13}
Merckelbach and Kranenburg (2004b)	≈100	-	-	2.76	3.68×10^{-14}
Merckelbach (2000)	81 (~80-90% clay) [(2)]	24 -	- -	2.67-2.75[(1)] 2.72-2.75[(2)]	$1.2 \times 10^{-15} – 4.5 \times 10^{-13}$ [(1)] $1.0 \times 10^{-16} – 1.4 \times 10^{-14}$ [(2)]
Winterwerp and van Kesteren (2004)	53	7	-	2.70	1.0×10^{-14}
te Slaa *et al.* (2013)	3-34	0.5-17	21-292	2.69-2.82	$1.04 \times 10^{-15} – 8.32 \times 10^{-13}$
Current work	83-330	83-528	-	2.70-2.89[(3)] 2.75-2.81[(4)]	$1.92 \times 10^{-15} – 3.03 \times 10^{-12}$

[(1)] Results for Caland-Beer Channel mud
[(2)] Results for Ems-Dollard Estuary mud
[(3)] ERT-EX1-5 - longer term tests (up to 72 *hours*)
[(4)] SET-EX1-9 - shorter term tests (up to 24 *hours*)

Furthermore, based on the above, Grasso *et al*. (2015) synthesised 22 settling experiments from the literature, for the settling and consolidation of natural sand-mud mixtures, and for which segregation occurrence was determined, based on sediment concentration and grain size vertical profiles (e.g. Bartholomeeusen *et al*. 2002; Merckelbach and Kranenburg 2004a; te Slaa *et al*. 2013; van and Pham Van Bang 2013 and Grasso *et al*. 2014). In these previous settling column studies, initial mixture conditions varied significantly (i.e. initial total mass concentration C_s ranging from 64 to 893 $kg\ m^{-3}$; sand content ranging from 2 to 80 %). Specifically, their analysis revealed that no segregation occurred for $C_{relmud} \geq 207\ kg\ m^{-3}$. As such, Grasso *et al.* (2015) suggested C_{relmud} ~200 $kg\ m^{-3}$ as a threshold for segregation within sand-mud mixtures. Applying these findings to the idealised sand-clay mixtures tested in the current study, using the appropriate notations $C_s^{cl} = C_{mud}$ and $\emptyset_{sand} = C_s^{sa}/\rho_s = \emptyset_s^{sa}$ in Equations (7-6), the corresponding values of C_{relmud} are estimated and presented in Table 7-1 (pg. 188). Clearly from Table (7-1), the calculated values of C_{relmud} for the sand-clay mixtures tested range from $C_{relmud} = 0$ (i.e. test ERT-EX1, 100 % sand) up to 356 $kg\ m^{-3}$ (i.e. test SET-EX9, 35 % sand). It is shown that the threshold for bed segregation occurs between $C_{relmud} = 227$ $kg\ m^{-3}$ (i.e. runs SET-EX4 to –EX7) and $C_{relmud} = 250\ kg\ m^{-3}$ (i.e. run ERT-EX4). This appears to be in broad accord with the findings of Grasso *et al*. (2015), but it does not provide further detail of the physical hindered settling processes under which sand-clay segregation may or may not occur.

7.6 Polydisperse Model for Hindered Settling of Sand-Clay Mixtures

The settling characteristics of monodisperse non-cohesive (e.g. Cheng, 1997) or cohesive sediment flocs (e.g. Winterwerp, 2002) suspensions have been extensively studied, with the exact form of the Richardson and Zaki (1954) formulae (see *section* 2.3.4.3; pg. 28) or some related variation being used for most hindered settling models employed to calculate sediment transport in coastal environments (Cuthbertson *et al*., 2008). By contrast, challenges associated with full theoretical description of settling characteristics, for high volumetric concentrations of polydispersed (i.e. multiple-species) particulate suspensions, still exist, in spite of contributions from various researchers (e.g. Batchelor, 1982; Davis and Gecol, 1994; Ha and Lui, 2002; etc.). As demonstrated in the current work and from previous studies, relative fractional (i.e. sand-clay) content within the mixture can strongly influence the fractional settling characteristics for the sand and mud constituents in concentrated suspensions. For example, in a suspension containing mainly

sand particles with a low mud content (i.e. "sand-rich" suspension), the generated return flow associated with the differential settling of sand particles, may be significant enough to initiate upward transport of the mud particles/flocs (Amy *et al*., 2006). However, if the sand particle content is much lower than the mud particle/floc content (i.e. "mud-rich" suspension) within the suspensions, the settling velocity of the sand particles can be significantly reduced by the increased apparent viscosity and return flow generated by the high mud content within the suspension (Winterwerp, 1998; Cuthbertson et al., 2008).

In this context, it is informative to consider the potential reciprocal influences that the sand and clay fractions are likely to have on each other in terms of their hindered settling characteristics within the sedimentation column experiments. To demonstrate this, an analytical hindered settling model for sand particle-clay floc mixtures, developed by Cuthbertson *et al.* (2008), has been used. Also, this analytical model is used, not least, to remove the restriction associated with the "mud-rich" assumption ($\emptyset_s << \emptyset_f$) [e.g. Winterwerp and Van Kesteren, 2004 and Cheng, 1997], as well as to account adequately for the relative size and density effects between the cohesive mud flocs and non-cohesive sand particles. The model is based on a polydisperse formulation from Batchelor (1982), whereby the fractional settling velocities w_{si}, for a suspension containing m different particle types with fractional volume concentrations $\emptyset_j$ within the polydisperse mixture can be determined by:

$$w_{si} = w_{si,0}\left(1 - \sum_{j=1}^{m} S_{ij}\emptyset_j\right) \tag{7-7}$$

where $w_{si,0}$ is the terminal settling velocity of a solitary particle from fraction i, and S_{ij} is an empirical polydisperse sedimentation parameter dependent on (i) the particle size ratio λ_{ij} (= d_j/d_i; (ii) the reduced density ratio $\rho_{ij} = [(\rho_j - \rho_f)/(\rho_i - \rho_f)]$ and (iii) the particle Péclet number (*Pe*). The particle Péclet number compares the ratio of particle advection to particle diffusion (i.e. *Pe* is defined as the ratio of mechanical to Brownian forces) and thus gives an estimate as to whether particle motions are predominantly advective (i.e. $Pe \gg 1$) or dominated by randomly diffusive (e.g. Brownian) motions ($Pe \ll 1$). The work of Batchelor (1982), discussed here, was extended by Davis and Gecol (1994), by considering a Richardson-Zaki-type relation [e.g. $w_{ss}/w_{ss,0} = (1 - \emptyset_s)^n$; see *section 2.3.4.3*], such that:

$$w_{si} = w_{si,0}(1-\emptyset)^{-S_{ii}}\left(1-\sum_{j\neq 1}^{m}(S_{ij}-S_{ii})\,\emptyset_j\right) \tag{7-8}$$

where $\emptyset$ is the total volumetric concentration of the mixture and S_{ii}, is the equivalent empirical sedimentation parameter for a monodisperse suspension. The application of this type of polydisperse hindered settling model to concentrated sand–mud suspensions, such as we have in the current work, is based on the assumption that, (i) the mud flocs and sand particles contained within the suspension are individually monodisperse (i.e. represented by single volumetric concentrations $\emptyset_f$ and $\emptyset_s$ and sizes d_f and d_s, respectively); and (ii) *Pe* >> 1 for each fraction (i.e. non-colloidal). Under these conditions, Cuthbertson *et al.* (2008) applied this polydisperse approach to consider mixed suspensions of uniform-sized sand particles and clay flocs, with hindered settling characteristics, w_s^{sa} and w_s^{floc}, respectively, given by:

$$w_s^{floc} = w_{s,0}^{floc}(1-\emptyset)^{-S_{ff}}\left[1+\left(S_{fs}-S_{ff}\right)\emptyset_s^{sa}\right] \tag{7-9}$$

$$w_s^{sa} = w_{s,0}^{sa}(1-\emptyset)^{-S_{ss}}\left[1+\left(S_{sf}-S_{ss}\right)\emptyset_{floc}\right] \tag{7-10}$$

The total mixture volumetric concentration $\emptyset = (\emptyset_{floc} + \emptyset_s^{sa})$ and volumetric clay floc concentration $\emptyset_{floc}$ after Winterwerp (2002), is:

$$\emptyset_{floc} = \left(\frac{\rho_s-\rho_f}{\rho_{floc}-\rho_f}\right)\frac{C_s^{cl}}{\rho_s} = \frac{C_s^{cl}}{\rho_s}\left(\frac{d_{floc}}{d_s^{cl}}\right)^{3-n_f} \tag{7-11}$$

where C_s^{cl} is the clay mass concentration ($kg\ m^{-3}$); ρ_s (= ρ_s^{sa}= ρ_s^{cl}) is the solid particle density; d_s^{cl} and d_{floc} are respectively, the clay primary particle and flocs sizes; and n_f is the fractal dimension of the flocs (n_f = 2.0 is assumed here). Although, Equations (7-9) and (7-10) include implicitly all induced hindered settling effects (i.e. return flow generation, increased viscosity and buoyancy of the sand-clay mixture, Winterwerp 2002). However, a further correction is necessary to account for the increased buoyancy effect resulting from the sum of the volumetric particle concentrations $\emptyset_s = (\emptyset_s^{cl} + \emptyset_s^{sa})$ rather than from the total mixture volumetric concentration $\emptyset = (\emptyset_{floc} + \emptyset_s^{sa})$. Therefore, Equations (7-9) and (7-10)] can be represented as:

$$w_s^{floc} = w_{s,0}^{floc}(1-\emptyset)^{-(S_{ff}+1)}(1-\emptyset_s^{cl}-\emptyset_s^{sa})\left[1+\left(S_{fs}-S_{ff}\right)\emptyset_s^{sa}\right] \tag{7-12}$$

$$w_s^{sa} = w_{s,0}^{sa}(1-\emptyset)^{-(S_{ss}+1)}(1-\emptyset_s^{cl}-\emptyset_s^{sa})\left[1+\left(S_{sf}-S_{ss}\right)\emptyset_{floc}\right] \qquad (7\text{-}13)$$

The sedimentation parameter S_{fs} and S_{sf} for the clay floc and sand particle fractions within Equations (7-12) and (7-13) can be estimated from an expression proposed by Ha and Lui (2002), following simulations by Batchelor and Wen (1982), such as;

$$S_{fs} = -2.5 - \left(\lambda_{fs}^2 + 3\lambda_{fs} + 1 - \frac{1.87\lambda_{fs}}{1+0.0024\lambda_{fs}^2}\right)\rho_{fs} \qquad (7\text{-}14)$$

$$S_{sf} = -2.5 - \left(\lambda_{sf}^2 + 3\lambda_{sf} + 1 - \frac{1.87\lambda_{sf}}{1+0.0024\lambda_{sf}^2}\right)\rho_{sf} \qquad (7\text{-}15)$$

where particle size ratios $\lambda_{fs} = d_s^{sa}/d_{floc}$ and $\lambda_{sf} = d_{floc}/d_s^{sa}$; while reduced density ratios, $\rho_{fs} = (\rho_s - \rho_f)/(\rho_{floc} - \rho_f)$ and $\rho_{sf} = (\rho_{floc} - \rho_f)/(\rho_s - \rho_f)$. By assuming $\lambda = \rho = 1$; S_{ff} and S_{ss} in Equations (7-12) and (7-13) respectively can be obtained as $S_{ff} = S_{ss} = -5.63$ from Equations (7-14) and (7-15). This assumption that the sedimentation parameters are both constant and equal is, according to Cuthbertson *et al.* (2008) deemed acceptable as a first approximation.

Thus, from the fractional hindered settling expressions in Equations (7-12) and (7-13), the hindered settling rates for clay floc fraction and sand particles within the tested mixtures in the current work, can be determined. In order to successfully apply the Cuthbertson *et al*. (2008) model, it is proposed in the current analysis that mixture condition under which no sand-clay segregation occurs will result when the initial clay concentration $C_s^{cl} \approx C_{gel}$ (i.e. gelling concentration). According to Winterwerp (2002), this condition occurs when the volumetric floc concentration $\emptyset_{floc} \rightarrow 1$, as such, from Equation (7-11), an expression for C_s^{cl} can be obtained as:

$$C_s^{cl} = C_{gel} = \rho_s\left(\frac{d_s^{cl}}{d_{floc}}\right)^{3-n_f} \qquad (7\text{-}16)$$

Additionally, for the purpose of the current analysis, C_{gel}= 330 *kg m*$^{-3}$ has been assumed. This is the largest clay mass concentration (i.e. C_s^{cl} = 330 *kg m*$^{-3}$) tested within the experimental runs under consideration here (see Table 7-1). Furthermore, $\rho_s = 2590$ *kg*

m^{-3}, n_f = 2.0 and d_s^{cl} = 2 μm (i.e. d_{50}) are equally used. It should be noted that in reality, this gelling concentration may be considerably lower, and has been reported (e.g. by Winterwerp and Van Kesteren, 2004) to be influenced by parameters such as fluid shear rate *G* and the fractal dimension n_f of the clay/mud flocs generated, which are either undefined or assumed within the current study. For the current hindered settling analysis within the sedimentation column experiments, d_{floc} = 15.6 μm, is the adopted representative clay floc size, which was obtained from Equation (7-16), substituting for n_f, d_s^{cl}, C_{gel} and ρ_s.

Figure 7.5 presents the predicted non-dimensional hindered settling characteristics (i.e. $w_s^{sa}/w_{s,0}^{sa}$ and $w_s^{floc}/w_{s,0}^{floc}$) for the sand particles and clay flocs obtained respectively from Equations (7-12) and (7-13). These hindered settling characteristics have been obtained for a range of volumetric mixture concentration $\emptyset$ = 0.3-1.0 and volumetric sand particle concentration $\emptyset_s^{sa}$ = 0.03-0.18, arbitrarily chosen to reflect the characteristics of the sand-clay mixtures under consideration (see Table 7-1).

Clearly from Figure 7.5, the predicted hindered settling regime of the sand fraction varies from $w_s^{sa}/w_{s,0}^{sa}$ = 0.19 to 0.31 at $\emptyset$ = 0.3 (i.e. depending on the $\emptyset_s^{sa}$ value), with $w_s^{sa}/w_{s,0}^{sa} \rightarrow 0$ as $\emptyset \rightarrow 1$ (for all $\emptyset_s^{sa}$ values). The corresponding hindered settling regime for the clay flocs (Equation 7-13), however, shows a contrasting trend, with all negative values obtained for $w_s^{floc}/w_{s,0}^{floc}$, for all the $\emptyset$ values considered, with $w_s^{floc}/w_{s,0}^{floc}$ values lower than -10 at $\emptyset$ values between 0.3 and 0.5 (depending on $\emptyset_s^{sa}$ values). The all negatives values obtained in the hindered settling regime for the clay flocs suggest that they are displaced upwards in the sedimentation column due to strong return flow effects generated by the settling sand fraction. Clearly, larger sand concentrations are shown to result in a stronger upward motion within the clay flocs (i.e. lower $w_s^{floc}/w_{s,0}^{floc}$ values). By contrast, larger clay concentrations $\emptyset_s^{cl}$ within the mixture (i.e. increased $\emptyset$ for given $\emptyset_s^{sa}$) are shown to reduce the upward motion of flocs and increase the hindered settling of sand particles, with the limit $w_s^{floc}/w_{s,0}^{floc} \rightarrow w_s^{sa}/w_{s,0}^{sa} \rightarrow 0$ as $\emptyset \rightarrow 1$ (Figure 7.5). It is therefore proposed that the generation of clearly segregated sand- and clay-dominated deposit layers in the column from initially well-mixed sand-clay suspensions requires the clay fraction (i.e. flocs) to be displaced upwards within the column while the sand fraction (i.e. particles) settles to the base of the column.

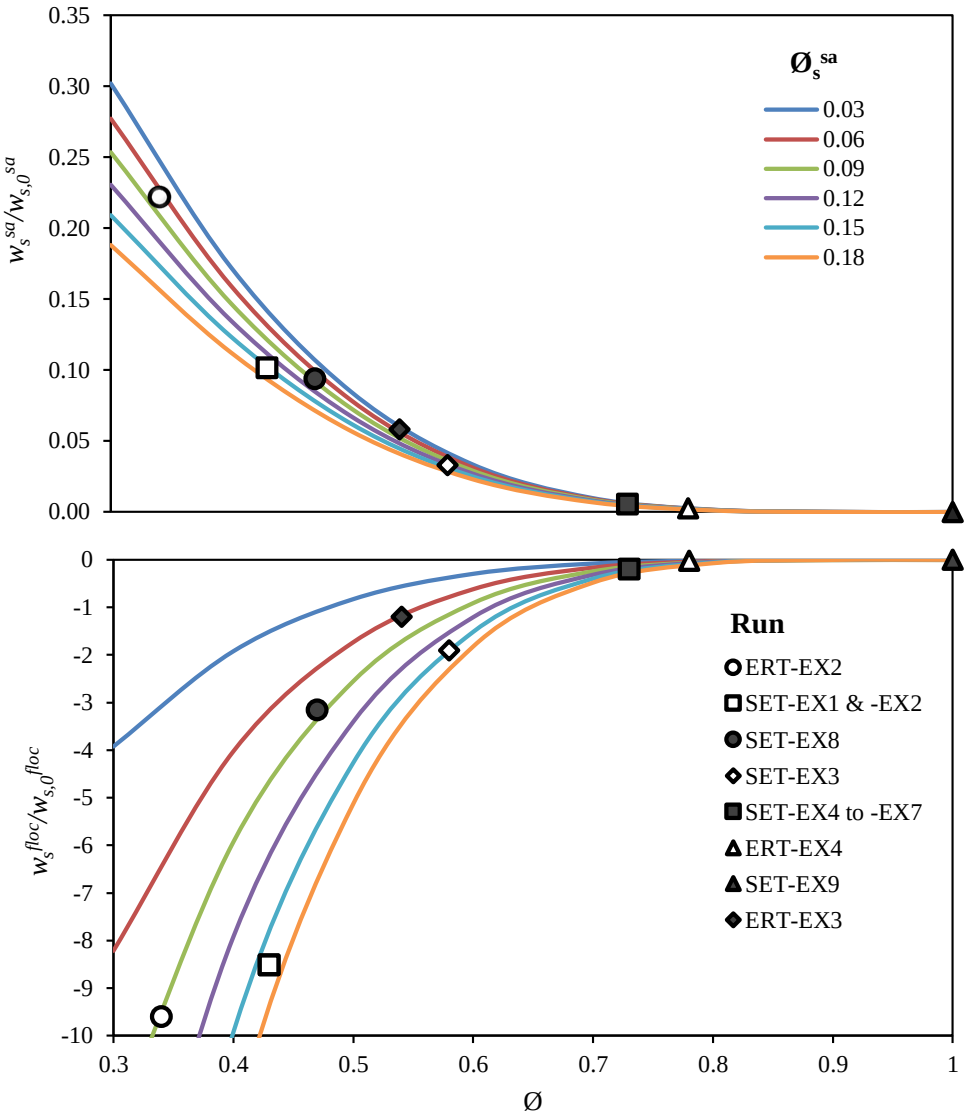

Figure 7.5 Predicted non-dimensional hindered (sand-clay) settling characteristics $w_s^{sa}/w_{s,0}^{sa}$ and $w_s^{floc}/w_{s,0}^{floc}$ versus volumetric mixture concentration Ø (for volumetric sand particle concentration $Ø_s$ values shown). Discrete data points show predicted $w_s^{sa}/w_{s,0}^{sa}$ and $w_s^{floc}/w_{s,0}^{floc}$ values for the tested sand-clay mixture (see Table 7-1).

In this context, the predicted $w_s^{floc}/w_{s,0}^{floc}$ and $w_s^{sa}/w_{s,0}^{sa}$ values [Equations (7-12) & (7-13)] are plotted as data points (Figure 7.5) for the individual sand-clay mixture conditions tested in the column (see Table 7.1). Clearly from the plot, sand-clay mixtures with lower volumetric concentrations $Ø < 0.5$ (i.e. runs ERT-EX2, SET-EX1, EX2 and EX8; Figure 7.5) have the largest predicted difference between hindered sand particle settling (i.e. $w_s^{sa}/w_{s,0}^{sa} \approx 0.1 \rightarrow 0.23$) and the upward clay floc motion (i.e. $w_s^{floc}/w_{s,0}^{floc} \approx -3.2 \rightarrow -9.7$). These runs are equally shown in Figures 5.2, 5.3 and 5.5(a) to generate the greatest degree of sand-clay layer segregation (and most well-defined interface) in the resulting bed deposits. In contrast, sand-clay mixtures in the range of $Ø \approx 0.55 \rightarrow 0.75$ (i.e. runs ERT-

EX3 and SET-EX3 to EX7, Figure 7.5) are shown to have lesser predicted differences between hindered sand particle settling (i.e. $w_s^{sa}/w_{s,0}^{sa} \approx 0.005 \rightarrow 0.06$) and upward floc motion (i.e. $w_s^{floc}/w_{s,0}^{floc} \approx -0.2 \rightarrow -1.5$). These predictions, show that the mixtures under consideration here (i.e. SET-EX3 to EX7) correspond to the structural conditions of bed deposits (i.e. in Figure 5.4), under which more transitional sand-clay segregation (i.e. with less well-defined interface between the *sand-rich* and *clay-rich* layers), are seen to occur. Finally, the two sand-clay mixtures with $\emptyset > 0.75$ (i.e. runs ERT-EX4 and SET-EX9, Figure 7.5) have the least difference in predicted settling rates between the clay and sand fractions (i.e. $w_s^{floc}/w_{s,0}^{floc} \approx w_s^{sa}/w_{s,0}^{sa} \rightarrow 0$ as $\emptyset \rightarrow 1$) and correspond to resulting bed deposit conditions where no vertical sand-clay segregation is observed (e.g. Figure 5.3b).

For the current set of settling experiments, a schematic representation (Figure 7.6) of relative sand and clay fraction motion within initial mixture, to develop fully segregated sand-clay bed deposit layers (Figure 7.6a) and transitional segregated sand-clay bed deposit layers (Figure 7.6b), has been drawn. Furthermore, it is informative to estimate the corresponding time scales over which the sand-clay segregation process occurs within the settling column for the majority of sand-clay mixture tested. Firstly, standard expressions by Cheng (1997) and Winterwerp (2002) [Equations (2-8) – (2.10); pg. 22] are used to estimate the settling rates for a single sand particle, d_s^{sa} (= 150 μm), as $w_{s,0}^{sa} \approx 20\ mm\ s^{-1}$ and clay floc, d_{floc} (= 15.6 μm), as $w_{s,0}^{floc} \approx 0.6\ mm\ s^{-1}$, respectively. Secondly, it is assumed that the nominal interface between the sand-dominated base layer and clay-dominated upper layer, forms at elevation z_{int} (Figure 7.6), then, an indicative time scale t_{seg} for the sand-clay segregation process can be estimated either from the hindered sand particle settling time, or clay floc rise time, over $z = 0.5h$ between the "centres of mass*"* of these two identified layers, i.e.:

$$t_{seg} \approx \frac{0.5h}{|w_s^{sa}|} \qquad \text{or} \qquad t_{seg} \approx \frac{0.5h}{|w_s^{floc}|} \tag{7-17}$$

where h is the total height of the settling column. For example, in sand-clay mixtures with highly segregated final bed deposit layers (e.g. SET-EX1 and -EX2, Table 7-2), the interface elevation is shown to form at $z_{int} \approx 0.125$ m = 0.25 h (i.e. Figures. 5.1a, b and 5.2). From Figure 7.5 and the estimated values of settling rates for a single sand particle and clay floc, the corresponding hindered sand particle settling velocity (i.e. $w_s^{sa} \approx 0.1$ x $w_{s,0}^{sa} = 2.0\ mm\ s^{-1}$) and upward floc motion (i.e. and $w_s^{floc} \approx -8.5 \times w_{s,0}^{floc} = -5.1\ mm\ s^{-1}$)

are predicted accordingly. Therefore, from Equation (7-17), the estimated segregation time scales can be calculated respectively as:

$$t_{seg} \approx \frac{0.5h}{|w_s^{sa}|} = 125\ s \quad \text{and} \quad t_{seg} \approx \frac{0.5h}{\left|w_s^{floc}\right|} = 49\ s$$

Interestingly, the $t_{seg} \approx 125\ s$ clearly falls within the time scale observed for the formation of predominantly sand base layer during sedimentation processes of the sand-clay mixtures under consideration here (i.e. t = 120 – 140 *s*; SET-EX1 and -EX2 in Figures 5.1a, b and 5.2). Following similar procedures for sand-clay mixtures that resulted in more transitional segregation within the bed (i.e. SET-EX4 to -EX7; Table 7-1), with the predicted $w_s^{sa} \approx 0.0051$ x $w_{s,0}^{sa} = 0.1\ mm\ s^{-1}$ and $w_s^{floc} \approx -0.204 \times w_{s,0}^{floc} = -0.12\ mm\ s^{-1}$; the estimated segregation time scales can again be calculated respectively as:

$$t_{seg} \approx \frac{0.5h}{|w_s^{sa}|} = 2500\ s\ (42\ mins) \quad \text{and} \quad t_{seg} \approx \frac{0.5h}{\left|w_s^{floc}\right|} = 2080\ s\ (34\ mins)$$

Again, this is shown to be in broad agreement with the observed time scale during actual sedimentation experiments, over which transitional segregational process occurs (i.e. t = 30 – 60 *mins*; SET-EX4 to EX7 in Figures 5.1d-f and 5.4). It should be noted that this initial segregation time scale t_{seg} is considerably shorter than the overall hindered settling time scale [i.e. t = 9000 – 18,000 *s* (150-300 *mins*); Figure 5.7] recorded during the settling experiments, prior to the onset of phase I consolidation in the upper clay-dominated bed layers.

In summary, as it has been demonstrated in the current section, the polydisperse hindered settling approach for sand-clay mixtures, proposed by Cuthbertson *et al*. (2008), provides improved representation of the physical mechanisms and reciprocal interactions between the sand and clay fractions that can lead to layer segregation within the bed deposit. Additionally, it has provided new insight into the parametric influences on these bed segregation patterns (e.g. sharp and transitional sand-clay interfaces) as well as information on the time scales over which this segregation would be expected to occur.

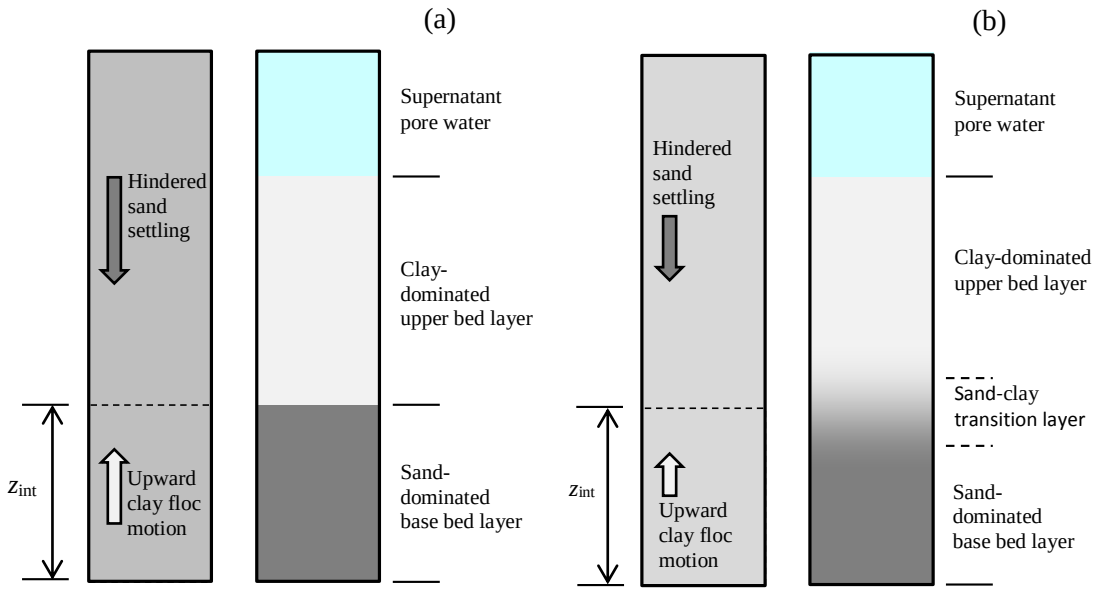

Figure 7.6 Schematic representation of relative sand and clay fraction motion within initial mixture, to develop (a) fully segregated sand-clay bed deposit layers and (b) transitional segregated sand-clay bed deposit layers.

7.7 Effect of Clay on Erosion of Sandy Bed

Occurrence of marine sediment as pure sand, silt or clay is very rare. In most sedimentary environments (e.g. tidal rivers, estuaries and coastal zones; etc.), sediments are usually found as mixtures of sand and mud (Torfs *et al*., 1996). The erosion and deposition processes of these mixed sediments are complex, even, a small quantity of clay particles in sand can significantly alter the fabric and shear strength of the mixed bed (Mehta, 2014). As shown in Figure 7.7, the sediment bed surface shear strength (τ_{so}) and the bed critical (or yield) shear stress (τ_{sc}) increase with increasing clay weight fraction, although the correlation especially for τ_{sc} is non-linear. It is particularly interesting to observe significant influence of low fraction of clay (i.e. from 0.02 to 0.1) on erosion rate of predominantly sandy beds (Figure 7.7). This finding is in good agreement with Lyle and Smerdon (1965), Panagiotopolos *et al* (1997), Torfs (1994) and Whitehouse *et al*. (2000), etc., where addition of clay particles to pure sand was found to initially increase τ_{sc} to a maximum value peaked at a clay weight fraction estimated to be in the order of 0.15 to 0.2. Previous studies (e.g. Smerdon and Beasley, 1959; Torfs. 1995; Raudkivi, 1998; Jacobs *et al*., 2011; Baas *et al*, 2013) suggested that once the cohesive sediment fractional weight within predominantly sandy bed exceeds 5-10% (i.e. critical cohesive fraction value), then the bed stops behaving as a non-cohesive bed and becomes a cohesive bed,

i.e. the bed moves from non-cohesive regime to cohesive regime (van Ledden, 2003; van Ledden, et al, 2004). This trend has been shown in the current study, where run EDT-EX3 [5% clay; Figures 6.8c (pg. 169) and 6.9c (pg. 170)] clearly appears to be a transitional bed between sand dominated and clay dominated behaviours. These measurable effects of small fraction of cohesive sediments on the erosion of predominantly non-cohesive sediments beds, call to question the widely used approach of modelling erosion fluxes of coarse and fine particle fractions as independent processes especially in cohesive regime (e.g. van Ledden, 2002; Sanford, 2008; etc.). For example, Sanford (2008) proposed a comprehensive model, based on two sediment classes, where the sand and mud fractions are eroded separately without the need to make a distinction between cohesive and non-cohesive regimes. The fact that this approach might be expedient and perhaps necessary to avoid some modelling difficulties and challenges, it is clearly not physically realistic and will unavoidably yield sediment transport models for predicting erosion in many sedimentary environments with limited successes.

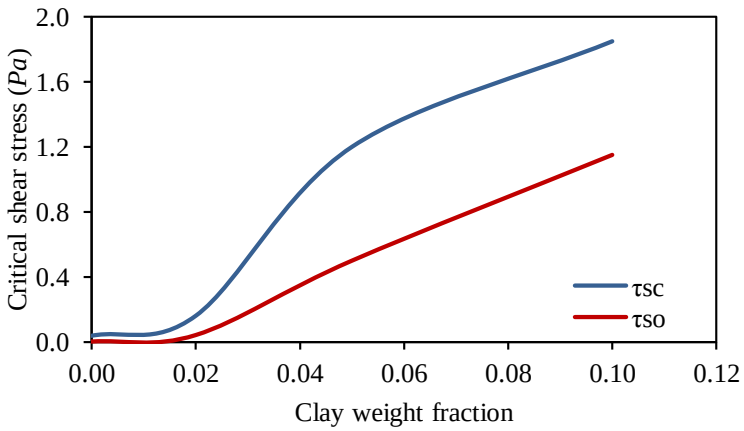

Figure 7.7 Plot showing the variance of critical shear stress with clay weight fraction within sandy-beds

7.8 Semi-Empirical Erosion Rate (E) Equations

For uniform beds, various mathematical expressions have been reported for the rate of erosion of cohesive sediment beds (e.g. Partheniades, 1965; Kandiah and Arulandan, 1975; Raudkivi and Hutchison, 1974; Thorn and Parsons, 1980; Parchure and Mehta, 1985; and Maa and Mehta, 1987; etc.) and mixed sediments beds (i.e. containing cohesive clay and non-cohesive sand) [e.g. van Ledden, 2003; van Ledden *et al*. 2004; Winterwerp and Van Kesteren, 2004; Jacobs *et al*., 2011]. Some of these expressions have been discussed in chapter 2 (see *sections 2.5.4* and *2.5.5*). Common to them, is expressing erosion rate or flux (***E***) as a function of excess shear stress ($\tau_b - \tau_{sc}$), i.e.

$$E = f(\tau_b - \tau_{sc}) \tag{7-18}$$

In general, these authors expressed the relationships between $\boldsymbol{E}$ and $(\tau_b - \tau_{sc})$ mostly as linear, power law or exponential model. The linear model for instance is applicable to initiation of motion at low shear stresses, while exponential model describes the erosion flux over a wider range of applied shear stresses and rates of erosion. These relationships were checked with the erosion results obtained from the tests considered to be in cohesive regime in the current study (i.e. runs EDT-EX3 to EX6). The results (i.e. Figure 7.8) reveal that quadratic (Figure 7.8b) and exponential (Figure 7.8c) models appear to give the best representation of the relationships between $\boldsymbol{E}$ and $(\tau_b - \tau_{sc})$, with power law being the least (Figure 7.8d). This is quite interesting as there has not been such quadratic relationship between $\boldsymbol{E}$ and $(\tau_b - \tau_{sc})$ recorded in the literature (to the best of the current author's knowledge). Therefore, in addition to existing empirical erosion formulae or models, the following quadratic erosion model [Equation (7-19)] has been proposed to estimate erosion processes of sand-clay mixture in cohesive regime (i.e. cohesive sediment fractional weight ≥ 5%), which obviously require further experimental validation.

$$E = M_1(\tau_b - \tau_{sc})^2 + M_2(\tau_b - \tau_{sc}) + M_3 \qquad for\ \tau_b > \tau_{sc} \tag{7-19}$$

M_1, M_2 and M_3 are erosion rate parameters which are believed to be strongly dependent on sediment composition or bed material characteristics. Although, exponential model (Figure 7.8c) appears to give the best representation (R^2 = 0.769); however, the physical basis of Equation (7-19) with R^2 = 0.765 is that, it may serve as a complementary model to the existing erosion empirical models.

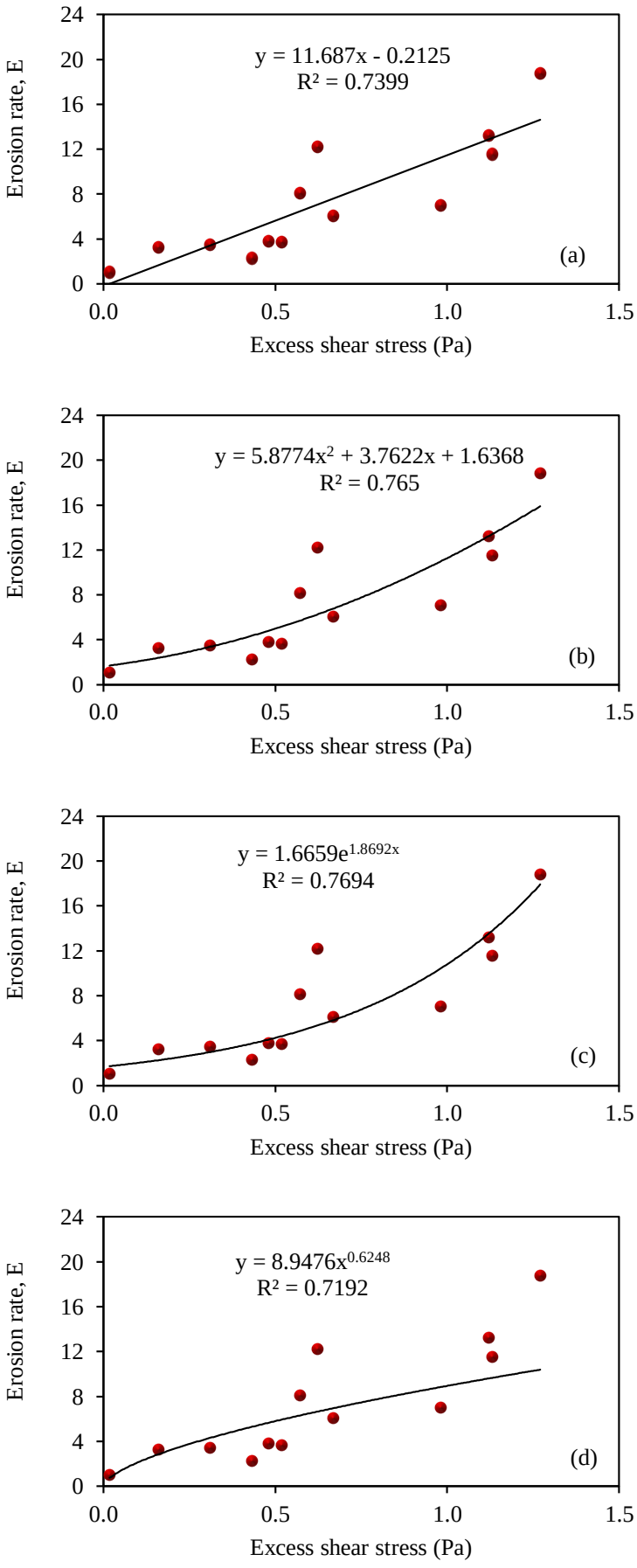

Figure 7.8 Semi-empirical expressions (or models) for the relationships between E and (τ_b-τ_c): (a) linear, (b) quadratic, (c) exponential, and (d) power relationships.

7.9 Critical Reflection

The previous chapters and sections have presented results, analyses and discussions of the experimental procedures designed to achieve the main aims and objectives of the current study (see *section* 7.1). Clearly, the findings reported here, are broadly in good agreement with related studies reported in the literature, especially in terms of parametric influence of ambient salinity, fractional sediment composition (i.e. relative sand and clay concentration) and initial sediment mass concentration on mixed sediment transport dynamics.

In general, parametric dependence of hindered settling, bed structural formation and onset of phase I consolidation, on sediment mixture fractional compositions, ambient fluid salinity and initial mixture concentration; for mixed sediments containing cohesive clay and non-cohesive sand, is shown to follow the generally accepted theories (e.g. Kynch, 1952; Imai, 1981; Bürger and Wendland, 2001; Grasso *et al*., 2014;2015; etc.). Furthermore, it has been shown that the resultant effects of the tested parametric conditions on these mixed sediment physical processes are significant. For instance, the settling characteristics of mixed sediment particles have been shown to be more complex and dynamic, especially at sufficiently large ambient salinity (> 15-ppt) and $C_s^{cl} \geq 100$ $kg\ m^{-3}$. As expected, the observed parametric influence of ambient salinity during the hindered settling stage, was absent during phase I consolidation stage. The material functions (e.g. K_k and n_f) or the so-called constitutive relationship parameters, governing the physical processes at this phase I consolidation stage (Winterwerp and van Kesteren, 2004), were found to largely depend on initial fractional composition of clay (C_s^{cl}) and, less on the initial mixed sediment mass concentration (C_s).

Furthermore, from the experimental results of the current study, more insight into the appropriate criteria describing the parametric conditions under which well mixed or segregated bed deposits are likely to be formed had been provided. The segregation mechanisms observed, clearly showed that, formation of segregated (sand-clay) bed layers within bed deposits is largely controlled by the initial fractional composition (i.e. fractional ratio of sand to clay). The results specifically indicate that segregated bed deposits are generally obtained for the range of sand-clay mixtures tested, with a sand-dominated layer deposited at the column base and subsequently overlain by a clay-dominated layer. The degree of segregation within these deposits is well described by the nature of the interface forming between these two layers, with a sharp, well-defined

interface obtained for mixtures with lower volumetric clay concentrations ($\emptyset_s^{cl} \leq 0.05$) or high sand ratio. This is thought to be primarily due to the weak network structure form by the cohesive clay particles in the settling phase, which cannot adequately support majority of the sand particles in its matrix. On the other hand, the mixtures with high volumetric clay fractions (i.e. $0.054 < \emptyset_s^{cl} < 0.076$), apparently result in the initial mixture concentration that has the potential of being above the structural density (i.e. the concentration at which a space-filling network occurs where particles within the mixture support each other at their loosest packing). Therefore, a network structure of predominantly cohesive flocs is formed, which significantly hindered the settling rate of sand particles within the mixture. Hence, generally results in transitional interfacial region developing for these mixtures. This appears to explain the co-existence of sand and mud in suspended sediment transport (e.g. Spearman *et al*., 2011) from weakly segregated bed deposits especially within high energy environments. Finally, for some mixtures with sufficiently high volumetric clay concentrations ($\emptyset_s^{cl} > 0.095$), no sand-clay layer segregation is shown to develop in the resulting bed deposits, irrespective of the corresponding sand concentration $\emptyset_s^{sa}$. In addition, the time evolution of the upper clay-water interface (i.e. via time-lapsed images) also provided information on the transition from hindered settling and phase I consolidation within the upper clay-dominant bed layer (see Figure 5.9), with the latter process shown to be well-represented by an existing consolidation model of Merckelbach (2000) [Figure 7.3].

An existing polydisperse hindered settling model of Cuthbertson *et al*. (2008), was used for further investigation into the main physical mechanisms underpinning the occurrence (or non-occurrence) of segregation (or degree of segregation) within the resulting bed deposits from the differential settling of sand-clay particles. This model was employed to predict the relative motion of sand particles and clay flocs during the sedimentation process and how these vary for the different mixture compositions under consideration. The model, specifically, predicted that hindered settling characteristics (i.e. $0 \leq w_s^{sa}/w_{s,0}^{sa} < 1$) will occur for the sand particles, while the clay flocs will be subjected to upward motion (i.e. $w_s^{floc}/w_{s,0}^{floc} \leq 0$) due to return flow effects from the settling sand fraction (Figure 7.5). Interestingly, the magnitude of the difference between these downward (sand) and upward (clay) motions was found to correlate qualitatively with the degree of sand-clay segregation observed within the resulting bed deposit for the actual experimental runs. Specifically, for mixtures with high sand $\emptyset_s^{sa}$ and low clay contents $\emptyset_s^{cl}$ (e.g. SET-EX1, -EX2, -EX8 and ERT-EX2), a well-defined segregation is observed,

between the sand and clay bed layers, where the difference in predicted fractional motions is maximal (see Figure 7.5). However, a contrasting trend is observed for mixtures with higher clay contents $\emptyset_s^{cl}$ (e.g. SET-EX4, to -EX7 and ERT-EX3); within their bed deposits, a more transitional sand-clay layer segregation is seen to occur, where this difference in fractional motion is equally observed to be relatively reduced. Lastly, in the remaining set of mixtures with $\emptyset_s^{cl} > 0.095$ (i.e. SET-EX9 and ERT-EX4), as mentioned above, no sand-clay layer segregation is observed, as the overall mixture concentration Ø is tending to unity ($Ø \rightarrow 1$; i.e. at the so-called gelling concentration, Winterwerp and van Kesteren, 2004). Furthermore, the prediction of relative sand-clay motions from the model, was used to estimate time scales, associated with these well-defined or transitional segregation processes. Interestingly, the results obtained are shown to agree quantitatively with experimental observations of layer development in the resulting bed deposits of the mixtures under consideration (see *section* 7.6).

Therefore, from combination of the experimental measurements and polydisperse model predictions from Cuthbertson *et al*. (2008), the physical processes under which sand-clay segregation occurs (as shown schematically in Figure 7.6), can be described qualitatively as follows:

- for sand-clay mixtures with lower clay concentrations (i.e. $\emptyset_s^{cl} \leq 0.05$): prior to the clay fraction in the mixture reaching gelling conditions, the sand fraction within the mixture, settles rapidly unhindered (and causing strong upward displacement of mud flocs)—the resulting deposit is separated by well-defined interface to form distinct sand and clay layers (Figure 7.6a);
- for mixtures with higher clay concentrations ($0.054 < \emptyset_s^{cl} < 0.076$): the increasingly hindered (i.e. reduced) sand settling rates (and reduced upward displacement of clay flocs) allow a greater proportion of clay to remain trapped in the developing sand-dominated base layer; while above this layer, the clay fraction reaches gelling point before the sand fraction is completely deposited—the resulting deposit forms a transitional segregation region (Figure 7.6b) where sand particles are trapped in patches within the clay dominated matrix (see Figure 5.4); and
- for mixtures with very high clay concentrations ($\emptyset_s^{cl} \geq 0.095$): very little or no motion is predicted for either fractions suggesting that the mixture is close to or at the gelling point under initial conditions (i.e. prior to sedimentation)—the

resulting deposit therefore shows no layer segregation (see Figure 5.5b), with the sand fraction trapped almost immediately within the developing clay matrix.

It should be noted here that the predictions obtained from the polydisperse model are based solely on the initial sand-clay mixture conditions and thus do not take account of temporal changes in sand or clay concentrations within the column during the sedimentation process itself. However, the correlation between the predicted hindered sand settling and/or upward clay motion and the time scales over which well-defined or transitional layer segregation occurs within the bed deposit layers appears to provide validation of the polydisperse model predictions for the first time.

As described in chapter 2, there are so many marine environments where mud and sand are found to co-exist in different fractions under different tidal and/or wave actions, resulting in either mixed or segregated bed layers. If the former occurs, it creates the potential for both the mud and sand fractions to be re-entrained into suspension especially in dynamic environment (i.e. where sediment is regularly re-suspended), and consequently combine within a flocculation matrix (Manning *et al*., 2007). Thus, the physical effect of having cohesive mud and non-cohesive sand co-existing as a mixture in the marine environments has been reported (e.g. Mitchener *et al*., 1996) to result in bed deposits of increased strength or stability, which has the potential of forming predominantly mixed sediment flocs whenever the bed deposit is re-entrained (Panagiotopoulus *et al*., 1997; Mitchener *et al*., 1996; Torfs 1994; Williamson and Ockenden 1993; etc.). On the other hand, if the latter occurs especially in the case of strongly segregated bed deposits, it would be expected that the textural and structural characteristics of the upper layer of the bed deposits will be dominated by clay-water matrix, which as a consequence, has the potential of forming predominantly mono sediment flocs whenever the bed deposit is re-entrained.

The general implications of the two scenarios described above (i.e. where mud and sand co-exist as either mixed or segregated bed layers) in sedimentary environments are (i) sediment transport from non-segregated bed deposits will result in mud and sand particles interacting to form sand-mud flocs (e.g. Manning *et al*., 2010, 2011; Cuthbertson *et al*., 2010), which will apparently exhibit characteristics such as sizes, settling velocity and structural density distinctly different from their compositional base; and (ii) sediment transport from fairly or well segregated bed deposits will result in mud and sand particles

within the suspended sediment acting independent of each other. This is largely because, for example, entrainment of natural sediment is dependent on the physical structure and particularly interactions of its subcomponents (Grabowski *et al*., 2011). Furthermore, segregation has been shown to clearly suggest minimal interaction between sand and mud fractions during settling and deposition processes (e.g. Torfs, 1994; Torfs *et al.,* 1996; Amy *et al.,* 2006; Manning *et al*., 2010). Therefore, in this context, Manning *et al*. (2013) suggested that, prediction of suspended sediment transport in mixed sediment estuarine environments is best based on sedimentary regimes determined by observational measurements rather than a priori determination. This of course is another source of complexity to numerical modelling of suspended sediment transport in such environments.

On the erosion of mixed (sand-clay) beds, in broad agreement with previous studies (e.g. Smerdon and Beasley, 1959; Torfs. 1995; Raudkivi, 1998; Jacobs *et al*., 2011; Baas *et al*, 2013), ~5% clay fractional concentration within sand-clay sediment bed, was identified as the critical cohesive fraction value that delineates the non-cohesive and cohesive bed erosion regimes (van Ledden, 2003; van Ledden *et al*, 2004). This implies that, below this critical clay fraction, the mixture behaves like pure sand, whereas above this critical value, the resistance to erosion increases with the clay fraction. Furthermore, it is a very common practice to use erosion rate (E), bed surface shear strength (τ_{so}) and bed characteristic shear strength (τ_{sc}) as measures of bed erosion or to quantify erosion resistance of sediment bed. However, it has been shown in the current work, especially at cohesive erosion regime, that the use of these parameters should be with care, as they are largely affected by properties and compositions of bed materials and specifically the history and mode of the bed formation (e.g. Lau and Droppo, 2000; Grabowski *et al*., 2011; etc.). For instance, results from runs EDT-EX4 to EX6, (Figure 6.5), show that, the τ_{sc} values of EDT-EX4 and EDT-EX6 are within a close range of 1.40-1.45 *Pa*, but the difference in their corresponding average erosion rates beyond τ_{sc} (i.e. 5 and 10 $g\ m^{-2}\ mins^{-1}$ respectively) is significant. This may be of significant implication on numerical models, which require these experimentally derived parameters as inputs for predictions of the transport and fate of sediments in rivers, lakes and estuaries. This suggests that modelling efforts which do not, in particular, take into account the history and mode of the bed formation, may give misleading information or results in underestimation of the bed erosion strength and as such, can result in erroneous predictions of sediment transport and fate, in agreement with Pattiaratchi and Collins (1984) and Lau and Droppo (2000).

CHAPTER EIGHT

Conclusions and Recommendations

"The only reason for time is so that everything does not happen at once"
— Albert Einstein

8.1 Summary of Main Experimental Findings

Knowledge of the dynamic sedimentation behaviour of sand-mud mixtures is crucial to the physical understanding and prediction of the time-dependent structure (i.e. mixed or segregated), composition and erodibility of sediment bed deposits developing within sedimentary environments such as estuaries and tidal inlets, etc. However, the co-existence of cohesive (i.e. mud: clay and silt, $D < 65\mu m$) and non-cohesive (i.e. sand, $D > 65\mu m$) sediments in different fractions, makes accurate prediction of sediment transport, fate and morphological changes in these sedimentary environments very challenging, not least as both types of sediments (i.e. cohesive and non-cohesive) can be mobilised easily under tidal and/or wave actions. These temporal and spatial changes and differences in sediment fractions distribution within sediment beds have consequences (e.g. economic, social, etc.) and to a large extent visible in changes in nearshore coastal zones morphology, siltation and erosion of navigation channels, dredging impact, etc. On this basis and in view of achieving the highlighted aims and objectives of the current study (see *section* 1.5), a series of settling column and erosion/deposition tests have been conducted to further investigate the complex underlying mechanisms of mixed-sediment sedimentation and erosion processes. The main findings from these series of experiments are thus re-iterated under the following sub-sections:

8.1.1 ES-1: Electrical resistivity measurement technique (ERMT)

Under this experimental programme, a new, non-invasive electrical resistivity measurement technique (ERMT) was developed and used to capture both temporal and spatial changes in density, porosity and composition of the evolving sand-clay bed deposits, resulting from the differential settling and erosion and deposition processes of

cohesive clay and non-cohesive sand mixtures. The main conclusions from ES-1 are summarised below:

- The main technical issues that must be given consideration when using ERMT are: (i) *electrode polarization* (ii) *temperature effects* (iii) *electrode configuration* and (iv) *CEC of clay* (or *surface conduction*). Nevertheless, provided a suitable calibration is carried out, it has been shown that ERMT can be deployed on variety of samples both at laboratory and field scales.
- Spatial resolution of the ERMT is shown to be significantly affected by electrode configuration (both vertical and horizontal) and geometry. When used to capture spatial changes within segregated bed deposits, the best spatial resolution was recorded with pin-electrodes array (i.e. 6 *mm* horizontal & 5 *mm* vertical spacing), whereas, plate electrodes spatial resolution was the least.
- Based on the findings of the current work, empirical relationships [i.e. Equations (4-4) and (4-5) respectively] are proposed between the normalized bulk density (γ_{bulk}/γ_p) and the porosity (φ) of the sediment bed deposit, as well as between the corresponding formation factor F and φ. These expressions require the following condition to be satisfied: γ_{bulk}/γ_p and $\varphi \rightarrow 1$ as $F \rightarrow 1$.

$$\frac{\gamma_{bulk}}{\gamma_p} = a.F^b \quad ; \quad \varphi = \hat{a}e^{-\hat{b}F}$$

The coefficients (a, b, $\hat{a}$ and $\hat{b}$) in these expressions are experimentally-derived.

8.1.2 ES-2: Mixed-sediment settling experiment

A series of settling column tests were conducted here to investigate the hindered settling and initial bed consolidation phases of a range of sand-clay mixtures to determine parametric conditions under which bed segregation occurs. The new, non-intrusive ERMT was used as described above, complimented by time-lapsed photographic and video images of the sedimentation process within the column. The main findings of this experimental series (ES-2) are summarised below:

- Pore fluid is seen being expelled upwardly through the near-vertical drainage paths (i.e. *dewatering* channels), formed within the predominantly clay suspensions just after the initiation of hindered settling phase. Also, sand grains are also observed to settle through these channels, an observation also recorded

by Merckelbach (2000). After the onset of primary consolidation phase, the *dewatering* channels later became smaller or even disappeared completely.

- Evidence of segregation immediately after the initiation of the tests in mixtures with lower initial clay fraction (i.e. $C_s^{cl} \leq 140\ kg\ m^{-3}$) was apparent between elapsed time $t = 10 \rightarrow 60$ s; while it became noticeable after $t = 300\ s$ in mixtures with $C_s^{cl} = 196\ kg\ m^{-3}$. Therefore, while it is observed during the sedimentation processes that some degree of bed deposit segregation occurred in majority of the sand-mud mixtures tested, the results clearly indicate that, the most highly segregated bed conditions tend to occur for sand-mud mixtures with higher $Ø_s^{sa}$ and lower $Ø_s^{cl}$ values, respectively. In general, the degree of segregation within the bed deposits is shown to become more transitional with a less well defined interface with increasing initial clay concentration.
- The two mixtures for which no segregation was observed in the deposit had the highest volumetric concentrations of clay [i.e. $Ø_s^{cl} = 0.095$ (ERT-EX4) and $Ø_s^{cl} = 0.110$ (SET-EX9), Table 5.1], irrespective of the corresponding volumetric sand content [i.e. $Ø_s^{sa} = 0.0314$ (ERT-EX4) and $Ø_s^{sa} = 0.20$ (SET-EX9), Table 5.1]. Clearly, a critical value of $Ø_s^{cl}$ exists where sand particles in the mixture are trapped within the overlying clay-dominated matrix and consequently prevented from settling and forming a segregated bottom layer within the settling column, analogous to a gelling concentration (i.e. Winterwerp and van Kesteren 2004).
- The transition region between the hindered settling stage and the onset of phase I consolidation (e.g. Imai, 1981) is thought to be largely initiated when the gelling point (e.g. Danker, 2006; te Slaa *et al*., 2013) or structural density (e.g. Sills, 1998; Been and Sills, 1981) of the upper clay-rich sediment is reached.
- During the hindered settling regime, the rate of downward interfacial displacement decreases steadily and occurs over a longer period of time for sand-clay mixtures with relatively high volumetric clay concentrations $Ø_s^{cl}$ and/or pore water salinity concentration. These results also indicate that, higher clay concentrations ($Ø_s^{cl}$) within the initial sand-clay suspension inhibit both the initial settling phase (in particular, hindered settling regime) and subsequent formation of the mixed bed deposit.
- Investigation into the parametric influence of salinity on sedimentation rates for identical sand-clay mixtures (e.g. SET-EX4 to –EX7; $C_{o,s}^{cl} = 196\ kg.m^{-3}$; See Table 5.1) clearly shows a negative correlation between pore water salinity and temporal displacement of the upper interfaces of these sand-clay mixtures.

Higher initial settling rates are distinctly shown for sand-clay mixtures with lower ambient pore water salinities; and earlier peak settling rates occur for sand-clay mixtures with reduced pore water salinities. Generally, in the context of the current study, these results specifically reveal that, if the salinity concentration of sand-clay mixture is sufficiently large (e.g. > 15-ppt), and in addition, the ratio of clay particles in the initial mixture is relatively high (e.g. ≥ 15%), the settling/consolidation rate will be significantly inhibited. It is apparent that, there is more significant hindrance to the particles settling rates due to combined effects of high clay content and salinity concentration.

- Higher clay mass concentrations C_s^{cl}, has been found to play a more significant role in defining particles settling rates in sand-mud mixtures. However, comparison between SET-EX6 (segregated bed; 65s:35c; C_s^{cl} = 196 $kg\ m^{-3}$; salinity = 30 *ppt*) and SET-EX9 (non-segregated bed; 65s:35c; C_s^{cl} = 285 $kg\ m^{-3}$; salinity = 30 *ppt*) revealed an opposite trend, with distinct differences in the transition behaviour of the two mixtures. It can therefore be hypothesised, whether or not the initial settling regime exists for non-segregating sand-clay mixtures, as the fact that the sand fraction has not segregated clearly suggests that the clay fraction has already reached the gelling concentration.
- The formation factor (F) colour maps, contour plots of γ_{bulk}/γ_p and lastly γ_{bulk}/γ_p profiles obtained from ERMT, clearly show the initial stages of the bed layer development for different sand-clay mixture compositions and indicate quantitatively how the individual deposit layer forms over time, as well as providing an indication of their composition and structure (i.e. through corresponding γ_{bulk}/γ_p and porosity ϕ values in the different bed regions).

In summary, the study has successfully employed new non-invasive electrical resistivity measurements technique (ERMT) and time-lapsed image techniques to investigate sedimentation and bed formation processes for mixed (sand-clay) suspensions. This study has highlighted the parametric conditions under which sand-clay segregation can occur in the resulting bed deposits, as well as providing a physical explanation for both the nature and time scale of this segregation.

8.1.3 ES-3: Mixed sediment bed erosion experiment

The erosion and deposition experiments on prescribed mixed sediment beds have been carried out with a testing facility (i.e. a 2 *m* diameter benthic annular flume, Voyager II)

and utilised in an idealised laboratory setting. The main aim was to investigate the effect flow-induced shear stresses, on the size-selective erosion and deposition of these mixed sediment beds, such as those conditions typically encountered in periodically-reversing (tidally-driven) estuaries or tidal inlets. The main findings of the experimental series are summarised below:

- After the initiation of erosion, quasi-linear relationship was found to exist between suspended sediment concentration (SSC) and applied bed shear stress (τ_b). Also, over the range of sediment proportions considered, a quasi-linear relationship was also found to exist between erosion rate (*E*) and applied bed shear stress (τ_b), once the erosion threshold is exceeded.
- The limitations highlighted in the current study notwithstanding, the erosion thresholds values are shown to vary from 0.08 to 1.45 Pa, which are in good agreement with reported data for low-cohesive sediment samples (e.g. Winterwerp and van Kesteren, 2004; Le Hir *et al*., 2008; Jacobs *et al*., 2011).
- A strong positive correlation between mixed sediment bed resistance to erosion and the proportion of cohesive fraction in the bed was further established. Specifically, the bed surface shear strength (τ_{so}) of the bed with 5% clay content is 1 and 2 order of magnitude more than that of the beds with 2% clay and 0% clay content respectively. Whereas, the spatial extent (i.e. height and width) of the sand deposits from all the experimental runs, is shown to reduce with increasing cohesive clay fraction within the bed.
- The results reveal that mixed sediment bed's initial resistance to erosion may be significantly reduced with further exposure to subsequent erosion cycles. This is established by significant reduction in both τ_{so} and τ_{sc} values when the resulting bed from erosion test of EDT-EX4 (i.e. erosion cycle-1) was further subjected to two sequential erosion cycles (i.e. cycle-2 and-3).
- The use of erosion rate (*E*), bed surface shear strength (τ_{so}) and bed characteristic shear strength (τ_{sc}) as measures of bed erosion in isolation may give misleading information as they are all largely affected specifically by bed materials' properties and compositions, and also significantly by antecedent conditions of the sediment beds. Therefore, in this context, prediction of sediment beds erosion characteristics in marine environments is best supported by adequate understanding of the sedimentary regimes, probably gained by observational measurements rather than a priori determination.

- Similar to the finding of Baas *et al*. (2013), clay dry weight fraction of ≥ 5.0 % within mixed (sand-clay) beds, will result in cohesive bed forces having more significant influence on bedform development and morphology. In general, a 5% clay fractional content within sand-clay sediment bed is observed in the current study, to be the critical cohesive fractional content that delineates the non-cohesive and cohesive bed erosion regimes (e.g. van Ledden, 2003; van Ledden, *et al*, 2004). This implies that, below this critical clay fraction, the mixture behaves like pure sand, whereas above this critical value, the resistance to erosion increases with the clay fraction.
- *Winnowing* of fine sediments from their compositional base, appears to be an important sediment transport process in the development of bedforms and also, in erosion and deposition processes of mixed (sand-mud) beds. Similar to findings of Baas *et al*. (2013).
- The results from the resistivity profiles, appear to support the adoption of *simultaneous bed exchange* model (e.g. Krone 1963; Mehta, 2014; etc.).

8.1.4 Analysis and discussion

Discussion, analysis and critical reflection on the current experimental results and findings have raised a number of observation and critical issues which are thought to have a wider implication on the existing knowledge of the physical processes controlling the dynamic behaviour of mixed (sand-clay) sediments within estuarine and coastal systems. Again, summary of some of these observations and findings are given below:

- From the analysis of the parametric influence of salinity on sedimentation processes, which appears to suggest that, higher salinities above ~15 *ppt* do not increasingly promote sedimentation. Therefore, on this premise, the following hypothesis is made: 'sediment distribution patterns (in terms of bed composition and structure) in marine environment with higher salinity (e.g. higher salinity basins) will be similar in certain degrees to those observed in marine environments with lower salinity (e.g. estuaries)'.
- A negative correlation is shown between w_{s-mean} and $\emptyset_s^{cl}$ according to a power law, hence, the following relationship has been proposed as an empirical measurement of the w_{s-mean} for the range of sediment mixtures tested:

$$w_{s-mean} = w_{s,0-mean}\left(\emptyset_s^{cl} \Big/ \emptyset_{s,0}^{cl}\right)^{-0.725}$$

The coefficients $\emptyset_{s,0}^{cl}$ and $w_{s,0-mean}$ are found to be 0.1274 and 0.0036 mms^{-1} respectively.

- The material functions (e.g. K_k and n_f) or the so-called constitutive relationship parameters in permeability regime (i.e. phase I consolidation regime), are specifically shown to largely depend on initial fractional composition of clay and less on the initial mixed sediment mass concentration. This is in good agreement with the findings of Grasso *et al*. (2015).
- From the polydisperse hindered settling approach for sand-clay mixtures, proposed by Cuthbertson *et al*. (2008); it is proposed that, the generation of clearly segregated sand- and clay-dominated deposit layers in the column from initially well-mixed sand-clay suspensions requires the clay fraction (i.e. flocs) to be displaced upwards within the column while the sand fraction (i.e. particles) settles to the base of the column. This analytical model has been demonstrated to be capable of providing (i) an improved representation of the physical mechanisms and reciprocal interactions between the sand and clay fractions that can lead to layer segregation within the bed deposit, (ii) insight into the parametric influences on these bed segregation patterns (e.g. sharp and transitional sand-clay interfaces), and as well as (iii) information on the time scales over which this segregation would be expected to occur.
- The Cuthbertson *et al*. (2008) model, specifically, predicted that hindered settling characteristics (i.e. $0 \leq w_s^{sa}/w_{s,0}^{sa} < 1$) will occur for the sand particles, while the clay flocs will be subjected to upward motion (i.e. $w_s^{floc}/w_{s,0}^{floc} \leq 0$) due to return flow effects from the settling sand fraction. Interestingly, the magnitude of the difference between these downward (sand) and upward (clay) motions was found to correlate qualitatively with the degree of sand-clay segregation observed within the resulting bed deposits for the actual experimental runs.
- In addition to existing empirical erosion formulae or models, a new quadratic erosion empirical model has been proposed, for estimation of erosion processes of sand-clay mixture in cohesive regime (i.e. cohesive sediment fractional weight $\geq 5\%$):

$$E = M_1(\tau_b - \tau_{sc})^2 + M_2(\tau_b - \tau_{sc}) + M_3 \qquad for\ \tau_b > \tau_{sc}$$

8.2 Potential Areas of Future Study

The experimental programmes designed to achieve the aims and objectives of the current study and their corresponding findings, have provided a premise on which further extensive experimental and analytical studies on influence of the fractional composition (i.e. relative sand and clay concentration) on mixed sediment dynamics can be conducted. In the course of the study, the following potential areas of further study have been identified:

- Comparison of runs SET-EX6 and EX9 in Figure 5.10 shows the parametric influence of initial mixture concentration (561 and 813 $kg\ m^{-3}$, respectively) for the same sand-clay mixture proportion (i.e. 65s:35c) and pore fluid salinity (i.e. 30 *ppt*). No sand-clay segregation occurs within the developing bed conditions for SET-EX9 while for SET-EX6, segregation does occur. As shown, for sand-clay mixtures demonstrating bed segregation (i.e. through sand deposition to the base of the column), the subsequent hindered settling characteristics and transition to phase 1 consolidation is expected to behave similar to a clay only suspension in the absence of sand after this initial segregation (e.g. Figures 5.1-5.3). However, it is unclear what influence the trapped sand fraction has on the sedimentation rate of sand-clay mixtures, in which segregation is inhibited (e.g. Figure 5.4b) or how it affects the transition between the settling regime and the onset of phase 1 consolidation. Therefore, it was hypothesised in chapter 5 that, the initial settling regime may not exist or at least be of a sufficiently short duration within non-segregating sand-clay mixtures, as the fact that the sand fraction does not segregate suggests that the clay fraction has reached the gelling concentration rapidly before segregation can occur. As such, it may be desirable to conduct further experiments to test this hypothesis.
- The results here, have demonstrated that, there appears to be a systematic dependency of the initial settling rates of sedimentation processes, on the pore water salinity; specifically, higher initial settling rates were recorded for sand-mud mixtures with lower pore water salinities. However, the electrical resistivity measurements, reveal that the key bed layer development characteristics and the corresponding physical properties (e.g. bulk density and porosity) for these mixtures are very similar, despite variations in their ambient pore fluid salinity. The formation of a sand-mud bed deposit clearly begins with the fractional settling of the sediments from the suspension (Cheng, 1997; Grasso *et al*., 2014; etc.), as such, any modification to the settling characteristics within the sand-mud

suspensions would be expected to correspondingly influence the physical properties and/or composition of the resulting bed deposit. Therefore, this lack of clearer parametric influence of salinity on the physical properties of the resulting bed deposits, may have partly been due to the EMRT yielding bulk values (e.g. bulk density). Therefore, a further systematic investigation into this issue is recommended. For example, the need to complement the characterisation technique with other *sediment sampling methodologies* for particle size distribution (PSD) analysis may be necessary.

- Finally, it is worth noting that the current study is clearly idealised both in terms of the cohesive and non-cohesive sediments used (i.e. 100 % kaolinite and superfine, high silica sand) and the environmental conditions under which the mixed sedimentation processes are studied. Further studies are therefore needed to validate the findings of this study for natural estuarine or coastal sediment deposits, which are characterised by larger ranges of particle sizes, mineralogical compositions (e.g. mud types), organic fractions and water chemistry. It is likely however, that the same sedimentation characteristics may be found in mixed sediment suspensions with different compositions from the ones already tested here. Albeit, the settling regimes boundaries or transition from settling regimes to phase I consolidation regimes, may not occur at the same volumetric or particle concentration values.

Appendices

Chapter Three

Appendix 3-1 The values of '$2\pi r$' for resistivity electrodes in ES-1 and ES-4

ES-1 (Figure 3-3b Column)			ES-4 (Resistivity box)	
Probe number from the base	2πr values (m)			
	6 mm spacing array	20mm spacing array	Probe number from the base	2πr values (m)
1	0.2648	0.6693	1	0.2209
2	0.3374	0.8618	2	0.3092
3	0.3458	0.9259	3	0.2909
4	0.3356	0.9724	4	0.3124
5	0.3548	0.9968	5	0.2956
6	0.3296	0.9932	6	0.2758
7	0.3431	1.0077	7	0.2646
8	0.3764	0.9932	8	0.3409
9	0.3623	0.9342	9	0.2246
10	0.3552	0.9968	10	0.2549
11	0.3431	1.0250	11	0.2240
12	0.3617	1.0126	12	0.2778
13	0.3450	0.9932	13	0.2571
14	0.3623	0.9667	14	0.2657
15	0.3510	0.9747	15	0.2917
16	0.3525	0.9921	16	0.2877
17	0.3311	1.0163	17	0.2947
18	0.3521	0.9932	18	0.2627
19	0.3364	0.9735	19	0.2928
20	0.3580	1.0163	20	0.1998
21	0.3451	0.9956	21	0.3009
22	0.3612	0.9311	22	0.2271
23	0.3487	0.9701	23	0.2557
24	0.3493	0.9815	24	0.2674
25	0.3469	0.9634	25	0.2882
26	0.3415	0.9491	26	0.2787
27	0.3374	1.0212	27	0.2428
28	0.3607	0.9168	28	0.2938
29	0.3573	1.0113	29	0.2441
30	0.3537	1.0430	30	0.2440
31	0.3320	0.9992		
32	0.3394	1.0101		
33	0.3393	0.9188		
34	0.3584	0.9535		
35	0.3367	0.9612		

Appendix 3-2(a) Standard geo-mechanical equations used for the calibration of ERMT

The following are the standard geo-mechanical equations employed for the ER calibration (Adapter from Craig, 1992):

- The *bulk density* (γ_{bulk}) of a soil sample is the ratio of the total mass (M) to the total volume (V), i.e.

$$\gamma_{bulk} = \frac{M}{V} \quad (kg\ m^{-3}\ or\ g\ cm^{-3})$$

- The *void ratio* (e) is the ratio of the volume of voids (V_v) to the volume of solids (V_s), i.e.

$$e = \frac{V_v}{V_s}$$

- Void ratio (e) can be expressed in terms of bulk density (γ_{bulk}), water content (w_c) and specific gravity (G_s) as:

$$e = G_s\ (1 + w_c)\frac{\gamma_{bulk}}{\gamma_{water}} - 1$$

- The *porosity* (φ) is the ratio of the volume of voids (V_v) to the total volume of the soil (V), i.e.

$$\varphi = \frac{V_v}{V}$$

- The void ratio (e) and porosity (φ) are inter-related as follows:

$$e = \frac{\varphi}{1-\varphi} \quad ; \quad \varphi = \frac{e}{1+e}$$

Appendix 3-2(b) Some important results obtained from the ERMT calibration processes

Sample (%) C-clay; S-sand	**Number of Trial**	**Specific Gravity (G_s)**	**Water Content (W_c)** *(%)*	**Bulk Density (γ_{bulk})** ($g\ cm^{-3}$)	**Void Ratio (*e*)**	**Porosity (φ)** *(%)*	**Average Formation Factor (*F*)**
100C:0S	1st	2.579	78.2	1.51	2.03	67.1	2.28
	2nd	2.587	88.0	1.49	2.25	67.2	
	3rd	2.592	89.9	1.49	2.29	67.5	
90C:10S	1st	2.590	83.0	1.53	2.09	66.4	2.40
	2nd	2.591	79.2	1.51	2.07	65.8	
	3rd	2.609	80.4	1.53	2.05	66.0	
60C:40S	1st	2.619	54.0	1.67	1.40	58.2	2.88
	2nd	2.612	52.0	1.67	1.37	57.8	
	3rd	2.613	54.1	1.69	1.37	57.8	
50C:50S	1st	2.617	45.2	1.75	1.14	53.8	3.18
	2nd	2.619	51.3	1.72	1.29	55.0	
	3rd	2.604	48.0	1.73	1.24	54.3	
40C:60S	1st	2.621	42.0	1.80	1.07	51.7	3.36
	2nd	2.626	36.3	1.82	0.96	52.0	
	3rd	2.615	38.0	1.82	0.99	51.4	
0C:100S	1st	2.632	21.0	1.97	0.67	40.0	4.45
	2nd	2.636	22.2	2.00	0.59	38.9	
	3rd	2.645	21.2	2.00	0.58	39.6	

Appendix 3-3 Custom-built tank to house the benthic flume for the erosion tests

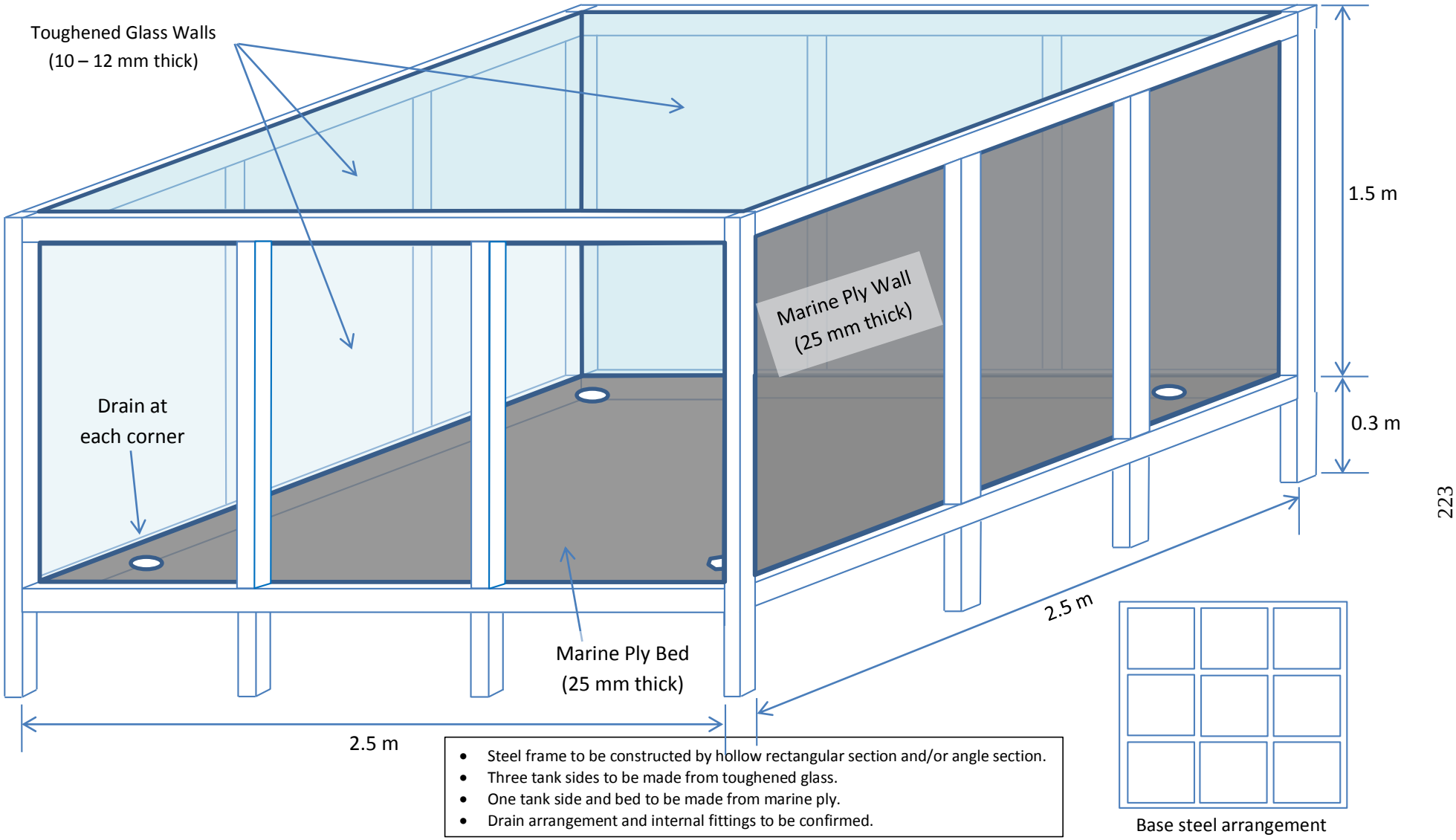

Appendix 3-4 The Creteangle Multi-Flow Rotary Mixer

(a) during mixing operation

(b) after mixing operation

Chapter Five

Appendix 5-1 Time-lapsed images of sand-clay sedimentation process at times *t* shown for run SET-EX2 (85s:15c)

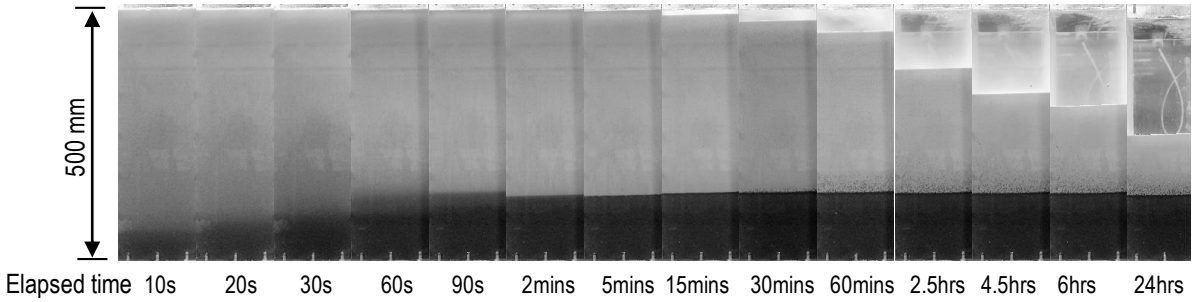

Appendix 5-2 Time-lapsed images of sand-clay sedimentation process at times *t* shown for runs with 65s:35c mixtures (a) SET-EX5 (b) SET-EX6 and SET-EX7

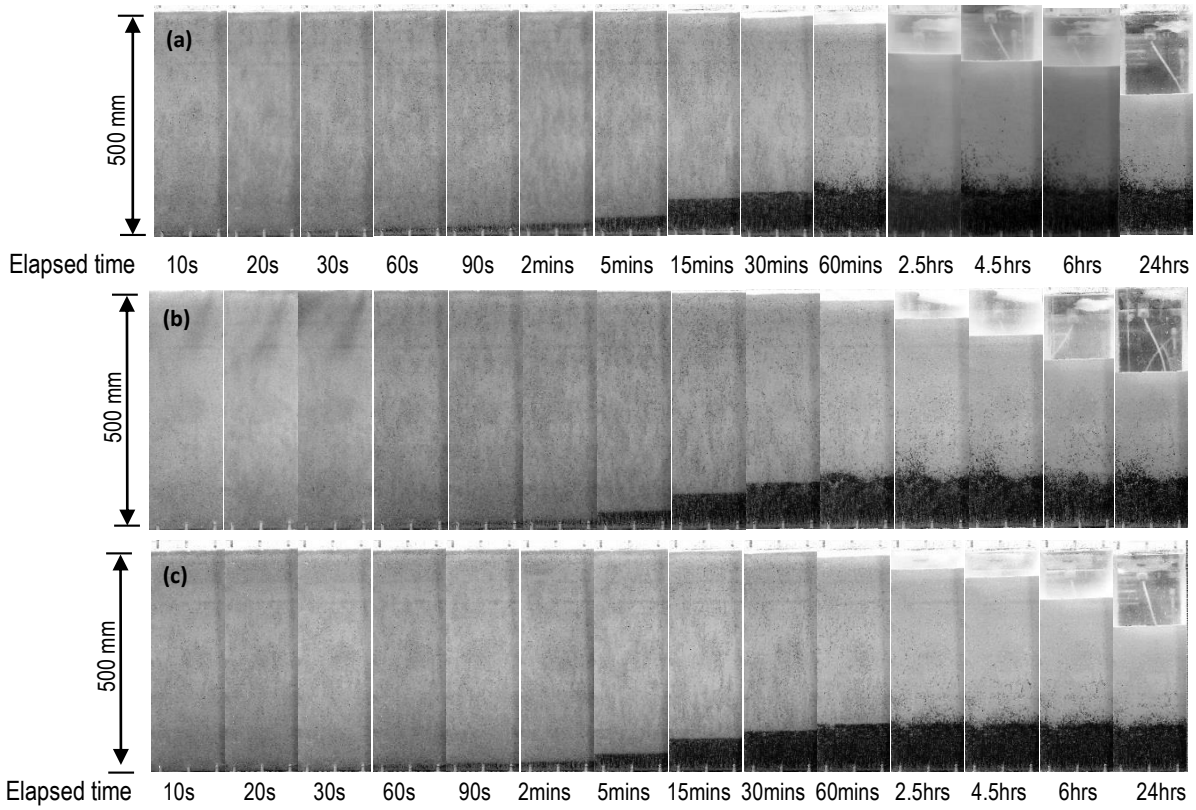

Appendix 5-3 Time series colour map plots of the variation in measure formation factor *F* profiles during the first hour of the sand-clay sedimentation process for (a) SET-EX1 and (b) SET-EX5.

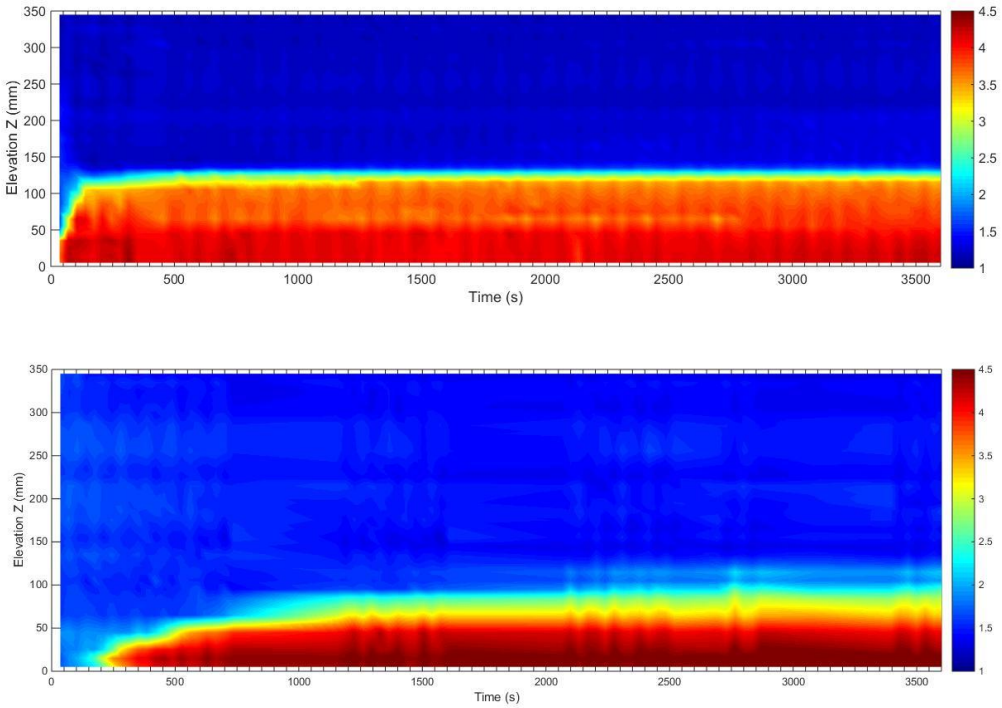

Appendix 5-4 Initial temporal development of normalised bulk density γ_{bulk}/γ_p within sand-clay bed deposit layers for (a) SET-EX1 (85s:15c; 15 ppt) and (b) SET-EX5 (65s:35c; 15ppt)

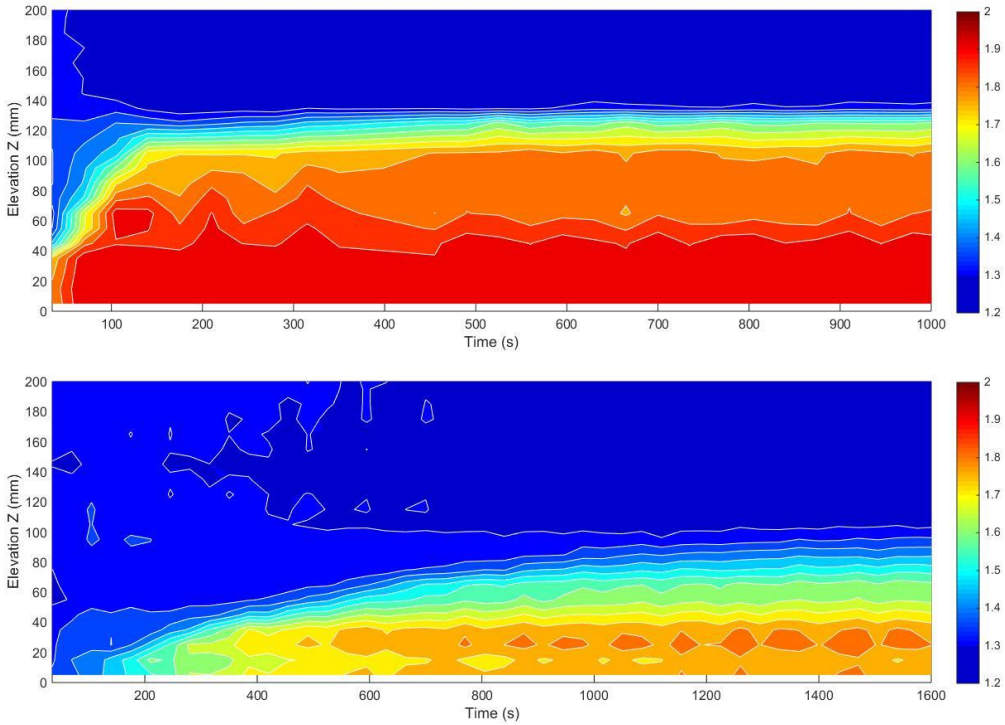

Appendix 5-5 Longer term temporal development in normalised bulk density γ_{bulk}/γ_p profiles at elapsed times shown for (a) SET-EX2(85s:15c) and (b) SET-EX5(65s:35c). [see Table 5.1]

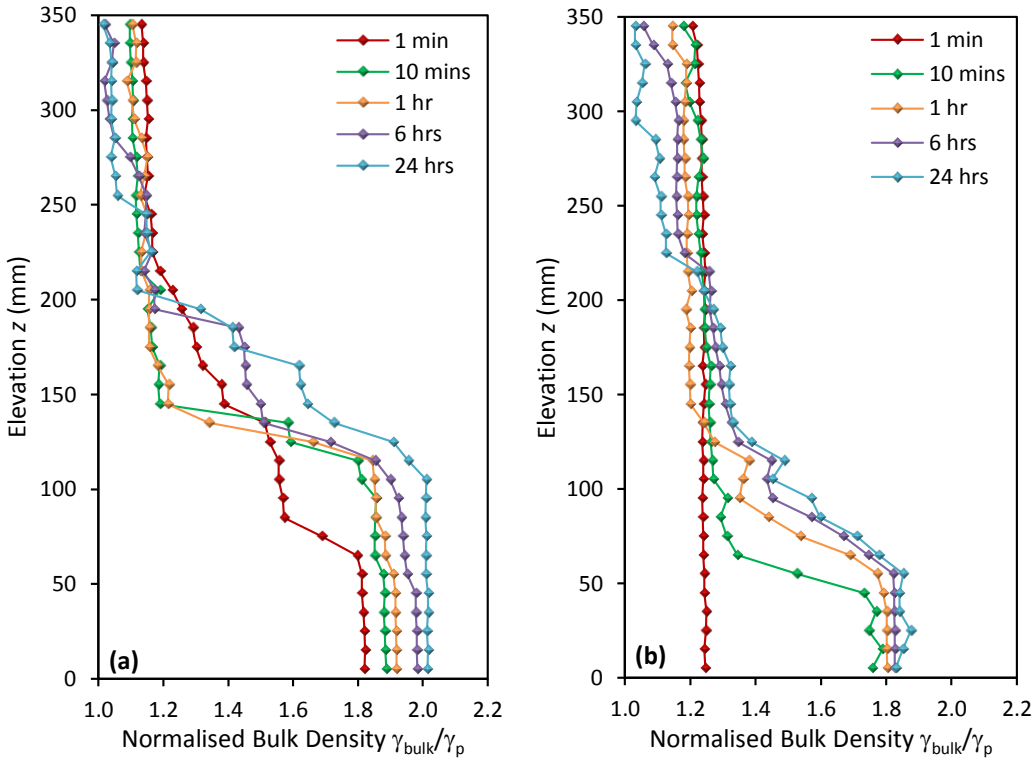

Chapter Six

Appendix 6-1 Total sediment mass eroded (g) per applied bed shear stress (Pa)

	Mean Bed Shear stress, τ_b (Pa)								
Erosion Tests	0.0003	0.0425	0.1816	0.4464	0.6997	1.0601	1.4186	1.8808	2.0205
ERT-EX1	0.00	12.95	244.24	Saturated	Saturated	Saturated	Saturated	Saturated	Saturated
ERT-EX2	0.00	17.03	229.51	488.89	530.81	Saturated	Saturated	Saturated	Saturated
EXT-EX3	0.00	1.57	1.83	2.10	8.65	29.87	52.66	100.35	163.49
ERT-EX4	0.00	0.26	0.26	0.26	0.26	0.26	2.79	19.45	70.48
ERT-EX5	0.00	0.52	0.52	0.52	0.52	0.52	8.81	32.75	106.11
ERT-EX6	0.00	0.52	0.79	0.79	0.79	28.03	31.70	61.05	115.02

Appendix 6-2 Mass per unit bed surface area (g/m^2) at the end of each applied bed shear stress (Pa)

	Mean Bed Shear stress, τ_b (Pa)								
Erosion Tests	0.0003	0.0425	0.1816	0.4464	0.6997	1.0601	1.4186	1.8808	2.0205
ERT-EX1	0.00	14.85	280.10	Saturated	Saturated	Saturated	Saturated	Saturated	Saturated
ERT-EX2	0.00	19.53	263.20	560.65	608.73	Saturated	Saturated	Saturated	Saturated
EXT-EX3	0.00	1.80	2.10	2.41	9.92	34.25	60.39	115.08	187.49
ERT-EX4	0.00	0.30	0.30	0.30	0.30	0.30	3.20	22.30	80.82
ERT-EX5	0.00	0.60	0.60	0.60	0.60	0.60	10.1	37.56	121.69
ERT-EX6	0.00	0.60	0.91	0.91	0.91	32.14	36.35	70.01	131.90

Appendix 6-3 Plots of Erosion rate against Bed shear stress. The fit lines for data points between B & C are extrapolated to the *x*-axis to determine the surface erosion threshold for all the experimental runs

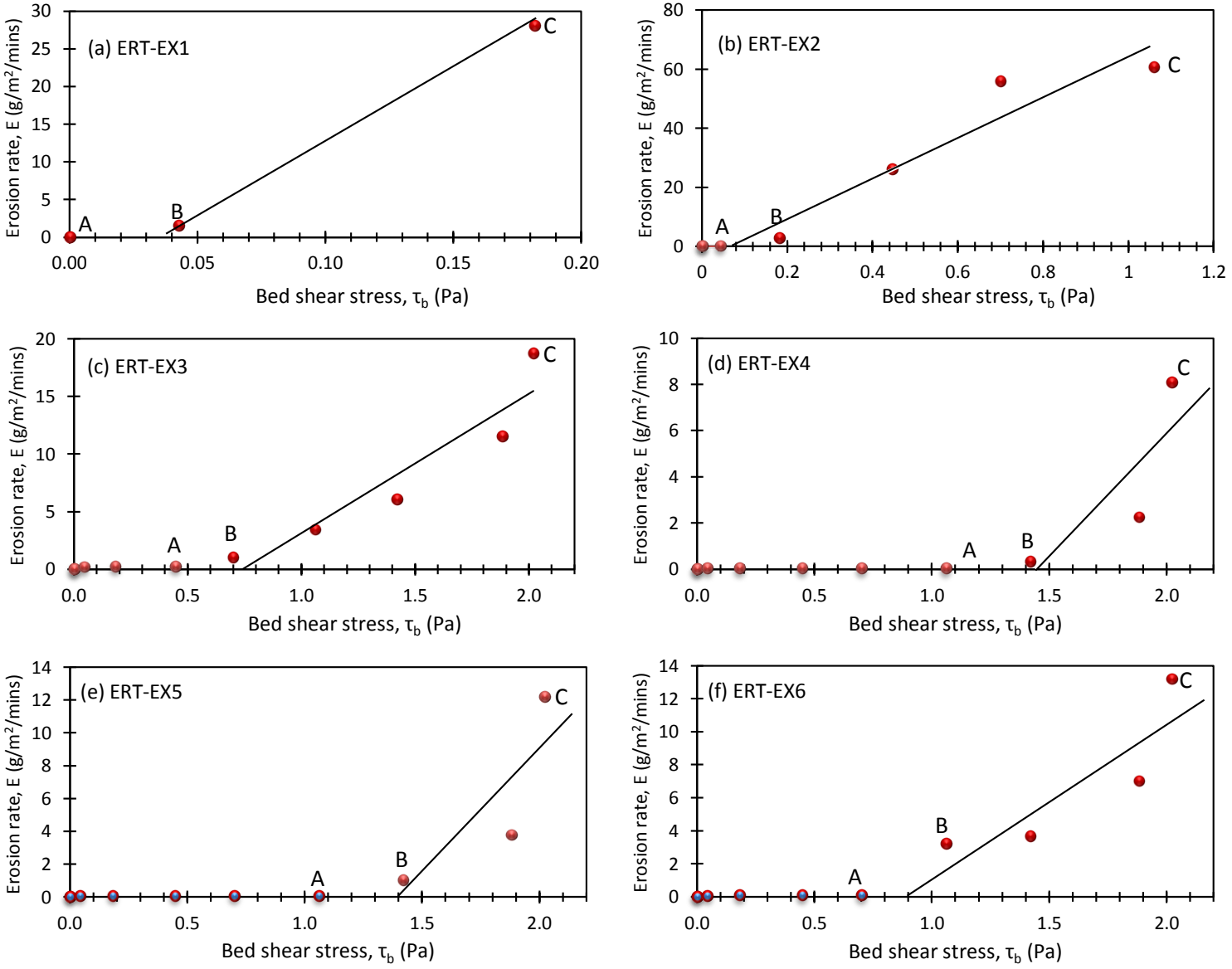

Appendix 6-4 Examples of typical results from erosion tests on predominantly sandy beds showing the linear extrapolation process for determination of erosion thresholds: (a) & (b) 70% & 90% sand respectively (Laksanalamai, 2007), and (c) 75% sand (Jacobs *et al.*,2011)

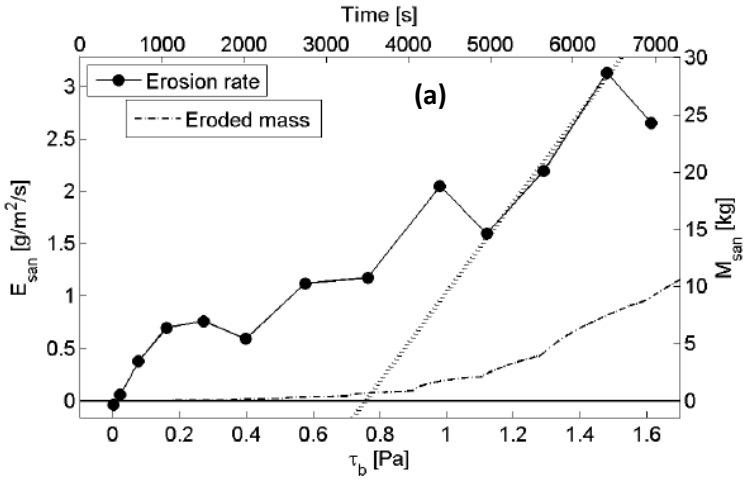

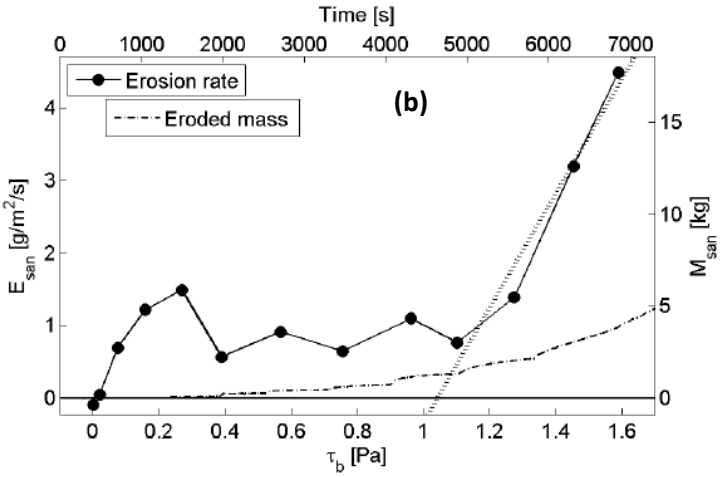

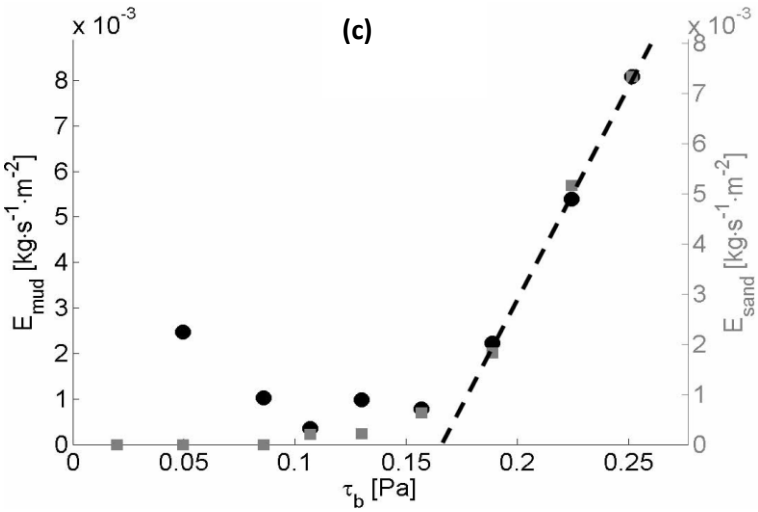

Appendices P-1 Monitoring and characterisation of sand-mud sedimentation processes (Sample of author's publication in Ocean Dynamics)

References

AINA, (2013). *Sustainable management of dredged material from inland waterways.* [Online] Available at: www.aina.org.uk
[Accessed 02 03 2015].

Allen, G.P. and Posamentier, H.W., (1993). Sequence stratigraphy and facies model of an incised valley fill; the Gironde Estuary, France. *Journal of Sedimentary Petrology,* 63(3), pp. 378-391.

Allen, R.C., (2000). *Triboelectric Generation: Getting Charged.* Marlboro, MA: Desco Industries Inc. (DII). Reproduced by permission:EE-Evaluation Engineering.

Amos, C. L., Grant, J., Daborn, R. and Black, K., (1992). Sea Carousel - A benthic annular flume. *Estuarine Coastal Shelf Sci.,* Volume 34, pp. 557-577.

Amos, C.L., Bergamasco, A., Umgiesser, G., Cappucci, S., Cloutier, D., DeNat, L., Flindt, M., Bonardi, M. and Cristante, S. , (2004). The stability of tidal flats in Venice Lagoon-the results of in-situ measurements using two benthic, annular flumes. *Journal of Marine Systems,* Volume 51, pp. 211-241.

Amy, L.A., Talling, P.J., Edmonds, V.O., Sumner, E.J. and Lesueur, A., (2006). An experimental investigation of sand-mud suspension settling behaviour: implications for bimodal mud contents of submarine flow deposits. *Sedimentology ,* 53(6), pp. 1411-1434.

Andersen, T.J., Lund-Hansen, L.C., Pejrup, M., Jensen, K.T., Mouritsen, K.N., (2005). Biological induced differences in erodibility and aggregation of subtidal and intertidal sediments: a possible cause for seasonal changes in sediment deposition. *Journal of Marine Systems,* 55(3-4), pp. 123-138.

Andersland, O.B. and Douglas, A.G., (1970). Soil Deformation rates and Activation Energies. *Geotechnique,* Volume 20, pp. 1-16.

Andreotti, B., Claudin, P., Devauchelle, O., Duran, O. and Fourriere, A., (2012). Bedforms in a Turbulent Stream:Ripples, Chevrons and Antidunes. *J. Fluid Mech.,* Volume 690, pp. 94-128.

Ani, S.A., Dyer, K.R. and Huntley, D.A., (1991). Measurement of the influence of salinity on floc density and strength.. *Geo-Marine Letters,* Volume 11, pp. 154-158.

Archie, G. E., (1942). The Electrical Resistivity Log as an Aid in Determining some Reservoir Characteristics. *Transaction of the American Institute of Mining and Metallurgical Engineers,* Volume 147, pp. 54-62.

Athaullah, M., (1968). *Prediction of Bedforms in Erodible Channels.,* Ph.D Thesis: Colorado State University.

Baas, J.H., Best, J.L., and Peakall, J., (2011). Depositional Processes, Bedform Development and Hybrid Bed Formation in Rapidly Decelerated Cohesive (mud-sand) Sediment Flows. *Sedimentology,* Volume 58, pp. 1953-1987.

Baas, J.H., Davies, A.G. and Malarkey, J., (2013). Bedform development in mixed sand-mud: The contrasting role of cohesive forces in flow and bed. *Geomorphology,* Volume 182, pp. 19-32.

Bale, A.J., Stephens, J.A. and Harris, C.B., (2007). Critical Erosion Profiles in Macro-tidal Estuary Sediments: Implications for the Stability of Intertidal Mud and the Slope of Mud Banks. *Continental Shelf Research,* 27(18), pp. 2303-2312.

Bassiouni, Z., (1994). *Theory, Measurement and Interpretation of Well Logs.* s.l.:SPE textbook series, vol. 4.

Batchelor G. K., (1982). Sedimentation in a dilute polydisperse system of interacting spheres: 1. General theory. *Journal of Fluid Mechanics,* Volume 119, pp. 379-408.

BBC, (2014). *Ancient Roman port 'larger than though', researchers find.* [Online]
Available at: www.bbc.co.uk/news/uk-england-27054163
[Accessed 01 03 2015].

Beach, R.A. and Sternberg, R.W., (1988). Suspended sediment transport in the surf zone: Response to cross-shore infragravity motion. *Marine Geology,* Volume 80, pp. 671-679.

Been, K. and Sills, G. C., (1981). Self-weight Consolidation of Soft Soils: An Experimental and Theoretical Study. *Geotechnique,* 31(4), pp. 519-535.

Been, K. and Sills, G. C., (1981). Self-weight Consolidation of Soft Soils: An Experimental and Theoretical Study. *Geotechnique,* 31(4), pp. 519-535.

Berlamont, J., Ockenden, M., Toorman, E. & Winterwerp, J., (1993). The characterisation of cohesive sediment properties. *Coastal Engineering,* Volume 21, pp. 105-128.

Bernard, J., Leite, O. and Vermeersch, F., (2004). *Multi-electrode Resistivity Imaging for Environmental and Mining Applications,* Orleans, France: IRIS Instruments.

Best J., (1996). The Fluid Dynamics of Small-scale Alluvial Bedforms. In: P. &. C. M. Dawson, ed. *Advances in Fluvial Dynamics and Stratigraphy.* West Sussex: John Wiley & Sons Ltd, pp. 67-125.

Blass, E., Jasman, A. and Shelly, S., (2010) . *Visioning 2035: The Future of the Higher Education Sector in the UK.* [Online]
Available at: http://uhra.herts.ac.uk/bitstream/handle/2299/4562/903760.pdf?sequence=1
[Accessed 22 02 2015].

Blewett, J., McCarter, W.J., Chrisp, T.M. and Starrs, G., (2001). Monitoring Sedimentation of a Clay Slurry. *Geotechnique,* 51(8), pp. 723-728.

Blewett, J., McCarter, W.J., Chrisp, T.M. and Starrs, G., (2003). An Experimental Study on Ionic Migration through Saturated Kaolin. *Engineering Geology,* Volume 70, pp. 281-291.

Boyce, R. E., (1968). Electrical Resistivity of Modern Marine Sediments from the Bering Sea. *Journal of Geophysical Research,* 73(14), pp. 4759-4766.

Breitzke, M., (2006). Physical Properties of Marine Sediments. In: H. D. a. Z. M. Schulz, ed. *Marine Geochemistry.* 2nd ed. Berlin Heidelberg: New York: Springer, pp. 28-69.

Brownlie, W.R. , (1981). *Prediction of flow depth and sediment discharge in open channels,* Pasadena, California: Report Number KH-R-43A, Keck Laboratory of Hydraulics and Water Resources, California Institute of Technology.

Buffington, J.M. and Montgomery, D.R., (1997). A systematic analysis of eight decades of incipient motion studies, with special reference to gravel-bedded rivers. *Water Resource Research,* Volume 33, p. 1993–2029.

Bürger, R. and Wendland, W.L., (2001) . Sedimentation and suspension flows: Historical perspective and some developments. *Journal of Engineering Mathematics,* 41(2), pp. 101-116.

Burt, T.N., (1986). Estuarine cohesive sediment dynamics. In: A. Mehta, ed. *Field settling velocities of Estuary muds.* s.l.:Springer-Verlag, pp. 126-150.

Camp, T.R., Stein, P.C. , (1943). Velocity gradients and internal work in fluid motion. *Journal of the Boston Society of Civil Engineers,* pp. 219-237.

Cao, Z., Pender, G. and Meng, J., (2006). Explicit formulation of the Shields diagram for incipient motion of sediment. *Journal of Hydraulic Engineering,* Volume 132, pp. 1097-1099.

Carling, P.A., (1984). Deposition of fine and coarse sand in an open-work gravel bed. *Canadian Journal of Fisheries and Aquatic Sciences,* 41(2), pp. 263-270.

Carrier, M. and Soga, K., (1999). A Four Terminal Measurement System for Measuring the Dielectric Properties of Clay at Low Frequencies. *Engineering Geology,* Volume 53, pp. 115-123.

Cerco, C.F., Kim, S.C. and Noel, M.R., (2013). Management modeling of suspended solids in the Chesapeake Bay, USA. *Estuarine, Coastal and Shelf Science,* Volume 116, pp. 87-98.

Charru, F. and Hinch, E.J., (2006). Ripple Formation on a Particle Bed sheared by a Viscous Liquid. Part 1. Steady Flow. *J. Fluid Mech.,* Volume 550, pp. 111-121.

Cheng. N. S., (1997). Effect of concentration on settling velocity of sediment particles. *Journal of Hydraulic Eng.,* 123(8), pp. 728-731.

Chisholm, H., (1911). *Encyclopædia Britannica.* 11th ed. s.l.:Cambridge University Press.

Christensen, R.W. and Das, B.M., (1974). *Hydraulic ERosion of Remolded Cohesive Soils,* s.l.: Special Report 135, Soil ERosion:Causes and Mechanisms, Prevention and Control, pp 8-19.

Christensen, R.W. and Wu, T.H., (1964). Analysis of Clays Deformations as a Rate Process. *Journal of the Soil Mechanics and Foundation Division, ASCE 90,* Volume No. SM6, Proc. Paper 4147.

Clavier, C., Coates, G. and Dumanoir, J., (1984). Theorectical and experimental bases for the dual-water model for interpretation of shaly sands. *Society of Petroleum Engineers Journal,* 24(2), pp. 153-168.

Cloutier, D., LeCouturier, M.N., Amos, C. L. and Hill, P.R., (2006) . The effects of suspended sediment concentration on turbulence in an annular flume. *Aquatic Ecology ,* Volume 40, p. 555–565.

Coleman, S.E. and Melville, B.W., (1996). Initiation of Bed Forms on a Flat Sand Bed. *J. Hydraulic Eng.,* 122(6), pp. 301-310.

Coleman, S.E. and Nikora, V.I., (2008). *Initiation and Growth of Fluvial Dunes.* Leeds, United Kingdom, Marine and River Dune Dynamics.

Colombini, M. and Stocchino, A., (2011). Ripples and Dune Formation in Rivers. *J. Fluid Mech.,* Volume 673, pp. 121-131.

Colombini, M., (2004). Revisiting the Linear Theory of Sand Dune Formation. *J. Fluid Mech.,* Volume 502, pp. 1-16.

Corrsin, S., (1963). Turbulence: experimental methods. *Handbuch der Physik,* Volume 8, pp. 524-587.

Craig, R.F., 1992. *Soil Mechanics.* 4th ed. London: Chapman & Hall.

Cuthbertson A. J. S., Dong, P. and Davies P. A., (2010). Non-equilibrium Flocculation Characteristics of Fine-grained Sediments in Grid-generated Turbulent Flow. *Coastal Engineering,* Volume 57, pp. 447-460.

Cuthbertson A., Dong, P., King, S. and Davies P. , (2008). Hindered Settling Velocity of Cohesive/non-cohesive Sediment Mixtures. *Journal of Coastal Engineering,* Volume 55, pp. 1197-1208.

Cuthbertson, A.J., (2001). *The Motion of Fine Sand Particles in Turbulent Open Channel Shaer Flows over Porous Bed Conditions.* s.l.:PhD Thesis, University of Glasgow.

Dade, W.B., Nowell, A.R.M. and Jumars, P.A., (1992). Predicting erosion resistance of muds. *Marine Geology ,* 105 (1–4), p. 285–297.

Dahlin, T., (2000). Short Note on Electrode Charge-up Effects in DC Resistivity Data Acquisition using Multi-electrode Arrays. *Geophysical Prospecting ,* Volume 48, pp. 181-187.

Dai, Q., Shan, H.X., Jia, Y.G., Meng, X.M., (2009). *Laboratory study on the relationship between suspended sediment concentration and electrical conductivity.* s.l., Proceedings of ASME 2009 28th Int'l Conf. on Ocean, Offshore and Arctic Engnr. Coll. of Environmental Sci. and Engnr., Qingdao, China.

Dallavalle, J., (1948). *The Technolology of Fine Particles.* s.l.:Pitman.

Dankers, P. and Winterwerp, J.C., (2007). Hindered settling of mud flocs: Theory and validation.. *Cont. Shelf Research ,* Volume 27, p. 1893–1907..

Dankers, P.J.T., (2006). *On the hindered settling of suspensions of mud and mud-sand mixtures.* PhD Thesis: TU Delft, The Netherland.

Davis, R.H. and Gecol, H., (1994). Hindered settling function with no empirical parameters for polydisperse suspensions. *AIChE Journal,* Volume 40, p. 570–575.

Davison, L., (2000). *Soil description and classification.* [Online]
Available at: http://environment.uwe.ac.uk/geocal/SoilMech/classification/soilclas.htm
[Accessed 06 05 2015].

de Boer, W.F., (2007). Seagrass-sediment interactions, positive feedbacks and critical thresholds for occurence: a review. *Hydrobiologia,* Volume 591, pp. 5-24.

De Silva, I.P.D., Fernando, H.J.S., (1992). Some aspects of mixing in a stratified turbulent. *Journal of Fluid Mechanics,* Volume 240, pp. 601-625.

De Silva, I.P.D., Fernando, H.J.S., (1994). Oscillating grids as a source of nearly isotropic turbulence. *Physics of Fluids,* 6(7), pp. 2455-2464.

Debnath, K., Nikora, V., Aberle, J. Westrich, B. and Muste, M., (2007). Erosion of cohesive sediments: resuspension, bed load and erosion patterns from field experiments. *Journal of Hydraulic Engineering-ASCE ,* 133(5), pp. 508-520.

DEFRA/EA, (2006). Integrated research results on hydrobiosedimentary processes in estuaries. Final report of the estuary process research project (EstProc). *Flood and Coastal Defence R & D Prog.*, p. 112.

Devarajan, S., Toumelin, E. and Torres-Verdin, C., (2006). *Pore-scale analysis of the Waxman-Smith shally sand conductivity model.* Vera Cruz, Mexico, SPWLA 47th Annual Logging Symposium.

Dowling, J.J., (1990). Estimating porosity of partially saturated sediment. *Engineering Geology,* Volume 29, pp. 139-147.

Dufois, F., (2008). *Modélisation du transport particulaire dans le Golfe du Lion en vue d'une application au devenir des traceurs radioactifs issus du Rhône.* PhD thesis: Univ. su Sud Toulon Var, p 409.

Dyer, K.R. and Manning, A.J., (1999). Observation of the size, settling velocity and effective density of flocs and their fractal dimensions. *Journal of Sea Research,* Volume 41, pp. 87-95.

Dyer, K.R., (1986). *Coastal and Estuarine Sediment Dynamics.* Chichester: John Wiley & Sons.

Dyer, K.R., (1989). Sediment processes in estuaries: future research requirements. *Journal of Geophysical Research,* 94(C10), pp. 14327-14339.

EC, (2004). Living with coastal erosion in Europe: Sediment and Space for Sustainability. *PART I - Major findings and Policy Recommendations of the EUROSION project*, p. 54.

EC, (2011). Guidelines on the implementation of the birds and habitats directives in estuaries and coastal zones with particular attention to port development and dredging. *EC Guidance Document*, p. 45.

Eisma, D., (1998). *Intertidal Deposits: River Mouths, Tidal Flats, and Coastal Lagoons.* Florida: CRC Press LLC.

Ellis, D. V.,, (1987). *Well Logging for Earth Scientists.* pp 532 ed. Amsterdam: Elsevier.

Eow, J.S., Speranza, A., Hayati, I. and Ghadiri, M., (2003). Mitigation of Segregation and Stratification in Bulk Granular Mixtures by the Electroclamping Method. *Power Technology,* Volume 92-104, p. 135–136.

Erchul, R. A. and Nacci, V. A., (1972). Electrical Resistivity Measuring System for Porosity Determination of Marine Sediments. *Marine Technology Society Journal,* 6(4), pp. 47-53.

Eugelund, F. and Hansen, E., (1967). *A monograph on sediment transport to alluvial streams,* s.l.: Copenhagen:Teknik Vorlag.

Evans, E.P., Simm, J.D., Thorne, C.R., Arnell, N.W., Ashley, R.M., Hess, T.M., Lane, S.N., Morris, J., Nicholls, R.J., Penning-Rowsell, E.C., Reynard, N.S., Saul, A.J., Tapsell, S.M., Watkinson, A.R., Wheater, H.S. , (2008). *An update of the Foresight Future Flooding 2004 qualitative risk analysis,* London: Cabinet Office.

Eyring, H., (1936). Viscosity, plasticity, and diffusion as examples of absolute reaction rates. *The Journal of Chemical Physics,* 4(4), pp. 283-291.

Falk, A. and Heckman, J.J., (2009). Lab experiments are a major source of knowledge in the social sciences. *Science,* 326(5952), pp. 535-538.

Feates, N., Hill, J. R., et al., (1999). *COSINUS Filed Experiemnt Tamar Estuary: Measurement of properties of suspended sediment flocs and bed properties,* s.l.: s.n.

Fernandes, S., Sobral, P. and Alcantara, F., (2009). Nereis diversicolor and copper contamination effect on the erosion of cohesive sediments: a flume experiment. *Estuarine Coastal and Shelf Science,* 82(3), pp. 443-451.

Fingerle, A., Roeller, K., Huang, K. and Herminghaus, S., (2008). Phase Transitions far from Equilibrium in Wet Granular Matter. *New Journal of Physics,* Volume 10, p. 10.

Fontein, W. and van der Wal, J., (2006). Assessing nautical depth efficiently in terms of rheological characteristics. In: Evolutions in Hydrography. *Proc. Int. Hydrographic Conference*, 6-9 November, Volume 55, pp. 149-152.

Friend, P.L., Ciavola, P., Cappucci, S. and Santos, R., (2003). Bio-dependent bed parameters as a proxy tool for sediment stability in mixed habitat intertidal areas. *Continental Shelf Research,* 23(17-19), pp. 1899-1917.

Futterer, D.K., (2006). The Solid phase of Marine Sediments. In: H. a. Z. M. Schulz, ed. *Marine Geochemistry.* 2nd ed ed. New York: Springer, Berlin Heidelberg, pp. 1-25.

Garde, R.J. and Ranga Raju, K.G., (1977). *Mechanics of sediment transportation and alluvial stream problems.* New Delhi: Wiley Eastern Ltd.

Gerbersdolf, S.U.,Jancke, T., Westrich, B. and Paterson, D.M.i, (2008). Microbial stabilization of riverine sediments by extracellular polymeric substances.. *Geobiology,* 6(1), pp. 57-69.

Gerbersdorf, S.U., Jancke, T. and Westrich, B., (2005). Physical-chemical and biological sediemnt properties determining erosion resistance of contaminated riverine sediment-

temporal and vertical pattern at the Lauffen reservoir/River Neckar, Germany. *Limnological,* 35(3), pp. 132-144.

Gibson, R.E., England, G.L. and Hussey, M.J.L, (1967). The theory of one dimensional consolidation of saturated clays. *Geotechnique,* Volume 17, pp. 261-273.

Glasstone, S., Laidler, K. and Eyring, H., (1941). *The Theory of Rate Process.* New York: McGraw-Hill.

Goldstein, S., (1929). The steady flow of viscous fluid past a fixed sperical obstacles at small Reynolds number. *Proc. of Royal Society London,* 123(A), pp. 225-235.

Grabowski, R.C., Droppo, I.G. and Wharton G., (2011). Erodibility of Cohesive Sedimnet: The Importance of Sediment Properties. *J. of Earth-Science Reviews,* Volume 105, pp. 101-120.

Grabowski, R.C., Droppo, I.G., Whaton, G., (2010). Estimation of critical shear stress from cohesive strength meter-derived erosion thresholds. *Limnology and Oceanography Methods,* Volume 8, pp. 678-685.

Grasso, F., Le Hir, P. and Bassoullet, P., (2014). Analysis of mixed-sediment consolidation experiments. *Proceedings of the 13th Journées Nationales Génie Côtier – Génie Civil, Dunkerque, France,* pp. 353-362.

Grasso, F., Le Hir, P. and Bassoullet, P., (2015). Numerical modelling of mixed-sediment consolidation. *Ocean Dynamics,* 65(4), pp. 607-616.

Gratiot, N. and Manning, A.J., (2004). An experimental investigation of floc characteristics in a diffusive turbulent flow. *Journal of Coastal Research,* Volume SI 41, pp. 105-113.

Gregory, J., (1997). The density of particle aggregates. *Water Science and Technology,* 36(4), pp. 1-13.

Guan, W.B., Kot, S.C. and Wolanski, E., (2005). 3-D fluid-mud dynamics in the Jiaojiang Estuary, China. *Estuarine, Coastal and Shelf Science (Journal),* 65(4), pp. 747-762.

Gularte, R.C., Kelly, W.E., and Nacci, V.A., (1980). Erosion of Cohesive Sediments as a Rate Process. *Ocean Engineering,* Volume 7, pp. 539-551.

Gust, G. and Walger, E., (1976). The influence of suspended cohesive sediments on boundary-layer structure and erosive activity of turbulent sea-water flow. *Marine Geology,* Volume 22, pp. 189-206.

Gust, G., (1976). Observations on turbulent-drag reduction in a dilute suspension of clay in sea-water. *J. Fluid Mech.,* Volume 75, pp. 29-47.

Ha, H. K., Maa, J., P-Y., Holland, C. W., (2010). Acoustic density measurements of consolidating cohesive sediment beds by means of non-intrusive “Micro-Chirp” acoustic system.. *Geo-Marine Letters,* 30(6), pp. 585-593 .

Ha, Z. and Lui, S., (2002). Settling velocities of polydisperse concentrated suspensions. *The Canadian Journal of Chemical Engineering,* Volume 80, pp. 783-790.

Hanes, D. M. and Bowen, A. J., (1985). A granular-fluid model for steady. *Journal of Geophysical Research,* 90(C5), pp. 9149-9158.

Harrison, A.J.M. and Owen, M.W., (1971). *Siltation of fine sediments in estuaries,* Paris, Paper D1: Proceedings of the XIV IAHR Congress.

Hauck, T.E., Dashtgard, S.E., Pemberton, S.G. and Gingras, M.K., (2009). Brackish-water ichnological trends in a microtidal barrier island-embayment system, Kouchibouguac national Park, New Brunswick, Canada. *Palaios,* 24(8), pp. 478-496.

Havel, F., (2004). *Creep in soft soils.* PhD Thesis: Norwegian University of Science and Technology.

Hill, P.S., (1998). Controls on floc size in the sea. *Oceanography,* 11(2), pp. 13-18.

Hirst, T.J., Rerlow, M. and Richards, A.F., (1975). Improved in situ gamma-ray transmission densitometer for marine sediments. *Ocean Engineering,* Volume 3, pp. 17-27.

Hirst, T.J., Rerlow, M. and Richards, A.F., (1975). Improved in situ gamma-ray transmission densitometer for marine sediments. *Oceans Eng.,* Volume 3, pp. 17-27.

HM Government, (2011). UK Marine Policy Statement. *The Stationary Office Ltd., London*, p. 47.

Hopfinger, E.J., Toly, J. A., (1976). Spatially-decaying turbulence and its relation to mixing across density interfaces. *Journal of Fluid Mechanics,* Volume 78, pp. 155-175.

Horn, D.P., (1992). A review and experimental assessment of equilibrium grain size and the ideal wave-graded profile. *Marine Geology,* Volume 108, pp. 161-174.

Houwing, E.J., (1999). Determination of the critical erosion threshold of cohesive sediments on intertidal mudflats along the Dutch Wadden Sea Coast. *Estuarine Coastal and Shelf Science,* 49(4), pp. 545-555.

Hoyal, D. and Sheets, B., (2009). Morphodynamic evolution of experimental cohesive deltas. *Journal of Geophysical Research,* Volume 114, p. F02009.

Hughes, S., (1993). Physical models and laboratorytechniques in coastal engineering. *Advanced Se-ries on Ocean Engineering,* Volume 7, World Scientific.

Hydramotion Ltd, (2013). *Engineer Live Magazine.* [Online] Available at: http://www.engineerlive.com/content/22329. [Accessed 23 07 2015].

Ibikunle, O.S., Cuthbertson, A.J.S. and McCarter, W.J.C., (2014). *Measuring Density and Porosity of Mixed-sediment Bed deposits using a Non-invasive Electrical Impedance Technique (EIT).* Ediburgh, Infrastructure and Environment Scotland 2nd PG Conference, pp. 25-31.

Ibikunle, S. O., Cuthbertson, A.J.S., Heynes, H. and McCarter, W.J., (2013). Exploring Electrical Impedance Techniques to Study Sedimentation and Bed Deposits of Sand-Mud Mixtures. *Proc. Intercoh 2013, Gainsville, Florida*, 21-24 October.

Imai, G., (1980). Settling Behaviour of Clay Suspension. *Soil and Foundation,* 20(2), pp. 61-77.

Imai, G., (1981). Experimental studies on sedimentation mechanism and sediemnt formation of clay materials. *Soils and Foundations,* 21(1), pp. 7-20.

Jackson, P. D., (1975). An Electrical Resistivity Method for Evaluating the In-Situ Porosity of Clean Marine Sands. *Marine Geotechnology,* 1(2), pp. 91-115.

Jacob, W., Eelkema, M. and Winterwerp, J.C., (2009). A new radiometric instrument for in situ measurements of physical sediment properties. *Marine & Freshwater Research,* Volume 60, pp. 727-736.

Jacobs, W., Le Hir, P., van Kesteren, W. and Cann, P., (2011). Erosion threshold of sand-mud mixtures. *Continental Shelf Research,* Volume 31, pp. S14-S25.

Jacobs, W., Van Kesteren, W.G.M. and Winterwerp, J.C., (2007). Strength of sediment mixtures as a function of sand content and clay mineralogy. In: T. Y. H. S. J. a. G. J. Kusuda, ed. *Sediment and Ecohydraulics, Intercoh 2005.* Saga, Japan: Proceedings in Marine Science, Vol. 9, pp. 91-107.

Janesch, J., (2013). *Keithley Instruments, Inc..* [Online]
Available at: www.keithley.co.uk/data?asset=57571
[Accessed 23 07 2015].

Jeffrey, J., (2012). *Investigating the performance of continuous helical displacement piles.* PhD Thesis: University of Dundee.

Johnson, C. P., Li, X. and Logan, B., (1996). Settling velocities of fractal aggregates. *Environmental Science & Technology,* Volume 30, pp. 1911-1918.

Jones, P., Lawton, J.H. and Shachak, M., (1997). Positive and negative effects of organisms as physical ecosystem engineers. *Ecology,* 78(7), pp. 1946-1957.

Julien, P.Y., (1995). *Erosion and Sedimentation.* New York: Cambridge University Press.

Jumars, P.A. and Nowell, A.R.M , (1984). Effects of Benthos on Sediment Transport-Difficulties with Functional Grouping. *Continental Shelf Research,* 3(2), pp. 115-130.

Kanagy, S.P. and Mann C.J., (1994). Electrical Properties of Eolian Sand and Silt. *Earth-Science Reviews ,* Volume 36, pp. 181-204.

Kandiah, A., (1974). *Fundamental aspects of surface erosion of cohesive soils.* PhD Thesis: University of California, Davis. Cited in Winterwerp and van Kesteren (2004).

Kaya, A., Yoshida, H., Tanigawa, H., Igata, H. and Tsuruya, H., (2008). Estimation of sea bottom density profile through analysis of ultrasonic echo signal. In: T. Y. H. S. J. a. G. J. Kusuda, ed. *Sediment and Ecohydraulics: Intercoh 2005.* Amsterdam: Elsevier, pp. 17-30.

Kelly, W.E. and Gularte, R.C., (1981). Erosion resistance of cohesive soils. *ASCE, Journal of the Hydraulics Division,* 107(10), pp. 1211-1224.

Khalil, M.A. and Santos, F.A.M., (2011). Influence of degree of saturation in the electric resistivity–hydraulic conductivity relationship. In: Dikinya O (ed) Developments in hydraulic conductivity research. *InTech, ISBN 978-953-307-470-2 ,* Volume 49–70, p. 282.

Klein, K. and Santamarina, (2002). Electrical Conductivity in Soils:Surface Conduction and Fabric Anisotropy Effects. *Journal of Geotech. Geoenviron. Engng (submitted).*

Kleinhans, M.G., van Dijk,W.M., van de Lageweg,W.I., Hoyal,D.C., Markies, H., van Maarseveen, M., Roosendaal, C., van Weesep, W., van Breemen, D., Hoendervoogt, R. and Cheshier, N. , (2014). Quantifiable effectiveness of experimentalscaling of river- and delta morphodynamicsand stratigraphy. *Scaling river- and delta morphodynamics and stratigraphy,* Volume ESR 133, p. 43–61.

Koncar-Djurdjevic, S. and Vukovic, D. , (1962). Separations in Fluidized Systems by means of Dielectric Charging of Materials. *Nature,* Volume 193, pp. 58-59.

Krank, K. and Milligan, T.C., (1992). Characteristics of suspendend particles at an 11 hour anchor station in San Francisco Bay. *Journal of Geophysical Research,* Volume 97, pp. 11373-11382.

Krone, R.B., (1962). *Flume studies of the transport of sediment in estuarial shoaling processes,* Hydraulic Engineering Laboratory and Sanitary Engineering Research Laboratory, University of California, Berkeley: Final Report.

Kuhnle, R.A., Horton, J.K., Bennett, S.J. and Best, J.L., (2006). Bed Forms in Bimodal Sand-Gravel Sediment: Laboratory and Field Analysis. *Sedimentology,* Volume 53, pp. 631-654.

Kunte, P.D., (2003). *National Institute of Oceanography (CSIR).* [Online]
Available at: http://drs.nio.org/drs/bitstream/2264/236/5/chap2%263.pdf
[Accessed 06 March 2012].

Kusuda, T., Umita, T., Koga, K., Futawatari, T and Awaya, Y., (1984). Erosional processes of cohesive sediment. *Water Science Engineering, Water Pollution Research Control,* Volume 117, pp. 891-901.

Kynch, G.J., (1952). A theory of sedimentation. *Transactions of the Faraday Society,* Volume 48, pp. 166-176.

Laksanalamai, J., (2007). *Erosion tests with annular flume,* M.Sc. Thesis: Delft University of Technology.

Lauder, K., (2010). *The performance of pipeline ploughs.* PhD Thesis: University of Dundee.

Le Hir, P., Canna, P., Waelesb, B., Jestina, H. and Bassoulleta, P., (2008). Erodibility of natural sediments: experiments on sand/mud mixtures from laboratory and field erosion tests. In: H. Y. J. S. a. J. Z. G. T. Kusuda, ed. *Sediment and Ecohydraulics — INTERCOH 2005.* Amsterdam: Elsevier, p. 137–153.

Le Hir, P., Cayocca, F. and Waeles, B., (2011). Dynamics of sand and mud mixtures: A multiprocess-based modelling strategy. *Continental Shelf Research,* 31(10), pp. S135-S149.

Le Hir, P., Ficht, A., Silva Jacinto, R., Lesueur, P., Dupont, J-P., Lafite, R., Brenon, I., Thouvenin, B. and Cugier, P., (2001). Fine sediment transport and accumulations at the mouth of the Seine estuary (France). *Estuaries,* 24(6B), pp. 950-963.

Letter, J.V., (2009). *Significance of probabilistic parameterisation in cohesive sediment bed exchange.* PhD Thesis: University of Florida, Gainesville.

Levinton, J.S., (1995). *Marine Biology: Function, Biodiversity, Ecology.* New York: Oxford University Press.

Lewis, W. K., Gilliland, E. R. and Bauer, W. C., (1949). Characteristics of Fluidized Particles. *Ind. Eng. Chem.,* Volume 41, pp. 1104-1117.

Libicki, C. and Bedford, K.W., (1989). Remote and in situ methods for sub-bottom sediment characterisation. *Journal of Coastal Research,* Volume 5, pp. 39-49.

Lick, W. and Lick, J., (1988). Aggregation and disaggregation of fine-grained lake sediments. *Journal of Great Lakes Research,* Volume 14, pp. 514-523.

Lick, W., , (1982). The transport of contaminants in the Great Lakes. *Annual Review of Earth and Planetary Science,* Volume 10, pp. 327-353.

Lick, W., Huang, H. and Jespen, R., (1993). Flocculation of fine-grained sediments due to differential settling. *Journal of of Geophysical Research ,* 98(C6), pp. 10279-10288.

Lick, W., In, L.J. and Gailani, J., (2004). Initiation of movement of quartz particles. *Journal of Hydraulic Engineering-ASCE,* 130(8), pp. 755-761.

Lintern, D.W., (2003). Influences of flocculation on bed properties for fine-grained cohesive sediment. *Ph.D Thesis, Oxford University, UK.*

Liu, H. K., (1957). Mechanics of Sediment-Ripple Formation. *J. Hyd. Div. ASCE,* 183(HY2), pp. 1-23.

Lovell, M. A., (1985). Thermal Conductivity and Permeability Assessment by Electrical Resistivity in Measurements in Marine Sediments. *Marine Geotechnology,* 6(2), pp. 205-240.

Lovell, M. A., (1985). Thermal Conductivity and Permeability Assessment by Electrical Resistivity in Measurements in Marine Sediments. *Marine Geotechnology,* 6(2), pp. 205-240.

Lundkvist, M. Grue, M. Friend, P.L. and Flindt, M.R., (2007). The relative contributions of physical and microbiological factors to cohesive sediment stability. *Continental Shelf Research,* 27(8), pp. 1143-1152.

Lyle, W.M. and Smerdon, E.T. , (1965) . Relation of compaction and other soil properties to erosion resistance of soils. *Transactions of the ASAE ,* Volume 8, p. 419–422.

Maa, J.P-Y. and Lee, D-Y., (2002). A preliminary study on using acostic waves to measure high resolution marine sedimnet bed structure. In: J. a. K. C. Winterwerp, ed. *Fine-sediment dynamics in the marine environment.* Amsterdam: Elsevier, pp. 469-481.

Maa, JP-Y., Sun, K-J and He, Q., (1997). Ultrasonic characterization of marine sediments: a preliminary study. *Marine Geology,* Volume 141, pp. 183-192.

Madsen, T.V. and Warncke, E., (1983). Velocities of currents around and within submerged aquatic vegetation. *Archiv Fur Hydrobiologie,* 97(3), pp. 389-394.

Mandl, F., (2008). *Statistical Physics.* 2nd ed. Manchester: John Wiley & Sons.

Manning, A.J., (2001). *A study of the effect of turbulence on the properties of flocculated mud.* Plymouth, England: PhD thesis, University of Plymouth .

Manning, A.J., Baugh, J.V., Spearman, J.R. and Whitehouse, R.J.S., (2010). Flocculation Settling Characteristics of Mud:Sand Mixtures. *Ocean Dynamics,* Volume 60, pp. 237-253.

Manning, A.J., Baugh, J.V., Spearman, J.R. and Whitehouse, R.J.S., (2010). Flocculation Settling Characteristics of Mud:Sand Mixtures. *Ocean Dynamics,* Volume 60, pp. 237-253.

Manning, A.J., Baugh, J.V., Spearman, J.R., Pidduck, E.L. and Whitehouse, R.J.S., (2011). The Settling Dynamics of Flocculating Mud-Sand Mixtures: Part1-Empirical Algorithm Development. *Ocean Dynamics,* Volume 61, pp. 311-350.

Manning, A.J., Baugh, J.V., Spearman, J.R., Pidduck, E.L. and Whitehouse, R.J.S., (2011). The Settling Dynamics of Flocculating Mud-Sand Mixtures: Part1-Empirical Algorithm Development. *Ocean Dynamics,* Volume 61, pp. 311-350.

Manning, A.J., Spearman, J.R., Whitehouse, R.J.S., Pidduck, E.P., Baugh, J. V. and Spencer, K. L., (2013). *Chapter 6: Flocculation Dynamics of Mud: Sand Mixed Suspensions.* [Online]
Available at: http://cdn.intechopen.com/pdfs-wm/43527.pdf
[Accessed 15 05 2015].

Manning, et al., Spearman, J.R., Whitehouse, R.J.S., Pidduck, E.L. and Spenser, K.L., (2013). Laboratory assessments of the flocculation dynamics of mixed mud:sand suspension. In: A. Dr Manning, ed. *Sediment Transport Processes and their Modelling Applications.* Rijeka, Croatia: InTech, pp. 119-164.

Mason, T.G., Levine, A.J., Ertas, D. and Halsey, T.C., (1999). Critical Angle of Wet Sandpiles. *Physical Review E,* 60(5), pp. 5044-5047.

McAnally, W., Friedrichs, C., Hamilton, D., Hayter, E., Shrestha, P., Rodriguez, H., Sheremet, A., Teeter, A., (2007). Management of Fluid Mud in Estuaries, Bays, and Lakes. I: Present State of Understanding on Character and Behavior. *Journal of Hydraulic Engineering,* 133(1), p. 9–22.

McAnally, W.H. and Mehta, A.J., (2001). Collisional aggregation of fine estuarial sediments. In: W. a. M. A. McAnally, ed. *Coastal and Estuarine Fine Sediment Processes.* s.l.:Elsevier Science B.V., pp. 19-39.

McAnally, W.H., (1999). *Transport of fine sediments in estuarial waters.* PhD Thesis: University of Florida, Gainesville.

McCarter, W. J. and Desmazes, P., (1997). Soil Characterisation using Electrical Measurements. *Geotechnique,* 47(1), pp. 179-183.

McCave, I.N., (1984). Size spectra and aggregation of suspended particles in the deap ocean. *Deep Sea Research,* 31(4), pp. 329-352.

McLean, S. R., (1990). The Stability of Ripples and Dunes. *Earth-Sciences Rev.,* Volume 29, pp. 131-144.

McNown, J.S. and Lin, P.N., (1952). Sediment concentration and fall velocity. *Proceedings, 2nd Midwest Conf. Fluid Mech. ,* pp. 401-411.

Mehta, A. J. , (1981). Review of erosion function for cohesive sediment beds. *Proceedings of the First Indian Conference on Ocean Engineering, Indian Institute of Technology, Madras, India,* Volume 1, pp. 122-130.

Mehta, A. J. and Partheniades, E., (1975). An investigation of the depositional properties of flocculated fine sediments. *Journal of Hydraulics Res.,* Volume 4, pp. 361-381.

Mehta, A.J., (2014). *An Introduction to Hydraulics of Fine Sediment Transport.* Toh Tuck Link, Singapore: World Scientific Publishing Company.

Mehta, A.J., Hayter, E., Parker, W., Krone, R. and Teeter, A., (1989). Cohesive Sediment Transport. I: Process Description. *Journal of Hydraulic Eng.,* 115(8), pp. 1076-1093.

Merckelbach, L. and Kranenburg, C., (2004a). Equations for effective stress and permeability of soft mud-sand mixtures. *Geotechnique,* 54(4), pp. 235-243.

Merckelbach, L. and Kranenburg, C., (2004b). Determining effective stress and permeability equations for soft mud from simple laboratory experiments. *Geotechnique,* 54(9), pp. 581-591.

Merckelbach, L.M., (2000). *Consolidation and strength evolution of soft mud layers.* Ph.D Thesis: Delft University of Technology.

Merckelbach, L.M., (2001). Consolidation and strength evolution of soft mud layers. *Civil Engineering. Delft, Technical University of Delft,* p. 151.

Mersch, E., Lumay, G., Boschini, F. and Vandewalle, N, (2010). Effect of an Electric Field on an Intermittent Granular Flow. *Physical Review E,* 81(4).

Metayer, J.-F., Richard, P., Faisant, A. and Delannay, R., (2010). Electrically Induced Tunable Cohesion in Granular System. *Journal of Statistical Mechanics,* Volume P08003.

Miedema, S.A., (2014). *The Delft sand, clay and rock cutting model.* 1st ed. Amsterdam, Netherlands: IOS Press Inc.

Migniot, C. , (1968). A study of the physical properties of different very fine sediments and their behaviour under hydrodynamic action. *La Houille Blanche,* Volume 7, p. 591–620.

Miller, C.O. and Logwink, A.K., (1951). Fluidized Studies of Solid Particles. *Ind. Eng. Chem.,* Volume 43, pp. 1220-1226.

Milligan, T.G. and Hill, P.S., (1998). A laboratoty assessment of relative importance of turbulence, particle composition and concentration in limiting maximal floc size and settling behaviour. *Journal of Sea Research,* Volume 39, pp. 227-241.

Mitchell, J. K., (1976). *Fundamentals of soil behaviours.* University of Michigan: John Wiley & Sons, Inc.

Mitchell, J., Camanella, R. and Singh, A., (1968). Soil creep as a rate process. *ASCE, Journal SMFD,* 94(1).

Mitchell, J.K., (1964). Shearing Resistance of Soils as a Rate Process. *Journal of the Soil Mechanicsand Foundation Division, ASCE 90,* Volume No. SM1, Proc. Paper 3773, pp. 29-61.

Mitchell, J.K., 1960. Components of Pore Water Pressure and theit Engineering Significance. *Clays and Clay Minerals,* 9(1), pp. 162-184.

Mitchener, H.J., Torfs, H. and Whitehouse, R.J.S., (1996). Erosion of mud/sand mixtures. *Coastal Engineering,* Volume 29, pp. 1-25 (Errata, 1997, 30, 319).

Mory, M., Gratiot, N., Manning, A.J. and Michallet, H., (2002). CBS layers in a diffusive turbulence grid oscillation experiment. In: J. a. K. C. Winterwerp, ed. *Fine sediment dynamics in the marine environment.* s.l.: Elsevier Science B.V. , pp. 139-154.

Nezu, I., Nakagawa, H., (1993). Turbulence in Open-Channel Flow. In: A. Balkema, ed. *IAHR Monograph Series.* Leiden, NL: s.n.

Nielsen, P., (1992). Coastal bottom boundary layers and sediment transport. In: P. Liu, ed. *Advanced Series on Ocean Engineering, Vol. 4.* Singapore: World Scientific, p. 324.

Novak, P. and Cabelka, J., (1981). *Models in Hydraulic Engineering: Physical Principles and Design Applications.* London: Pitman Advanced Publishing Program.

Nowak, S., Samadani, A. and Kudrolli, A., (2005). Maximum Angle of Stability of a wet Granular Pile. *Nature Physics,* Volume 1, pp. 50-52.

Ockelford, A. and Haynes, H., (2013). The Impact of Stress History on Bed Structure. *Earth Surface Processes and Landforms ,* Volume 38, p. 717–727.

Ockenden, M.C. and Delo, E.A., (1988). *Consolidation and erosion of estuarine mud and sand mixtures – an experimental study,* s.l.: HR Wallingford Report, SR 149..

Odd, N.V.M., (1982). The feasibility of using mathematical models to predict sediment transport in the Severn Estuary. In: *The Severn Barrage.* London: Thomas Telford Ltd, pp. 195-202.

Oseen, C., (1927). Hydrodynamik. In: *Akademische Verlags Gesellschaft.* Leipzig: AVG.

Owen, M.W., (1970). *A detailed study of settling velocities of an estuary mud,* s.l.: Hydraulics Research Station, Report INT 78.

Paarlberg, A.J., Gjermansen, M. and Tolker-Nielsen, T., (2005). Biological influences on morphology and bed composition of an intertidal flat. *Estuarine Coastal and Shelf Science,* 64(4), pp. 544-590.

Pahtz, T., Herrmann, H.J. and Shinbrot, T., (2010). Why do Particle Clouds generate Electric Charges?. *Nature Physics,* Volume 6, pp. 364-368.

Panagiotopoulos, I. Voulggaris, G. and Collins, M.B., (1997). The influence of clay on the threshold of movement of fine sandy beds. *Coastal Engineering,* 32(1), pp. 19-43.

Pane, V. and Schiffman, R.L., (1997). The Permeability of Clay Suspensions. *Geotechnique,* 47(2), pp. 273-288.

Pant, H.R., (2013). *Erosional resistance of cohesive sediments in coastal saltmarshes.* MSc Thesis: Louisiana State University.

Paola, C., Straub, K., Mohrig, D. and Reinhardt, L., (2009). The “unreasonable effectiveness” of stratigraphicand geomorphic experiments. *Earth-Science Re-views,* Volume 97, p. 1–43.

Paphitis, D., (2001). Sediment movement under unidirectional flows: an assessment of empirical threshold curves. *Coastal Engineering,* Volume 43, pp. 227-245.

Parchure, T. M. and Mehta, A. J. , (1985). Erosion of soft cohesive sediment deposits. *Journal of Hydraulic Engineering, ASCE,* 3(10), pp. 1308-1326.

Partheniades, E., (1965). Erosion and deposition of cohesive soils. *Journal of the Hydraulics division proceedings of the American Society of Civel Engineers,* Volume 91, pp. 105-139.

Pattiaratchi, C.B. and Collins, M.B. , (1984). Sediment transport under waves and tidal currents: A case study from the northern Bristol Channel, U.K.. *Marine Geology,* 56(1-4), pp. 27-40.

POL, (2009). *UK Sediment Initiative 2009: Developing multidisciplinary sediment dynamics research in a strategic context,* Liverpool: SOFI Workshop Report, April 2009.

Pye, K., (1994). Properties of sediment particles. In: K. Pye, ed. *Sediment Transport and Depositional Processes.* Oxford: Blackwell Scientific Publications, pp. 1-24.

Rasband, W.S., (2008). *ImageJ, U.S. National Institutes of Health. Bethesda, Maryland.* [Online] Available at: http://rsb.info.nih.gov/ij/index.html
[Accessed 13 Dec. 2014].

Raudkivi, A.J. and Hutchinson, D.L., (1974). Erosion of Kaolinite by Flowing Water. *Proc. R. Soc. A.,* Volume 337, pp. 537-554.

Raudkivi, A.J., (1966). Bed Forms in Alluvial Channels. *J. Fluid Mech.,* 26(part 3), pp. 507-514.

Raudkivi, A.J., (1990). *Loose boundary hydraulics.* 3rd ed. Oxford, England: Pergamon Press.

Raudkivi, A.J., (2007). Transition from Ripples to Dunes. *J. Hydraulic Eng.,* Volume 132, pp. 1316-1320.

Raven, E. K., Lane, S. N. and Bracken, L.J. , (2010). Understanding sediment transfer and morphological change for managing upland gravel-bed rivers. *Progress in Physical Geography,* 34(1), pp. 23-45.

Richards, K.J., (1980). The Formation of Ripples and Dunes on an Erodible Bed. *J. Fluid Mech.,* Volume 99, pp. 597-618.

Richardson, J. F. and Zaki, W. N., (1952). Sedimentation and Fluidisation: Part 1. *Transactions of the Institution of Chemical Engineers,* 32(1), pp. 35-53.

Richardson, J.F. and Zaki, W.N., (1954). The sedimentation of a suspension of uniform spheres under conditions of viscous flow. *Chem. Eng. Sci.,* Volume 3, pp. 65-73.

Righetti, M. and Lucarelli, C. , (2007). May the Shields theory be extended to cohesive and adhesive benthic sediemnts?. *Journal of Geophysical Reserach-Oceans,* Volume 112, p. C05039.

Roberts, J., Jepsen, R., Gotthard, D. and Lick, W., (1998). Effects of particle size and bulk density on erosion of quartz particles. *Journal of Hydraulic Engineering-ASCE,* 124(12), pp. 1262-1267.

Roberts, J.J. and Wildenschild, D., (2004). Electrical Properties of Sand-Clay Mixtures Containing Trichloroethylene and Ethanol. *JEEG,* 9(1), pp. 000-000.

Robinson, K.S. and Jones, T.B., (1984). Particle-Wall Adhension in Electropacked Beds. *IEEE Trans. Ind. Appl.,* IA-20(6), pp. 1573-1577.

Ross, M.A., (1988). *Vertical structure of estuarine fine sediment suspensions.* PhD Thesis: University of Florida, Gainesville.

Rubey, W., (1933). Settling velocities of gravel, sand and silt particles. *American J. of Science,* 25(148), pp. 325-338.

Ruffet, C., Gueguen, Y. and Darot, M., (1991). Complex Conductivity Measurements and Fractal Nature of Porosity. *Geophysics,* Volume 56, pp. 758-768.

Saffman, P.G. and Turner, J.S., (1956). On the collision of drops in turbulent clouds. *Journal of Fluid Mechanics,* 1(1), pp. 16-30.

Salem, H. S., (2001). The Influence of Clay Conductivity on Electrical Measurements of Glacial Aquifers. *Energy Sources,* Volume 23, pp. 225-234.

Samouëlian A., Cousin I., Tabbagh A., Bruand A. and Richard G., (2005). Electrical Resistivity Survey in Soil Science: A Review. *Soil and Tillage Research,* Volume 83, pp. 173-193.

Samouëlian A., Cousin I., Tabbagh A., Bruand A. and Richard G., (2005). Electrical Resistivity Survey in Soil Science: A Review. *Soil and Tillage Research,* Volume 83, pp. 173-193.

Sampath, A., (2009). *Sedimentation of Lake Apopka mud and comparison with other sediments.* MS Thesis: University of Florida, Gainesville.

Sanford, L.P., (2008). Modelling a dynamically varying mixed sediment bed with erosion, deposition, bioturbation, consolidation, and armoring.. *Computer and Geosciences,* 34(10), pp. 1263-1283.

Schiffman, R. L., Pane, V. and Sunara, V., (1986). Sedimentation and Consolidation. In: B. a. S. P. Moudgil, ed. *Engineering Foundation Conference, Flocculation,Sedimentation and Consolidation.* New York, NY: AICE.

Schlaberg, H. I., Baas, J. H., Wang, M., Best, J. L., Williams, R. A. and Peakall, J., (2006). Electrical Resistance Tomography for Suspended Sediment Measurements in Open Channel Flows Using a Novel Sensor Design. *Part. Part. Syst. Charact.,* Volume 23, pp. 313-320.

Schofield, A.N and Wroth, C.P., (1968). *Critical state soil mechanics.* London: McGraw-Hill.

Schon, J. H., (1996). Physical Properties of Rocks - Fundamentals and Principles of Petrophysics. In: *Handbook of Geophysical Exploration 18, Section I, Seismic Exploration.* Oxford: Pergamon Press, p. 583.

Scott, K.J., (1984). *Hindered settling of a suspension of spheres; Critical evaluation of equations relating settling rate to mean particle diameter and suspension concentration,* Pretoria, South Africa: Technical Report 497. Chemical Engineering Research Group.

Sen P. N., Scala, C. and Cohen, M. H., (1981). A Self-Similar Model from Sedimentary Rocks with Application to Dielectric Constant of Fused Glass Beads. *Geophysics,* Volume 46, pp. 781-795.

Sgro, L., Mistri, M. and Widdows, J., (2005). Impact of the infaunal Manila clam, 'Ruditapes philippinarum', on sediment stability. *Hydobiologia,* Volume 550, pp. 175-182.

Sheng, Y.P., (1984). A turbulent transport model of coastal processes. *Proceedings 19th Int'l Conf. on Coastal Engineering, ASCE,* pp. 2380-2396.

Sills, G., 1998. Development of structure in Sedimenting Soils. *Phil. Trans. R. Soc. Lond. A,* Volume 356, pp. 2515-2534.

Sills, G.C., Bartholomeeusen, G., Lintern, D.G., Harbottle, M and Lear, G., (2004). The Structure of Soil. In: R. P. D. a. H. K. Jardine, ed. *Advances in Geotechnical Engineering: The Skempton Conference.* London : American Society of Civil Engineers, pp. 630-639.

Simons, D.B., and Richardson, E.V., (1963). Form of Bed Roughness in Alluvia Channels. *Trans. ASCE,* Volume 128, pp. 284-323.

Small, C. and Nicholls, C.J., (2003). A Global Analysis of Human Settlement in Coastal Zones. *Journal of Coastal Research,* 19(3), pp. 584-599.

Smerdon, E.T. and Beasley, R.P., (1959). The tractive force theory applied to stability of open channels in cohesive soil. *Agricultural Experimental Stability Research Bulletin,* Volume 715, pp. 1-36.

Smith J.D. and McLean, S.R., (1977). Spatially averaged flow over a wavy surface. *Journal of Physical Oceanography,* 82(12), pp. 1735-1746.

Soulsby, R., (1997). *Dynamics of Marine Sands.* London: Thomas Telford Publications.

Soulsby, R.L. and Whitehouse, R.J.S., (1997). *Threshold of sediment motion in coastal Environments.* Christchurch, New Zealand, pp 149–154, Proceedings of combined Australasian coastal engineering and port conference.

Spearman, J.R., Manning, A.J. and Whitehouse, R.J.S, (2011). The settling dynamics of flocculating mud:sand mixtures: Part 2 – Numerical modelling. *Ocean Dynamics,* INTERCOH 2009 special issue(DOI: 10.1007/s10236-011-0385-8).

Spears, B. M., Saunders, J.E., Davidson, I., Paterson, D.M., (2008). Microalgal sediment biostabilisation along a salinity gradient in Eden Estuary, Scotland: unravelling a paradox. *Marine and Freshwater Research ,* 59(4), pp. 313-321.

Sridharan, A. and Prakash, K. , (1999). Influence of Clay Mineralogy and Pore-medium Chemistry on Clay Sediment Formation. *Canadian Geotechnical Journal ,* Volume 36, pp. 961-966.

Steves, R., (2015). *Osita Antica, Near Rome.* [Online]
Available at: www.rickstevens.com/watch-read-listen-/read/articles/osiia-antica-near-rome
[Accessed 07 03 (2015)].

Stoke, G.G., (1851). On the effect of internal friction of fluids on the motiom of pendulums. *Transactions, Cambridge Philosophical Society,* 9(2), pp. 8-106.

Stolzenbach, K.D. and Elimelich, M., (1994). The effect of density on collision between sinking particles: implication for particle aggregation in the ocean. *Journal of Deep Sea Research I,* 41(3), pp. 469-483.

Subhasish, D., (2011). Entrainment threshold of loose boundary. In: P. Rowinski, ed. *Experimental Methods in Hydraulic Research.* Berlin Heidelberg: Springer-Verlag, pp. 29-48.

Summer, B. M. and Bakioglu, M., (1984). On the Formation of Ripples on an Erodible Bed. *J. Fluid Mech.,* Volume 144, pp. 177-190.

Sutherland, B.R., Barret, K.J. and Gingras, M.K., (2014). Clay settling in fresh and salt water. *Environ Fluid Mech,* 15(1), pp. 147-160.

Sutherland, T.F., Amos, C.L. and Grant, J., (1998). The effect of buoyant biofilms on the erodibility of sublittoral sediments of a temperate microtidal estuary. *Limnology and Oceanography,* 43(2), pp. 225-235.

Syvitski, J.P.M., Vorosmarty, C.J., Kettner, A.J. and Green, P., (2005). Impact of humans on the flux of terrestrial sediment to the global coastal ocean. *Science ,* Volume 308, p. 376–380.

Taylor Smith, D., (1975). *Geological Assessment of Sea-Floor Sediment Properties.* Brighton, UK, Oceanology International 1975 Conference Papers, pp. 235-267.

Te Slaa, S., He, Q., van Maren, D.S., Winterwerp, J.C., (2013). Sedimentation processes in silt-rich sediment mixtures. *Ocean Dynamics,* Volume 63, pp. 399-421.

Ternat, F., Boyer, P., Anselmet, F. and Amielh, M., (2008). Erosion threshold of saturated natural cohesive sediments: modelling and experiments. *Water Resources Research,* Volume 44, p. W11434.

Terzaghi, K. , (1943). *Theoretical Soil Mechanics.* New York: John Wiley and Sons..

Terzaghi, K., (1923). Die Berechnung des Durchlassigkeitsziffer des Tones aus des Verlauf des hydrodynamischen Spannungerscheinungen. *Sitz Akad Wissen Wien Math Naturwiss Kl. Abt IIa ,* Volume 132, p. 125–138.

Thompson, C.E.L., Amos, C.L., Angelaki, M., Jones, T.E.R. and Binks, C.E., (2006). An evaluation of bed shear stress under turbid flows. *Journal of Geophysical Research,* Volume 111, pp. 1-8.

Thompson, S.M., Turner, J.S., (1975). Mixing across an interface due to turbulence generated by an oscillating grid. *Journal of Fluid Mechanics,* 67(2), pp. 349-368.

Thomsen, L. and Gust, G., (2000). Sediment erosion thresholds and characteristics of resuspended aggregates on the western European continental margin. *Deep-Sea Research Part-I - Oceanographic Research Papers,* 47(10), pp. 1881-1897.

Thomsen, L., Gust, G., (2000). Sediment erosion thresholds and characteristics of resuspended aggregates on the western European continental margin. *Deep-Sea Research Part I-Oceanographic Research Papers,* 47 (10), p. 1881–1897.

Tolhurst, T.J., Consalvey, M. and Paterson, D.M., (2008). Changes in cohesive sediemnt properties associated with the growth of a diatom biofilm. *Hydrobiologia,* Volume 596, pp. 225-239.

Toorman, E. A. and Berlamont, J. E., (1993). Settling and Consolidation of Mixtures of Cohesive and Non-cohesive Sediments. *Adv. Hydro-Sci. Eng.,* Volume 1, pp. 606-613.

Toorman, E.A. , (1996). Sedimentation and self-weight consolidation: general unifying theory. *Géotechnique ,* 46(1), p. 103–113.

Toorman, E.A., (1999). Sedimentation and sel-weight consolidation: constitutive equations and numerical modelling. *Geotechnique,* 49(6), pp. 709-726.

Toorman, E.A., (2001). Cohesive sediment transport modeling: European perspective. In: W. M. &. A. Mehta, ed. *Proceedings in Marine Science, Vol.3: Coastal and Estuarine Fine Sediment Processes .* Proc. INTERCOH'98, Seoul, May 1998: Elsevier Science, Amsterdam, pp. 1-18.

Torfs, H. , (1994). Erosion of Layered Sand-Mud Beds in Uniform Flow. *Proceedings of the International Conference on Coastal Engineering,* Volume No. 24 , pp. 3360-3368..

Torfs, H., Jiang, J. and Mehta, A.J., (2001). Assessment of the erodibility of fine/coarse sediment mixtures. In: W. M. a. A. Mehta, ed. *Coastal and Estuarine Sediment Processes. Vol. 3 Proceedings in Marine Science.* Amsterdam: Elsevier, pp. 109-123.

Torfs, H., Mitchener, H., Huysentruyt, H. and Toorman, E., (1996). Settling and Consolidation of Mud/Sand Mixtures. *Coastal Engineering,* Volume 29, pp. 27-45.

Torfs, H., Mitchener, H., Huysentruyt, H. and Toorman, E., (1996). Settling and Consolidation of Mud/Sand Mixtures. *Coastal Engineering,* Volume 29, pp. 27-45.

Townsend, F.C. and McVay, M.C., (1990). SOA: Large strain consolidation predictions. *Journal of Geotechnical Engineering, ASCE,* 116 (2), pp. 222-243.

Uncles, R.J., Stephens, J.A. and Harris, C. , (1998). Seasonal variability of subtidal and intertidal sediments distributions in a muddy, macrotidal estuary: the Humber-Ouse, UK. In: K. P. D. a. C. A. Black, ed. *Sedimentary Processes in the Intertidal Zone.* London: Geological Society, Special Publications, 139, pp. 211-219.

Uncles, R.J., Stephens, J.A. and Law, D.J., (2006). Turbidity maximum in the macrotidal, high turbid Humber Estuary, UK; flocs, fluid mud, stationary suspensions and tidal bores. *Estuarine, Coastal and Shelf Science,* 67(1-2), pp. 30-52.

USGCRP, (2009). Global Climate Change Impacts in the United States . In: T. J. M. a. T. P. Karl, ed. *United States Global Change Research Program .* New York, NY, USA.: Cambridge University Press.

van Ledden, M., (2003). *Sand-mud segregation in estuaries and tidal basins.* PhD Thesis, Delft University of Technology: The Netherlands.

van Ledden, M., Kesteren, W.G.M. and Winterwerp, J.C., (2004). A conceptual framework for the erosion behaviour of sand-mud mixtures. *Continental Shelf Research,* Volume 24, pp. 1-11.

Van Lessen, W., (1988). *Aggregation of particles, settling velocity of mud flocs: A review.* Berlin, Springer-Verlag, pp. 427-445.

van Leussen, W. and Winterwerp, J. C., (1990). Laboratory experiemnts on sedimentation of fine-grained sediments: A state-of-the-art review in the light of experiemnts with the Deft Tidal Flume. In: R. Cheng, ed. *Coastal and Estuary Studies: Residual Current and Long-term Transport.* N.Y.: Springer-Verlag, p. 241 – 259.

Van Leussen, W., (1994). Estuarine Macroflocs and their Role in Fine-grained Sediment Transport. *Ph.D Thesis, University van Utrecht,* p. 488.

Van Leussen, W., (1997). The Kolmogorov microscale as a limiting value for the floc sizes of suspended fine-grained sediment in estuaries. In: N. P. R. a. W. J. Burt, ed. *Cohesive Sediments.* Chichester, UK: John Wiley & Sons, pp. 45-62.

Van Olphen, H., (1977). *An Introduction to Clay Colloid Chemistry.* 2nd ed. New York: Wiley.

van Rijn, L.C. , (1984). Sediment transport, part I: bed-load transport. *Journal of Hydraulic Engineering,* Volume 110, pp. 1431-1456.

Van Rijn, L.C., (1985). *Sutrench-model: two-dimensional vertical mathematical model for,* s.l.: WL|Delft Hydraulics, Report S488, part IV..

Van Rijn, L.C., (1993). *Principles of Sediment Transport in Rivers, Estuaries and Coastal Seas.* The Netherlands: AQUA Publications.

Van, L.A. and Pham Van Bang, D., (2013). Hindered settling of sand-mud flocs mixtures: From model formulation to numerical validation. *Advances in Water Resources,* Volume 53, pp. 1-11.

Villaret, C. and Paulic, M., (1986). *Experiments on the erosion of deposited and placed chesive sediemnts in an annular flume and a rocking flume,* Gainesville: Coastal and Oceaographic Engineering Dept. University of Florida.

Waeles B., Le Hir P., Lesueur P. and Delsinne N., (2007) . Modelling sand/mud transport and morphodynamics in the Seine river mouth (France): an attempt using a process-based approach.. *Hydrobiologia,* Volume 588 , pp. 69-82.

Waeles, B., Le Hir P. and Lesueur, P., (2008). A 3D morphodynamic process-based modelling of a mixed sand/mud coastal environment: the Seine estuary, France. In: *Sediment and Ecohydraulics: INTERCOH 2005.* s.l.:Elsevier.

Wang, Z., Nestmann, F., and Dittrich, A, (1995). Fall velocity of sediment in clay suspensions. *Sixth International Symposium on River Sedimentation, New Delhi,* p. 314–322.

Waxman M. H. and Smits, L. J. M., (1968). Electrical Conductivities in Oil Bearing Shaly Sandstones. *Society of Petroleum Engineering,* Volume 8, pp. 107-122.

Whitehouse, R.J.S., Soulsby, R., Roberts, W and Mitchener, H.J., (2000). *Dynamics of Estuarine Muds.* London: Thomas Telford Publication.

Widdows, J., Brinsley, M.D. and Pope, N.D., (2009). Effect of Nereis diversicolor density on the erodability of estuarine sediment.. *Marine Ecolody-Progess Series,* Volume 378, pp. 135-143.

Wildenschild, D., Roberts, J.J., and Carlberg, E.D., (2000). Electrical Properties of Sand-Clay Mixtures: The Effects of Microstructure. *Geophys. Res. Lett.,* Volume 27, pp. 3085-3089.

Williamson, H. J. and Ockenden, M. C., (1992). *Tidal Transport of Mud/Sand Mixtures, Laboratory Tests,* s.l.: Wallingford, Report SR 257.

Williamson, H. J., (1991). Tidal Transport of Mud/Sand Mixtures. Sediment Distributions- A Literature Review. *HR Wallingford, Report,* Volume SR 286.

Williamson, H.J. and Ockenden, M.C., (1993). Laboratory and field investigations of mud and sand mixtures. In: S. S. Wang, ed. *Advances in Hydro-science and Engineering, Proceedings of the First International Conference on Hydro-science and Engineering.* Washington D.C.: s.n., pp. 622-629, volume 1.

Winsauer, W. O., Shearin, H. M., Masson, P. H. and Williams, M., (1952). Resistivity of Brine-Saturated Sands in Relation to Pore Geometry.. *American Society of Petroleum Geologists Bulletin,* Volume 36, pp. 253-277.

Winterwerp, J. C., van Kesteren, W. G. M., van Prooijen, B. and Jacobs, W., (2012). A conceptual framework for shear flow–induced erosion of soft cohesive sediment beds. *Journal of Geophysical Research,* 117(C10), pp. 1-17.

Winterwerp, J.C. and Van Kesteren, W.G.M., (2004). *Introduction to the Physics of Cohesive Sediment in the Marine Environment.* Amsterdam, The Netherlands: Elsevier B.V..

Winterwerp, J., (2002) . On the flocculation and settling velocity of estuarine mud. *Continental Shelf Research,* Volume 22, pp. 1339-1360.

Worthington, P.F., (1993). The uses and abuses of the Archie equations, 1: the formation factor–porosity relationship. *Journal of Applied Geophysics,* 30(3), p. 215–228.

Wu, T.H., Resendiz, D. and Neukirchner, R.J., (1966). Analysis of Consolidation by Rate Process Theory. *Journal of the Soil Mechanics and Foundation Division, ASCE 92,* Volume No. SM6, Proc. Paper 4991, pp. 229-248.

Xu, G., Gao, Y., Hong, Z. and Ding, J., (2012. Sedimentation Behaviour of Four Dredged Slurries in China. *Marine Georesources & Geotechnology,* Volume 30, pp. 143-156.

Yalin, M.S. and Karahan, E. , (1979). Inception of sediment transport. *Journal of the Hydraulics Division,* Volume 105, p. 1433–1443.

Yalin, M.S., (1964). Geometrical Properties of Sand Waves. *J. Hydraulic Div. ASCE,* 90(HY5), pp. 105-119.

Yalin, M.S., (1972). *Mechanics of Sediment Transport.* Oxford, UK: Pergamon Press.

Yallop, M.L., Paterson, D.M. and Wellsbury, P., (2000). Interrelationships between rates of microbial production, exopolymer production, microbial biomass, and sediment stability in biofilms or intertidal sediments. *Microbial Ecology,* 39(2), pp. 116-127.

Young, H.D. and Freedman, R.A., (2008). *University Physics – With Modern Physics.* 12th ed. s.l.:Addison-Wesley (Pearson International).

Zhao, G., Mu, X., Strehmel, A. and Tian, P., (2014). Temporal Variation of Streamflow, Sediment Load and Their Relationship in the Yellow River Basin, China. *PLoS ONE,* 9(3), pp. 1-13.

Zhou, D. and Mendoza, C., (2005). Growth Model for Sand Wavelets. *J. of Hydraulic Engineering (ASCE),* 131(10), pp. 866-876.

Zhou, D. and Mendoza, C., (2009). On Bedform Growth and Nonequilibrium Sediment Transport. *Can. J. Civ. Eng.,* Volume 36, pp. 1634-1642.